The Climate Response to Antarctic Sea Ice Loss

Submitted by Holly Cara Ayres, to the University of Exeter as a thesis for the degree of Doctor of Philosophy in Mathematics in December 2020.

I certify that all material in this thesis which is not my own work has been identified and that any material that has previously been submitted and approved for the award of a degree by this or any other University has been acknowledged.

Holly Cara Ayres

Abstract

Antarctic sea ice is projected to decrease in response to increasing greenhouse gas concentrations. Antarctic sea ice and its changes are known to strongly modulate the climate of the high-latitude Southern Hemisphere, but sea-ice loss may also affect the large-scale atmospheric and oceanic circulation. Limited studies so far have examined the coupled atmosphere-ocean response to Antarctic sea-ice loss. This thesis provides the first comprehensive examination of the climate response to Antarctic sea-ice loss, isolating the atmospheric and oceanic responses, and their coupled interactions, using several modelling approaches. It provides the first multi-model assessment of the atmospheric response to Antarctic sea-ice loss, and novel bespoke coupled model experiments, to assess the oceanic response and the importance of ocean-atmosphere coupling. Lower tropospheric warming over regions of sea-ice loss and the nearby Southern Ocean is robust across all models and experimental approaches. Ocean coupling allows the warming response to spread globally, including to the Antarctic interior, Arctic Ocean and tropical upper troposphere, and throughout the global oceans. A weakening and slight equatorward shift of the Southern Hemisphere tropospheric eddy-driven jet is also common across all models and experiments, but of greater magnitude in the coupled model. The oceanic response features a 20% reduction in Antarctic Circumpolar Current transport, likely due to reduced surface wind stress. Surface waters warm, becoming more stable and more stratified in the Southern Ocean, with similar changes, but of lesser magnitude, in the Arctic Ocean, where sea ice declines. These results demonstrate that the ocean governs the widespread effects of Antarctic sea-ice loss, and is also important in determining the magnitude of its effects over the Southern Hemisphere high latitudes.

Acknowledgments

To start, I would like to thank my lead supervisors; James Screen and Tom Bracegirdle who have helped to develop and discuss ideas, and support me throughout the entire process, reading draft after draft of thesis chapters! James has been tremendously supportive, and an outstanding supervisor throughout every step of PhD.

An enormous thank you to those that have supported me on the modelling at the Met Office and NCAS. Chiefly, Ed Blockley, who gave truly invaluable instruction on manipulating the sea ice model code. Not to mention, Grenville Lister and the team, who have answered many of my questions at the Unified Model helpdesk.

A thank you to my internal examiners; Mat Collins and Nadine Unger for their continued support, questions and suggestions that have helped shape this thesis and challenge my ideas. Also, to everyone at the climate dynamics department at the University of Exeter, for moral support, keeping me smiling, and the occasional problem-solving discussion.

I am hugely grateful for the funding to complete (and enjoy!) this project, provided by the University of Exeter College of Engineering, Mathematics and Physics, and the NERC Real Projections Project.

Thank you to David Ferreira for offering me a postdoc position to start straight away after submission and accepting my delay, meaning I could focus solely on the thesis over the final months.

On a personal level, thank you to my friends and family, who have supported, listened, and tried their absolute best to understand me when I excitably discuss my work and climate science. Not to mention, my exercise instructor, Vicki, for keeping me physically and mentally well throughout. On an even cheesier note,

I would like to thank my Mum, who has supported my journey since the age of 7, when I first decided I wanted to be a climate scientist, despite still not fully understanding ‘what it is that I do’! I would specifically like to thank my husband Jamie, who has supported and encouraged every step, in addition to making me laugh, even on the hardest of days.

Finally, I would like to thank you, the reader, be it examiner, researcher, or friend, for reading the work that has been my life and passion for just over three years.

List of publications

Ayres, H. C., & Screen, J. A. (2019). Multimodel Analysis of the Atmospheric Response to Antarctic Sea Ice loss at Quadrupled CO_2. Geophysical Research Letters, 46(16), 9861–9869. https://doi.org/10.1029/2019GL083653

Table of Contents

Abbreviations ..... **x**
List of Figures and Tables ..... **xi**
1 Introduction **1**
2 Literature Review **5**
2.1 The geographic setting 5
2.1.1 Tropospheric atmospheric circulation 6
2.1.2 Stratospheric atmospheric circulation 10
2.1.3 Ocean circulation 12
2.1.4 Sea ice 18
2.2 Antarctic sea ice trends 20
2.2.1 Trends 20
2.2.2 Causes of positive trends 22
2.2.3 Recent and predicted Antarctic sea ice trends 26
2.3 Modelling limitations 28
2.4 Impact of global climate change on the Antarctic region 30
2.5 Climate response to polar sea-ice loss 33
2.5.1 Climate response to Arctic sea-ice loss 33
2.5.2 Climate response to Antarctic sea-ice loss 35
2.6 Chapter summary 37
3 Data and Methods **39**
3.1 The CMIP5 multi-model response. 39
3.1.1 CMIP5 models 39
3.1.2 Multi-model response 40

3.2 Bespoke simulations 42

3.2.1 HadGEM3.GC3.1 model 42

3.2.2 Forcing 47

3.2.3 Model sensitivity tests 49

3.3 HadGEM3 Atmospheric only 55

3.3.1 Model and forcing 55

3.3.2 Tests 56

3.4 Diagnostic metrics and statistics 59

3.5 Summary of Chapter 3 63

4 Multi-Model Analysis of the Atmospheric Response to Antarctic Sea-Ice Loss at Quadrupled CO_2 64

4.1 Introduction 65

4.2 Results 68

4.2.1 Sea ice 68

4.2.2 Atmosphere 70

4.2.3 Zonal-mean atmospheric responses 75

4.2.4 Jet, SPV and SAM dynamics 79

4.3 Discussion 82

4.4 Summary of Chapter 4 85

5 Atmospheric Response to Abrupt Antarctic Sea-Ice Loss in HadGEM3-GC3.1. 86

5.1 Introduction 86

5.2 Results 89

5.2.1 Sea ice 89

5.2.2 Spatial pattern of atmospheric response 94

5.2.3 Vertical structure of atmospheric response 99

5.2.4 Fast and slow responses 101

5.2.5 Response to quadrupled CO_2 104

5.3 Discussion 107

5.4 Summary of Chapter 5 111

6 Oceanic Response to Abrupt Antarctic Sea-Ice Loss in HadGEM3-GC3.1. 113

6.1 Introduction 113

6.2 Results 118

6.2.1 Global Ocean 118

6.2.2 The Southern Ocean 127

6.2.3 The Tropics 135

6.2.4 The Arctic and the AMOC 136

6.3 Discussion 138

6.4 Summary 141

7 Role of Ocean Coupling in the Atmospheric Response to Abrupt Antarctic Sea-Ice Loss 143

7.1 Introduction 143

7.2. Results 146

7.2.1 Sea ice 146

7.2.2 Spatial pattern of atmospheric response 149

7.2.3 Vertical structure of atmospheric response 155

7.3. Discussion 161

7.4. Summary 164

8 Conclusions 165

8.1 Key findings 165

8.2 Future work and possible extensions 170

Bibliography 174

Data Sources 214

Abbreviations

Acronym	Definition
AABW	Antarctic Bottom Water
AAIW	Antarctic Intermediate Water
ACC	Antarctic Circumpolar Current
ASL	Amundsen Sea Low
AAIW	Antarctic Intermediate Water
CDW	Circumpolar Deep Water
CMIP	Coupled Model Intercomparison Project
ENSO	El Niño Southern Oscillation
ITCZ	Intertropical Convergence Zone
MOC	Meridional Overturning Circulation
MSLP	Mean sea level pressure
NADW	North Atlantic Deep Water
NPDW	North Pacific Deep Water
PSC	Polar stratospheric clouds
PCH	Polar cap height
RCP	Representative Concentration Pathway
SAM	Southern Annular Mode
SAMW	Sub-Antarctic Mode Water
SIA	Sea ice area
SIC	Sea ice concentration
SIT	Sea ice thickness
SPV	Stratospheric Polar Vortex
SSH	Sea surface height
SST	Sea surface temperature
TAS	Surface air temperature
U500	Zonal wind at 500 hPa
Z500	Geopotential height at 500 hPa

List of figures and tables

Figure 2.1: The Southern Ocean by region..... 6

Figure 2.2: The Amundsen Sea Low (ASL) 7

Figure 2.3: The SAM index as a time series since 1957 to 2016..... 8

Figure 2.4: Schematic of ENSO physical mechanisms..... 10

Figure 2.5: The Antarctic Circumpolar Current frontal dynamics schematic 13

Figure 2.6: The dynamic front locations of the Southern Hemisphere 14

Figure 2.7: Southern Ocean overturning circulation 16

Figure 2.8: Mean Antarctic sea-ice loss since accurate satellite records began (1979 - 2019)..... 21

Figure 2.9: Annual-mean variation in regional sea ice concentration distribution in the Antarctic..... 21

Figure 2.10: The monthly sea ice extent (SIE) trends over the 40-year satellite period by region..... 22

Figure 2.11: 2016 -2017 sea ice concentration anomalies by region..... 27

Figure 2.12: Minimum and maximum sea ice and SST trends for the Arctic and Antarctic 30

Figure 2.13: The response of the ocean and atmospheric dynamics of the high-latitude Southern Hemisphere 32

Figure 3.1:The annual mean SST in (a) N96ORCA1 and (b) N216ORCA025, and the bias against ESA CCI satellite observations 44

Figure 3.2: Antarctic Circumpolar Current volume transport, for 500 years of the Preindustrial Control N96ORCA1 model, and 300 years of the Preindustrial Control N216ORCA025..... 45

Figure 3.3: The mean Antarctic sea ice extent in winter with (a) HadGEM3 -GC3 and (b) HadGEM3 GC3.1..... 45

Figure 3.4: The annual cycle of sea ice volume for the HadGEM3 model GC2 and GC3, for the (a) the Arctic and (b) the Antarctic..... 46

Figure 3.5: Sea ice area annual cycle comparison, for Hadgem2-ES RCP8.5, Abrupt4XCO_2 and Preindustrial Control simulations, with the HadGEM3 GC3.1 experiments..... 51

Figure 3.6: Sea ice area percentage loss annual cycle comparison, for Hadgem2-ES RCP8.5 and Abrupt4XCO_2 difference to the Preindustrial Control simulations, with the HadGEM3 GC3.1 experiments..... 52

Figure 3.7: Sea ice concentration response to full meltpond experiments..... 53

Figure 3.8: Annual average sea ice area anomaly between HadGEM3 GC3.1 perturbed and Preindustrial Control..... 54

Figure 3.9: Sea ice area comparison between the atmosphere-only and coupled model..... 57

Figure 3.10: Sea ice concentration output from atmospheric only model, against input from coupled model..... 57

Figure 3.11: Sea ice thickness comparrison of the controls of the atmospheric-only and coupled model..... 58

Figure 4.1: Multi-model-mean sea ice concentration and heat flux response to quadrupled CO_2..... 69

Figure 4.2: Multi-model-mean inferred spatial variables..... 72

Figure 4.3: Austral winter (July-September) multi-model-mean spatial variable response to Antarctic sea-ice loss comparrison to Abrupt4xCO_2. 73

Figure 4.4: Austral spring (October-December) multi-model-mean spatial variable response to Antarctic sea-ice loss comparrison to Abrupt4xCO_2..... 74

Figure 4.5: Multi-model-mean inferred zonal-mean response to Antarctic sea-ice loss..... 76

Figure 4.6: Austral spring (October-December) multi-model-mean zonal-mean response to Antarctic sea-ice loss comparrison to Abrupt4xCO_2 77

Figure 4.7: Multi-model-mean, zonal-mean zonal wind at 850hPa (U850) monthly averages for (a) Abrupt4xCO_2 response to PiControl (b) AMIP SST+CO_2 response to AMIP and (c) the inferred response to Antarctic sea-ice loss 78

Figure 4.8: Multi-model-mean inferred zonal-mean geopotential height response to Antarctic sea-ice loss with time over the Antarctic polar cap. 79

Figure 4.9: Multi-model-mean inferred large scale atmospheric dynamics response to Antarctic sea-ice loss and the combined response to SST and CO_2 as a function of calendar month. 82

Figure 5.1: Annual average sea ice for the control and perturbed simulations. 90

Figure 5.2: Total sea ice and heat flux response to Antarctic sea-ice loss as a function of calendar month 92

Figure 5.3: Annual average sea ice and heat flux difference between perturbed and PIcontrol data for Antarctic and Arctic 93

Figure 5.4: Sea ice concentration and heat flux response to Antarctic sea-ice loss 94

Figure 5.5: Spatial variable response to Antarctic sea-ice loss..... 97

Figure 5.6: Continental surface response to Antarctic sea-ice loss 97

Figure 5.7: Mean annual total precipitation per day in tropical region. 98

Figure 5.8: Zonal-mean response to Antarctic sea-ice loss..... 100

Figure 5.9: The Southern Hemispheric tropospheric jet latitude response to Antarctic sea-ice loss (black line). (b) As (a), for jet strength..... 101

Figure 5.10: Annual average near surface temperature difference between perturbed and PIcontrol data 102

Figure 5.11: Annual zonal wind velocity at 500 hPa at the Southern Hemisphere tropospheric jet difference between perturbed and PIcontrol data 103

Figure 5.12: Annual average tropical total precipitation difference between perturbed and PIcontrol data 103

Figure 5.13: Spatial variable Abrupt4xCO_2 response from PIcontrol and response to Antarcitc sea ice loss 105

Figure 5.14: Zonal-mean Abrupt4xCO_2 response from PIcontrol and response to Antarcitc sea ice loss 107

Figure 6.1: Sea ice response to Antarctic sea-ice loss 119

Figure 6.2: Zonal-mean potential seawater temperature, salinty and density as a response to Antarctic sea-ice loss 122

Figure 6.3: Zonal-mean vertical velocity as a response to Antarctic sea-ice loss 124

Figure 6.4: Zonal-mean zonal velocity as a response to Antarctic sea-ice loss 125

Figure 6.5: Zonal-mean meridional velocity as a response to Antarctic sea-ice loss 126

Figure 6.6: Change in Antarctic Circumpolar Current (ACC) transport as a response to Antarctic sea-ice loss 128

Figure 6.7: Zonal-mean zonal velocity as a response to Antarctic sea-ice loss (spatial maps) 129

Figure 6.8: Temperature and salinity profiles at latitude bands of the Southern Ocean 132

Figure 6.9: Sea surface temperature (SST) gradient transcet along the Greenwhich Meridian (0° E) throughout the Southern Ocean (70° S to 30° S) 134

Figure 6.10: Zonal-mean tropical Pacific surface upwelling as a response to Antarctic sea-ice loss, in the top 100 m 135

Figure 6.11: Temperature and salinity profiles of the Equator 136

Figure 6.12: T-S profiles at 85° N of the Arctic Ocean 137

Figure 6.13: Annual average change in North Atlantic Meridional Streamfunction transport (Sv) at 26.5° N 138

Figure 7.1: Sea ice and heat flux response to Antarctic sea-ice loss 148

Figure 7.2: Spatial variable response to Antarctic sea-ice loss 150

Figure 7.3: Spatial varialbe comparrison to Antarctic sea-ice loss in austral cold season 153

Figure 7.4: Spatial varialbe comparrison to Antarctic sea-ice loss in austral warm season 154

Figure 7.5: Zonal-mean response to Antarctic sea-ice loss 156

Figure 7.6: Zonal-mean comparrison to Antarctic sea-ice loss in austral cold season 158

Figure 7.7: Zonal-mean comparrison to Antarctic sea-ice loss in austral warm season. 159

Figure 7.8: The Southern Hemispheric tropospheric jet latitude response to Antarctic sea-ice loss 160

Table 3.1: Models used for the CMIP5 mult-model ensemlbe 40

Table 3.2: Summary of the main model outputs used throughout this thesis, and their acronyms 61

Table 3.3: Summary of model experiments and data used for throughout this thesis 62

Chapter 1

Introduction

The polar regions are especially sensitive to global climate change leading to polar amplification, the phenomenon of greater warming at high latitudes compared to the global average (e.g., Bromwich et al., 2013; Collins et al., 2013; Meredith et al., 2019). The Antarctic is currently warming at a slower rate than the Arctic, with many theories as to why that may be (e.g., Gupta & England, 2006; Polvani et al., 2011; Solomon et al., 2016; Turner et al., 2009), although parts of the Antarctic Peninsula and West Antarctica are warming rapidly. If greenhouse gas concentrations continue to rise, Antarctic warming is projected to become more widespread and severe (Collins et al., 2013).

Over the satellite era, since 1979, the annual-mean Antarctic sea ice extent (SIE) has increased by a small, yet significant 54 thousand square kilometres per decade (Fetterer et al., 2017). This counterintuitive increase, in a warming world, is in contrast to the decline in the Arctic over the same time period, and the decline simulated for Antarctica in models over the historical period (e.g., Meredith et al., 2019). The observed trend of increasing sea ice has become weaker in recent years, and less statistically significant (Parkinson, 2019), after the record low sea ice extent (SIE) in austral winter 2016 (Turner et al., 2017), the causes of which remain unclear. Models project Antarctic sea-ice loss over this century in response to increasing greenhouse gas concentrations (Collins et al., 2013).

The Northern Hemisphere response to Arctic sea-ice loss has been assessed extensively, with robust features including thermodynamically driven warming and moistening of the atmosphere (e.g., Deser et al., 2010; England et al., 2018; Screen & Simmonds, 2010; Screen et al., 2013). Large scale circulation changes of the mid-latitude westerly jet and North Atlantic Oscillation (NAO) have also been suggested in response to Arctic sea-ice loss (e.g., Blackport & Kushner, 2016; Blackport & Screen, 2020; Kay et al., 2015; Kim et al., 2014; Peings & Magnusdottir, 2014; Screen & Simmonds, 2013; Screen et al., 2013), although these are still highly debated in the literature.

The response to Antarctic sea-ice loss has been less studied by comparison. The limited studies so far have focused on the high-latitude Southern Hemispheric response, rather than the possible global implications, and have revealed contrasting results. For example, there is disagreement on the impact of sea-ice loss on the location of the westerly jet, although most studies agree that there is a reduction in its strength (Bader et al., 2013; England et al., 2018; Kidston et al., 2011; Menéndez et al., 1999). Furthermore, the vast majority of studies have used atmosphere-only models, as opposed to fully coupled atmosphere-ocean models.

The use of fully coupled ocean-atmosphere models is known to be important in capturing the full global response to Arctic sea-ice loss (e.g., Blackport & Kushner, 2016; Deser et al., 2016, 2015; Oudar et al., 2017; Sun et al., 2020; Tomas et al., 2016). Seminal work by Deser et al. (2015) found the response to Arctic sea-ice loss was confined to north of 30° N in an atmosphere-only model,

whereas in a coupled model with equivalent forcing, the response was global. Since then, the widespread effects of Arctic sea-ice loss has been well established (e.g., Chemke et al., 2019; Deser et al., 2015; Smith et al., 2017; Sun et al., 2018; Sun et al., 2020; Tomas et al., 2016).

Coupled models have only very recently been used to isolate the response to Antarctic sea-ice loss, with only two published papers based on the same set of experiments with a single model (England et al, 2020a; 2020b). These authors suggested that ocean coupling is crucial in capturing a global response to Antarctic sea-ice loss, which was found to be much alike the global response to Arctic sea-ice loss. However, further confirmation from other coupled climate models is needed to fully determine the coupled climate responses to Antarctic sea-ice loss. It is clear from the above studies that the ocean may play an important role in the climate response to Antarctic sea-ice loss. Yet, the impact of Antarctic sea-ice loss on the ocean has not been assessed in any detail.

The thesis advances the science on the climate response to Antarctic sea-ice loss in four main ways. First, it provides the first multi-model assessment of the atmospheric response to Antarctic sea-ice loss. Second, it uses a novel coupled modelling framework to isolate the atmospheric response to Antarctic sea-ice loss, building on the work of England et al (2020a; 2020b), and assessing local and global effects. Third, it provides the first detailed examination of the oceanic response to Antarctic sea-ice loss. Fourth, it provides the clearest yet determination of the role of ocean coupling in the climate response to Antarctic sea-ice loss.

This thesis is organised as follows. Chapter 2 provides a detailed literature review, expanding on the topics introduced here. Chapter 3 contains details of the data, modelling and statistical methods used throughout the thesis. Chapter 4 uses the CMIP5 “ensemble of opportunity” to infer the multi-model atmospheric response to Antarctic sea-ice loss. Chapters 5 and 6 examine the atmospheric and oceanic components, respectively, of the climate response to Antarctic sea-ice loss, estimated from a bespoke sea ice perturbation experiment in a coupled model. Chapter 7 evaluates results from an analogous experiment but with an atmosphere-only model, to assess the role of ocean coupling in the atmospheric response to Antarctic sea-ice loss. Finally, Chapter 8 summarises the main conclusions of the thesis and discusses their implications for the field.

Chapter 2

Literature Review

This chapter reviews the literature related to Antarctic sea ice and its role in the global climate system, as follows. First, Section 2.1 introduces the geography and climate dynamics of the mid-to-high latitudes of the Southern Hemisphere, including the atmosphere, ocean, and sea ice. This is followed by a review of Antarctic sea ice trends in Section 2.2 including recent changes, their causes, and future projections. In Section 2.3, modelling limitations of specific relevance to the Southern Hemisphere extratropics are discussed. Section 2.4 focuses on greenhouse gas-induced climate change over Antarctica and the Southern Ocean. Sections 2.5.1 and 2.5.2 respectively, examine the climate responses to Arctic and Antarctic sea-ice loss. This is followed by a short summary of the literature in Section 2.6.

2.1 The geographic setting

Geographically, Antarctica and the Arctic are opposites in almost every sense of the word. The Arctic is an ocean surrounded by landmasses whereas Antarctica is a continent surrounded by ocean. A strong westerly eddy-driven tropospheric jet and the corresponding Antarctic Circumpolar Current (ACC) encircle Antarctica, protecting the continent from the impact of warm surface currents and meridional air masses. The Antarctic coast is situated between 83° and 63° S, with the Southern Ocean extending up to 35° S. The winds and currents flow uninterrupted by land, with the narrowest constriction at Drake Passage, between 80° and 50° W. The continent itself consists of a vast, mountainous, icy desert, with its tallest peak, Mt. Vinson Massif, at an altitude of 4,892 metres (Figure 2.1).

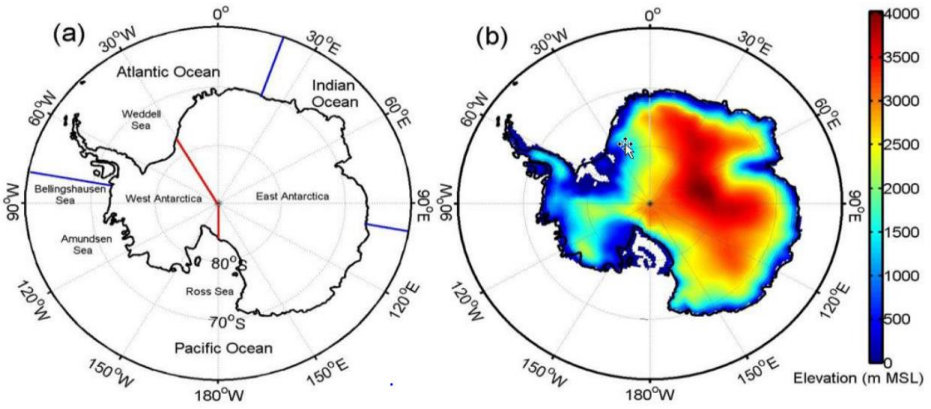

***Figure 2.1**: The Southern Ocean by region (a) and Antarctic continent topography (b). Figure from Yu et al. (2020).*

2.1.1 Tropospheric atmospheric circulation

The large-scale tropospheric circulation surrounding Antarctica is simplified by the zonal symmetry of the region in comparison to the Northern Hemisphere. The mid-latitude westerly tropospheric eddy-driven jet encircles Antarctica at approximately 50° S, with easterly winds at higher latitudes around the Antarctic coast. Over the continent, the near-surface winds are dominated by katabatic (downslope) flow from the high-altitude plateau to the coast. There is limited meridional transport across the westerly eddy-driven jet, with varying wave patterns shifting throughout the year, formed from topography and regions of warming and cooling over the Southern Ocean (e.g., Turner et al., 2017). Key pressure systems and teleconnections connecting the region to the rest of the globe include the Amundsen Sea Low (ASL), the Southern Annular Mode (SAM), and El Niño Southern Oscillation (ENSO).

The ASL is a quasi-stationary, cyclonic low pressure system stretching from the Antarctic Peninsula to the Ross Sea (60° – 70° S, 220° – 250° E) (Figure 2.2), which shifts eastwards and westwards (Hosking et al., 2013), and is a key controller of regional sea ice in the Ross and Amundsen Seas (e.g., Hosking et al., 2013; Turner et al., 2016). The clockwise rotation of the ASL brings warm, poleward air into the Antarctic Peninsula and Bellingshausen Sea regions, and cold equatorward air over the Ross Sea. The ASL is the most variable atmospheric system over the Antarctic and is thought to exhibit significant correlations with SAM and ENSO (e.g,. Lefebvre et al., 2004; Turner et al., 2013).

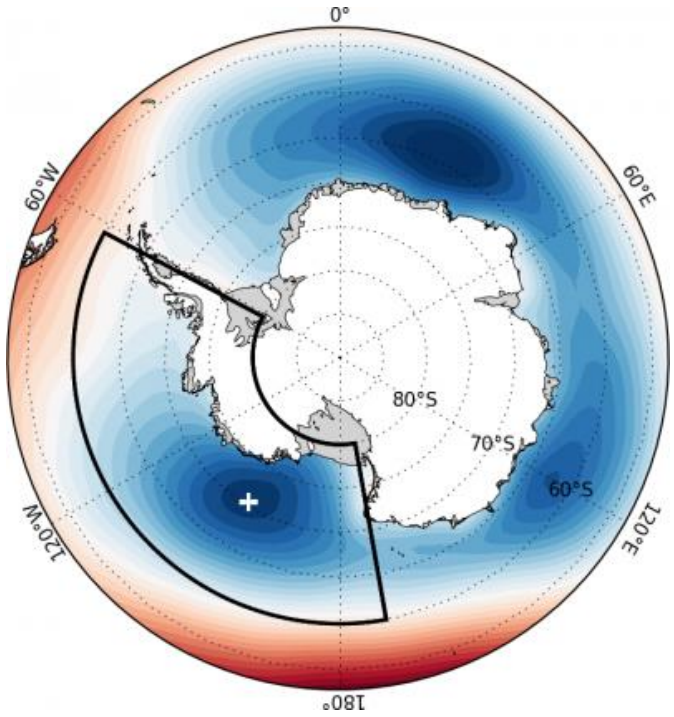

Figure 2.2*: The Amundsen Sea Low (ASL) region, with the centre of low pressure marked with a '+', and the full region marked inside the black outlined box. Figure from Hosking et al. (2020).*

The SAM is the dominant mode of variability in the extratropical Southern Hemisphere and describes variations in the intensity of zonal westerly winds over the Southern Ocean (Gong & Wang, 1999; Thompson & Wallace, 2000). The phase of the SAM index also relates to the position of cold fronts and mid-latitude storm tracks, affecting climate variability across the Southern Hemisphere extratropics (Klekociuk & Wienecke, 2017). A positive SAM index occurs when the pressure over the continent is anomalously low and pressure in mid-latitudes is anomalously high. It is associated with a strong westerly tropospheric eddy-driven jet, a wave one pattern (minimal meridional transport), with a slight poleward shift of the jet. A negative SAM index occurs with the opposite pressure anomalies and is associated with a weaker westerly tropospheric eddy-driven jet, a wave 3 pattern (increased meridional transport) and a slight equatorward shift of the jet. Since satellite records began in the 1970s, the SAM index has transitioned towards its positive phase, notably strongest in Austral summer. (Figure 2.3) (Gong & Wang, 1999; Marshall, 2003; Thompson & Wallace, 2000).

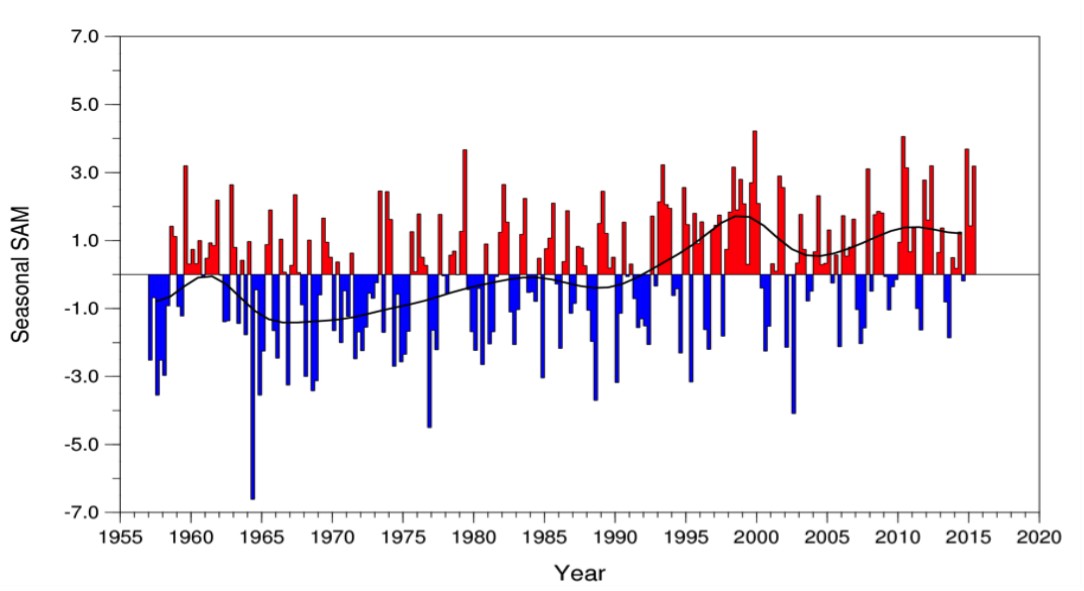

***Figure 2.3**: The SAM index as a time series since 1957 to 2016. Figure from Marshall et al. (2018).*

The primary dynamics of ENSO occur in the tropical South Pacific (Figure 2.4), but the phenomenon has a significant influence on the Southern Ocean and Antarctica. This teleconnection occurs through the process of atmospheric anomalies triggered by tropical Pacific convection, which then propagate south-eastward in the form of a Rossby wave train (e.g., Karoly, 1989; Mo & Higgins, 1998; Yu et al., 2012). The influence of ENSO in high latitudes is most notable in the Ross, Amundsen and Bellingshausen Sea regions (Kwok & Comiso, 2002; Simmonds & Jacka, 1995; Turner, 2004; Yuan, 2004), with strongest correlations in austral winter and spring (Jin & Kirtman, 2009; Mo & Higgins, 1998; Simpkins et al., 2012).

ENSO can be separated into two phases: El Niño and La Niña. El Niño events trigger a high-pressure anomaly in the Amundsen-Bellingshausen Sea region, weakening the ASL (e.g., Clem et al., 2016; Turner, 2004; Turner et al., 2013; Yuan, 2004; Yuan & Li, 2008). The response to a La Niña event generally shows a strengthening and broadening effect on the ASL (Fogt et al., 2011; Houseago-Stokes & McGregor, 2000; Simpkins et al., 2012; Turner et al., 2013; Yuan, 2004). The relationship between ENSO and the SAM index is still debated. Most studies imply a negative correlation, that is El Niño coincides with negative SAM and La Niña with a positive SAM (Fogt & Bromwich, 2006; Fogt et al., 2011; Stammerjohn et a.,2008).

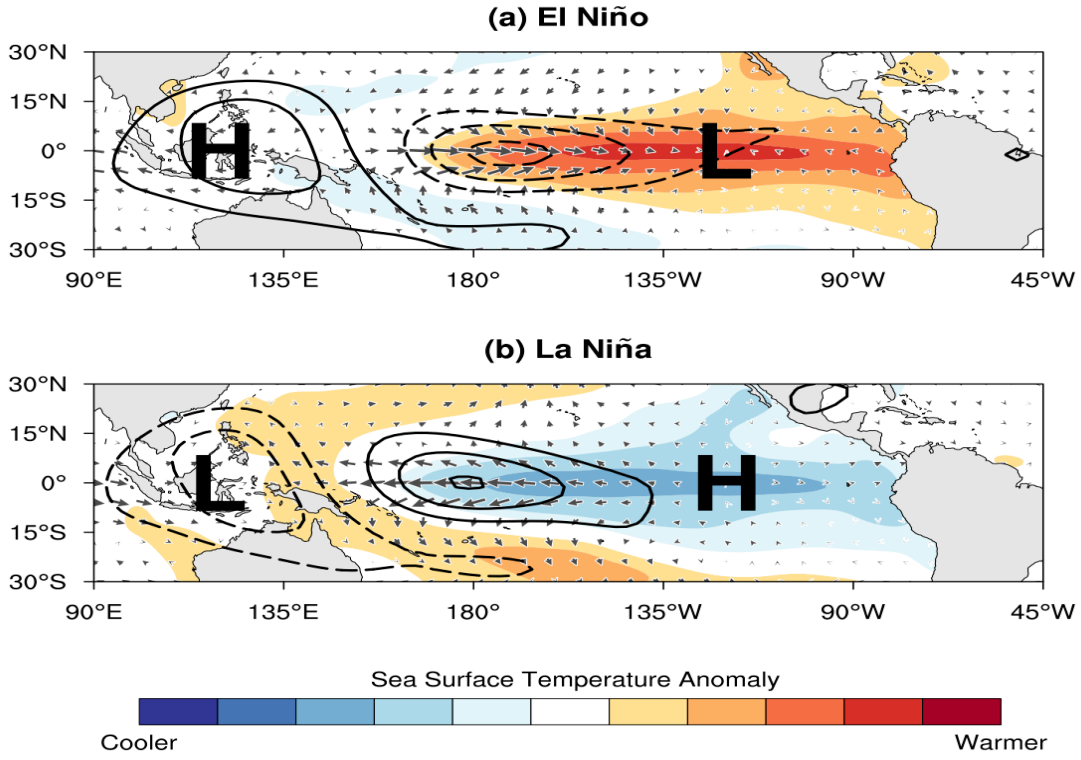

***Figure 2.4**: Schematic of ENSO physical mechanisms, whereby the SST (shaded), outgoing longwave radiation index (OLR) (contours), surface zonal and meridional winds (vectors), and sea level pressure, regulate the wintertime Multivariate ENSO Index (MEI) during (a) El Niño and (b) La Niña events. Figure from NOAA (2020) and Zhang et al. (2019).*

2.1.2 Stratospheric atmospheric circulation

The stratospheric circulation over Antarctica is dominated by the stratospheric polar vortex (SPV). The SPV is defined by close-to-zonal westerly winds, persistent low pressure, and extreme cold temperatures contained by the winds (Rafferty et al., 2017). The SPV is strongest in the winter in both hemispheres, and the extreme cold temperatures within the SPV allow polar stratospheric cloud (PSC) formation, triggering rapid ozone loss in the late winter and early spring (e.g., Hassler et al., 2011; Thompson & Wallace, 2000). The SPV system extends

from 8km in the upper troposphere, to up to 50km in the stratosphere. The Southern Hemisphere SPV is stronger and has a longer life cycle than that of the Northern Hemisphere, due to lesser planetary wave activity and muted seasonality of stationary waves (arising from the more zonally-symmetric continental geography) (Waugh & Randel, 1999). Destabilisation of the SPV can occur via stratospheric sudden warming events, although these are less frequent in the Southern Hemisphere than in the Northern Hemisphere (Thompson et al., 2011): they occur approximately every other year in the Northern Hemisphere winter. Ozone depletion in the Southern Hemisphere stratosphere has led to the SPV final warming occurring later in the year, from late October in the 1970s and 1980s to late November in more recent years (Mayewski et al., 2009).

Ozone depletion has been a critical driver of climate change in recent decades, affecting the surface climate most strongly in austral summer (Thompson et al., 2011). This depletion of ozone (as well as increased greenhouse gas concentrations) has caused a stratospheric cooling, which in turn triggers a stronger SPV and therefore, a positive SAM index (e.g., Bandoro et al., 2014; Gillett & Thompson, 2003; Randel et al., 2009; Thompson et al., 2005; Thompson & Solomon, 2002). Ozone depletion has contributed to stronger westerly winds in the troposphere and a poleward shift of the jet, through downward wave propagation of stratospheric anomalies to the surface (Klekociuk & Wienecke, 2017), with broad effects on summertime weather and climate across the Southern Hemisphere (Thompson et al., 2011). However, there is evidence that these effects will be reversed as the ozone hole recovers over the next few decades. In summer, the opposing effects of ozone recovery and increased greenhouse gases may lead to a muted SAM trend (Thompson et al., 2011).

However, during other seasons, the effect of increased greenhouse gases is expecting to dominate and for the positive SAM trend to continue, shifting the jet further poleward (Klekociuk & Wienecke, 2017).

2.1.3 Ocean circulation

The Southern Ocean is a critical component of the global climate system: it forms a major part of the Meridional Overturning Circulation (MOC), and is a considerable global carbon and heat sink, through vertical transport and water mass transformation (Frölicher et al., 2015; Shi et al., 2018). Air-sea interactions drive the transport of heat, momentum, freshwater, carbon, and tracers. Understanding of these processes is essential to the global energy budget, and for accurate weather and climate prediction (e.g., Dong et al., 2010; Trenberth & Fasullo, 2010). The consistent strong zonal winds and seasonal sea ice extent (SIE) make the Southern Ocean a central regulator of the global climate (e.g., Frölicher et al., 2015; Rintoul, 2018; Sabine et al., 2004).

The eastward zonal transport of the ACC is driven by the westerly wind stress of the tropospheric eddy-driven jet, air-sea fluxes, friction, and the bottom drag of topography (Gnanadesikan & Hallberg, 2000; Rintoul et al., 2001). Flowing between ~45° S and ~65° S (Sokolov & Rintoul, 2009), the ACC transports approximately 173.3 ± 10.7 × 10^6 m^3 s^{-1} of water (Donohue et al., 2016). The transport is governed and maintained by geostrophic balance between the westerly wind stress and ocean heat loss (changing buoyancy) to the south. The ACC is divided by sharp transitional zones of water properties, namely fronts (Figure 2.5), with temperatures between -1 °C and 5 °C and salinities of 34.7 psu

and 34.9 psu (Emery, 1977). These fronts make it possible to define the location and development of key water masses within the region, and can be roughly defined by where the zonal flow is the greatest (Sokolov & Rintoul, 2009).

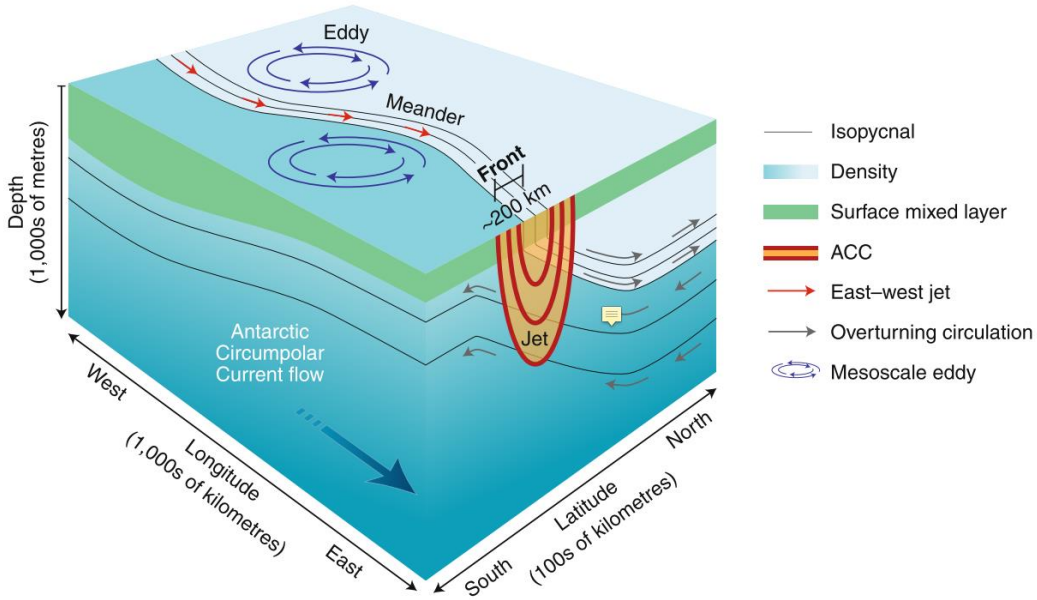

***Figure 2.5**: The Antarctic Circumpolar Current (ACC) frontal dynamics schematic. Figure from Chapman et al. (2020).*

From north to south (Figure 2.6), these fronts can be recognised by water properties as the Sub-Tropical Front (STF), the Sub-Antarctic Front (SAF), the Antarctic Polar Front (PF), and the South Antarctic Circumpolar Front (SACCF) (Belkin & Gordon, 1996; Orsi et al., 1995; Pollard et al., 2002). The SAF and PF zones are where most of the ACC transport takes place (Sokolov & Rintoul, 2002). Located south of the SAFCCF, a separate, westward, coastal current flows around the continent, and can be defined with a temperature of -1 °C or less. However, these definitions are not fixed and can be determined with both 'local' and 'global' definitions, making it difficult to maintain a uniform consensus

(Chapman et al., 2020). The locations of these fronts are primarily determined by bathymetry. However, meridional migration of the ACC and its fronts has been detected in paleo-records and modelling during the glacial – interglacial periods, linked to wind stress forcing (e.g., Ferry et al., 2015; Gersonde et al., 2005; Crosta et al., 2004).

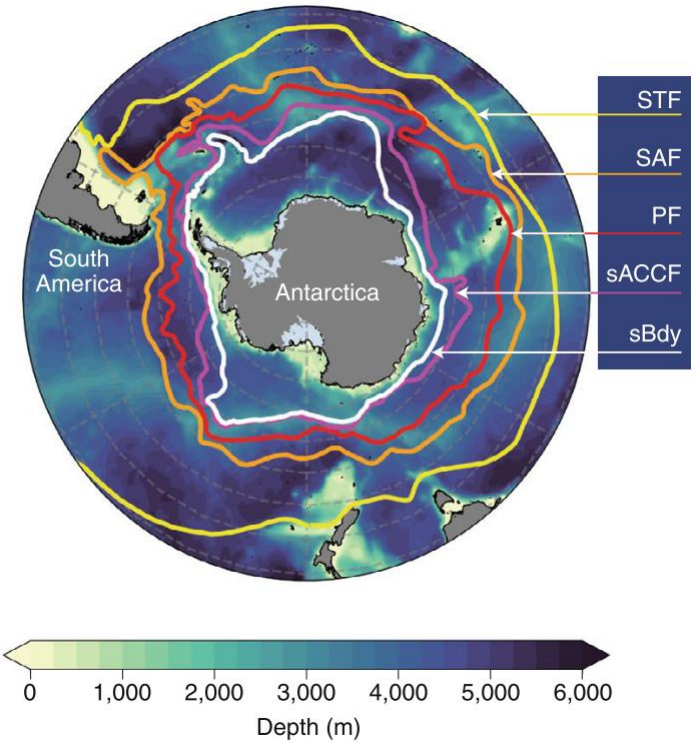

***Figure 2.6**: The dynamic front locations of the Southern Ocean. Figure from Chapman et al. (2020).*

Water mass formation and vertical transport are key processes in the Southern Ocean. Water mass transformation occurs when Deep Water masses, such as North Atlantic Deep Water (NADW) and North Pacific Deep Water (NPDW), are upwelled and mixed, and then downwelled to sub-surface layers (Whitworth et

al., 1998). The Southern Ocean transforms and overturns the largest volume of water in the world's oceans (Iudicone et al., 2008).

NADW is upwelled at the Antarctic Convergence Zone (Figure 2.7), which is then mixed with surface waters and modified into Antarctic Surface Water (ASW). ASW is then transported north through Ekman transport as Antarctic Circumpolar Water (ACCW). When ACCW reaches the polar front, it is downwelled as Antarctic Intermediate Water (AAIW) and Subantarctic Mode Water (SAMW), then ejected and upwelled into the surrounding oceans (Sabine et al., 2004). Antarctic Bottom Water (AABW), is the deepest water mass in all oceans, and connects the Southern Ocean to the global ocean system (through the MOC). AABW is formed through sea ice formation, mostly in polynyas in the Weddell and Ross Seas, in addition to ice-shelf melt, which creates fresh, but dense (cold) water (Jacobs, 2004; Nicholls et al., 2008; Ohshima et al., 2013; Orsi & Wiederwohl, 2009). Models project that with increased greenhouse gasses, the subduction of these water masses will decrease, from the warming and freshening of surface waters (Downes et al., 2010). AABW volume and its production are currently decreasing (Purkey & Johnson, 2012, 2013). Changes to the production of AABW have the potential to greatly impact the Atlantic Meridional Overturning Circulation (AMOC) (e.g., Patara & Böning, 2014). The seasonal cycle of sea ice controls the Southern Ocean surface mixed layer. Deep destabilisation in winter from changes to air-sea fluxes, Ekman transport and vertical entrainment, all act to change the profile of the water column and create a deepened mixed layer (e.g., Dong et al., 2007; Ren et al., 2011; Sallée et al., 2006). In the summer, the mixed layer depth is comparatively shallower and more

stratified due to reduced wind stress and higher irradiance (e.g., Panassa et al., 2018).

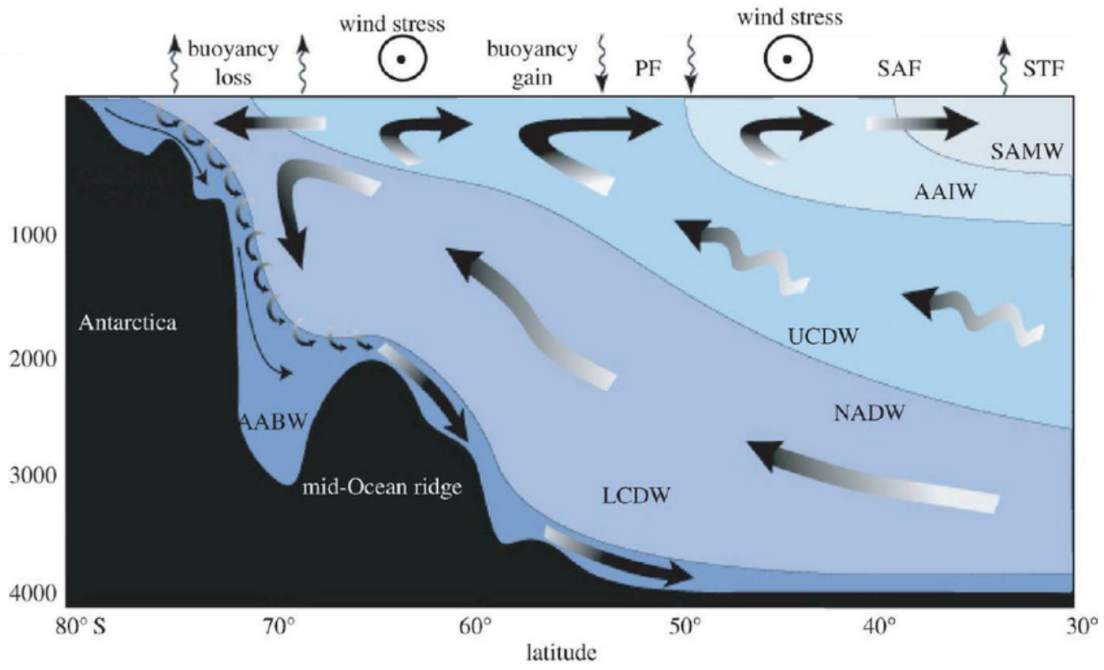

***Figure 2.7**: Southern Ocean overturning circulation, including water masses. fronts, and atmospheric wind stress and buoyancy fluxes. Water masses from left to right; Antarctic Bottom Water (AABW), Lower Circumpolar Deep Water (LCDW), North Atlantic Deep Water (NADW), Upper Circumpolar Deep Water (UCDW), Antarctic Intermediate Water (AAIW), Subantarctic Mode Water (SAMW) Figure from Speer et al. (2000).*

The strength of the tropospheric eddy-driven jet is thought to have minimal impact on the transport and isopycnic tilt of the ACC, due to the balance of changes in eddy-induced and Eulerian mean transports (e.g., Böning et al., 2008; Farneti & Delworth, 2010; Hallberg and Gnanadesikan, 2006). In support of this view, the annual mean ACC transport has remained stable throughout the instrumental period (Chidichimo et al., 2014; Donohue et al., 2016). Also, there has also been

no significant shift in the position of the ACC (Chambers et al., 2018; Chapman & Sallée, 2017; Gille, 2014; Swart et al., 2015). Over the longer term, palaeoceanographic records since the last glacial suggest minimal ACC transport changes (McCabe et al., 2013). It is thought that this small sensitivity to changes in wind stress may be due to eddy saturation (an energy cascade into the smaller-scale eddy field) (Munday et al., 2013). In an eddy-permitting coupled simulation, a poleward shift and intensification of the westerly winds, a known response to increased sea ice, led to a small increase in the net ACC transport and a slight shift in its position (Downes et al., 2011). Enhanced wind stress also led to a stronger northward Ekman transport of colder surface waters, and an associated increase in the winter mixed layer depth and in the subduction rates of SAMW and AAIW between the SAF and PF (Downes et al., 2011). This study did not, however, directly investigate the impact of sea ice forcing. A study by Haumann et al. (2016), demonstrated that the 20 ± 10% increase in meridional sea ice transport between 1982 and 2008, associated with increased westerly wind strength, may have driven a freshening of $0.002 \pm 0.001\ yr^{-1}$ in the surface and intermediate waters of the Southern Ocean.

The influence of the Southern Ocean on the AMOC is debated in the literature. The AMOC is primarily driven by the southward transport of NADW and the northward transport of AABW (e.g., Lumpkin & Speer, 2007). Some studies suggest that the Southern Ocean surface buoyancy forcing controls the AMOC depth, shallowing the AMOC (Ferrari et al., 2014; Jansen & Nadeau, 2016). However, these theories were challenged, where models did not include diabatic processes and diapycnal mixing in the Southern Ocean (Newsom & Thompson, 2018; Sun et al., 2018). Others suggest that the North Atlantic surface forcing or

interior diabatic mixing are more dominant, deepening the AMOC (e.g. Muglia & Schmittner, 2015; Wolfe & Cessi, 2014). A recent study, (Sun et al., 2020), suggests that the AMOC depth is more strongly constrained by changes to the surface density, rather than the buoyancy fluxes, suggesting that the surface density fields in both the Southern Ocean and North Atlantic control the AMOC depth.

Changes in the Southern Ocean have been found to impact global paleoclimates in the past, most notably through the bipolar seesaw hypothesis (e.g., Blunier & Brook, 2001; Broecker, 1998; Marino et al., 2015; Pedro et al., 2018). This hypothesis theorises that the Southern Ocean drives the Northern Hemisphere climate through the NADW circulation and transformation. Proxy records of the last glacial and deglacial periods show that warming in the northern high-latitudes and cooling in the southern high-latitudes coincide with each other, and vice versa (e.g., Blunier & Brook, 2001; Pedro et al., 2011; Blunier et al., 1998). Studies suggest that this phenomenon is driven by deep ocean circulation at the poles (Knutti et al., 2004; Stocker, 1998; Stocker & Johnsen, 2003).

2.1.4 Sea ice

Antarctic SIE is connected to all of the above processes and is highly seasonal with little multiyear sea ice (Maksym et al. 2012). Globally, sea ice is formed via two methods, pancake and frazil ice formation. In the Southern Ocean, sea ice is primarily formed as pancake ice, and is thinner and shorter lived than Arctic sea ice. This is due to being at lower latitudes than the Arctic, although not as warm, rougher seas, and the westerly winds surrounding Antarctica transporting older

ice away. SIE is expanded by westerly winds surrounding Antarctica and associated northward Ekman transport, but limited in spatial extent by the ACC (Gupta & England, 2006; Hall & Visbeck, 2002).

Polynyas and leads are natural openings in the sea ice. Sensible heat polynyas tend occur in the deep ocean and are often driven by topographic upwelling. Latent heat polynyas occur in shallower coastal regions, where ocean water is at freezing point and where katabatic winds off the continent flow in a persistent direction away from the coast. Examples in the Antarctic are the Maude Rise and Weddell Sea polynyas, which are sensible heat polynyas and sites of large ocean-to-atmosphere heat fluxes and AABW formation (Jacobs, 2004; Nicholls et al., 2008; Ohshima et al., 2013; Orsi & Wiederwohl, 2009). Leads are narrow, linear cracks that form as ice diverges, or shears as floes move parallel to each other. Leads are found to reduce the albedo of sea ice and contribute to the summer melt, absorbing more solar incoming radiation than the surrounding ice. They are also sites of large ocean to atmosphere heat fluxes, where warmer water is exposed to the colder atmosphere, and are a source of clouds and precipitation. Melt ponds are another feature which affect the sea ice albedo, but are less common in Antarctic sea ice than in the Arctic, due to the greater snow cover on Antarctic sea ice (Scott & Feltham, 2010).

Antarctic SIE rarely extends beyond 65° S in the winter, with the maximum winter SIE reaching 12.8 $x10^6$ km^2 in 2014 (Parkinson, 2019), and a minimum winter SIE of 10.7 $x10^6$ km^2 in 2017 (Parkinson, 2019). The annual minimum sea ice extent

always occurs in February, but the maximum varies between September and October.

2.2 Antarctic sea ice trends

2.2.1 Trends

Since accurate satellite records of polar sea ice began in 1979, annual-mean Antarctic SIE has increased by a small, but still significant, ~54 thousand square kilometres per decade (Fetterer et al., 2017) (Figure 2.8). The counterintuitive Antarctic average SIE increase is in defiance of expectations from greenhouse gas increases and not what historical model simulations show. The increasing trend has become weaker and less statistically significant after the sudden decrease in austral winter 2016 (Turner et al., 2017). Between 2014 and 2017, SIE has decreased from 12.8 x10^6 km^2 to 10.7 x10^6 km^2, an amount comparable to 30 years of Arctic sea ice decline (Parkinson, 2019).

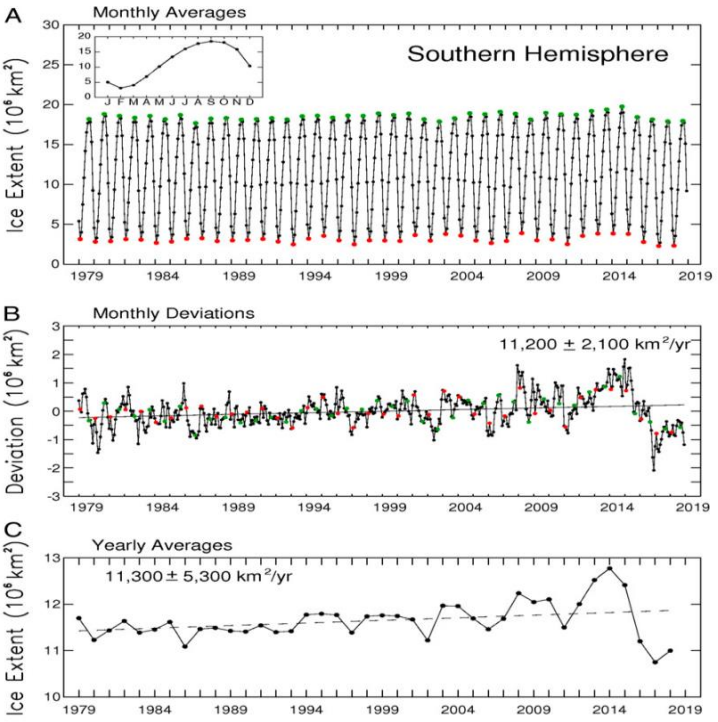

***Figure 2.8**: Mean Antarctic sea-ice loss since accurate satellite records began (1979 - 2019), with monthly averages (A), monthly deviations (B), and yearly averages (C). Figure from Parkinson (2019).*

Antarctic sea ice trends have been highly variable between regions (Figure 2.9 & 2.10). SIC has generally increased in the coastal margins, while SIC has decreased in deeper waters (Wang & Wu, 2020). The Weddell Sea has seen the greatest increase in annual-mean of up to 1.15% per year, with the Amundsen and Ross Seas seeing the greatest decrease of a smaller, but still significant, -0.76% per year; although these trends vary by season (Figure 2.8) (Holland, 2014; Parkinson, 2019). These regionally varying trends partly counteract each other, giving rise to small Antarctic-mean trends. In the Arctic, trends are more regionally consistent (Holland, 2014).

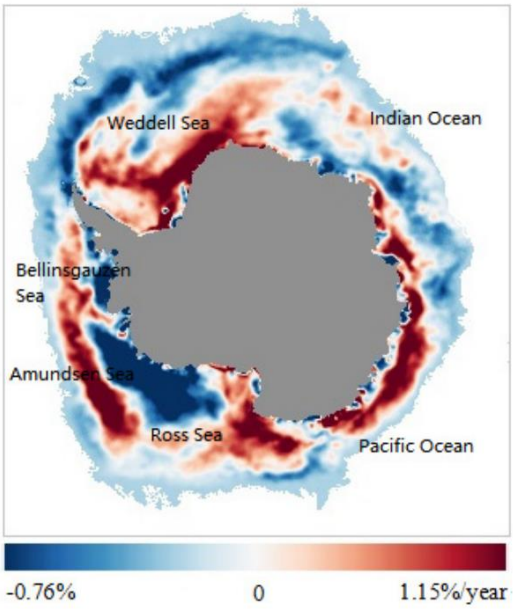

***Figure 2.9**: Annual-mean variation in regional sea ice concentration distribution in the Antarctic from 1989 to 2018. Figure from Wang & Wu (2020)*.

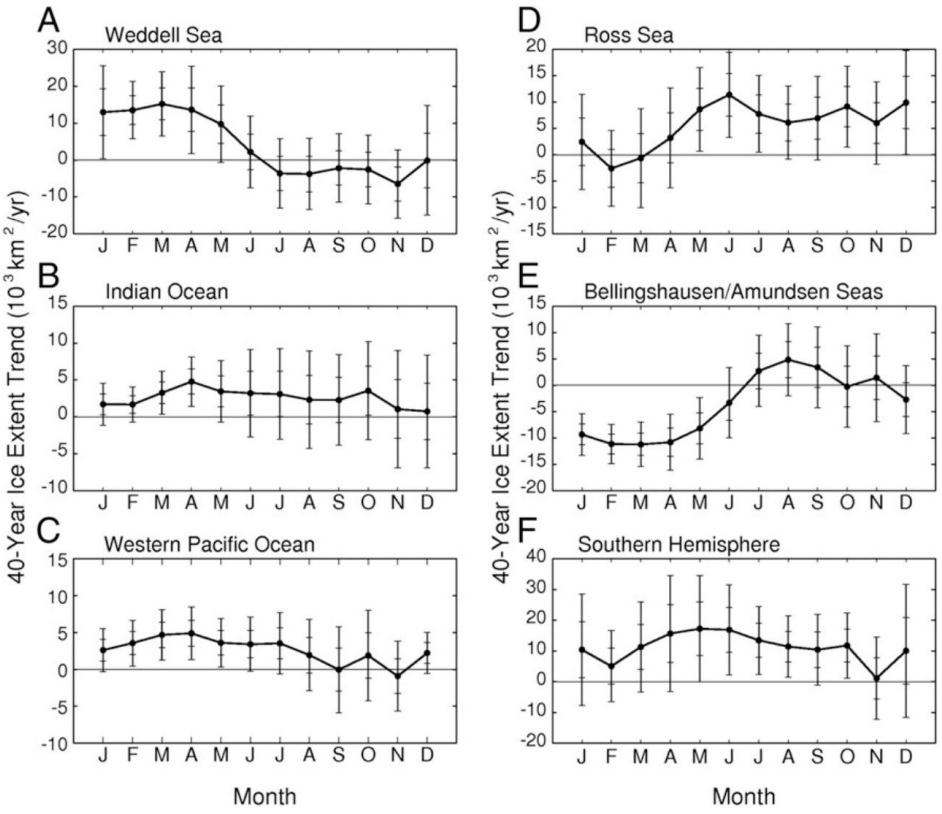

Figure 2.10*: The monthly sea ice extent (SIE) trends over the 40-year satellite period by region. Figure from Parkinson (2019).*

2.2.2 Causes of positive trends

Many possible explanations for Antarctic sea ice area (SIA) increase have been suggested. In 2009, Turner et al. argued that this unprecedented increase may be a result of stratospheric ozone loss over Antarctica, which has driven a strengthening of the tropospheric eddy-driven jet and enhanced northward Ekman transport of colder waters (e.g., Polvani et al., 2011). However, others have since contested that stratospheric ozone loss may actually cause an increase in SIA, as strengthened wind stress also triggers enhanced poleward heat transport through enhanced upwelling and invigoration of ocean eddies (Bitz & Polvani, 2012; Landrum et al., 2017; Sigmond & Fyfe, 2010; Solomon et al., 2016).

The SAM index has been trending positive since observations began (e.g., Marshall, 2003). Via Ekman theory, the increased westerly winds drive the northward transport of sea ice, expanding the SIE (Gupta & England, 2006; Hall & Visbeck, 2002). Another study shows that a positive SAM anomaly is followed by anomalously cold SSTs leading to an increase in SIE, whereas negative SAM anomalies are proceeded by the opposite SST and SIE response (Doddridge & Marshall, 2017). However, other studies have found the opposite, whereby a positive SAM trend would, in the long-term, cause a decrease in the SIE: initially SIE may increase for the aforementioned reasons, but then decreases through the Ekman pumping of warm Circumpolar Deep Water (CDW) (Ferreira et al., 2015; Sigmond & Fyfe, 2010) and/or invigoration of poleward eddy heat transport (e.g., Meredith & Hogg, 2006; Screen et al., 2009).

The ASL is the largest permanent pressure system in the region and is a large source of meridional flow. Connections have been found between ASL variability and to regional sea ice trends in the Ross and Amundsen Seas in autumn and winter (e.g Hosking et al., 2013; Turner et al., 2016). Here, the SIE is expanded outward by a greater meridional flow around the ASL. The role of the ASL in the Ross Sea is less clear in the summer, when the ASL has a greater influence on sea ice in the Bellingshausen Sea, as ASL migrates seasonally (Coggins & McDonald, 2015).

Ocean circulation changes may also play a role in the sea ice trends, specifically in terms of surface mixed layer temperature and salinity. Interactions with sea ice

may come from incoming solar radiation, entrainment of warm water from below or meridionally through surface currents (summarised in Hobbs et al., 2016). The relatively cool and fresh surface mixed layer sits atop warmer saltier CDW, which upwells via Ekman pumping. Brine rejection from ice formation can help to entrain this deep water via the process of double diffusion (de Boyer Montégut et al., 2004; Martinson, 1990). In the spring, the water column stabilises again. The mechanisms related to ice growth depend on the background state of the water column and the consideration of horizontal sea ice transport (Goosse & Zunz, 2014; Hobbs et al., 2016; J. Zhang, 2007). Increased ocean stratification may play a crucial role here (Parkinson & Cavalieri, 2012). Multiple theories are available in the literature. One being that increased precipitation over the Southern Ocean freshens the surface waters (Liu & Curry, 2010) and promotes sea-ice growth. Another, is that freshwater input from ice-sheet melt has freshened the surface mixed layer (Bintanja et al., 2013), although sea ice sensitivity to ice-sheet melt is inconsistent across modelling studies (Pauling et al., 2016; Swart & Fyfe, 2013).

An additional ocean related theory is the oceanic asymmetry between the two poles. In the North Atlantic, transport comes from warm surface water and is transformed through sinking, whereas in the Southern Ocean, transformation comes solely from upwelled deep ocean water, which may have been subducted for centuries and therefore not yet been impacted by anthropogenic warming (e.g., Armour et al, 2016; Marshall et al., 2014). This would lead to a delayed warming impact from anthropogenic greenhouse gas in the Antarctic compared to the Arctic.

Another alternative, yet debated influence, is that of ENSO. Multiple studies have found a strong sea ice response to tropical SST anomalies on interannual timescales (Kwok & Comiso, 2002; Simmonds & Jacka, 1995; Simpkins et al., 2012; Turner, 2004; Yuan, 2004). However, other observational studies show that there is minimal influence on ENSO on multi-decadal sea ice trends (Kohyama & Hartmann, 2016; Simpkins et al., 2012). Nevertheless, it has been suggested that West Antarctic temperatures are related to multi-decadal tropical Pacific Ocean variability (Ding et al., 2011; Schneider & Steig, 2008), with recent studies linking the abrupt sea ice decrease in 2016 to ENSO (Schlosser et al., 2017; Stuecker et al., 2017). A secondary influence through the SAM may also be possible. However as discussed in Section 2.1.1, the connection between SAM and ENSO is complex.

There is also a possible link between multi-decadal tropical Atlantic Ocean variability and Antarctic sea ice (Li et al., 2014; Simpkins et al., 2014), suggested to occur via a Rossby wave train propagating from the tropical Atlantic to the Amundsen Sea region. Warmer Atlantic SSTs are suggested to deepen the ASL and thus, may influence the SIE in the Ross Sea (Fan et al., 2014; Li et al., 2014; Simpkins et al., 2013; Simpkins et al., 2014). Other studies find that there may be atmospheric teleconnections to Antarctica from both the tropical Atlantic and Pacific, but neither is sufficient to fully explain the observed sea ice trends in the Ross Sea (e.g., Hobbs et al., 2016).

2.2.3 Recent and predicted Antarctic sea ice trends

In austral spring 2016, Antarctic SIE decreased at an abnormal rate (Figure 2.11), 18% quicker than in the previous record melt rate in the satellite record, and 46% quicker than the climatological average melt rate (Turner et al., 2017). Possible explanations for the sudden 2016 decline include influences from ENSO and an enhanced zonal wavenumber-3 pattern of the westerly jet (Schlosser et al., 2017; Stuecker et al., 2017). In addition, research has shown that the rapid sea-ice loss led to ocean warming and enhanced upward propagation of planetary scale waves, triggering a rare stratospheric warming event, subsequently influencing the westerly jet and further enhancing ice melt (Meehl et al., 2019; Wang et al., 2019).

Another possible contributor may have been the unprecedented opening of the polynya near the Maud Rise in 2016, the most significant polynya event since the 1970s (Turner et al., 2020). Polynyas increase summer melt by reducing the albedo and enhancing short-wave radiation absorption, thereby warming neighbouring regions. In 2016 and 2017, the polynya expanded due to the anomalously warm ocean temperatures (Turner et al., 2020) and since 2016, Antarctic SIE has tracked below its long-term average.

It is unclear if this substantial reduction is temporary or if the Southern Hemisphere sea ice is entering a new era of decline (Ludescher et al., 2018). However, the recent decline has made an impact on the overall trend since the 1970s, lessening it (Parkinson, 2019). More recently, another notable stratospheric sudden warming event occurred in 2019, and although the SAM

index was highly negative as a response (Shen et al., 2020), there has yet to be another sea ice minimum (Comiso et al., 2020).

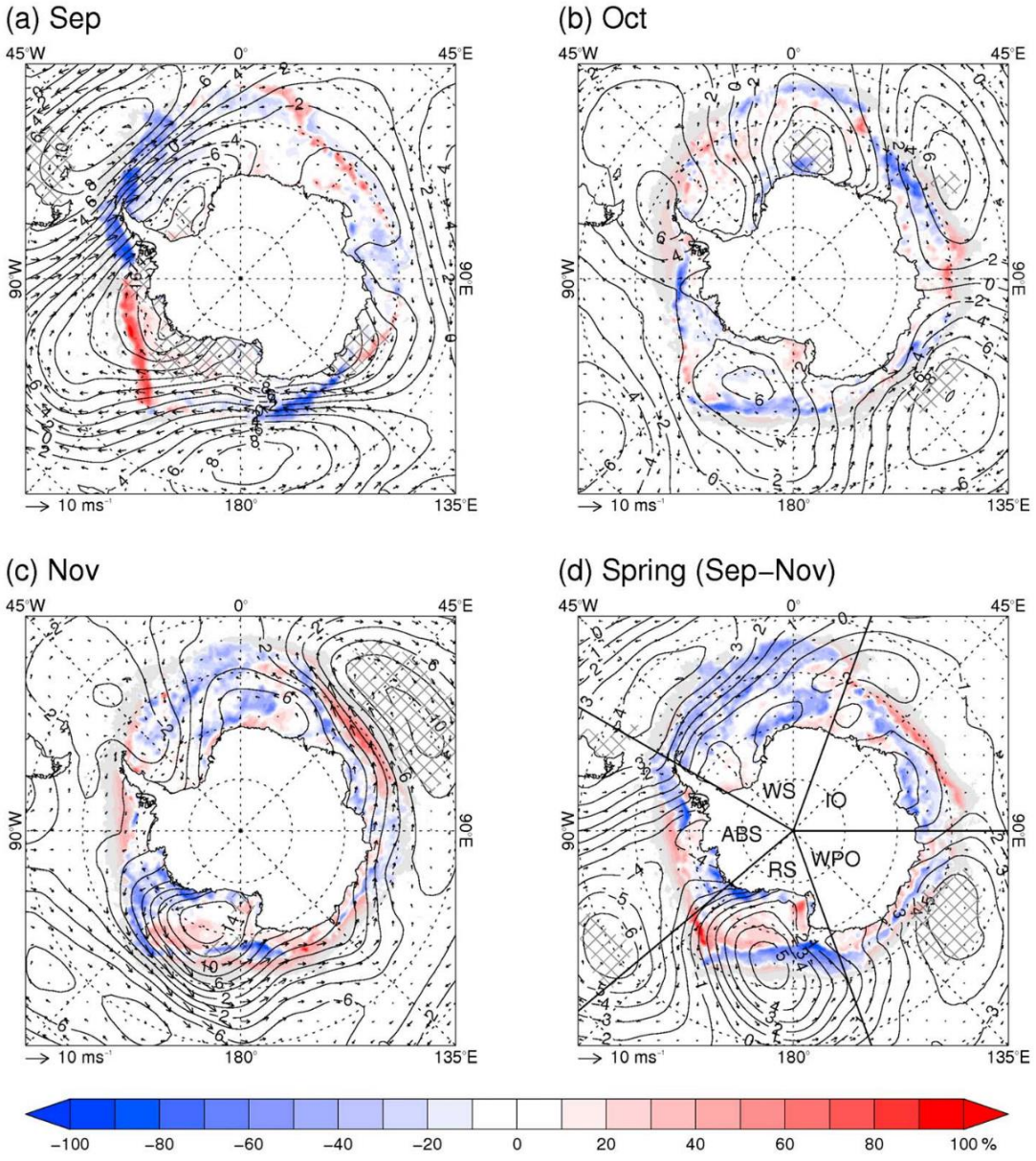

***Figure 2.11**: 2016 -2017 sea ice concentration anomalies by region. Figure from Turner et al. (2017).*

2.3 Modelling limitations

The observed increasing trend in sea ice is not reproduced in the CMIP3 and CMIP5 global climate models, and despite some improvement in CMIP6, the latest models still generally simulate decreasing trends over the historical period (Roach et al., 2018; Turner et al., 2015; Zunz et al., 2013), as well as failing to reproduce the observed regional patterns (Turner et al., 2013). The few models that do simulate a loss of sea ice over the observed period, do not reproduce observed seasonality and spatial pattern (Turner et al., 2015). The largest single-model initial-condition ensemble, the 40-member Community Earth System Model (CESM1), did not contain a single member simulating increased SIA over the observed period (Kay et al., 2015; Rosenblum & Eisenman, 2017).

This striking disagreement between observations and models remains poorly understood (Turner et al., 2013), but possible explanations include internal climate variability (Polvani & Smith, 2013; Roach et al., 2018; Zunz et al., 2013), model biases (e.g., Bracegirdle et al., 2013; Bracegirdle et al., 2018; Holland et al., 2017; Lecomte et al., 2016; Purich et al., 2016; Roach et al., 2018; Schroeter et al., 2017; Turner et al., 2013) or unresolved processes in models such as ice-sheet-ocean interactions (e.g., Schneider & Deser, 2018). The same models project that Antarctic sea ice will continue to decline significantly by 2100 (Figure 2.12) (e.g., Collins et al., 2013; Vaughan, 2013), if greenhouse gas concentrations continue to rise, although there is significant divergence between models in the magnitude of the projected decline.

Some studies have found that modelled internal variability captures the observed trends across CMIP5, with the forced response being small in comparison to the natural variability (Polvani & Smith, 2013; Roach et al., 2018; Zunz et al., 2013). In addition, observations prior to the satellite period show the presence of multi-decadal variability over the Southern Ocean (Fan et al., 2014; Gagné et al., 2015). However, a recent study from Chemke & Polvani (2020), has shown that internal variability cannot account for the model discrepancy, stating instead that biases in the models' forced response to external forcing are the root cause. A variety of model biases and unresolved processes have been suggested to explain the contrast between modelled and observed Antarctic sea ice trends, including warm upper ocean biases (Schneider & Deser, 2018), and biases in the ocean-atmosphere thermodynamic coupling (Chemke & Polvani, 2020). A common theme is that sea ice trends are sensitive to mean state biases in, for example, the westerly jet position (e.g., Bracegirdle et al., 2018), mixed layer depth (Sallée et al., 2013) and initial SIE state (Chemke & Polvani, 2020).

One of the greatest issues, however, is that in-situ observations, particularly in the autumn and winter months, are extremely sparse (e.g., Pellichero et al., 2017; Swart et al., 2018). Lack of understanding of sea ice-ocean processes that are needed to feed into the models, leads to large errors in not only models, but also reanalysis and even remote sensing configuration (e.g., Yu & Weller, 2007). This is due to subsequent biases in SSTs, surface mixed layer dynamics, and cloud cover (e.g., Bodas-Salcedo et al., 2014; Hermanson et al., 2018; Hyder et al., 2018; Schneider & Reusch, 2016).

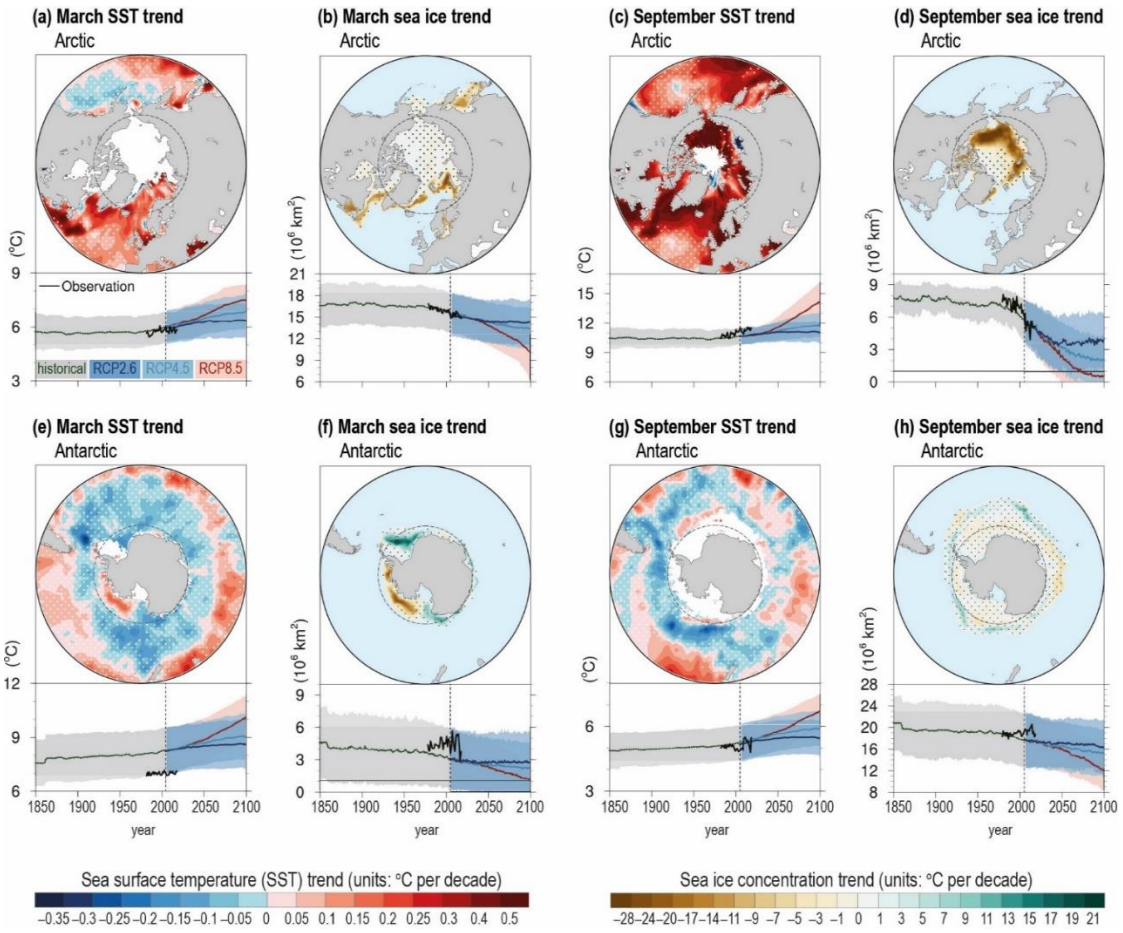

***Figure 2.12**: Minimum and maximum sea ice and SST trends for the Arctic and Antarctic, with historical and modelled trend lines. Figure from Meredith et al. (2019).*

2.4 Impact of global climate change on the Antarctic region

The poles are the regions most rapidly impacted by global climate change (Figure 2.13) (e.g., Bromwich et al., 2013). The Antarctic is currently warming at a slower rate than the Arctic, but is predicted to warm rapidly during this century if greenhouse gas concentration continue to rise (Collins et al., 2013). This contrast in warming rates between the Arctic and Antarctic is thought to be due to Southern Ocean heat uptake and deep ocean mixing, which suppresses polar amplification in the Southern Hemisphere (Armour et al., 2016). Antarctic

warming over the past 30-50 years has been non-uniform, with minimal change over East Antarctica but large warming over parts of West Antarctica and the Antarctic Peninsula (Jones et al., 2016; Nicolas & Bromwich, 2014; Turner et al., 2016).

The strength of the westerly eddy-driven winds has increased since the 1960s, reflected in the positive trend in the SAM and associated with cooler conditions over the interior Antarctic continent (Gong & Wang, 1999; Marshall, 2003; Thompson & Wallace, 2000). Over this period, Antarctic ozone depletion is thought to be the main driver of the SAM trend (e.g., Polvani et al., 2011). It is projected that with increasing greenhouse gases, the strengthening of the westerly winds will continue (Bracegirdle et al., 2013).

An increase in the westerly wind corresponds with an increase in the Southern Ocean eddy field. However, there has been no change in the ACC transport during the instrumental period (Chidichimo et al., 2014; Donohue et al., 2016). Projections show that through a combination of increased freshening from sea-ice loss and increased precipitation (both related to warming), Southern Ocean circulation changes may emerge in the future (Downes & Hogg, 2013). Models indicate that with the maintained increase in the westerly jet, the eddy field will continue to also grow (Morrison & Hogg, 2013; Munday et al., 2013). Due to the freshening and warming of surface waters, it is projected that the formation of AABW will continue to decrease (Heuzé et al., 2015). As such, the subduction of intermediate and mode waters within the ACC is predicted to increase (Sallée et al., 2013), and the overall transport of the Southern Ocean upper overturning

circulation may increase by up to 20% (Downes & Hogg, 2013). It should be noted however, that these processes are some of the most poorly resolved in global climate models due to their inability to explicitly resolve mesoscale eddies and related processes (Gent, 2016). Therefore, projected changes to Southern Ocean processes that are related to eddies should be interpreted with low confidence (Meredith et al., 2019).

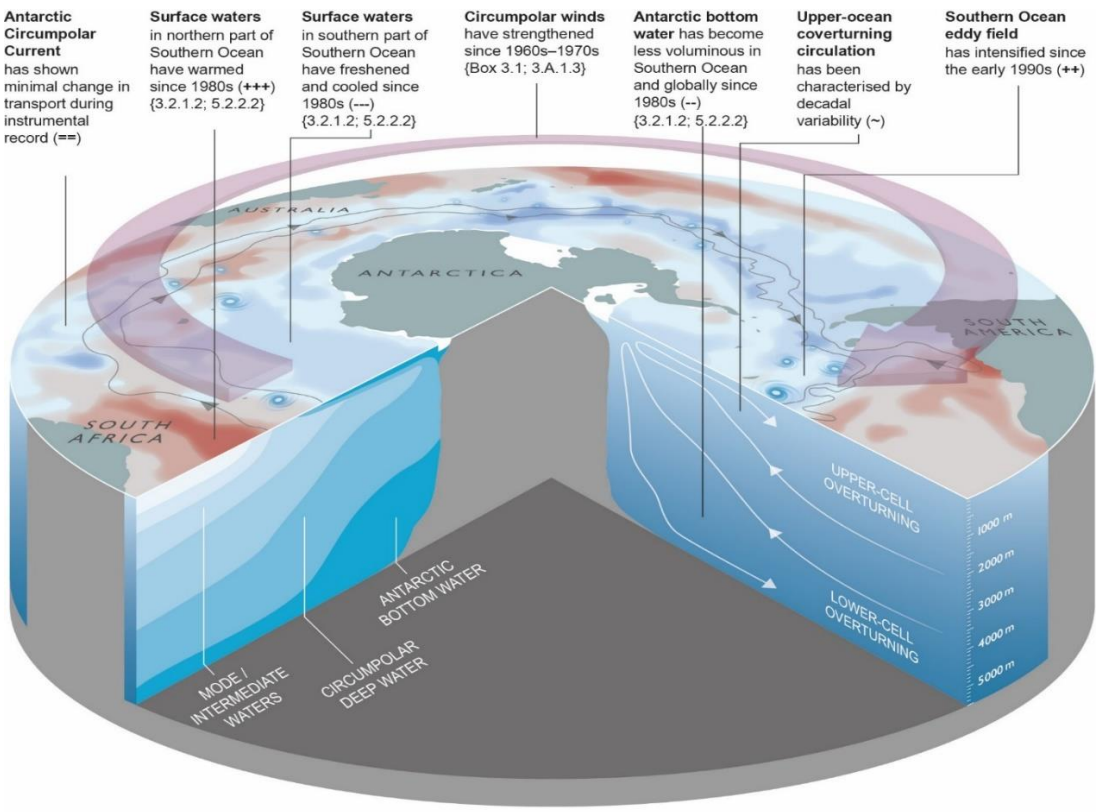

***Figure 2.13**: The response of the ocean and atmospheric dynamics of the high-latitude Southern Hemisphere over the satellite era. Figure from Meredith et al. (2019).*

2.5 Climate response to polar sea-ice loss

2.5.1 Climate response to Arctic sea-ice loss

The climate response to Arctic sea-ice loss has been extensively studied, motivated by the current reduction of sea ice extent at over 4% per decade (Vaughan et al., 2013) and the expectation that Arctic sea ice decline will continue to decline this century (Collins et al., 2013; Stocker et al., 2013). As a result, it is well understood that Arctic sea-ice loss is influencing high-latitude weather and climate in the Northern Hemisphere, with thermodynamically induced warming and moistening of the atmosphere, amongst other changes (e.g., Deser et al., 2010; England et al., 2018; Screen & Simmonds, 2010; Screen et al., 2013). There is also emerging evidence that reduced Arctic sea ice may influence the large-scale atmospheric circulation, for example, through weakening of the mid-latitude westerly winds (e.g., Peings & Magnusdottir, 2014) and a negative shift in the North Atlantic Oscillation (NAO) index (Blackport & Kushner, 2016; Deser et al., 2015; Kim et al., 2014; Peings & Magnusdottir, 2014; Screen & Simmonds, 2013; Screen et al., 2013).

It is becoming increasingly apparent that coupled ocean-atmosphere models are needed to study the climate response to Arctic sea-ice loss, as atmosphere-only models do not fully capture the global reach or magnitude of changes in response to Arctic sea-ice loss (Deser et al., 2015; 2016; Smith et al., 2017; Tomas et al., 2016; Blackport & Kushner, 2016; Oudar et al., 2017; Sun et al., 2020). For example, (Deser et al., 2015) found the responses to Arctic sea-ice loss were limited to north of 30°N in an atmosphere-only model, whereas in a coupled model, responses were seen globally, including tropical upper-tropospheric warming, an enhanced global hydrological cycle, and an equatorward shift of the

Intertropical Convergence Zone (ITCZ). Within the Northern Hemisphere extratropics, ocean coupling enhanced the response to Arctic sea-ice loss by up to 50%, but did not appreciably change its overall spatial pattern (Deser et al., 2016). The tropical response to Arctic sea-ice loss has been well studied in recent years. Tropical SST warming enhances convection and drives upper tropospheric warming, with a resultant effects on the strength and location of the subtropical jet and Hadley Cell (e.g., Chemke et al., 2019; Deser et al., 2015; Smith et al., 2017; Sun et al., 2018; Sun et al., 2020; Tomas et al., 2016).

The global response appears to be highly dependent on whether the atmospheric model is coupled to either a slab ocean or full-depth ocean model. For example, the atmospheric warming response simulated when using a full-depth ocean model was largely symmetric around the equator, whereas it was antisymmetric response when a slab ocean model was used (Tomas et al., 2016). More recently Chemke et al. (2019) found a weakening and expansion of the Hadley Cell in response to Arctic sea-ice loss when using a slab ocean model, but a narrowing of the Hadley Cell when using a full-depth ocean model.

The stratospheric response to Arctic sea-ice loss is highly debated. Sea-ice loss may weaken the SPV and increase the chance of cold winters in mid-latitude regions (e.g., Kim et al., 2014; Nakamura et al., 2016; Zhang et al., 2018). These studies suggest that decreased sea ice in the autumn and early winter months increase the upward propagation of planetary-scale waves, and lead to a weakening of the polar vortex in later winter months. Other studies have suggested that the stratospheric response varies across models, dependent on

geographical location of sea-ice loss (Screen et al., 2018; Screen & Blackport, 2019; Screen et al., 2018), indicating a non-robust response. A recent study by Labe et al. (2019) found that the response of the polar vortex response is highly dependent on the state of the Quasi-biennial Oscillation (QBO). These authors found that the SPV response to sea-ice loss was greater during the westerly phase of the QBO compared to the easterly phase.

2.5.2 Climate response to Antarctic sea-ice loss

The climate response to Antarctic sea-ice loss is a lot less studied, compared to the response to Arctic sea-ice loss. Within the limited existing literature, there is large disagreement on the response to projected Antarctic sea-ice loss. With the possibility of future Antarctic sea-ice loss due to greenhouse gas increases (Collins et al., 2013), improving our understanding of the response to Antarctic sea-ice loss is imperative.

The observed gradual growth of Antarctic sea ice has been suggested to result in a slight poleward shift of the tropospheric jet in the austral winter months (Smith et al., 2017). Raphael et al. (2011) suggested that negative summer sea ice anomalies were linked to a more negative SAM index, and vice versa. Atmospheric-only modelling studies, prescribed with projected Antarctic sea-ice loss, present contrasting results. For example, there is divergence on the impact on the location of the mid-latitude tropospheric eddy-driven jet, though generally agreement that there is a reduction in its strength (Bader et al., 2013; England et al., 2018; Kidston et al., 2011; Menéndez et al., 1999). Kidston et al. (2011) found no significant response in jet latitude, whereas Bader et al. (2013) and Menéndez

et al. (1999) both found a clear equatorward shift of the tropospheric jet in austral winter. Bracegirdle et al. (2018) found when comparing CMIP5 models, that although there was a robust jet weakening, latitudinal jet shifts were not robust. Also, the initial position of the jet mediated the jet shift. More recently, England et al. (2018) used the WACCM4 model to compare responses to Arctic and Antarctic sea-ice loss. These authors found a significant equatorward shift of the eddy-driven jet in the hemisphere in which sea ice was reduced, for both Arctic and Antarctic sea-ice loss. They also found that the tropospheric and stratospheric responses to Antarctic sea-ice loss were of smaller amplitude, more vertically confined, and had less seasonal variation than in response to Arctic sea-ice loss.

Up until recently, all model experiments to isolate the response to Antarctic sea-ice loss have been either atmospheric- or ocean-only runs. Studies on the response to Arctic sea-ice loss, mentioned above, have highlighted the importance of using coupled models. England et al. (2020a) was the first published study to assess the impact of Antarctic sea-ice loss in a coupled model. It showed that ocean dynamics are important for capturing the global response to Antarctic sea-ice loss. These authors found that the tropical response to Antarctic sea-ice loss is much alike that to Arctic sea-ice loss, particularly in the eastern equatorial Pacific. They found enhanced tropospheric warming and an equatorward intensification of the ITCZ. Antarctic sea-ice loss also caused a ‘mini global warming’ signal (i.e., a pattern similar to that in response to increased greenhouse gases, but of lesser magnitude), comparable to the ‘mini global warming’ simulated in response to Arctic sea-ice loss. Further research by the same authors (England et al., 2020b), suggests that the response to Antarctic sea-ice loss has the potential to cause subsequent Arctic sea-ice loss, and a

surface temperature warming of up to 1 °C in the Arctic, in response to Antarctic sea-ice loss projected in the RCP8.5 scenario.

Studies have found that the observed increase in SIE has increased stratification and reduced entrainment of warm deep waters into the mixed layer. With increased SIE, the seasonal cycle is enhanced, with a greater freshwater flux from sea-ice loss in the melt season and increased brine transport from sea ice formation in growth season (Abernathey et al., 2016; Goosse & Zunz, 2014; Lecomte et al., 2017). This seasonal cycle of the surface mixed layer, in response to sea ice change, is prominent in the subpolar gyre regions (Barthélemy et al., 2015; Petty et al., 2014; Ren et al., 2011), and is associated with the formation of AABW and upwelling of deep waters (Rintoul et al., 2001). Here, in both current and paleoclimates, increased sea ice cover enhances AABW formation, accompanied by a stronger poleward export of CDW, and increased brine rejection leading to enhanced deep ocean stratification and decreasing vertical mixing (Shin et al., 2003; Stein et al., 2020).

2.6 Chapter summary

Since accurate satellite records began 41 years ago, Antarctic sea ice has displayed small, but significant, increasing overall trend, with large regional variation. The reason for this net increase in Antarctic sea ice remains unresolved and may be some combination of factors including multi-decadal internal variability, a wind-induced response to stratospheric ozone depletion, or buoyancy-induced response to changes in freshwater input. Global coupled climate models are yet to replicate this trend, again for reasons that remain poorly

understood. Despite this uncertainty over the historical period, models robustly project a significant decrease in Antarctic sea ice by the end of this century. While the climate response to the Arctic sea-ice loss has been well assessed, the response to projected Antarctic sea-ice loss has not. It is clear that both the atmosphere and the ocean play a crucial role in shaping the global climate response to sea-ice loss. This thesis aims to assess the climate impacts of projected Antarctic sea-ice loss, using multiple modelling approaches, and examining the atmospheric and oceanic responses and their coupled interactions.

Chapter 3

Data and Methods

This study uses a combination of CMIP5 multi-model ensembles and bespoke sea ice perturbation model experiments to examine, indirectly and directly, the atmospheric and oceanic responses to projected Antarctic sea-ice loss. The indirect method uses data from eleven CMIP5 models to infer a multi-model estimate of the response to Antarctic sea-ice loss at quadrupled CO_2 (Section 3.1). The direct method uses sea ice perturbation experiments with the HadGEM-GC3.1 coupled model to explicitly isolate the response to Antarctic sea-ice loss in the coupled system (Section 3.2). Additionally, atmosphere-only experiments with the HadGEM3-A atmosphere-only model are used to demonstrate the importance of atmosphere-ocean coupling (Section 3.3). Section 3.4 discusses the main diagnostic metrics and statistical methods used throughout the study.

3.1 The CMIP5 multi-model response

3.1.1 CMIP5 models

Zappa et al. (2018) introduced a novel method of estimating the response to projected sea-ice loss using existing CMIP5 simulations. Their study applied this method to analyse the wintertime atmospheric response to projected Arctic sea-ice loss and in particular, that of the North Atlantic jet. Here, a very similar methodology was applied to examine the seasonal atmospheric response to Antarctic sea-ice loss when the CO_2 concentration is quadrupled. The outputs from 11 climate models were used (Table 3.1), which had all the required experiments. Prior to analysis and to facilitate averaging across models, data were interpolated onto a T42 grid (summarised in Table 3.3).

***Table 3.1**: Models used for this study. All models used monthly data from r1i1p1, apart from AMIP, where the ensemble mean was used. Models with both Abrupt4xCO_2, Preindustrial Control and AMIP, AMIP4xCO_2, AMIPFuture were used for determining sea-ice loss (see equation 1).*

Model name	***Institution***	***Abrupt4xCO_2, PiControl***	***AMIP, AMIP4xCO_2, AMIPFuture***
1 BCC-CSM1-1	BCC, China	1	1
2 CANESM2	CCCma, Canada	1	1 (CanAM4)
3 CCSM4	NCAR, USA	1	1
4 CNRM-CM5	CNRM, France	1	1
5 HadGEM2-ES	MOHC, UK	1	1 (HadGEM2-A)
6 IPSL-CM5A-LR **7 IPSL-CM5B-LR**	IPSL, France	1 1	1 1
8 MIROC5	MIROC, Japan	1	1
9 MPI-ESM-LR **10 MPI-ESM-MR**	MPI–M, Germany	1 1	1 1
11 MRI-CGCM3	MRI, Japan	1	1

3.1.2 Multi-model response

To estimate the coupled climate response to quadrupled CO_2, 100-year means (years 50-150) from the CMIP5 'abrupt4xCO_2' simulations and 100-year climatologies from the preindustrial control simulations ('piControl'), were compared. This study chose to use 'abrupt4xCO_2' rather than any of the Representative Concentration Pathway (RCP) experiments (Zappa et al. (2018)

used RCP8.5), to avoid the complicating influences of non-CO_2 climate drivers, such as ozone and aerosols, which are included in the RCPs but not in 'abrupt4xCO_2'. Furthermore, the use of 'abrupt4xCO_2' results in scaling factors (described below) closer to unity, which reduces this study's reliance on the assumption of linear scalability of the atmospheric response to SST warming and CO_2 increase. The atmospheric response to quadrupled CO_2 was estimated by comparing 30-year means (years 1979-2008) from the 'amip4xCO_2' simulations to those in the 'amip' simulations. Likewise, the atmospheric response to SST warming was estimated by comparing 30-year means from the 'amipFuture' and 'amip' simulations. The 'amip' simulations were prescribed with observed variability in sea ice concentrations (SICs), sea surface temperatures (SST) and atmospheric composition for the period 1979-2008. The 'amipFuture' simulations are identical to 'amip', except that they have added SST perturbations derived from the CMIP3 'abrupt4xCO_2' multi-model response, scaled to have a global average warming of 4 K. The 'amip4xCO_2' simulations are identical to 'amip' except that the CO_2 concentration was quadrupled. Sea ice is kept unchanged at present day values in both 'amip4xCO_2' and 'amipFuture', so is identical to that in 'amip'. The fact that sea ice is unchanged, but that either SST or CO_2 is changed, allows for the response to sea-ice loss to be estimated as the residual between the coupled climate response ('abrupt4xCO_2' minus 'piControl') and the combined and scaled atmospheric responses to SST warming and quadrupled CO_2, termed $AMIP_{sst+co2,}$ ('$AMIP_{sst+co2}$' *equal to 'AMIP'*) where:

$$AMIP_{sst+co2} - AMIP = k_{sst}.(AMIP_{Future} - AMIP) + k_{co2}.(AMIP_{4xCO2} - AMIP) \quad (1)$$

Here, k_{sst} is the temperature scaling factor derived as the ratio of tropical 30°S-30°N zonal-mean warming at 100-300 hPa in 'amipFuture' (relative to 'amip') to that in 'abrupt4xCO_2' (relative to 'piControl'). This scaling was chosen to capture the tropical upper tropospheric warming, which is a dominant feature (or 'fingerprint') of global warming. k_{sst} was calculated for each of the eleven models, with an average of $k_{sst} = 0.8047$. k_{co2} is the scaling of CO_2 radiative forcing, which, for the purposes of this study, is unity. Hereafter, this study refers to the multi-model-mean difference between the coupled climate response and $AMIP_{sst+co2}$, as the inferred response to sea-ice loss. The estimate of the inferred response to sea-ice loss is derived as a residual from coupled model experiments and so, it includes any effects of ocean coupling on the response to sea-ice loss (see, e.g., Deser et al., 2015). However due to the scaling (k_{sst}), it is expected that any tropical response to sea-ice loss, and any feedback of sea ice-induced tropical changes on the extratropics, would be missed by this method and instead apportioned to SST change.

The results of this analysis are presented in Chapter 4 of this thesis.

3.2 Bespoke simulations

3.2.1 HadGEM3.GC3.1 model

The bespoke sea ice perturbation experiments use the HadGEM3-GC3.1 low resolution (n96 ORCA1) global coupled model configuration (Table 3.3), which is participating in phase 6 of the Coupled Model Intercomparison Project (CMIP6) (Williams et al., 2017). The model uses the GA7.1 (Walters et al., 2017) global atmosphere configuration, with the JULES GL7.0 land surface component model

(Walters et al., 2017), the NEMO GO6.0 ocean model (Storkey et al., 2018), and CICE GSI8.1 sea ice model (Rae et al., 2015; Ridley et al., 2018). This version has an atmosphere with 85 vertical levels and horizontal resolution of (~135 km at mid-latitudes (n96). The ocean model used has 75 vertical levels with a 1° horizontal resolution on a tripolar grid. Atmosphere-ocean coupling occurs every three hours through the OASIS-MCT coupler (Ocean Atmosphere Sea Ice Soil Model Coupling Toolkit; Valcke, 2006). An advantage of using the N96ORCA1 model over the N216ORCA025 model, is that it requires an order of magnitude less computing power per model year, yet maintains almost the same quality in representation of the global climate (Kuhlbrodt et al., 2018), and for this study in particular, performs better for Antarctic sea ice. The 1° ocean resolution requires a parameterization for eddy-induced transports (Kuhlbrodt et al., 2018), which here is a globally uniform coefficient.

For the purpose of this study, it is important to understand how well the model simulates the relevant processes, and any known biases that may impact the results. One of the most well-known problems, across multiple models, is the Southern Ocean warm bias (Kuhlbrodt et al., 2018; Menary et al., 2018; Ridley et al., 2018; Williams et al., 2017). The previous configuration of the HadGEM3 model (GC2) contained a warm bias, thought to be caused by excess solar insulation from too little cloud cover (Williams et al., 2017). This also impacted the temperature with depth in the high-latitude Southern Ocean. However in the current configuration (GC3.1), there is only a slight cold bias in the mid to high latitudes (Figure 3.1), which is an improvement over prior versions (Kuhlbrodt et al., 2018). This improvement in simulating realistic extratropical SST has other benefits, such as an improved seasonal cycle of sea ice and more realistic ACC

transport, in the N96ORCA1 GC3.1 simulation (Kuhlbrodt et al., 2018; Ridley et al., 2018) compared to either the older version of the model (GC2) or the higher resolution (N216ORCA025) version of GC3.

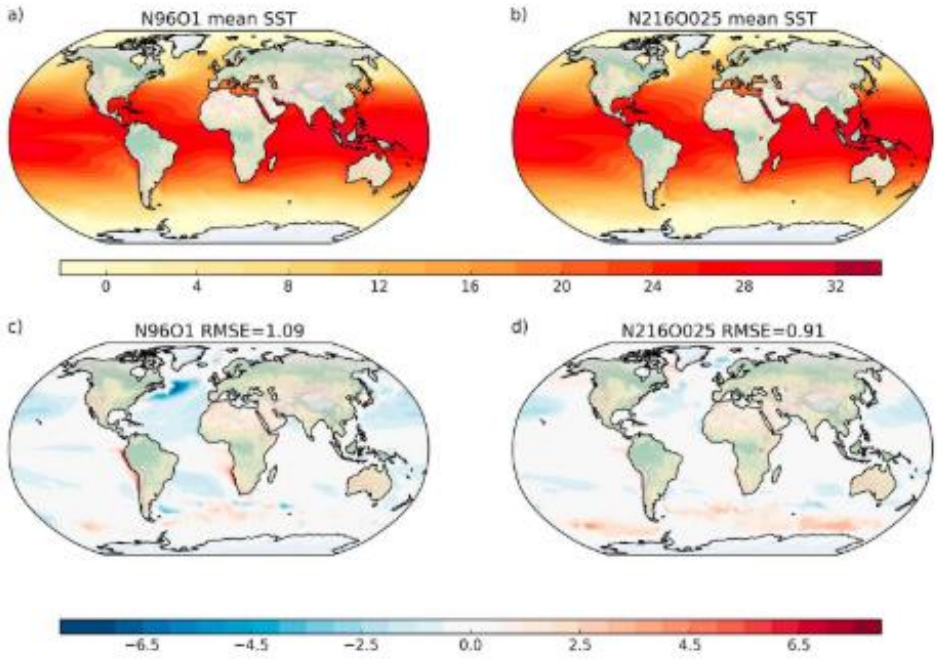

Figure 3.1*: The annual mean SST in (a) N96ORCA1 and (b) N216ORCA025, and the bias against ESA CCI satellite observations for (c) N96ORCA1 and (d) N216ORCA025.Temperature scale in Celsius. Figure from Kuhlbrodt et al. (2018).*

The ACC transport in the N96ORCA1 model reproduces the observed (and reanalysis-estimated) transport better than the N216ORCA025, with an average of 136 Sv and 54 Sv respectively (Figure 3.2) (Menary et al., 2018), compared to the observed 173.3 ± 10.7 Sv (Donohue et al., 2016). The low transport rate of the N216ORCA025 model is thought to be in response to too much deep convection in the Weddell Sea (Menary et al., 2018).

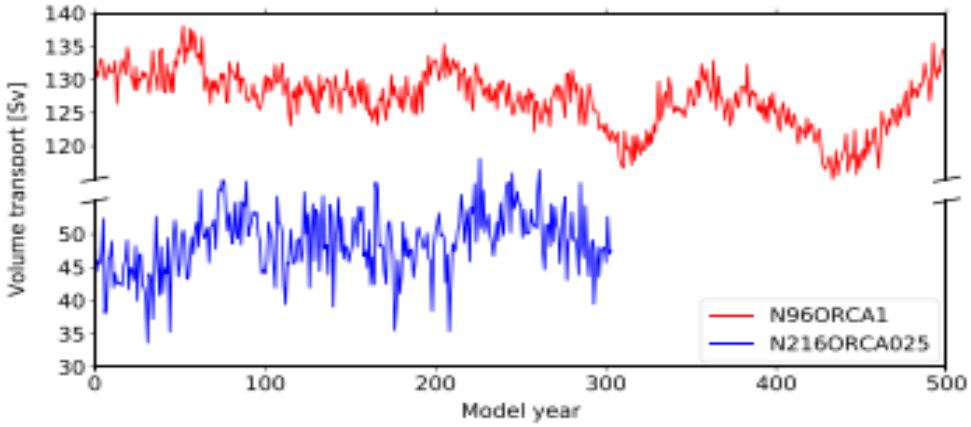

***Figure 3.2**: Antarctic Circumpolar Current (ACC) volume transport, for 500 years of the Preindustrial Control N96ORCA1 model (Red), and 300 years of the Preindustrial Control N216ORCA025. Figure from Menary et al. (2018).*

Antarctic SIE is comparatively better in the GC3.1 configuration of the model too. SIE reaches latitudes comparable to observations (Figure 3.3) (Ridley et al., 2018). In terms of the seasonal cycle of sea ice, the model simulates autumn Antarctic sea ice volume well, however, spring sea ice volume is estimated too high (Ridley et al., 2018) (Figure 3.4).

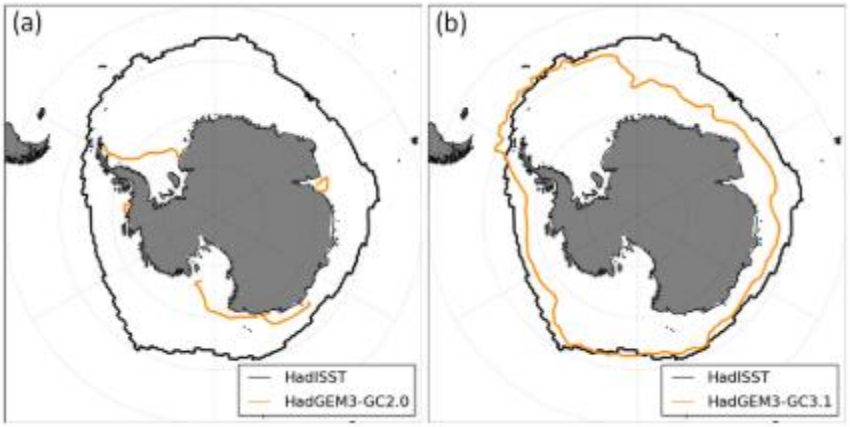

***Figure 3.3**: The mean Antarctic sea ice extent in winter (June, July, and August) with (a) HadGEM3 -GC3 and (b) HadGEM3 GC3.1 (orange). With HadISST1.2 sea ice analysis for comparison (back). Figure from Ridley et al. (2018).*

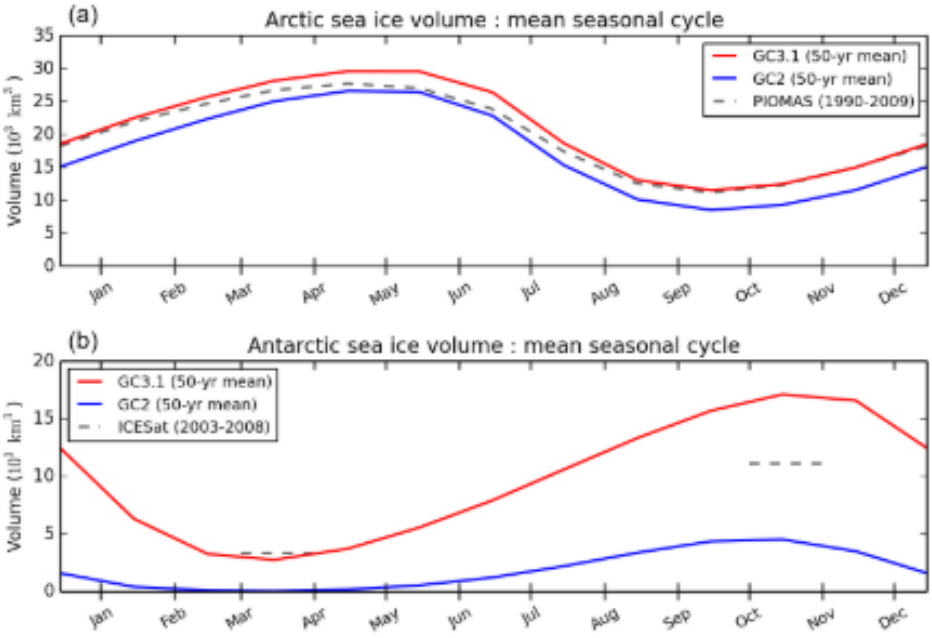

Figure 3.4*: The annual cycle of sea ice volume for the HadGEM3 model GC2 (blue) and GC3 (red), for the (a) the Arctic and (b) the Antarctic. For comparison, estimates from PIOMAS model reanalysis for the Arctic, and ICESat for the Antarctic, is included (grey). Figure from Ridley et al. (2018).*

Biases away from the Southern Ocean include a cold bias in the Arctic, where sub-surface ocean temperatures are up to 2 K colder in the N96ORCA1 compared to reanalyses and observations at the end of winter, leading to thicker sea ice (Kuhlbrodt et al., 2018). This is thought to be due to problems representing the Gulf Stream and Kuroshio currents, which are common issues in low resolution models (Bryan et al., 2007). Another related bias is in the AMOC, with all configurations of the model having an AMOC upper cell that is too shallow, and heat transport at 26.5 °N that is too weak (Menary et al., 2018).

3.2.2 Forcing

The control experiment was the CMIP6 'Preindustrial Control' simulation (Eyring et al., 2016), which was spun-up using CMIP6 Preindustrial forcing (Menary et al., 2018). In the sea ice perturbation experiment, sea-ice loss was induced in the Southern Hemisphere alone, via an albedo feedback method. More specifically, all sea ice in the Southern Hemisphere was set to be covered by melt ponds with 30 cm depth. This perturbation caused an abrupt reduction in sea ice albedo, leading to the increased absorption of shortwave radiation and thus, abrupt Antarctic sea-ice loss. All other forcings were kept constant at preindustrial levels. Although melt ponds are naturally rare in the Antarctic due to thick snow cover (Scott & Feltham, 2010), modifying the melt pond scheme was an effective way to control the sea ice in one hemisphere and not the other. Other albedo parameters, for example the sea ice albedo, are coded to be globally consistent.

The CICE model governs the spatial and temporal evolution of the ice thickness distribution via the processes of advection, thermodynamics, and mechanical redistribution and ridging (Ridley et al., 2018). The latest version of CICE (GSI8.1) (Rae et al., 2015; Ridley et al., 2018) has prognostic melt ponds (Ridley et al., 2018) within the albedo scheme. This scheme has separate albedos for visible and near-infrared wavelengths and includes the impact of surface melt ponds (Ridley et al., 2018). The melt pond area fraction, fp(n), and depth, hp(n), for ice in thickness category n, are calculated using the CICE topographic melt pond formulation (Flocco et al., 2010; 2012; Hunke et al., 2015). When pond depth is less than 4mm, melt pond depth has no impact on the albedo for that ice thickness category n, such that the ponded ice albedo is equal to that of bare ice, αi (Ridley et al., 2018). Conversely, where melt pond depth is greater than 20 cm, the bare

ice albedo has no impact, and the ponded ice albedo is equal to that of a melt pond, *αp*. For melt pond depths between these two values, the ponded ice albedo is a function of the underlying bare ice albedo and the pond albedo (Ridley et al., 2018; Briegleb & Light, 2007):

$$\alpha_{p_i}(n) = \frac{h_p(n)}{0.2}\alpha_p + \left(1 - \frac{h_p(n)}{0.2}\right)\alpha_i \quad (2)$$

The snow albedo, *αs(n)*, is a simple function of temperature:

$$\alpha_s(n) = \begin{cases} \alpha_c & if\ T(n) < T_c \\ \alpha_c + \left(\frac{\alpha_m - \alpha_c}{T_m - T_c}\right)(T(n) - T_c) & if\ T(n) \geq T_c \end{cases} \quad (3)$$

Where $T(n)$ is the surface skin temperature, T_m is the melting snow temperature, α_c and α_m are the albedos of cold and melting snow respectively, and T_c is the threshold temperature, below T_m, whereby the surface melting impacts the albedo (Ridley et al., 2018). Together, the scheme calculates the total grid-box albedo, *α(n)*, of each sea ice thickness category n, for each of the wavelength bands (Ridley et al., 2018). This is calculated as the combined ponded ice albedo, *αpi(n)*, bare ice albedo $\alpha_i(n)$, and snow albedo, *αs(n)*, weighted by the melt pond fraction *fp(n)* and snow fraction *fs(n)*:

$$\alpha(n) = f_p(n)\alpha_{p_i}(n) + \left(1 - f_p(n)\right) \times \left(f_s(n)\alpha_s(n) + \left(1 - f_S(n)\right)\alpha_i\right) \quad (4)$$

Equation (4) dictates that when the melt pond fraction is one, the total albedo is solely dependent on the ponded ice albedo, whereas when melt pond fraction is zero, the total albedo is solely dependent on the snow albedo and bare ice

albedo. For the purposes of this work, the melt pond fraction and depth can be changed to perturb the albedo.

3.2.3 Model sensitivity tests

The melt pond albedo method was tested for five years, disregarding the first two years as spin-up, with different combinations of melt pond fraction and depth, applied to Southern Hemisphere sea ice only. Four separate combinations were tested: the first with maximum pond area fraction and depth (1, 0.3 m), the second with maximum pond area fraction but smaller depth (1, 0.1 m), the third with half pond area fraction and maximum depth (0.5, 0.3 m), and the fourth with zero pond area fraction. These test simulations were compared to the HadGEM3 GC3.1 'Preindustrial Control' simulation, and the CMIP5 HadGEM2-ES Preindustrial Control, RCP8.5 and Abrupt4xCO_2 simulations, with two aspects in mind; the magnitude, and the seasonal cycle of SIA loss.

The three experiments with pertubed melt ponds all have reduced SIA compared to the control run, in all months (Figure 3.5 & 3.6). Of these three, the largest sea-ice loss relative to the control was achieved with the maximum melt pond fraction and depth (1, 0.3 m), as might be expected. The other two experiments still produced signifianct ice loss, closely comparable to each other but lesser in magnitude than the first experiment. The fourth experiment, with no melt ponds, showed a slight increase in SIA compared to the control, highlighting that in free-running simulations, the snow fraction is the dominant term in the albedo determination.

It is informative to compare the magnitude of sea-ice losses induced through the melt pond perturbations to those simulated in the CMIP5 experiments (described in section 3.1). All three melt pond perturbation experiments yield greater ice losses in summer than either quadrupled CO_2 or the RCP8.5 scenario by the end of the twenty-first century, relative to the respective preindustrial control runs. This shows the albedo method is very effective for reducing summer sea ice. In winter, the picture is rather different, with even the largest melt pond perturbation yielding lesser ice losses than either quadrupled CO_2 or the RCP8.5 scenario. In October, the largest melt pond perturabtion results in an approximate 20% reduction in SIA compared to 60% at quadrupled CO_2 and 40% at the end of the 21st century in RCP8.5. This highlights a limitation of the albedo method in that is has a relatively disproportionately large effect in the sunlit portion of the year. However, unlike nudging approaches which can better mimic the seasonal cycle of projected sea-ice loss, the albedo method conserves energy (Sun et al., 2020). Using the albedo method, it is impossible to accurately mimic the seasonal cycle of projected sea-ice loss: matching the CMIP5 results in summer would lead to a larger underestimation of ice loss in winter. Matching the winter sea-ice losses seen in CMIP5 is not possible within this albedo perturbation framework. In these experiments, changing the melt pond fraction or depth individually, or in combination, led to similar seasonality of the resultant ice loss.

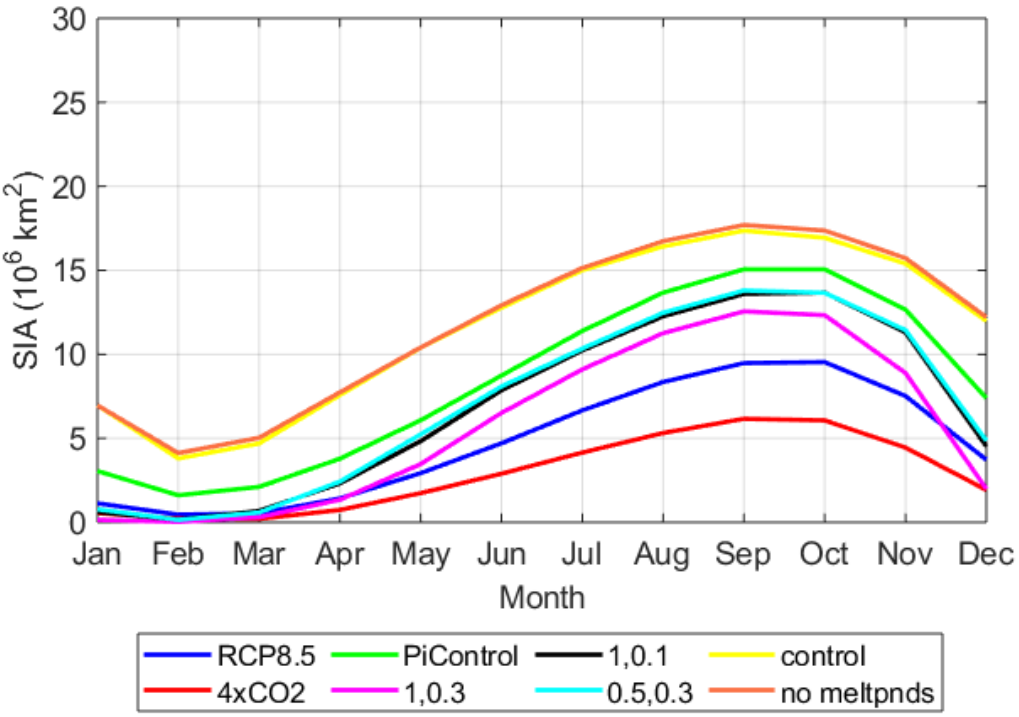

***Figure 3.5**: Sea ice area (SIA) annual cycle comparison, for Hadgem2-ES RCP8.5, Abrupt4XCO₂ and Preindustrial Control simulations (blue, red, and green, respectively), with the HadGEM3 GC3.1 full meltpond grid cell and maximum depth (1, 0.3 m), full meltpond grid cell and small depth (1, 0.1 m), half meltpond grid cell and full depth (0.5, 0.3 m), the preindustrial control, and no meltpond simulations (magenta, black, aqua, yellow, and orange, respectively).*

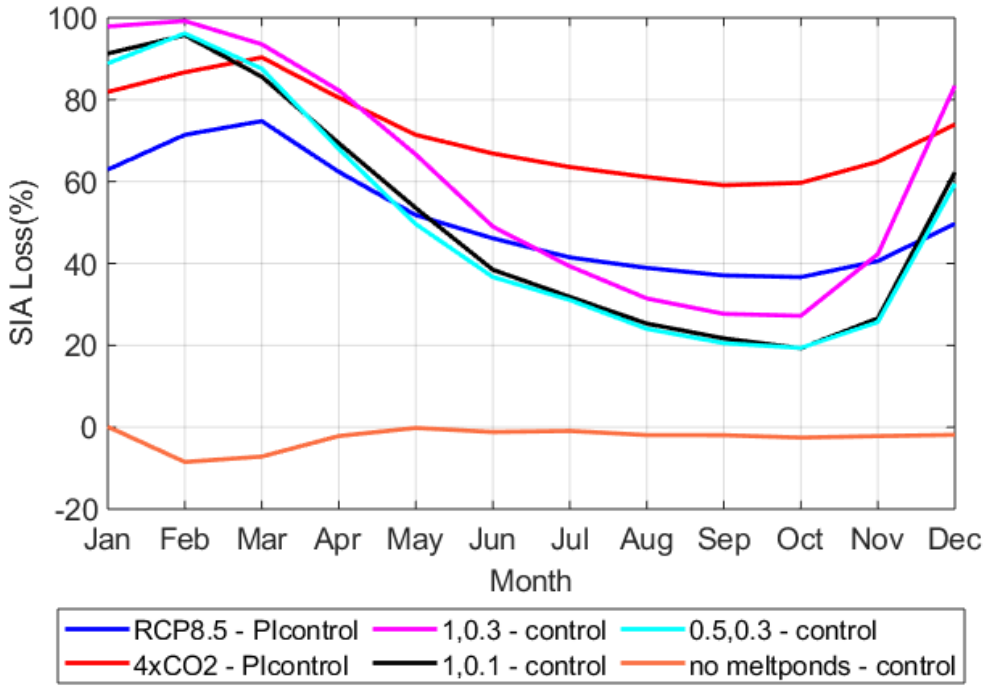

***Figure 3.6**: Sea ice area (SIA) percentage loss annual cycle comparison, for Hadgem2-ES RCP8.5 and Abrupt4XCO₂ difference to the Preindustrial Control simulations (blue and red, respectively), with the HadGEM3 GC3.1 full meltpond grid cell and maximum depth (1, 0.3 m), full meltpond grid cell and small depth (1, 0.1 m), half meltpond grid cell and full depth (0.5, 0.3 m), and the no meltpond simulations, difference to the Preindustrial Control, (magenta, black, aqua, and orange, respectively).*

The spatial differences between the melt pond perturbation experiments and the control run (top to bottom, Figure 3.7 a-l), show that in each case, sea-ice loss occurs at all longitudes. In austral summer, sea-ice loss occurs in all ice-covered regions. In austral winter, sea-ice loss occurs near the ice edge, where the ice is thinner and is more exposed to the surrounding ocean. The fourth experiment (Figure 3.7 m-p) shows an increase in sea ice where melt ponds would have been present previously. These include regions at the sea ice edge in the Weddell and

Amundsen Sea. Interestingly, there is a decrease in sea ice in the Ross Sea and South Pacific Ocean, however, this may be noise from the short three years of comparison.

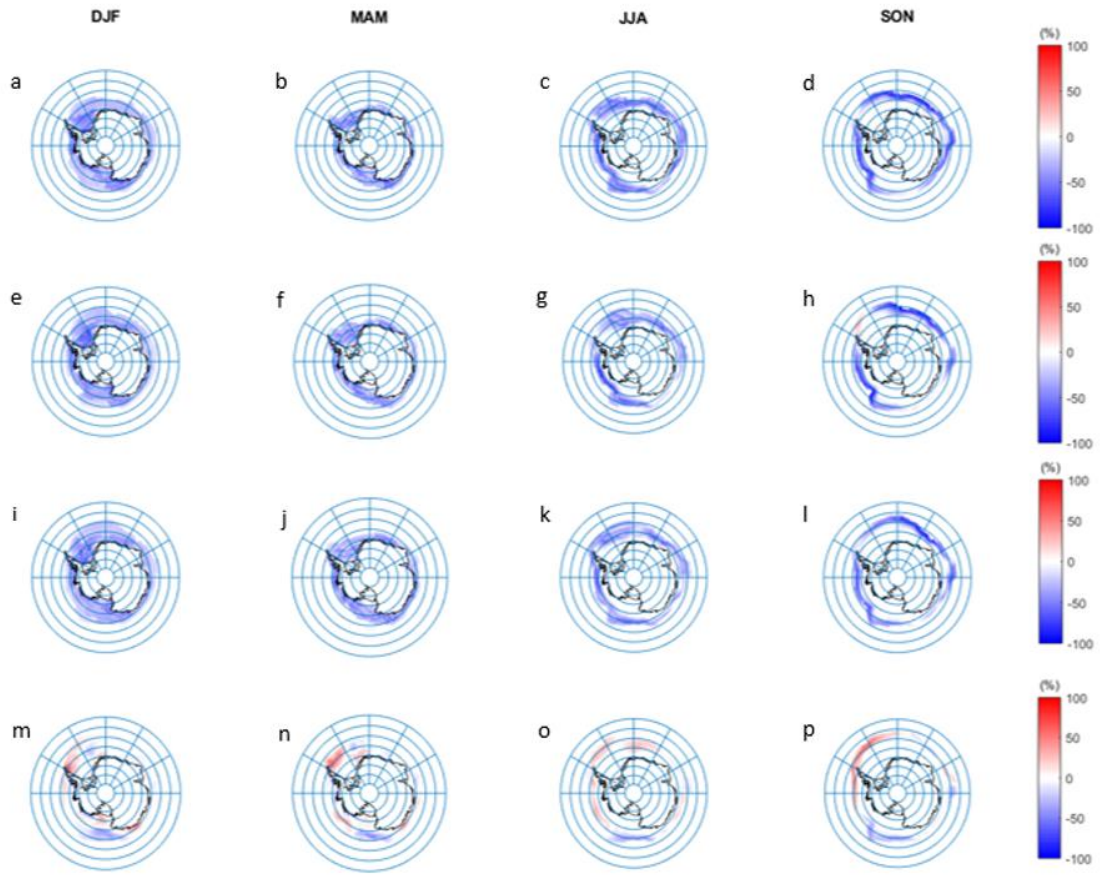

***Figure 3.7**: Sea ice concentration (SIC) response to full meltpond grid cell and full depth (1, 0.3 m) in austral (a) summer (December-February; DJF), (b) autumn (March-May MAM), (c) winter (June-August; JJA) and (d) spring (September-November SON). (e-h) As (a-d) for full meltpond grid cell and a small depth (1, 0.1 m). (i-l) As (a-d) for half meltpond grid cell and full depth (0.5, 0.3 m). (m-p) As (a-d) for no melt ponds.*

Based on these experiments, the forcing chosen was the maximum melt pond fraction and depth (1, 0.3 m). With the largest sea-ice loss relative to the control, this forcing was chosen to increase the signal-to-noise, and to maximise winter sea-ice loss to be closer to projected values. This forcing was applied continually in a 300-year perturbation simulation, sufficiently long to allow the ocean circulation to reach a new equilibrium state (Deser et al., 2016). Antarctic sea-ice loss was abrupt and quasi-equilibrium was reached within the first 20 years, with only a slow continued decline thereafter (Figure 3.8).

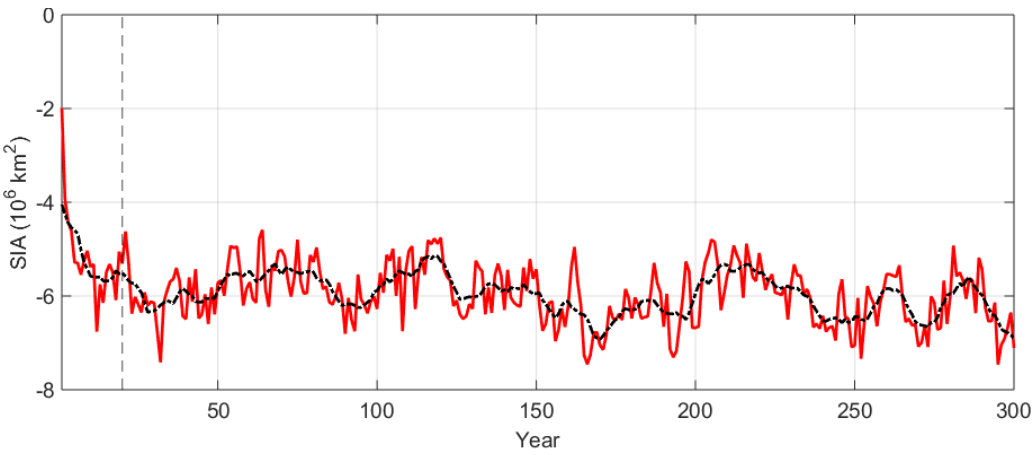

***Figure 3.8**: Annual average sea ice area (SIA) anomaly between HadGEM3 GC3.1 perturbed and Preindustrial Control data with ten year running mean (black dashed line).*

The results of this analysis are presented in Chapters 5 and 6 of this thesis.

3.3 HadGEM3 atmospheric only

3.3.1 Model and forcing

In chapter 7, the HadGEM3-A low resolution (N96) global atmosphere-only model is used, in the same configuration as participating in the CMIP6 (Walters et al., 2017) (Table 3.3). The atmosphere and land component models are the same as in HadGEM3-GC3.1, but are not coupled to either an ocean or sea ice component model.

Sea ice concentrations and sea surface temperatures were taken from the coupled control and perturbed albedo simulations. In the uncoupled control simulation, both the prescribed sea ice concentrations and sea surface temperatures were taken from the coupled control simulation, averaged over years 50-300. In the uncoupled sea ice perturbation experiment, sea ice concentrations in the Southern Hemisphere were taken from the coupled albedo perturbation experiment, average over years 50-300, whilst those in the Northern Hemisphere were taken from the coupled control simulation. Sea surface temperatures were set to the values from coupled albedo perturbation experiment over regions of Antarctic sea-ice loss, but to the values from the coupled control simulations elsewhere. All external forcings were kept constant at preindustrial levels.

The model was run following the Polar Amplification Modelling Intercomparison Project (PAMIP) protocol (Smith et al., 2018). More specifically, the model was run for 14 months, starting 1st April, with a total of 200 members, each starting from a different atmospheric initial condition. The first 2 months of each run were

discarded and the remaining 200 years averaged to remove internal variability (Mori et al., 2014; Screen et al., 2014).

3.3.2 Tests

Tests were conducted to ensure that after assimilation into the model, the sea ice and SSTs fields were as prescribed. These tests identified a problem, in that after ingestion by the model, sea ice concentrations were slightly lower than the prescribed sea ice input (Figure 3.9). This difference, whilst small, warranted further investigation. Comparing the input and output sea ice concentrations, grid-point by grid-point (Figure 3.10), revealed the problem was confined to locations with a sea ice concentration between 0 and 0.3. After discussion with model users and developers at the Met Office, the problem was found to relate to a quirk in model code, which constrained prescribed sea ice concentrations less than 0.3 (30%) to be zero. This issue could not be fixed within the scope of this work. The problem is manifest particularly near the ice edge (Figure 3.7), where sea ice concentrations are low. However, the discrepancies in sea ice area are very small (Figure 3.10), especially in comparison to the differences between the control and perturbation experiments, and unlikely to strongly affect the results.

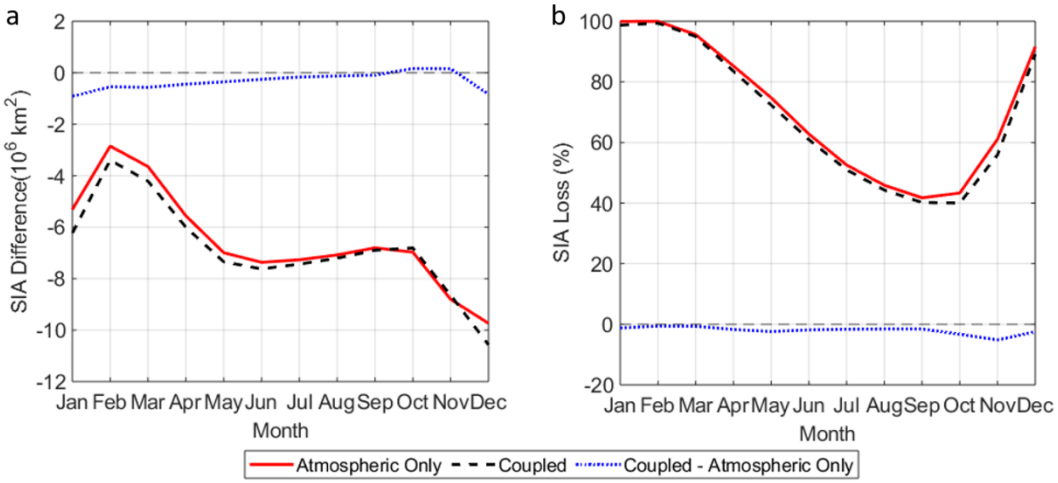

***Figure 3.9**: Sea ice area (SIA) comparison between the atmospheric only (red) and coupled model (black dashed) Antarctic sea ice output, and their difference (blue dotted).*

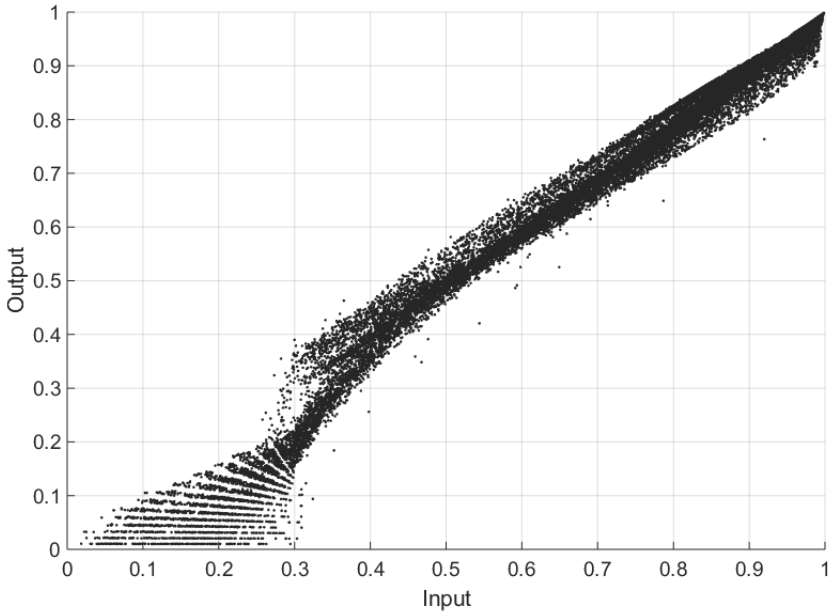

***Figure 3.10**: Sea ice concentration output from atmospheric only model, against input from coupled model. A linear relationship is expected; however, this is not the case for inputs less than 0.3 (30%).*

A difference in SIT between the coupled and atmosphere-only models was found to be related to the creation of sea ice conditions for the atmosphere-only model. The SIT (Figure 3.11) of the coupled model displays a maximum in austral summer, and a minimum in austral winter. Studies have found that in summer, after seasonal melt, sea ice of greater SIT remains, leading to a higher seasonal mean (Kurtz & Markus, 2012; Worby et al., 2008). In winter, there is greater SIC, but the majority of this ice is thin and short lived. The AMIP-II method, used to calculate SIT from SIC, outputs the wrong seasonal cycle for SIT. The differences between the perturbed and control experiments show a reduction in SIT in both models, but this reduction is slightly greater in the coupled model, with a different seasonality. However, unlike in the Arctic, there is less multi-year ice in the Antarctic, therefore, changes in SIT are likely secondary to changes in SIC for the atmospheric response. Despite this difference, the heat flux response from the ocean to the atmosphere of both models are of similar magnitude.

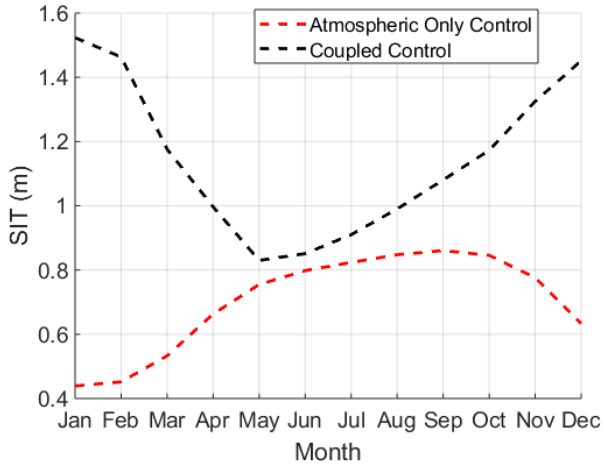

***Figure 3.11**: Sea ice thickness (SIT) for the controls of the atmospheric only (red) and coupled model (black).*

The results of this analysis are presented in Chapter 7 of this thesis.

3.4 Diagnostic metrics and statistics

Sea ice area was calculated by multiplying the sea ice fraction of each grid cell by the true area of each grid cell, and summing over the hemisphere of interest, and has units of square kilometres. The turbulent heat flux was used to calculate the heat exchange between the atmosphere and ocean, and is defined here as the sum of the sensible and latent heat fluxes, with positive values in the upward direction. The area-weighted turbulent heat flux, averaged over grid cells where sea ice concentration decreased between control and perturbed experiments, was used to estimate the forcing on the atmosphere from sea-ice loss. Model output variables are summarised in Table 3.2.

The mid-latitude tropospheric eddy-driven jet was characterised in terms of its strength (the maximum velocity) and latitude, calculated as follows, consistent with Ceppi et al. (2018) and Zappa et al. (2018). First, the jet strength was determined from the zonal average of the monthly-mean climatological zonal wind ($\bar{u}$) at 850 hPa and was calculated over the extratropics between 35° S and 65° S. Next, the jet latitude (ϕ_{jet}) was defined as the mean latitude (ϕ) of westerlies weighted by the square of the westerly wind speed:

$$\overline{u_0}(\phi) = \max(0, \bar{u}(\phi)) \tag{5}$$

$$\phi_{jet} = \int_{-35^\circ}^{-65^\circ} \phi \bar{u}_0^2 \, d\phi \,/\, \int_{-35^\circ}^{-65^\circ} \bar{u}_0^2 \, d\phi \tag{6}$$

The SAM index was calculated using the Gong & Wang (1999) method, defined as the normalized zonal-mean sea level pressure difference between 40 °S and

65 °S. The SPV strength was calculated as the 10 hPa zonal-mean zonal wind velocity at 60 °S.

The ACC volume transport was calculated as the vertically integrated volume transport across Drake Passage (54.5° S – 61° S, 61° W). The AMOC was measured as the meridional streamfunction at 26.5° N in the Atlantic Ocean region.

Statistical significance was calculated with the Student's t-test (Student, 1908):

$$t = \frac{\bar{x}-\mu}{s/\sqrt{n}} \quad (7)$$

Whereby $\bar{x}$ is the sample mean, μ is the population mean, s is the standard deviation, and n is the sample size. Significance is indicated when the p-value is less than 0.05. Throughout the thesis, statistical significance was shown via hatching, contours, or additional methods described in the figure caption. Where no additional definition of significance was shown, all results presented in a figure were statistically significant.

Where seasonal means were used, the seasons were defined as December, January and February for austral summer (boreal winter); March, April and May for austral autumn (boreal spring); June, July and August for austral winter (boreal summer); and September, October and November from austral spring (boreal autumn), unless defined as otherwise. The text refers to the austral seasons, unless otherwise stated.

***Table 3.2**: Summary of the main model outputs used throughout this thesis, and their acronyms.*

Surface level		*Atmosphere on pressure level*		*Ocean on depth levels*	
Sea ice concentration	SIC	Zonal wind	UA	Potential temperature	T
Sea ice thickness	SIT	Meridional wind	VA	Salinity	S
Mean sea level pressure	MSLP	Geopotential height	ZG	Density	Rho
Total precipitation	Pr	Temperature	TA	Zonal velocity	U
Surface air temperature	TAS			Meridional velocity	V
Sea surface temperature	SST			Vertical velocity	W
Sea surface salinity	SOS				
Surface latent heat flux	HFLS				
Surface sensible heat flux	HFSS				

***Table 3.3**: Summary of model experiments and data used for throughout this thesis.*

Model Experiment	***Grid***	***Version***	***Experiment ID***	***Years/ members***	***Period***	***Chapters for data feature***
CMIP5 Ensemble	T42	See Table 3.1.	PiControl Abrupt4xCO_2 AMIP AMIPFuture AMIP4xCO_2	100 years 30 years 11 models	1850-1950 1979-2008	Chapter 4
HadGEM3-GC3.1	N96 ORCA1 (LL)	GA7.1 UM10.7	PiControl Albedo	300 years 1 member	1850-2149	Chapter 5 & 6
HadGEM3-A	N96 (LL)	GA7.1 UM10.7	AMIP AMIP Albedo	1 year 200 members	2000-2001	Chapter 7

3.5 Summary of Chapter 3

Three separate methods were used in this thesis to assess the effects of projected Antarctic sea-ice loss. First, was to indirectly infer the atmospheric response from the CMIP5 “ensemble of opportunity”, using eleven models to estimate the multi–model response to sea-ice loss at quadrupled CO_2 (Chapter 4). Second, was by conducting a bespoke HadGEM3 GC3.1 experiment with sea-ice loss induced through a novel method of perturbing the melt pond albedo in the Southern Hemisphere only. This allowed quantification of the response to sea-ice loss in the coupled climate system, including both the atmospheric (Chapter 5) and oceanic impacts (Chapter 6). Third, was a HadGEM3-A atmosphere-only experiment, prescribed with sea ice conditions from the coupled model experiments, to determine the importance of ocean-atmosphere coupling (Chapter 7). Together these three approaches facilitate the most comprehensive study so far on the coupled climate response to Antarctic sea-ice loss.

Chapter 4

Multi-Model Analysis of the Atmospheric Response to Antarctic Sea-Ice Loss at Quadrupled CO_2

Sections of this chapter are published as - Ayres, H. C., & Screen, J. A. (2019). Multimodel Analysis of the Atmospheric Response to Antarctic Sea Ice loss at Quadrupled CO_2. Geophysical Research Letters, 46(16), 9861–9869. https://doi.org/10.1029/2019GL083653

Antarctic sea ice cover is projected to significantly decrease by the end of the 21st century if greenhouse gas concentrations continue to rise, with potential consequences for Southern Hemisphere weather and climate. This chapter examines the atmospheric response to projected Antarctic sea-ice loss at quadrupled CO_2, inferred from eleven CMIP5 models, and is the first multi-model analysis of the atmospheric response to Antarctic sea-ice loss. Section 4.1 discusses the previous literature on the atmospheric response to Antarctic and Arctic sea-ice loss. Sections 4.2.1 to 4.2.4 show the projected Antarctic sea-ice loss, the spatial character of inferred atmospheric response to Antarctic sea-ice loss, the zonal-mean atmospheric response, and jet stream response, respectively. Finally, Section 4.3 discusses these results, with a brief summary in Section 4.4.

4.1 Introduction

Accurate satellite records of polar sea ice began in 1979. Since this time, annual-mean Arctic SIE has decreased significantly by ~960 thousand square kilometres per decade (Fetterer et al., 2017), whereas annual-mean Antarctic SIE has increased by a lower, but still significant, ~54 thousand square kilometres per decade (Fetterer et al., 2017).

In spring 2016, Antarctic SIE decreased at an abnormal rate, 18% quicker than in any previous melting season in the satellite record, and 46% quicker than the average melt rate (Turner et al., 2017). Possible explanations for the sudden 2016 decline include influences from the ENSO and an enhanced zonal wavenumber-3 pattern of the westerly jet (Schlosser et al., 2017; Stuecker et al., 2017). In addition, new research has shown that the rapid sea-ice loss led to ocean warming and enhanced upward propagation of planetary scale waves, triggering a stratospheric warming event, subsequently influencing the westerly jet and further enhancing ice melt (Meehl et al., 2019; G. Wang et al., 2019). Since 2016, Antarctic SIE has tracked well below its long-term average. It is unclear if this dramatic reduction is temporary or if the Southern Hemisphere sea ice is entering a new era of decline (Ludescher et al., 2018).

The CMIP5 climate models simulate, on average, a loss of sea ice over the historical period, and not an increase as has been observed. This disagreement between observations and models remain poorly understood (Turner et al., 2013), but possible explanations include internal climate variability (Polvani & Smith, 2013), model biases (e.g., Bracegirdle et al., 2013; Bracegirdle et al.,

2018; Holland et al., 2017; Lecomte et al., 2016; Purich et al., 2016; Roach et al., 2018; Schroeter et al., 2017; Turner et al., 2013) or unresolved processes in models such as ice-sheet-ocean interactions. The same models project that Antarctic sea ice will continue to decline significantly to 2100 (e.g., Collins et al., 2013; Vaughan, 2013) if greenhouse gas concentrations continue to rise, although there is significant divergence between models in the magnitude of the projected decline. Nevertheless, future trends in Antarctic sea ice may have numerous impacts on the surrounding atmosphere.

It is well understood that Arctic sea-ice loss is influencing high-latitude weather and climate in the Northern Hemisphere, with thermodynamically induced warming and moistening of the atmosphere, amongst other changes. There is also emerging evidence that reduced Arctic sea ice may influence the large-scale atmospheric circulation, for example, through weakening of the mid-latitude westerly winds (e.g., Peings & Magnusdottir, 2014) and a negative shift in the North Atlantic Oscillation index (Blackport & Kushner, 2016; Deser et al., 2015; Kim et al., 2014; Peings & Magnusdottir, 2014; Screen & Simmonds, 2013; Screen et al., 2013). Several review papers have been published on the atmospheric response to Arctic sea-ice loss, including Cohen et al. (2014), Vavrus (2018) and Screen et al. (2018). The potential for such atmospheric responses to Antarctic sea-ice loss has been less well studied.

The observed gradual growth of Antarctic sea ice has been suggested to result in a slight poleward shift of the tropospheric jet in the winter months (Smith et al., 2017). Raphael et al. (2011) suggested that negative summer sea ice anomalies

were linked to a more negative SAM index and vice versa. Studies examining the atmospheric response to projected Antarctic sea-ice loss have revealed contrasting results, with Kidston et al. (2011) finding no significant impacts whereas Bader et al. (2013) and Menéndez et al. (1999) both found an equatorward shift of the tropospheric jet. More recently, England et al. (2018) used the WACCM4 model to compare impacts of Arctic and Antarctic sea-ice loss. These authors found a significant equatorward shift of the eddy-driven jet in response to sea-ice loss in either hemisphere. They also found that the tropospheric and stratospheric responses to Antarctic sea-ice loss were of smaller amplitude, more vertically confined, and with less seasonal variation than in response to Arctic sea-ice loss.

In this chapter, the methods developed by Zappa et al. (2018), were adapted and applied to the Antarctic. This method was originally used to analyse the wintertime atmospheric response to projected Arctic sea-ice loss and in particular, that of the North Atlantic jet. Here, a very similar methodology is applied to examine the seasonal atmospheric response to Antarctic sea-ice loss when the CO_2 concentration is quadrupled. The output from 11 CMIP5 models was used to calculate the indirect response as discussed in section 3.1 of this thesis. All stated seasons refer to the austral seasons, unless otherwise specified.

4.2 Results

4.2.1 Sea ice

In response to quadrupled CO_2, Antarctic sea ice concentrations are reduced in all seasons and in all sectors of the Southern Ocean (Figure 4.1 a-d). During the warmer months, sea-ice loss is mostly limited to high southern latitudes, particularly the Weddell and Ross Seas. In the colder months, sea ice reductions are simulated all around Antarctica and extend further to the north, reaching 55° S in the Atlantic sector. The loss of sea ice is of greatest magnitude in the late autumn through to summer (May-December) and of weaker magnitude in the late summer and early autumn (January-April). The loss of sea ice area (Figure 4.1e) is greatest in September (7.7×10^6 km^2) and least in February (1.6×10^6 km^2).

As would be expected, the loss of sea ice leads to an increase in the ocean-to-atmosphere heat flux at the ocean surface. Figure 4.1f shows the area-weighted surface turbulent (sensible plus latent) heat flux response, summed over Southern Hemisphere grid points where the sea ice concentration differs between the preindustrial and quadrupled CO_2 states. The inferred heat flux response to the sea-ice loss (Figure 4.1f) is largest in the winter (July-September), reaching a maximum of 300 TW in August, and smallest in spring to summer, with a minimum of 50 TW in January. The annual cycle of the surface heat flux response closely follows the annual cycle of sea ice area loss; although the monthly maximum and minimum heat flux responses occur one month prior to the maximum and minimum sea ice area loss. The heat flux response peaks in August, despite sea-ice loss being largest in August-September, because the climatological heat flux is at a maximum in July-August (not shown).

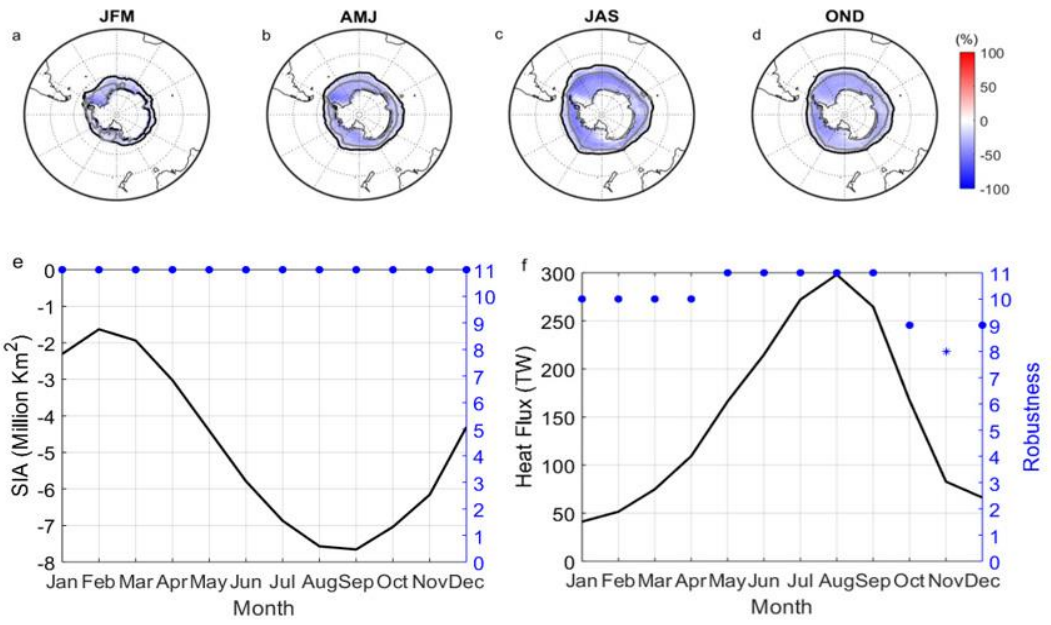

Figure 4.1: *Multi-model-mean sea ice concentration response to quadrupled CO_2 in (a) summer (January-March; JFM), (b) autumn (April-June; AMJ), (c) winter (July-September; JAS) and (d) spring (October-December). The black and grey contours show the sea ice edge (15% concentration) in the quadrupled and control simulations, respectively. (e) Multi-model-mean sea ice area (SIA) response to quadrupled CO_2 as a function of calendar month. The right-hand vertical axis (in blue) shows the number of models that have the same signed response as the multi-model mean, with filled dots indicating nine or more models have the same signed response as the multi-model mean and stars indicating fewer than nine models have the same signed response as the multi-model mean. (f) As (e), but for the inferred surface turbulent heat flux response, calculated as the area-weighted surface turbulent (sensible plus latent) heat flux response, summed over Southern Hemisphere grid points where the sea ice concentration differs between the preindustrial and quadrupled CO_2 states. The heat flux is defined as positive in the upward direction.*

4.2.2 Atmosphere

Near-surface air temperatures are significantly increased in regions of sea-ice loss (Figure 4.2 a-d), consistent with an enhanced ocean-to-atmosphere heat flux. The seasons and geographical regions of greatest warming are consistent with both the magnitude of sea-ice loss and of the surface heat flux response. Warming reaches a maximum of 7.2 K in the Amundsen Sea in winter. The near-surface warming does not extent far inland, probably due to the high elevation of the Antarctic continent and predominantly down-slope winds, in agreement with England et al. (2018).

The inferred mean surface level pressure (MSLP) response to sea-ice loss (Figure 4.2 e-h) resembles the spatial pattern of the negative phase of the SAM, with increased MSLP at high latitudes and reduced MSLP in mid-latitudes, particularly in the spring and summer. An increase in MSLP is simulated over the Antarctic continent in all seasons. The MSLP response is highly zonally symmetric in spring and summer. In winter, and to a lesser extent in autumn, the ring of reduced MSLP in mid-latitudes is punctuated by increased MSLP in the East Pacific sector (i.e., south of Australia and New Zealand). Also, in winter, MSLP is increased in the Amundsen-Bellingshausen Sea, which implies a reduction in the intensity of the ASL. The inferred response of the westerly wind in the mid-troposphere (U500 hPa; Figure 4.2 i-l) is best described as decrease in westerly wind velocity around Antarctica centred at 65° S and an increase in mid-latitudes centred at 45° S. This general pattern is simulated in all seasons but is of greatest magnitude in spring and summer, consistent with the MSLP response. The inferred geopotential height response (Z500 hPa; Figure 4.2 m-p) is also consistent with the MSLP response.

A comparison between the total response to quadrupled CO_2, the estimated component due to SST and CO_2 change, and the inferred sea ice responses for winter and spring, shows corresponding increase in near air surface temperature in all three cases (Figure 4.3 & 4.4 a-c). Sea-ice loss represents a large fraction of the total warming response over the high-latitude Southern Ocean. For MSLP, U500 and Z500 (Figure 4.3 & 4.4 d-l), the inferred response to sea-ice loss is of the opposite sign to that in response to quadrupled CO_2, indicating the competing effects of increased greenhouse gas concentrations and sea-ice loss. The total response to quadrupled CO_2 shows a MSLP decrease at high latitudes and an increase in mid-latitudes, resembling the positive phase of the SAM. In contrast, the inferred sea-ice loss response shows increased MSLP at high latitudes and a decrease at mid-latitudes, most prominent in spring and resembling the negative SAM phase. The zonal wind and geopotential height responses at 500 hPa, show a similar competition between the total response to quadrupled CO_2 and the inferred component due to sea-ice loss, particularly in spring. It is important to note however, that the combined response to SST and CO_2 is of a greater magnitude than is the response to sea-ice loss and thus sea-ice loss only partially offsets the response to SST and CO_2.

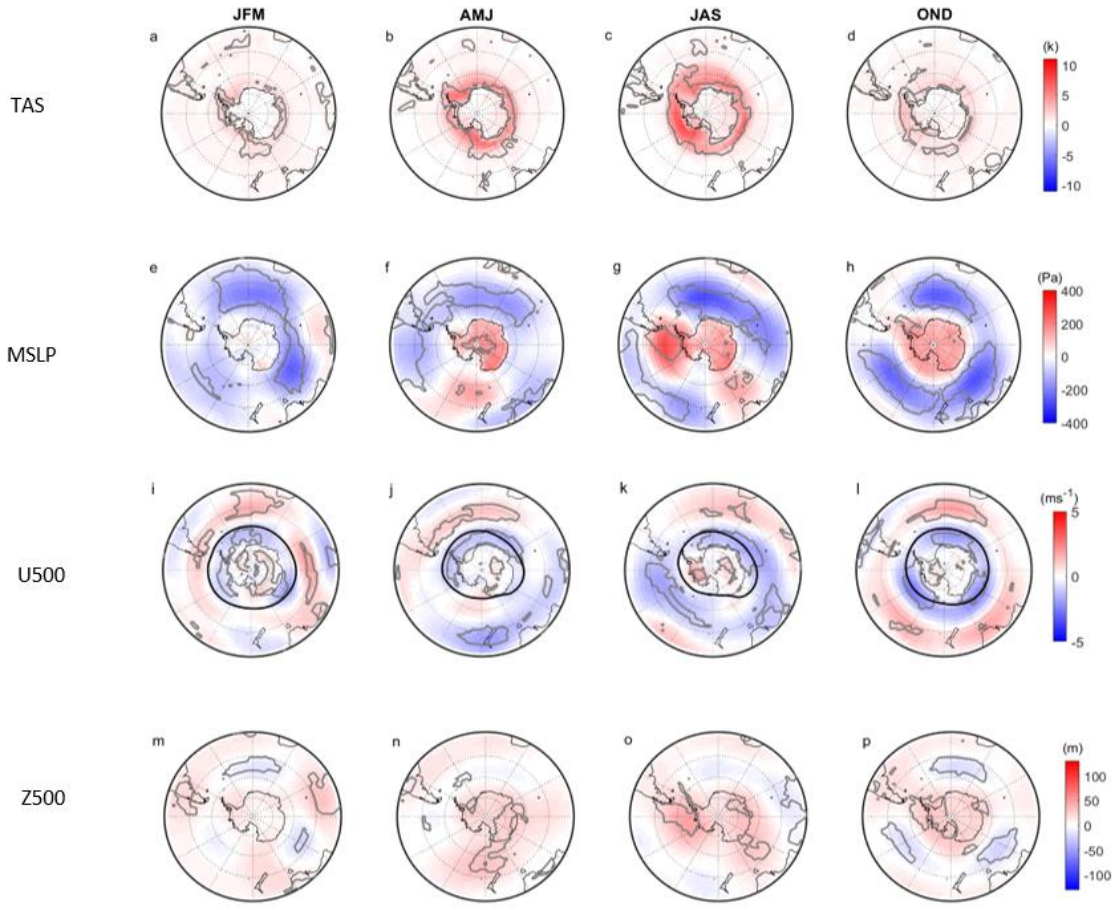

Figure 4.2: *Multi-model-mean inferred surface air temperature (TAS) response to Antarctic sea-ice loss in (a) summer (January-March; JFM), (b) autumn (April-June; AMJ), (c) winter (July-September; JAS) and (d) spring (October-December; OND). In areas enclosed by the grey contours nine or more models have the same signed response as the multi-model mean. (e-h) As (a-d), for mean sea level pressure (MSLP). (i-l) As (a-d), for 500 hPa westerly wind (U500). The thick black line represents the climatological jet position. (m-p) As (a-d), but for 500 hPa geopotential height (Z500).*

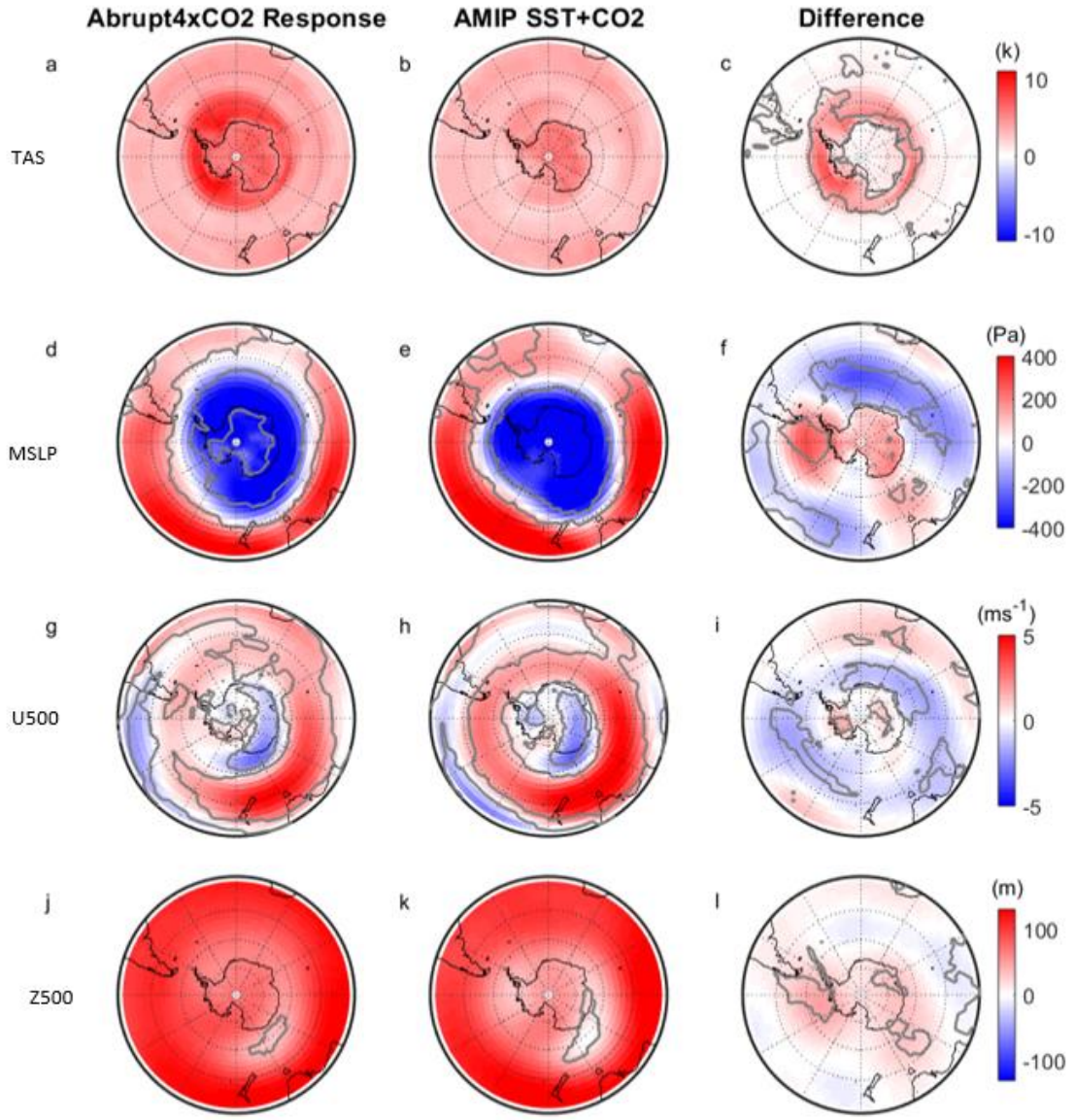

***Figure 4.3**: Austral winter (July-September) multi-model-mean surface air temperature (TAS) for (a) Abrupt4xCO_2 response to PiControl (b) AMIP SST+CO_2 and (c) inferred response to Antarctic sea-ice loss. In areas enclosed by the grey contours nine or more models have the same signed response as the multi-model mean. Note that all areas have ten or more models agree in a and b. (d-f) As (a-c), for mean sea level pressure (MSLP). (g-i) As (a-c), but for 500 hPa westerly wind (U500). (j-l) As (a-c), for 500 hPa geopotential height (Z500).*

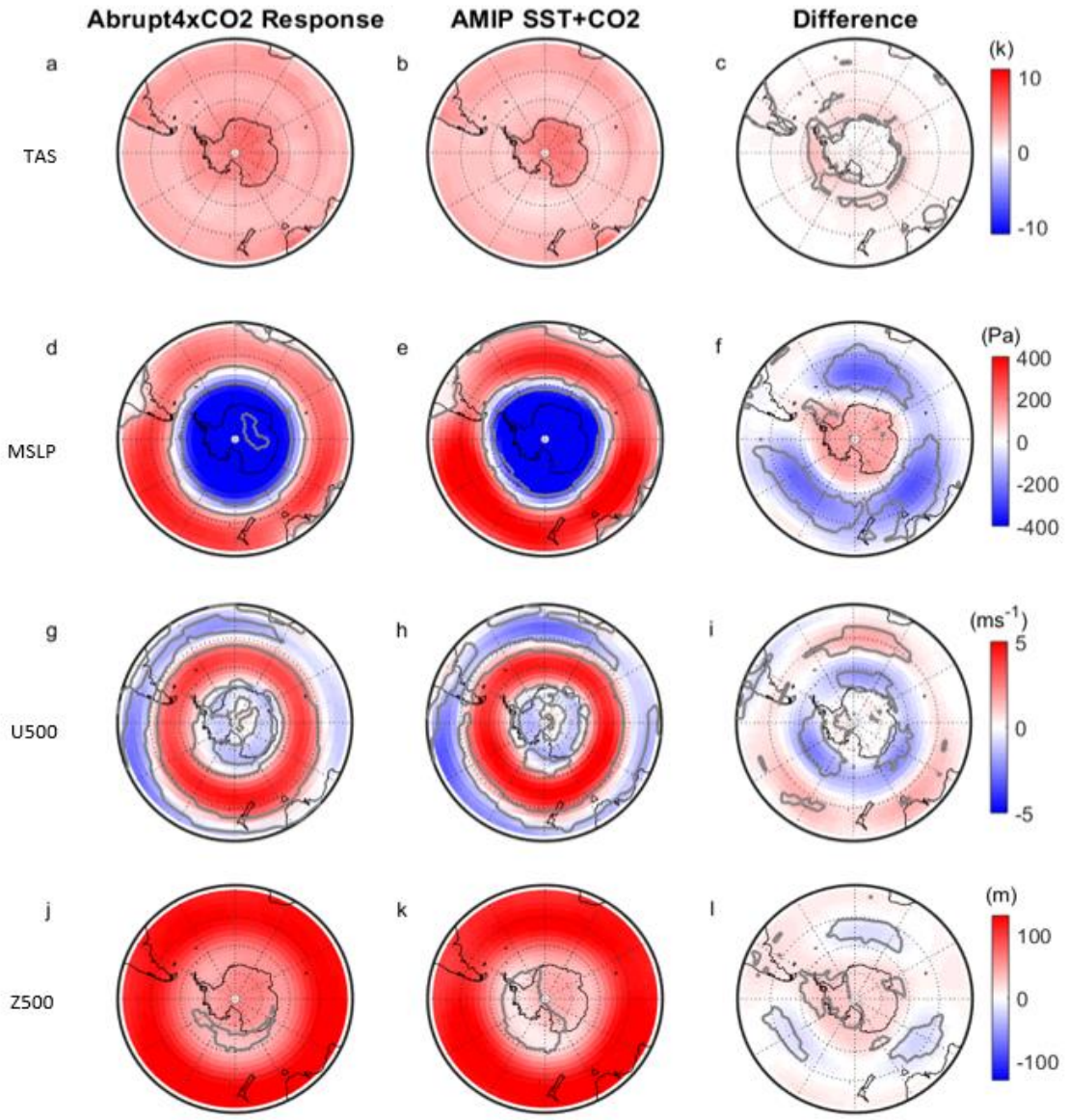

***Figure 4.4**: Austral spring (October-December) multi-model-mean surface air temperature (TAS) for (a) Abrupt4xCO_2 response to PiControl (b) AMIP SST+CO_2 and (c) inferred response to Antarctic sea-ice loss. In areas enclosed by the grey contours nine or more models have the same signed response as the multi-model mean. Note that all areas have ten or more models agree in a and b. (d-f) As (a-c), for mean sea level pressure (MSLP). (g-i) As (a-c), but for 500 hPa westerly wind (U500). (j-l) As (a-c), for 500 hPa geopotential height (Z500).*

4.2.3 Zonal-mean atmospheric responses

Figure 4.5 a-d shows the vertical profile of the inferred zonal-mean air temperature response to sea-ice loss. The near-surface warming previously discussed is confined to the lower troposphere, below 500 hPa. The most notable features of the temperature response aloft are general cooling of the stratosphere across a range of latitudes and seasons and polar stratospheric warming in spring. Note that the former may be an artefact of the method, as both SST warming and quadrupled CO_2 favour a cooler stratosphere (Figure 4.6 a-c). The polar stratospheric warming in spring, however, is not seen in the response to either SST warming or quadrupled CO_2 and may indicate a weakened SPV in response to sea-ice loss.

The inferred zonal-mean westerly wind response to sea-ice loss (Figure 4.5 e-h) shows a weakening of the westerly wind at 60° S, on the poleward flank of the eddy-driven jet, from the surface to the mid-stratosphere in all seasons, but of largest magnitude in winter and spring. In October, the models depict a robust slowdown of SPV by 4.5 ms^{-1} (~10 % of the climatological SPV strength in this month). Throughout the year (although to a lesser degree in autumn) there is strengthened westerly wind at 40° S, predominantly in the core of the subtropical jet. The tropospheric response is largest when there is a coincident and same-signed stratosphere response, suggesting troposphere-stratosphere coupling. This result is in accordance with previous studies that have suggested increased stratosphere-troposphere coupling in the spring when the SPV breaks down (e.g., Kidston et al., 2015).

Over Antarctica the inferred zonal-mean geopotential height response to sea-ice loss shows a baroclinic increase from the surface to the stratosphere and from autumn through to spring, when the response is of largest magnitude (Figure 4.5 i-l).

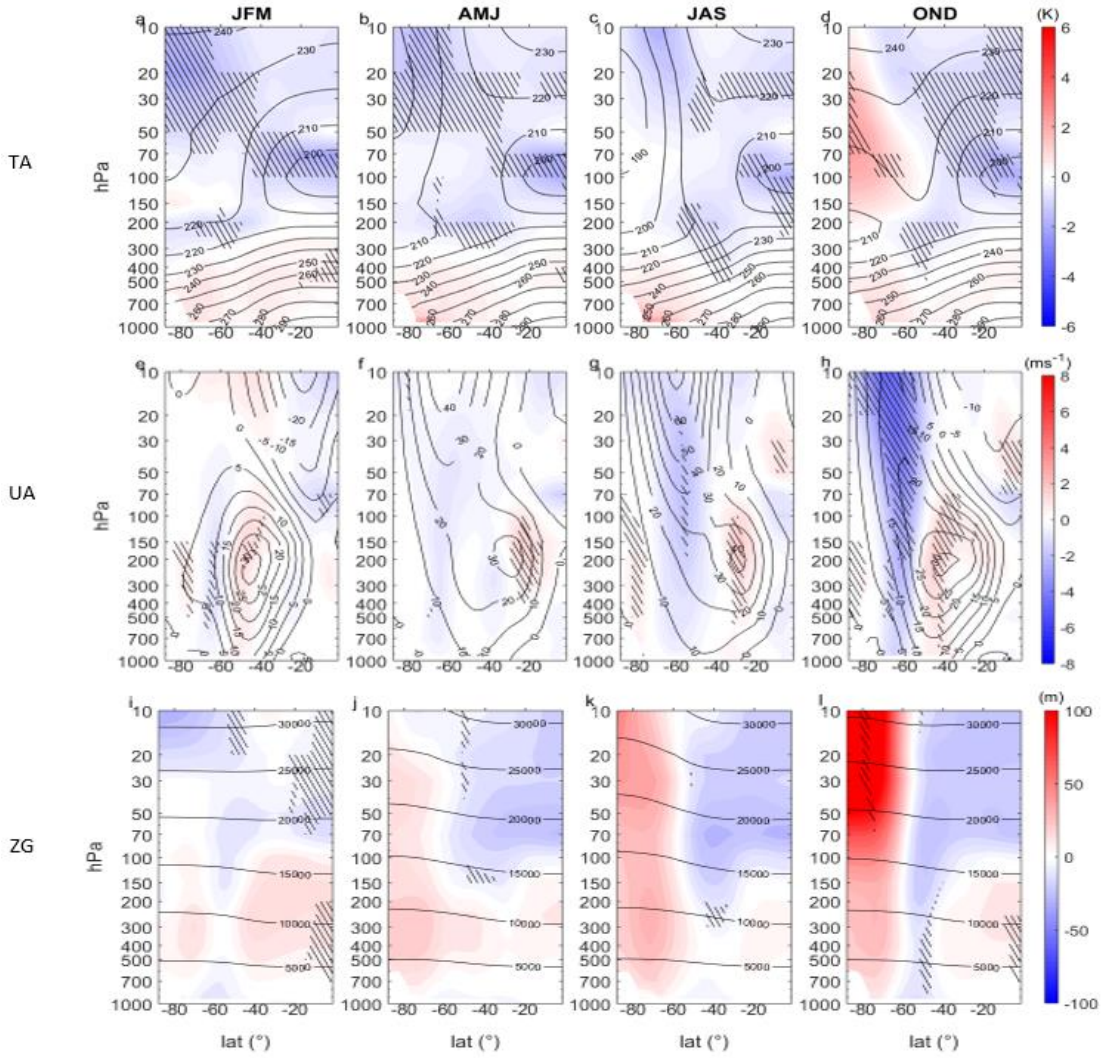

Figure 4.5*: Multi-model-mean inferred zonal-mean air temperature response to Antarctic sea-ice loss in (a) summer (January-March; JFM), (b) autumn (April-June; AMJ), (c) winter (July-September; JAS) and (d) spring (October-December; OND). The black contours show the baseline climatology and hatching indicates where nine or more models have the same signed response as the multi-model mean. (e-h) As (a-d), for zonal-mean westerly wind. (i-l) As (a-d), for zonal-mean geopotential height.*

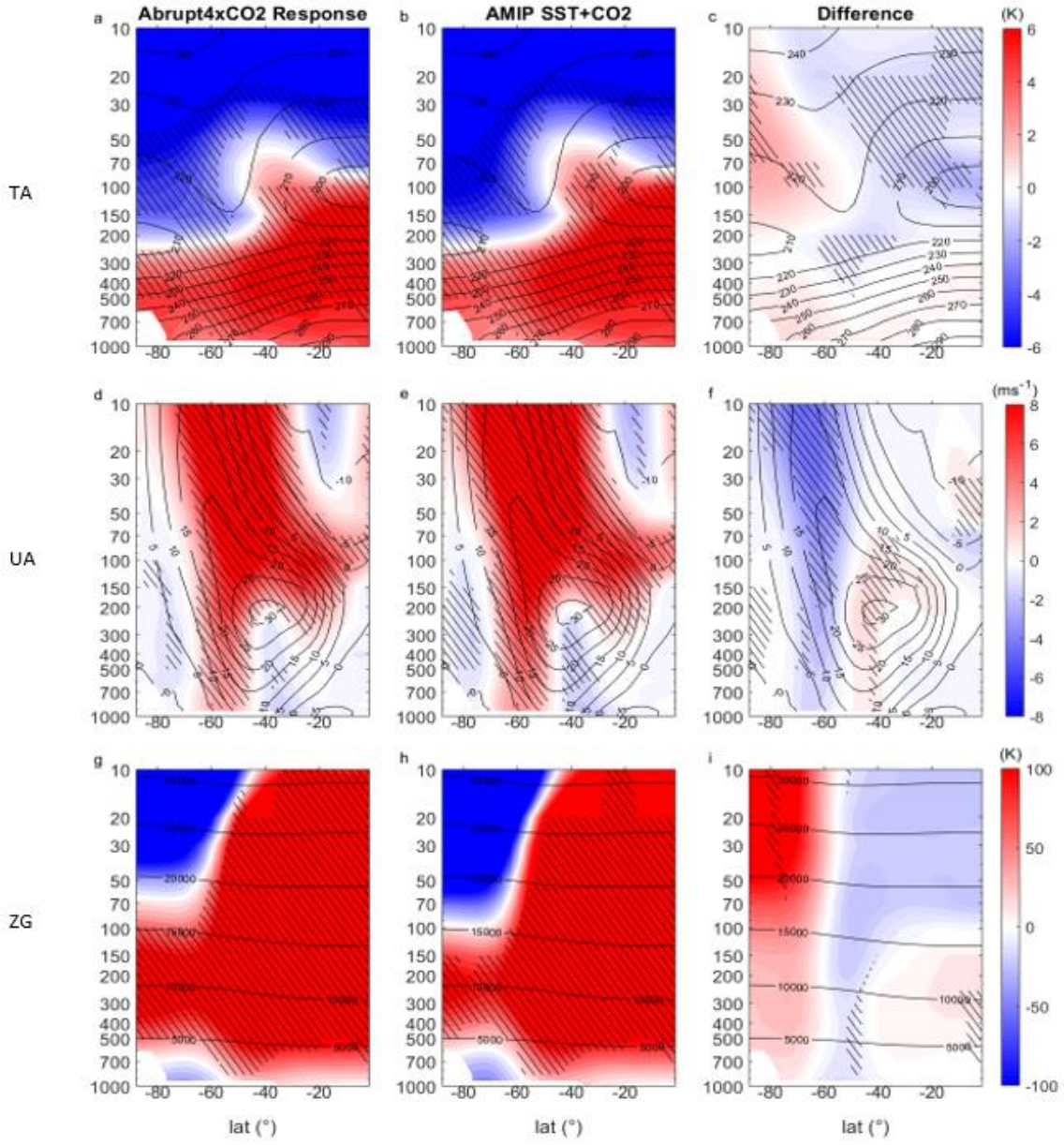

***Figure 4.6**: Austral spring (October-December) multi-model-mean zonal-mean air temperature for (a) Abrupt4xCO_2 response to PiControl (b) AMIP SST+CO_2 and (c) inferred response to Antarctic sea-ice loss. The black contours show the baseline climatology and hatching indicates where nine or more models have the same signed response as the multi-model mean. (d-f) As (a-c), for zonal-mean westerly wind. (g-i) As (a-c), for zonal-mean geopotential height.*

Zonal-mean 850 hPa zonal wind changes as a function of calendar month show a strengthening and poleward shift of the tropospheric eddy-driven jet in the total response to quadrupled CO_2 and the component due to combined SST and direct CO_2 change (Figure 4.7 a&b). In contrast, the inferred response to sea-ice loss (Figure 4.7c) displays a weakening of the jet in all months, with the largest decrease in spring and summer. During these months there is also an increase in wind westerly wind component on the equatorward flank of the jet, associated with a slight northward jet shift.

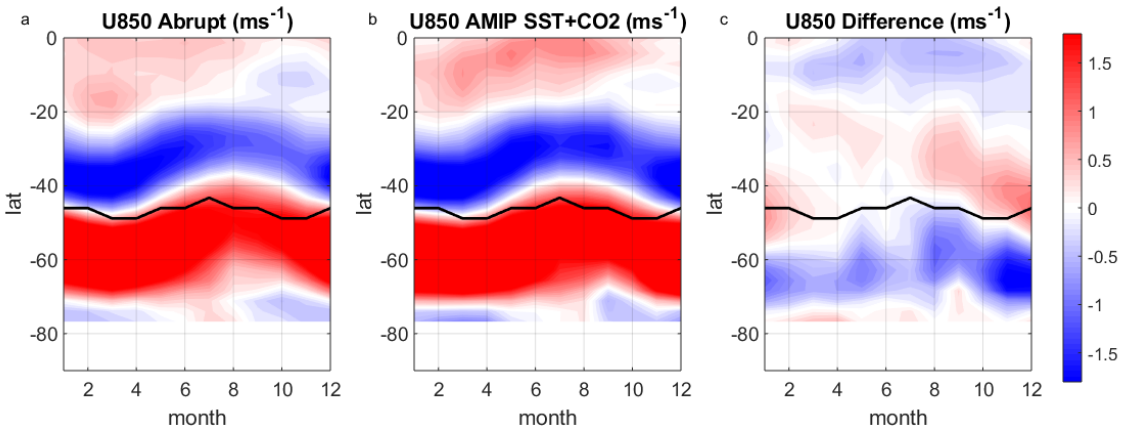

***Figure 4.7**: Multi-model-mean, zonal-mean zonal wind at 850hPa (U850) monthly averages for (a) Abrupt4xCO_2 response to PiControl (b) AMIP SST+CO_2 response to AMIP and (c) the inferred response to Antarctic sea-ice loss. The thick black line represents the climatological jet position.*

Figure 4.8 shows the inferred polar cap height (PCH; geopotential height averaged south of 90° – 70° S) response to sea-ice loss as a function of month and altitude. From winter to spring, PCH increases, from the mid-troposphere to lower stratosphere, the latter indicating a weakening of the polar vortex. In spring

and early summer (September-December) PCH also increases in the upper stratosphere (Turner et al., 2017).

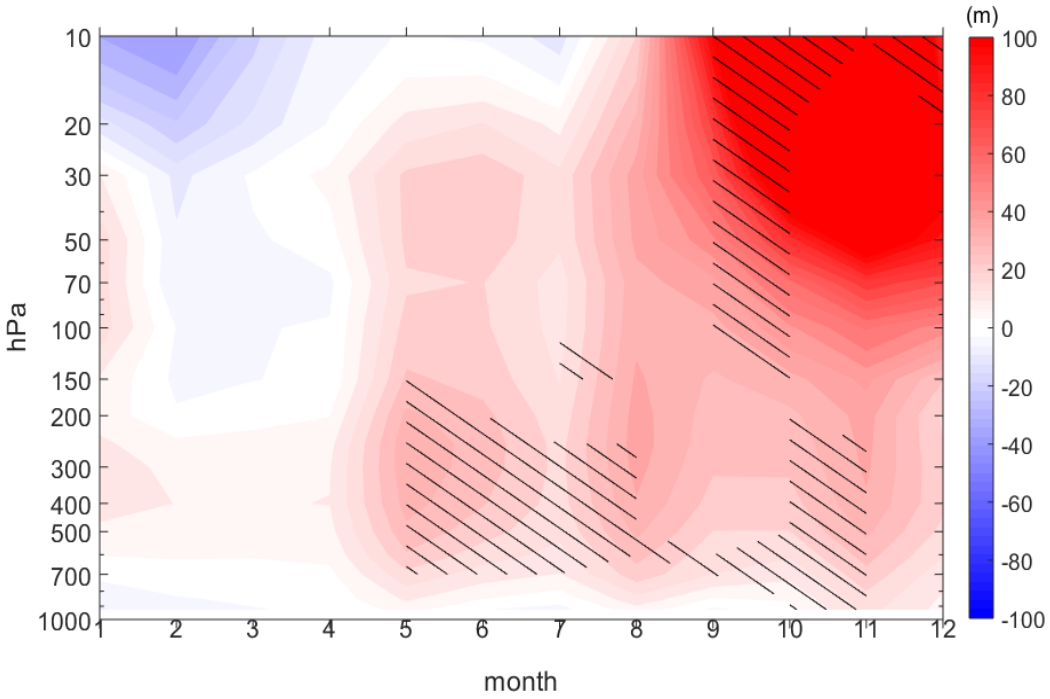

***Figure 4.8**: Multi-model-mean inferred zonal-mean geopotential height response to Antarctic sea-ice loss with time over the Antarctic polar cap (90° – 70° S). Hatching indicates where nine or more models have the same signed response as the multi-model mean.*

4.2.4 Jet, SPV and SAM dynamics

Figures 4.2 and 4.5 suggest changes in the westerly jet in response to sea-ice loss, which can be better quantified using the jet latitude and jet strength metrics. The inferred jet latitude response (Figure 4.9a) shows an equatorward shift in August to February, of 1.5° latitude at its maximum in December. December and April are the only months when eight models agree on the sign of the jet latitude response, with approximately seven or fewer models agreeing on the sign of the response in other calendar months. The eddy-driven jet strength is decreased

from August to December, with the biggest reduction in jet strength of 0.75 ms^{-1} found in November and corroborated by 9 models (Figure4.9b). Changes in the SAM index mimic those of jet strength (Figure 4.9e).

The simplest dynamical explanation for the eddy-driven jet weakening is the reduction in the near-surface temperature gradient and resultant decreased baroclinicity (Kidston et al., 2011). It is noted that the jet responses to sea-ice loss are small and, in most months, of opposite sign compared to those simulated in response to SST and CO_2. The jet strength and in particular, jet latitude responses are less robust than the 500 hPa westerly wind and zonal-mean zonal wind responses described earlier. This study posits that more varied jet responses reflect differences in the average latitude of the jet across the models. Models with a more southerly located jet tend to simulate a poleward-shifted jet in response to sea-ice loss, whereas those with a more northerly located jet tend to simulate an equatorward-shifted jet in response to sea-ice loss, with correlation coefficients of -0.84 in winter, and -0.62 in spring, demonstrating a strong negative relationship, most prominent in winter (Figure 4.9c). The models that depict a strengthening jet in response to sea-ice loss have their jets too far north, at around 40° S, at latitudes where the westerly wind increases (Figure 4.5). The zonal-mean westerly wind decrease is largest at 60 °S (Figure 4.5), poleward of the mean jet, and thus, the models with more poleward-located jets are also those that simulate the largest reductions in jet strength in response to sea-ice loss, with slightly lower correlation coefficients of 0.79 in winter, and 0.56 in spring (Figure 4.9d). These relationships are strongest in winter and spring (not shown for other seasons) and are reminiscent of similar dependencies seen for the

projected jet response to increased greenhouse gas concentrations (e.g., Bracegirdle et al, 2018a; Kidston & Gerber, 2010)

Figure 4.5 suggests a weakening of the SPV in the spring. To explore the seasonality of the polar vortex further, Figure 4.9f shows the annual cycle of the SPV strength change in response to sea-ice loss. It is noted that the SPV breaks down each year in November/December and reforms in the following autumn. The inferred response to sea-ice loss shows decreases in SPV strength between September and December, corroborated by eight (or more) models, with a maximum weakening of 4.5 ms^{-1} in October.

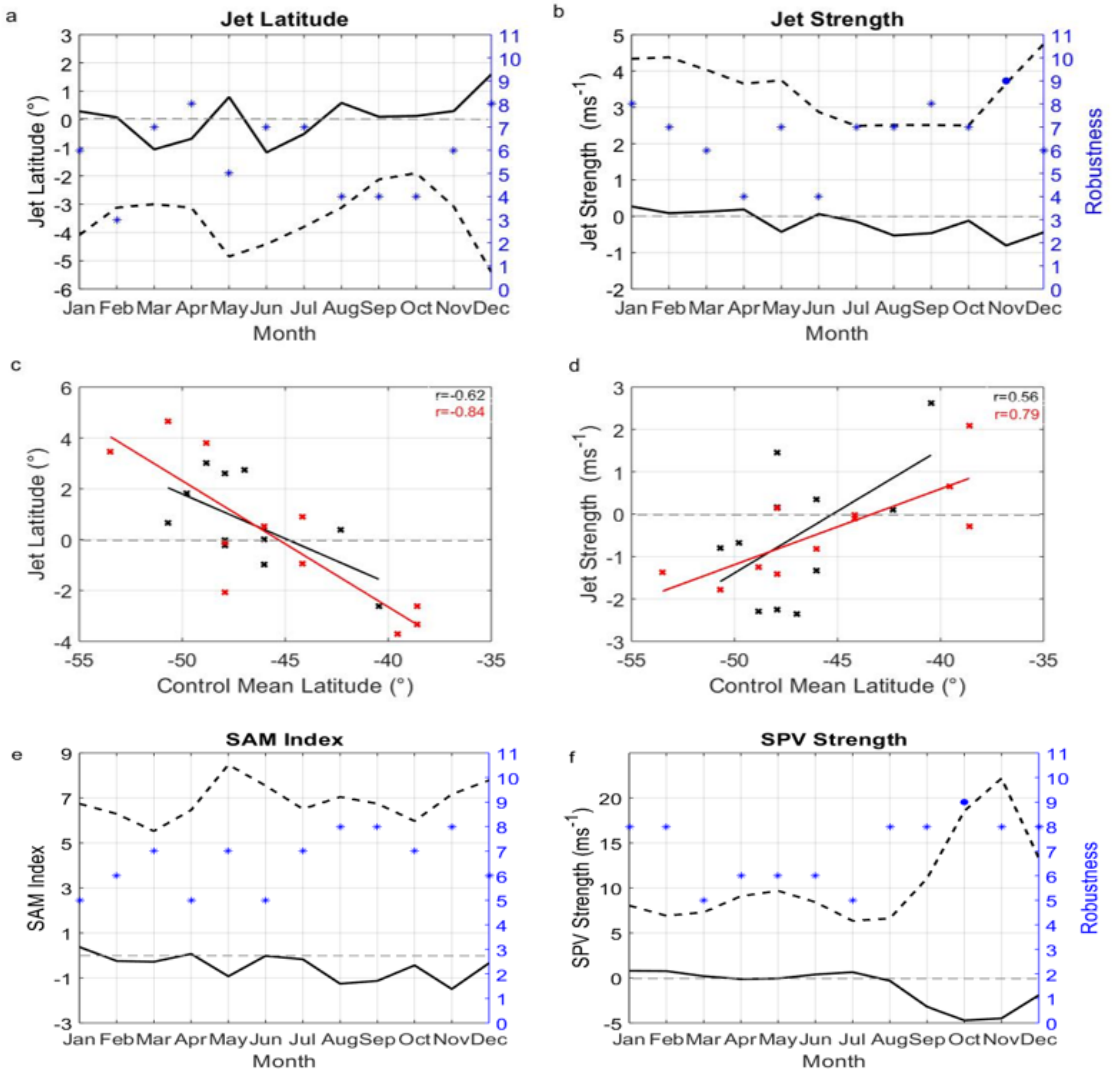

***Figure 4.9**: Multi-model-mean inferred jet latitude response to Antarctic sea-ice loss (black line) and the combined response to SST and CO_2 (dashed line) as a function of calendar month. The right-hand vertical axis (in blue) shows the number of individual models that have the same signed response to sea-ice loss as the multi-model-mean, with filled dots indicating nine or more models agree and stars indicating fewer than nine models agree. (b) As (a), but for jet strength. (c) Jet latitude response to Antarctic sea-ice loss as a function of the climatological jet latitude in the preindustrial control simulation for each model (crosses) and for winter (red) and spring (black). Also shown are the linear relationships and their associated correlation coefficients. (d) As (c) but for jet strength. (e) As (a), but for the Southern Annular Mode (SAM). (f) As (a), but for the stratospheric polar vortex strength (SPV). The SAM index was defined as the standardized zonal-mean sea level pressure difference between 40° S and 65° S. The SPV strength was calculated as the 10 hPa zonal-mean zonal wind velocity at 60° S.*

4.3 Discussion

The results suggest an overall weakening of the eddy-driven jet and negative shift in the SAM index in response to projected Antarctic sea-ice loss, particularly in spring. These results are in broad agreement with past studies using individual models (Bader et al., 2013; England et al., 2018; Menéndez et al., 1999; Raphael et al., 2011; Smith et al., 2017), but this is the first to provide evidence from a multi-model ensemble. The weakening of the eddy-driven jet and negative SAM in response to sea-ice loss counteract, but only partially offset, the projected jet strengthening and positive SAM in response to increased CO_2. Thus, projected sea-ice loss acts to slightly weaken the jet and SAM response to increased CO_2.

This study has shown that the SAM response to projected sea-ice loss primarily reflects changes in eddy-driven jet strength and to a lesser extent, changes in jet latitude, consistent with England et al. (2018).

This suggests that variations in sea ice are more closely tied to the jet strength than the jet latitude. Bracegirdle et al. (2018) found a similar result but considering uncertainty in the projected jet response. These authors found that half of the variance in the strengthening of the jet across different models is related to different historical representation of SIA, and that links between the projected jet shift and SIA were much weaker.

The results suggest a feedback between sea ice and the SAM, although the sign of this feedback is unclear. On interannual timescales, the SAM affects sea ice through changes in wind-driven near-surface ocean circulation. During the positive SAM phase, enhanced northward Ekman transport of colder waters can cause the ice pack to expand (Gupta & England, 2006; Purich et al., 2016). Conversely during negative SAM, anomalous southward Ekman transport can reduce the sea ice cover. If sea-ice loss causes a more negative SAM, as the results suggest, then this may reinforce sea-ice loss. However, it has been suggested that relationships between the SAM and sea ice may be opposite on decadal or longer timescales, with the slow response being governed by changes in eddy heat transport and upwelling rather than surface wind-driven currents (Ferreira et al., 2015; Kostov et al., 2017; Screen et al., 2009). If negative SAM is associated with Southern Ocean cooling and sea ice expansion, then the negative SAM response to sea-ice loss could suppress sea-ice loss.

In many respects, the multi-model-mean response to projected Antarctic sea-ice loss is analogous to that in response to projected Arctic sea-ice loss. Consistent features of the multi-model responses to Arctic and Antarctic include the weakening of the eddy-driven jet, shift towards the negative phase of the annular mode, and weakening of the SPV, albeit with some differences in seasonality as also noted by England et al. (2018) for one model. One difference between the results and that for the multi-model-mean response to projected Arctic sea-ice loss is that near-surface temperature response to Antarctic sea-ice loss does not extend over the Antarctic continent (Figure 2), whereas the surface temperature response to Arctic sea-ice loss does spread to the northern high-latitude continents (e.g., Zappa et al., 2018). It is speculated that the high elevation of Antarctica isolates the continent from the low-level sea ice-induced warming. In contrast, Krinner et al. (2014) found a large temperature response over the continent in atmosphere-only simulations with prescribed changes in sea ice and SST. This implies that broader SST warming is key to warming over the Antarctic plateau.

The results suggest a different seasonality to the stratospheric response to projected Antarctic sea-ice loss to that in England et al. (2018). This study found a robust multi-model-mean weakening of the stratospheric zonal wind only in spring, whereas in the single model experiments of England et al. (2018), the stratospheric zonal wind was weakened in autumn and winter, but not in spring. The seasonal timing of maximum stratospheric response shown here is more in line with that in response to projected Arctic sea-ice loss. In the Northern Hemisphere, sea-ice loss appears to enhance the upward propagation of

planetary scale waves causing a weakening of the polar vortex in late boreal winter or spring (e.g., Kim et al., 2014). However, it is unclear whether this mechanism operates in the Southern Hemisphere and the zonal symmetry of multi-model-mean tropospheric circulation response implies only small changes in upward wave propagation. Further work with dedicated sea ice perturbation experiments, were assessed throughout this thesis, however, this result was not reproduced in the latter chapters.

4.4 Summary of Chapter 4

This study has presented the first multi-model analysis of the atmospheric response to projected Antarctic sea-ice loss. Some aspects of the atmospheric circulation response to sea-ice loss were robust across eleven models, despite large differences between the models in many other aspects. The results suggested that projected sea-ice loss caused a robust weakening of the tropospheric westerly jet and favoured the negative phase of the SAM, of greatest magnitude and robustness in spring and summer. In these regards, the response to sea-ice loss acts to weakly damp the strengthening westerly jet and positive SAM responses to increased CO_2. The SAM response to sea-ice loss primarily reflected a reduction in jet strength and to a lesser extent, an equatorward shift in the jet. In spring, this study found multi-model evidence for a weakening polar stratospheric vortex and coupling between the stratospheric and tropospheric zonal wind responses. Sea-ice loss induces warming in the lowermost atmosphere over the high-latitude Southern Ocean, but this warming did not penetrate over the Antarctic continent.

Chapter 5

Atmospheric Response to Abrupt Antarctic Sea-Ice Loss in HadGEM3-GC3.1.

This chapter examines the atmospheric component of the coupled low resolution HadGEM3-GC3.1 response to abrupt Antarctic sea-ice loss. Section 5.1 discusses the previous literature on the atmospheric response to Antarctic and Arctic sea-ice loss, and the importance of ocean-atmosphere coupling. Sections 5.2.1 to 5.2.3 describe the albedo-induced Antarctic sea-ice loss and associated changes in ocean-to-atmosphere heat fluxes, the spatial pattern of the atmospheric response, and the vertical structure of the atmospheric response, respectively. Section 5.2.4 examines the fast and slow components of the response, and Section 5.2.5 compares the response to Antarctic sea-ice loss to that in response to quadrupled CO_2. Lastly, Section 5.3 discusses these results, with a summary in Section 5.4.

5.1 Introduction

The climate response to Arctic sea-ice loss has been well studied (e.g., Blackport & Kushner, 2016; Blackport, Screen, 2020; Cohen et al., 2014; Deser et al., 2015; Kim et al., 2014; Peings & Magnusdottir, 2014; Screen et al., 2018; Screen & Simmonds, 2013; Screen et al., 2013; Vavrus, 2018; Zappa et al., 2018). By comparison however, only a handful of modelling studies have been conducted on the impacts of Antarctic sea-ice loss. Model studies forced by observed sea ice trends suggest that the growth in Antarctic sea ice results in a slight poleward shift of the tropospheric eddy-driven jet and a positive SAM anomaly in winter

months (Raphael et al., 2011; Smith et al., 2017). Modelling studies, using atmosphere-only model configurations prescribed with projected Antarctic sea-ice loss, have found contrasting results on the impact on the location of the mid-latitude tropospheric eddy-driven jet, but generally agree that there is a reduction in its strength (Bader et al., 2013; England et al., 2018; Kidston et al., 2011; Menéndez et al., 1999). In addition to the impacts on the jet, England et al. (2018) found that the responses to Antarctic sea-ice loss were more vertically confined, of smaller amplitude, and less seasonally variable than the well-studied response to Arctic sea-ice loss. Non-direct methods using the CMIP5 multi-model ensemble to estimate the response to Antarctic sea-ice loss (Ayres & Screen, 2019; Bracegirdle et al., 2018), suggest that there is a weakening of the eddy-driven jet but not a significant equatorward shift, and a corresponding negative shift in the SAM index. Atmosphere-only experiments show an increase in surface temperatures over the regions of sea-ice loss, extending over neighbouring parts of the high-latitude Southern Ocean, but not over the Antarctic continent or into lower latitudes (Ayres & Screen, 2019; England et al., 2018).

Up until recently, all model experiments on the response to Antarctic sea-ice loss have used either atmosphere- or ocean-only simulations (i.e., uncoupled). It is becoming increasingly apparent that coupled models are needed to fully capture the global scale and magnitude of the response to Arctic sea-ice loss (Deser et al., 2016; Smith et al., 2017; Tomas et al., 2016). These coupled model experiments indicate that the influence of Arctic sea-ice loss may extend across the globe and not only be manifest in high latitudes (Blackport & Kushner, 2016; Deser et al., 2016; Deser et al., 2015; Oudar et al., 2017). One study found that when an atmosphere-only model was used, the response to Arctic sea-ice loss

was limited to north of 30° N, but with ocean-atmosphere coupling, the responses were seen over the whole globe (Deser et al., 2015). Remote responses included tropical upper-tropospheric warming, an enhanced global hydrological cycle, and an equatorward shift of the ITCZ (Deser et al., 2016, 2015).

Studies on the response to Arctic sea-ice loss, mentioned above, have highlighted the importance of using coupled models. England et al., (2020) was the first study to use a coupled climate model to assess the impact of Antarctic sea-ice loss and showed that ocean dynamics are important in capturing the global response to Antarctic sea-ice loss, just as is the case for the response to Arctic sea-ice loss. These authors found that the tropical response to Antarctic sea-ice loss is alike that to Arctic sea-ice loss, particularly in the eastern equatorial Pacific. It has been well studied that Arctic sea-ice loss triggers a zonal asymmetric response in tropical SSTs, with greatest warming in the eastern equatorial Pacific enhancing tropospheric warming, which impacts the strength and location of the Hadley Cell (e.g., Chemke et al., 2019; Deser et al., 2015; Smith et al., 2017; Sun et al., 2018; Sun et al., 2020; Tomas et al., 2016). An equatorward intensification of the ITCZ was also simulated. Antarctic sea-ice loss induced a ‘mini global warming’ signal, comparable to that in response to Arctic sea-ice loss, having a spatial pattern like that seen in response to increased greenhouse gas concentrations, but with smaller magnitude. A second paper by the same authors describes a robust Arctic warming in response to Antarctic sea-ice loss, propagated through the tropical Pacific and associated teleconnections to the Aleutian Low (England et al., 2020).

This chapter presents the atmospheric results from the coupled HadGEM3-GC3.1 abrupt Antarctic sea-ice loss experiment described in Section 3.2. Recall, this experiment used the HadGEM3-GC3.1 n96 ORCA1 global coupled model, adapting the CICE code to set all Antarctic sea ice to have the albedo of a melt pond rather than bare ice, triggering an abrupt loss of Antarctic sea ice. The model was run for 300 years to quasi-equilibrium, in order to assess both the fast and slow responses. All stated seasons refer to the austral seasons, unless otherwise specified.

5.2 Results

5.2.1 Sea ice

Annual-mean Antarctic SIA is 13.5×10^6 km^2 in the control simulation (Figure 5.1a), averaged across years 20-300. Following the albedo perturbation, SIA decreases to 8×10^6 km^2 in year 5, then to 7×10^6 km^2 by year 20. After this, SIA continues to decrease slowly to 6×10^6 km^2 in year 300. The control simulation also exhibits a slight decreasing trend and thus, the anomaly (perturbation minus control) remains fairly level from year 20 to 300, but with interannual and (multi-)decadal variability (Figure 5.1b). Total annual-mean Antarctic SIT decreases by 0.25 m within the first two years, then remains constant with small variations throughout the time series (Figure 5.1c).

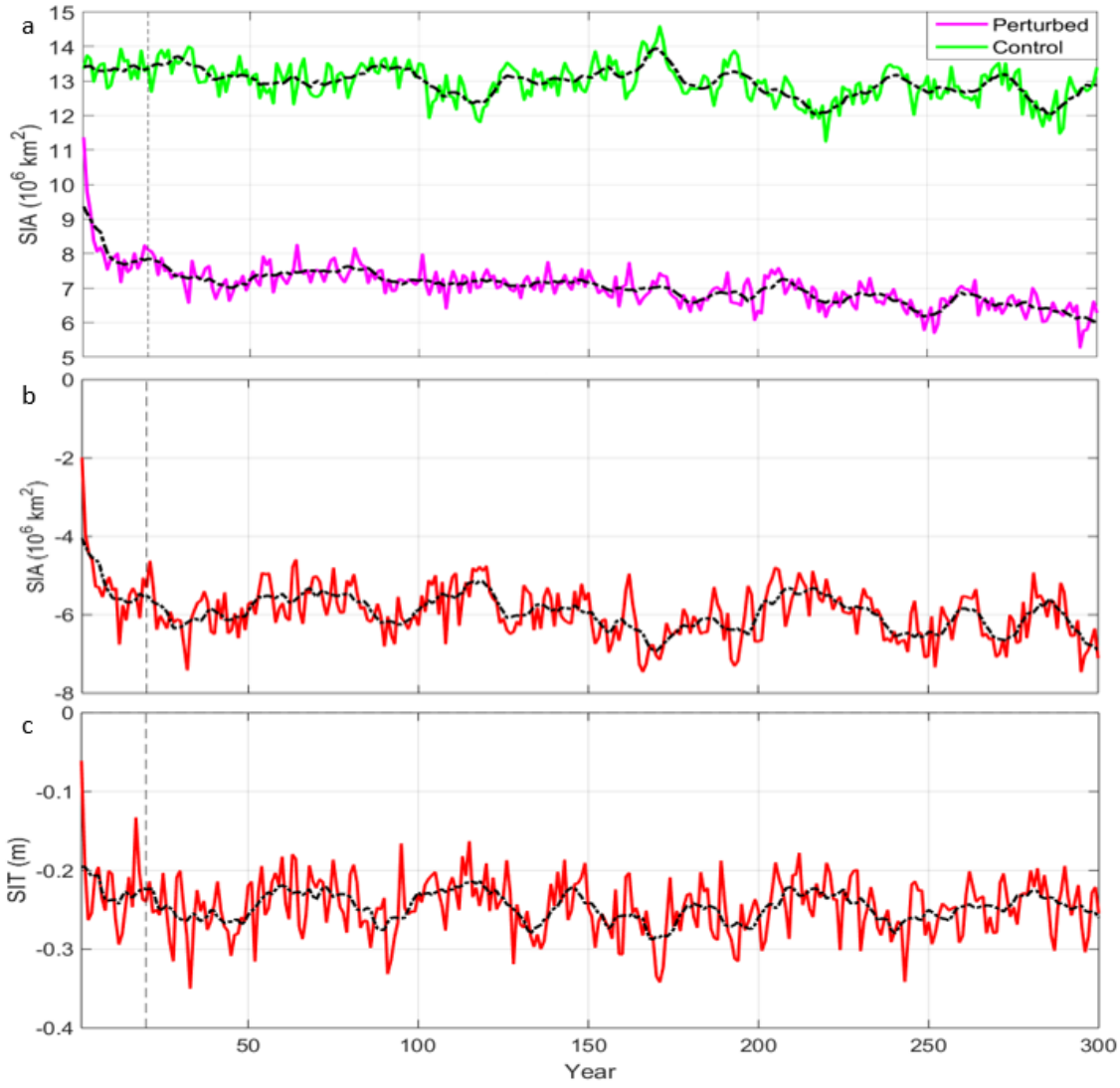

***Figure 5.1**: Annual average sea ice area (SIA) for the control (green) and perturbed (purple) simulations, with ten year running mean (black dashed line) (a). Annual average sea ice area (SIA) anomaly between perturbed and PiControl data with ten year running mean (black dashed line) (b). Dashed line indicating end of spin up period. (c) As (b) for sea ice thickness (SIT).*

The perturbed albedo simulation exhibits a complete loss of sea ice in summer and a 40% loss in SIA in winter, relative to the preindustrial control state (Figure 5.2 a&b). The seasonal cycle of SIA loss in real terms (i.e., in square kilometres) is largest in early summer, when the effect of the albedo change is largest, owing

to maximum incoming solar radiation, and smallest in late summer, when there is little ice to start with. This overall loss is comparable to sea-ice loss projected under quadrupled CO_2 or in the high emission RCP8.5 scenario by the end of the 21st century (Section 3.2), although yielding greater ice loss in the summer, and a considerable lesser ice loss in winter. This seasonal cycle of ice loss is a characteristic of the albedo reduction method, which has greatest influence in summer when incoming solar radiation is at a maximum (Sun et al., 2019).

SIT in the Southern Hemisphere displays a decrease in all seasons except December, with a maximum change of -0.82 m in March (Figure 5.2c). The total turbulent heat flux to the atmosphere peaks in winter at 500 TW and is smallest in summer at less than 100 TW (Figure 5.2d). This seasonal cycle reflects both the magnitude of sea-ice loss in each month and the magnitude of the air-sea temperature difference. Although the albedo was only changed in the Southern Hemisphere, Arctic SIA shows 24% loss in boreal summer and 5% loss in boreal winter, which, although considerably lesser in magnitude than in the Southern Hemisphere, demonstrates a significant reduction of Arctic sea ice in response to Antarctic sea-ice loss.

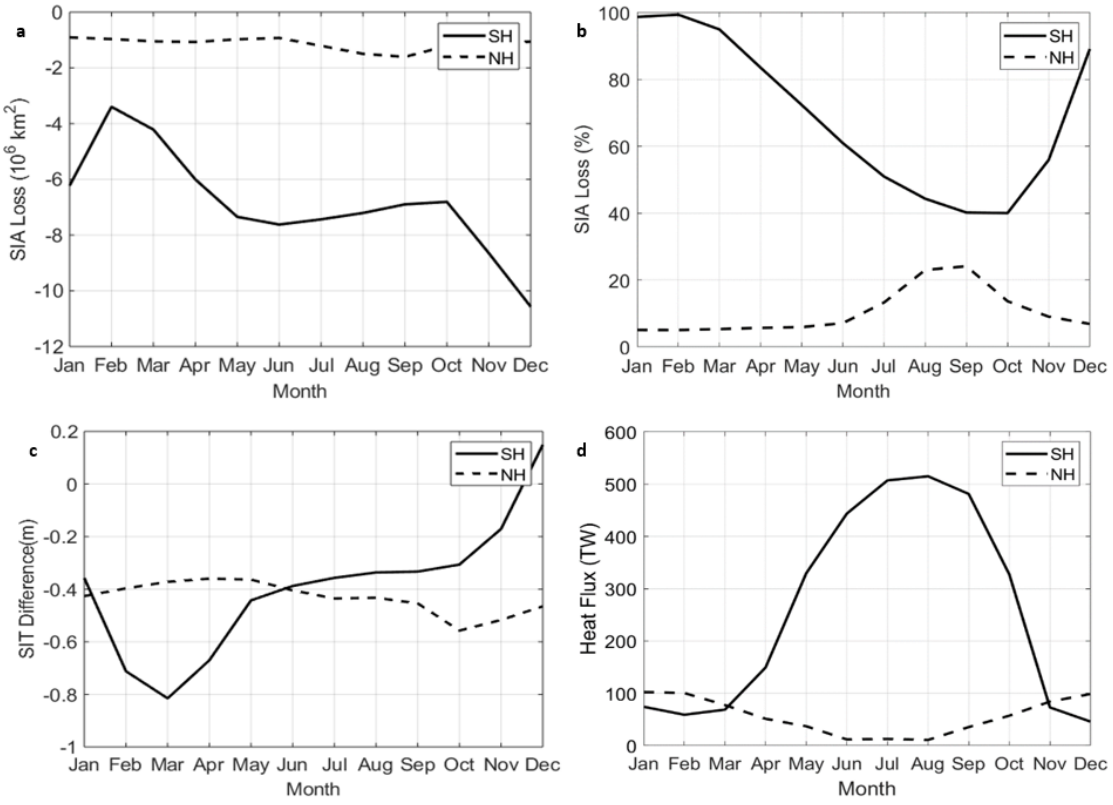

Figure 5.2*: Total sea ice area (SIA) response to Antarctic sea-ice loss as a function of calendar month (a), with the solid line showing the Southern Hemisphere ice response and the dashed line showing Northern Hemisphere ice response. (b) As (a) for percentage of sea ice area (SIA) loss. (c) As (a) for sea ice thickness (SIT). (d) As (a) for the surface turbulent heat flux response, calculated as the area- weighted surface turbulent (sensible plus latent) heat flux response, summed over grid points where the sea ice concentration differs between the control and the Antarctic sea-ice loss states. The heat flux is defined as positive in the upward direction.*

The Arctic sea ice response is delayed by twenty years compared to the imposed sea ice reduction in the Antarctic (Figure 5.3). This delay suggests that the pole-to-pole response may be governed by slow oceanic processes, a concept returned to later in Section 5.2.4.

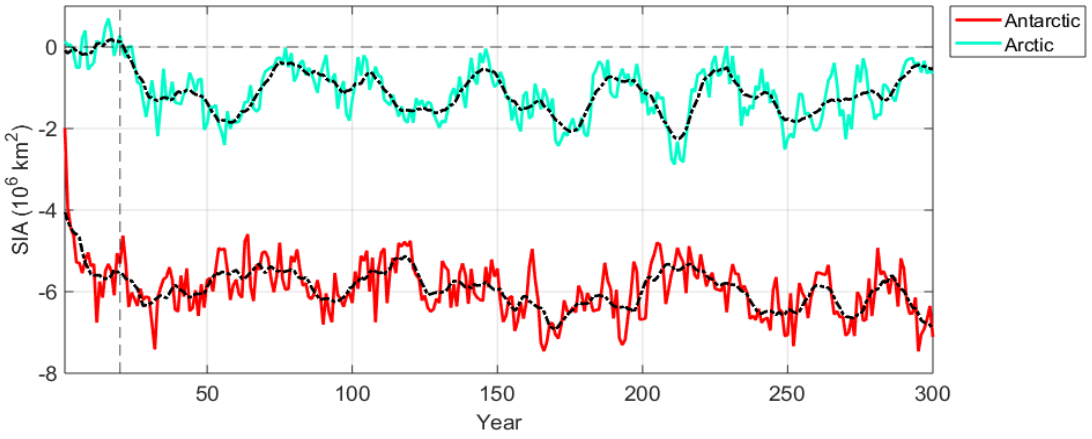

***Figure 5.3**: Annual average sea ice difference between perturbed and PiControl data for Antarctic (red) and Arctic (blue), with ten year running mean (black dashed line). Dashed line indicating end of spin up period.*

SIC is reduced all year round in the Southern Hemisphere (Figure 5.4 a-d), being of greatest magnitude near the ice edge, which migrates with the seasons. In the Arctic, there is less than 5% SIC reduction, mostly in the Barents Kara Sea in boreal winter and spring, but extending across the Arctic Ocean in boreal summer and autumn. SIT in both the Antarctic and Arctic is reduced in all seasons (Figure 5.4 e-h). The spatial pattern of the net heat flux responses (Figure 5.4 i-l) largely mimics that of SIC, with largest increases in the ocean-to-atmosphere heat exchange in regions of ice loss, and seasonally greatest in autumn and winter. Reductions in the net heat flux (atmosphere- to-ocean) are seen northward of the

sea ice edge in the Southern Ocean, reflecting anomalous heat input. In the Arctic, increased heat fluxes are simulated in the colder boreal seasons and in regions of SIC loss, namely the Barents-Kara Sea.

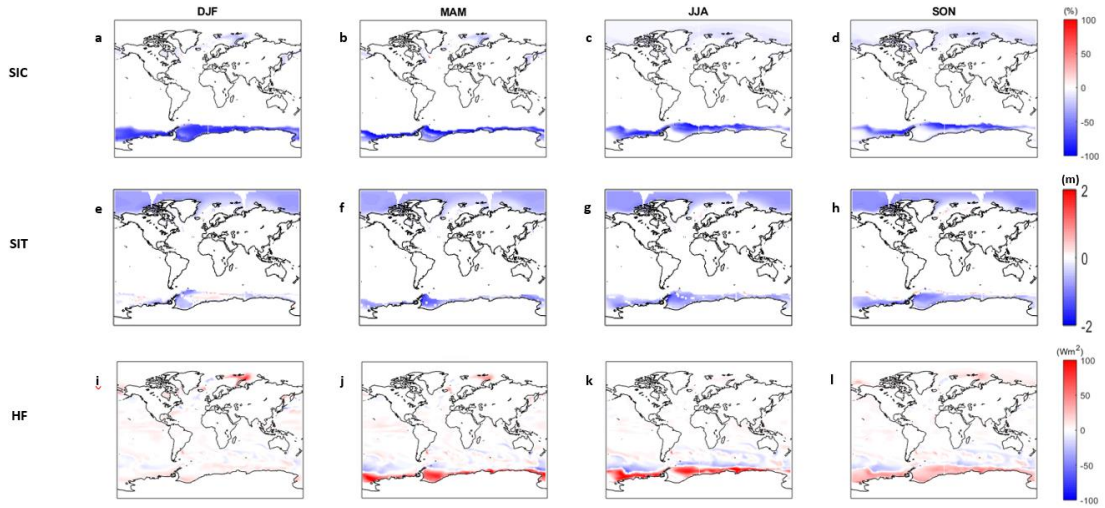

***Figure 5.4**: Sea ice concentration (SIC) response to Antarctic sea-ice loss in austral (a) summer (December-February; DJF), (b) autumn (March-May MAM), (c) winter (June-August; JJA) and (d) spring (September-November SON). (e-h) As (a-d) for sea ice thickness (SIT) response. (i-l) As (a-d) for surface turbulent heat flux response. The heat flux is defined as positive in the upward direction.*

5.2.2 Spatial pattern of atmospheric response

The near-surface air temperature response is global in reach, reaching as high as 15 K over regions of Antarctic sea-ice loss (Figure 5.5 a-d). In polar regions, there is a clear seasonal cycle, with the largest warming in autumn and winter, in each hemisphere, as expected from the heat flux response (Figure 5.2). An increase in temperature over the Antarctic continent is present in all seasons (Figure 5.6 a-d), with coastal regions warming the most, by up to 5 K in winter

and spring, but significant warming extending to the high-altitude plateau in all seasons. There is substantial warming of up to 4 K in the northern regions of the Southern Ocean. Over the tropics, surface warming is similar in each season, albeit of smaller magnitude than at the poles. In the high latitudes of the Northern Hemisphere, north of 50° N, there is an increase in near-surface air temperature of between 3 K and 8 K, in all seasons apart from boreal summer. The largest increases in near-surface air temperature are in the Barents-Kara Sea in boreal winter, again consistent with the spatial and seasonal pattern of the heat flux response

The mean sea level pressure (MSLP) response (Figure 5.5 e-h) to Antarctic sea-ice loss shows an increase over Antarctica, up to 220 Pa, with the largest and most significant increase in autumn. This high-latitude MSLP increase maps onto the negative phase of the SAM. However, the MSLP response over the Southern Ocean is not zonally symmetric. There is a clear weakening of the ASL from autumn to spring (i.e., increased MSLP), and decreased MSLP in the Weddell Sea in all seasons. North of 50° S, one notable feature is the MSLP decrease over the North Pacific, reflecting a strengthened Aleutian Low in boreal winter and spring.

The zonal wind response at 500 hPa (U500) (Figure 5.8i-l) displays a decrease over the latitudes of the westerly jet in all seasons, suggesting a weakening of the jet, which is largest in autumn and winter. The maximum decrease, in winter, amounts to an ~10 % reduction in the mean westerlies. The increase of the equatorward flank of the westerly is less significant. The zonal velocity increases

over the Antarctic continent. Over the Equatorial Pacific, there is a decrease in the easterly equatorial trade winds in December to January. The zonal wind increases over the northern sub-tropics in boreal winter and spring, suggesting a strengthening of the subtropical jet; and decreases in northern mid-latitudes, suggesting a weakening of the eddy-driven jet, again largest in boreal winter and spring.

Precipitation (Figure 5.5 & 5.6 e-h) significantly increases over areas of Antarctic sea-ice loss and the surrounding Southern Ocean, extending to 40° S in the Atlantic. Over the Antarctic continent, there is an increase of up to 0.5 mm/day in the coastal regions, with higher latitudes and altitudes seeing a smaller but significant increase in all seasons. In addition, a small increase in Arctic precipitation is simulated in boreal autumn and winter in the regions of Arctic sea-ice loss. An interesting remote response is simulated in the tropics, which is worthy of closer examination.

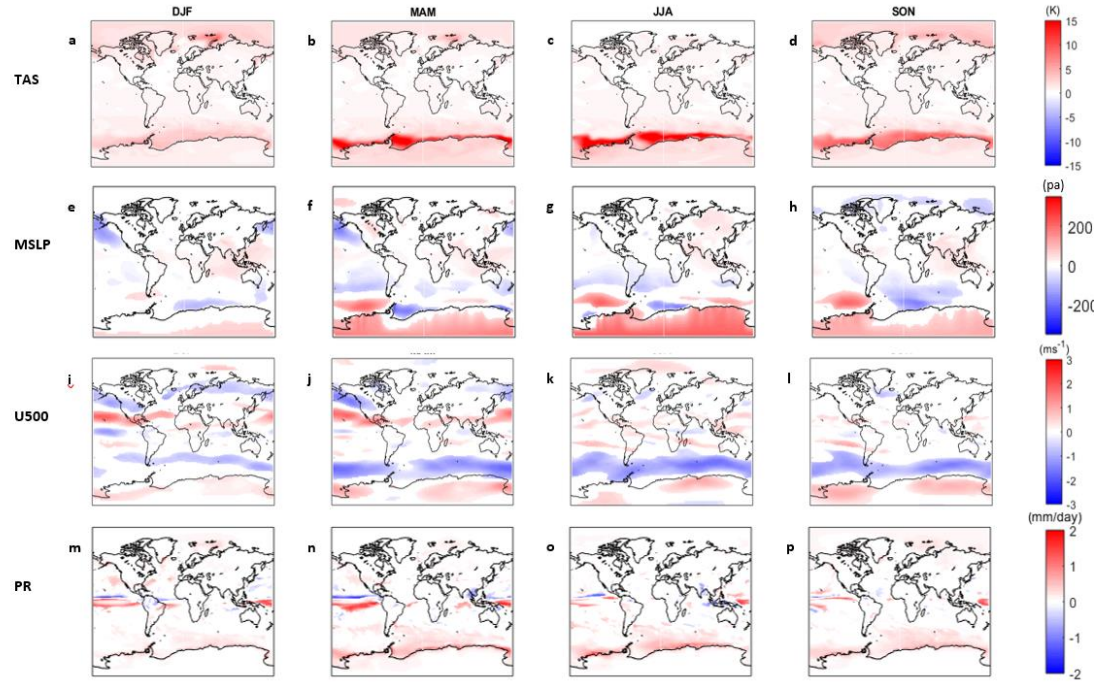

***Figure 5.5**: Surface air temperature (TAS) response to Antarctic sea-ice loss in austral (a) summer (December-February; DJF), (b) autumn (March-May MAM), (c) winter (June-August; JJA) and (d) spring (September-November SON). (e-h) As (a-d), for mean sea level pressure (MSLP). (i-l) As (a-d), for 500 hPa westerly wind (U500). (m-p) as (a-d) for total precipitation (PR).*

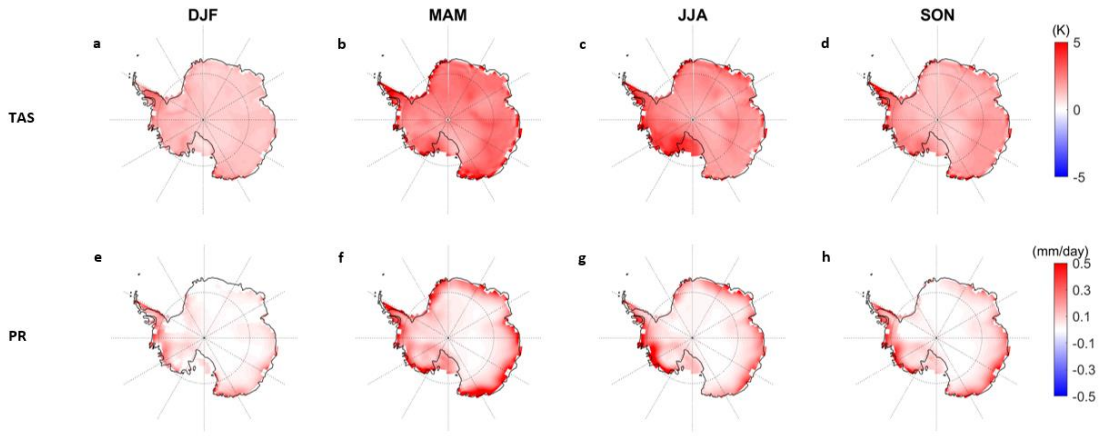

***Figure 5.6:** Continental Surface air temperature (TAS) response to Antarctic sea-ice loss in austral (a) summer (December-February; DJF), (b) autumn (March-May MAM), (c) winter (June-August; JJA) and (d) spring (September-November SON). (e-h) As (a-d) for total precipitation (PR).*

The annual-mean precipitation response over the tropical Pacific (Figure 5.7 a&b) shows a decrease in a band north of the equator, which is climatologically wetter, and an increase along the equator, which is climatologically drier. This suggests a shift of the ITCZ, analogous but of smaller magnitude to that simulated in response to increased greenhouse gas concentrations (Collins et al., 2013). The spatial pattern of the tropical precipitation response resembles that of SST, with increased precipitation in regions of greater ocean surface warming, relative to the global mean, and reduced precipitation in regions of lesser ocean surface warming, again relative to the global mean (Figure 5.7c). The mechanisms for this tropical SST warming will be returned to later.

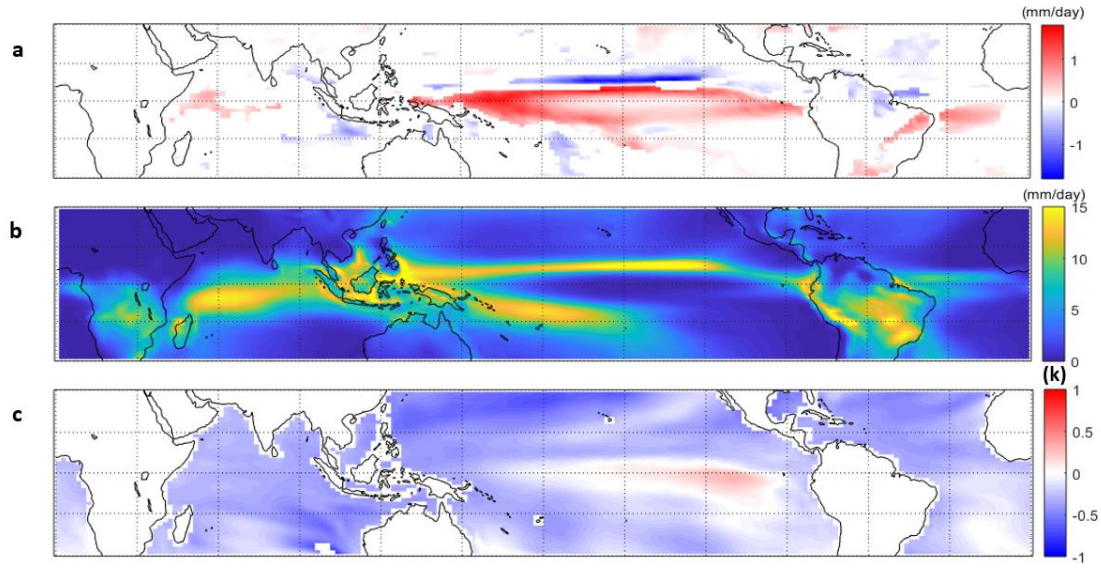

***Figure 5.7**: Mean annual total precipitation per day in tropical region. (a) Response to Antarctic sea-ice loss, (b) control climatology. (c) As (a) for tropical sea surface temperature (SST) with the global mean response removed.*

5.2.3 Vertical structure of atmospheric response

The zonal-mean temperature response to Antarctic sea-ice loss displays warming throughout the troposphere, with the biggest increase over the high southern latitudes in the lower troposphere (Figure 5.8 a-d). In the upper troposphere, there is a warming at lower latitudes, akin to a classic global warming temperature signature. The stratosphere cools in the Southern Hemisphere, in all seasons apart from winter. In contrast, the Northern Hemisphere stratosphere warms in all seasons apart from boreal autumn.

Turning now to the zonal-mean zonal wind response (Figure 5.8 e-h), the velocities decrease in the core and on the poleward flank of the westerly jet, suggesting a weakening and slight equatorward shift of the jet. In the Northern Hemisphere, velocities increase in the core of the subtropical jet, most strongly in boreal winter and spring. Velocities decrease on the poleward flank of the northern tropospheric eddy-driven jet, suggesting an equatorward shift.

The Southern Hemisphere mid-latitude jet shifts equatorwards in most months, with a maximum of 1.39° in September (Figure 5.9a). The jet weakens throughout the entire year, with maximum weakening of -0.64 ms^{-1} in September (Figure 5.9b). Thus, the months of maximum jet weakening broadly correspond to the months with the largest equatorward shifts.

In the Northern Hemisphere, the jet moves equatorward in all months (Figure 5.9a), with a maximum of 0.79° in March. The jet strength (Figure 5.9b) increases

in the boreal winter, spring, and autumn, by a maximum of 0.22 ms^{-1} in December, but decreases in boreal summer, with a maximum of -0.18 ms^{-1} in August. Thus, the eddy-driven jets are shifted equatorward in both hemispheres, but the jet weakening is more apparent in the Southern than Northern Hemisphere.

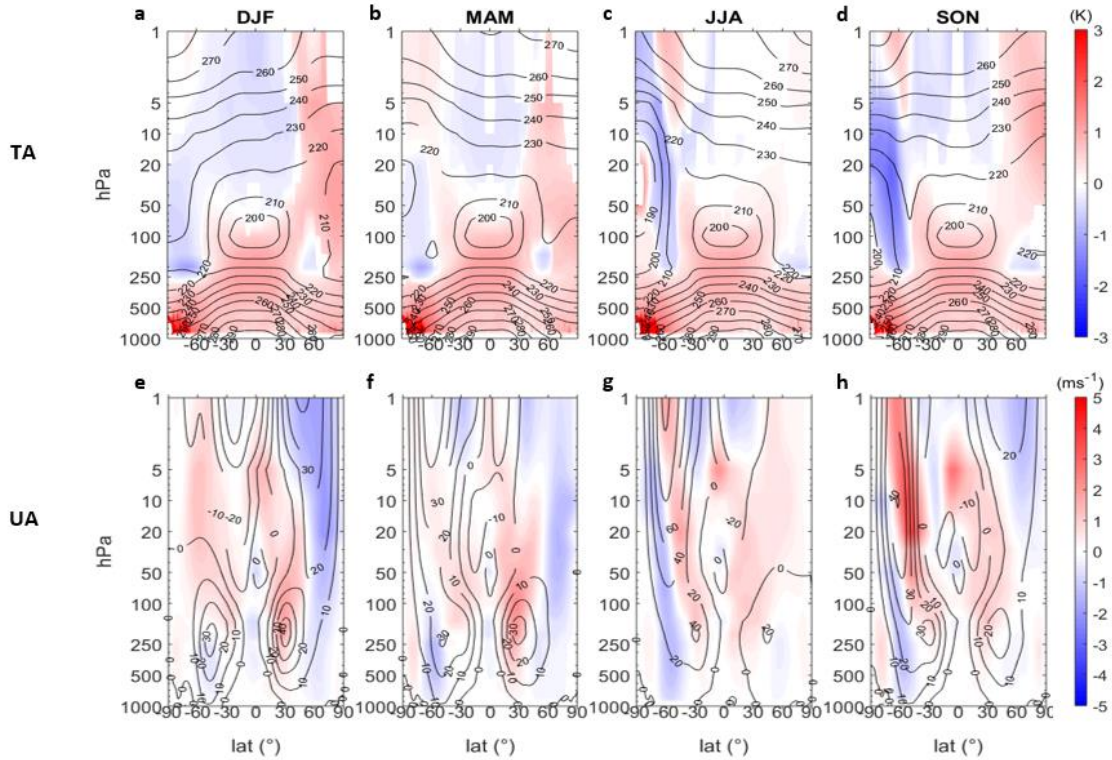

Figure 5.8: *Zonal-mean air temperature response to Antarctic sea-ice loss in austral (a) summer (December-February; DJF), (b) autumn (March-May MAM), (c) winter (June-August; JJA) and (d) spring (September-November SON). (e-h) As (a-d), for zonal-mean westerly wind.*

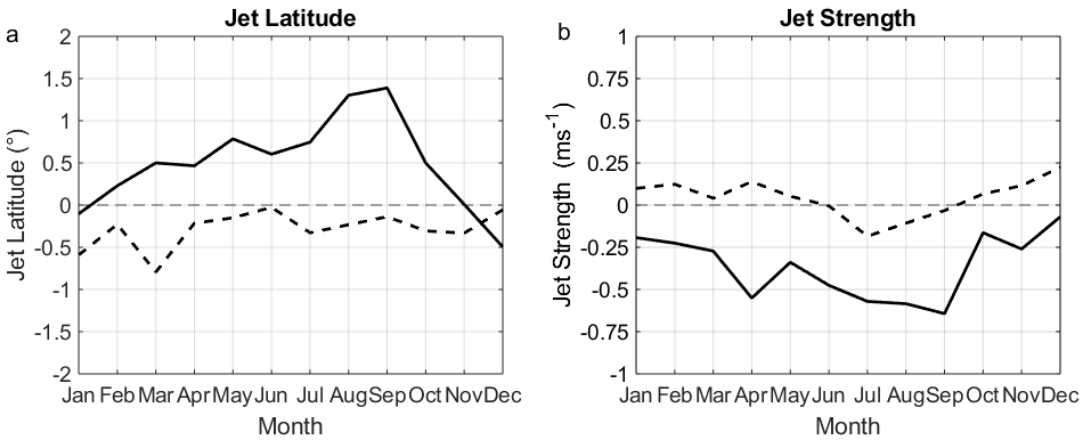

Figure 5.9*: The Southern Hemispheric (black line), and Northern Hemisphere (dashed line) tropospheric jet latitude response to Antarctic sea-ice loss. (b) As (a), for jet strength.*

5.2.4 Fast and slow responses

This subsection analyses the time evolution of the atmospheric response, to determine its fast and slow components. Surface warming over the Southern Hemisphere extratropics occurs rapidly following the abrupt loss of sea ice (Figure 5.10a), reaching 2 K within 5 years and levelling out around 2.5 K after about 30 years, with small fluctuations due to multi-decadal variability. In the tropics (Figure 5.10b), there is a gradual warming over the first 60 years before quasi-equilibrium is reached. In the Northern Hemisphere extratropics (Figure 5.10c), there is little response in the first 20 years. This delay suggests a role for oceanic processes, which evolve more slowly than atmospheric processes. Recall, a similar lag was seen in the Arctic sea ice response (Figure 5.3). Warming becomes apparent thereafter, reaching equilibrium after around 60 years.

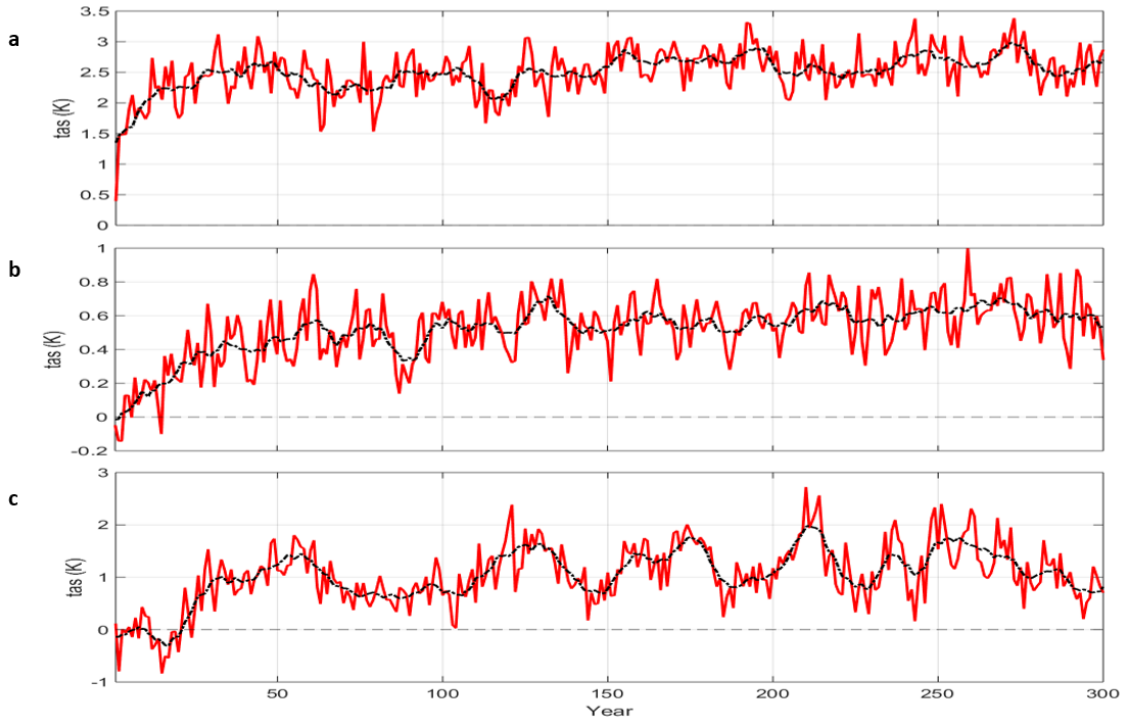

***Figure 5.10**: Annual average near surface temperature (TAS) difference between perturbed and PiControl data with ten year running mean (black dashed line) in the Southern Hemisphere (a). (b) As (a) for the tropics. (c) As (a) for the Northern Hemisphere.*

The time evolution of the annual-mean Southern Hemisphere tropospheric eddy-driven jet (Figure 5.11) exhibits a decrease in the zonal velocity from the beginning of the simulation. This signifies a fast jet weakening response. After the first seventy years, the jet response becomes more variable, reflecting the impact of tropical warming re-establishing a stronger pole-to-equator near-surface temperature difference, but does not recover back to its original state.

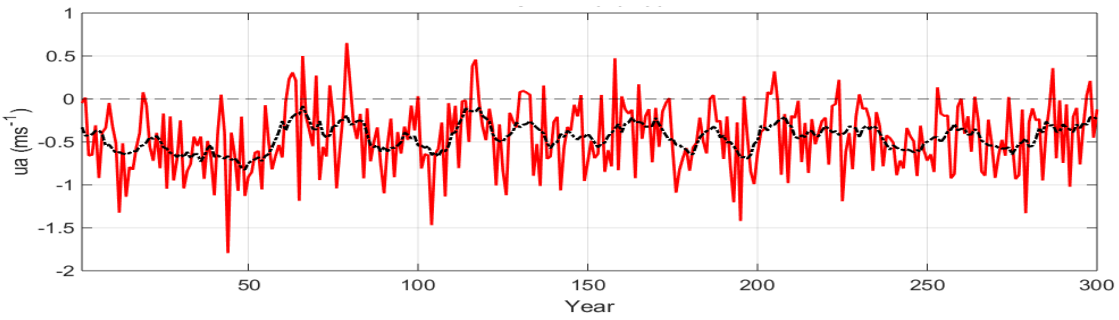

Figure 5.11: *Annual zonal wind velocity at 500 hPa at the Southern Hemisphere tropospheric jet difference between perturbed and PiControl data with ten year running mean (black dashed line).*

The time evolution of the annual-mean tropical precipitation and SST responses (Figure 5.12 a&b) follow the same trajectory as tropical surface air temperature (Figure 5.10b), with a gradual increase over the first 60 years before levelling out. Thus, the tropical air temperature, SST and precipitation responses appear to be governed by similar 'slow' processes, involving the ocean.

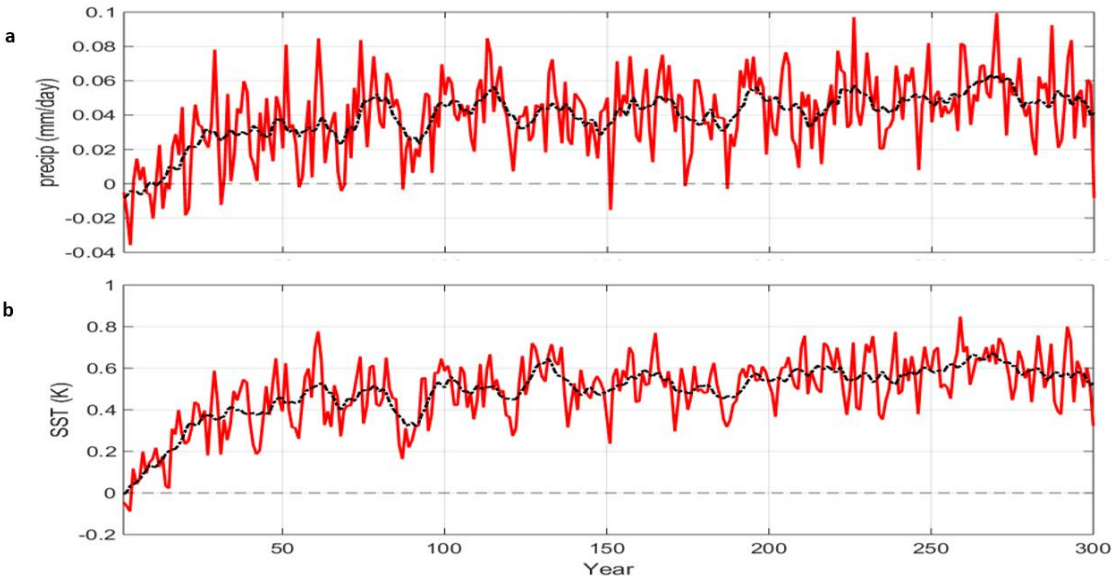

Figure 5.12*: Annual average tropical total precipitation difference between perturbed and PiControl data with ten year running mean (black dashed line) (a). (b) As (a) for tropical sea surface temperature (SST).*

5.2.5 Response to quadrupled CO_2

The purpose of this subsection is to compare the atmospheric response to Antarctic sea-ice loss to the response to quadrupled CO_2. To assess the latter, the CMIP6 Abrupt4xCO_2 and preindustrial control simulations of HadGEM3-GC3.1 were differenced (Figure 5.13). Antarctic sea-ice loss and quadrupled CO_2 both cause warming in near-surface air temperature over the southern high latitudes, with warming in response to quadrupled CO_2 (Figure 5.13 a&b) being approximately double that in response to Antarctic sea-ice loss (Figure 5.13 c&d). Notably, loss of sea ice is less in the albedo case than in the quadrupled CO_2. However, the MSLP responses are of the opposite sign over the Southern Hemisphere, with decrease in pressure over high latitudes and a large increase at mid-latitudes in response to quadrupled CO_2 (Figure 5.13 e&f), in contrast to the increase in pressure over high latitudes in response to Antarctic sea-ice loss The MSLP response to quadrupled CO_2 is of larger magnitude, more zonally and hemispherically symmetric, and more seasonally consistent compared to the response to Antarctic sea-ice loss (Figure 5.13 g&h).

Correspondingly, the 500 hPa zonal wind responses (Figure 5.13 i&j) are also of opposite sign over the Southern Ocean between the response to Antarctic sea-ice loss and the response to quadrupled CO_2 (Figure 5.13 k&l). While the tropospheric eddy-driven jet velocity decreases in response to Antarctic sea-ice loss, its velocity increases in response to quadrupled CO_2, albeit with greater magnitude. The decrease in velocity in the response to sea-ice loss is ~10-20 % of the magnitude of the increase in velocity in response to quadrupled CO_2.

The precipitation response to quadrupled CO_2 features wetting in the high latitudes of both hemispheres and pronounced changes in the tropics (Figure 5.13 m&n). The response to Antarctic sea-ice loss shows similar wetting over the Southern Ocean and captures aspects of the tropical changes, but has much weaker changes in the Arctic, compared to that due to quadrupled CO_2 (Figure 5.13 o&p).

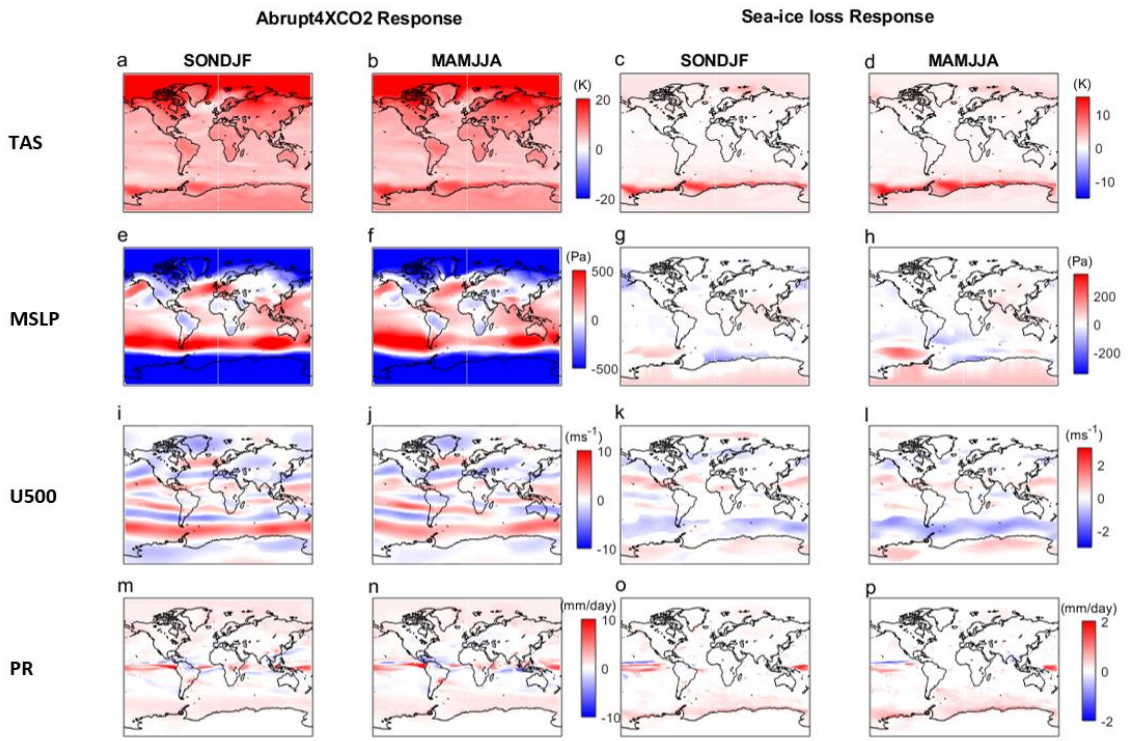

***Figure 5.13**: Surface air temperature (TAS) Abrupt4xCO_2 response from PiControl in austral (a) warm season (September-February; SONDJF), (b) cold season (March-August; MAMJJA). (c&d) As (A&b) for the response to Antarctic sea-ice loss. (e-h) As (a-d), for mean sea level pressure (MSLP). (i-l) As (a-d), for 500 hPa westerly wind (U500). (m-p) As (a-d) for total precipitation (PR).*

Comparing the zonally averaged temperature response to quadrupled CO_2 (Figure 5.14 a&b) and Antarctic sea-ice loss (Figure 5.13 c&d) indicates similarities in the troposphere, but differences in the stratosphere. Notably, both responses show the typical tropospheric warming that is global in scale, albeit weaker in response the Antarctic sea-ice loss than in response to quadrupled CO_2, with warming maximum in the high-latitude lower troposphere and the tropical upper troposphere. This is a typical global warming fingerprint, which is why the temperature response to Antarctic sea-ice loss can be thought of as a 'mini global warming', as also argued for the response to Arctic sea-ice loss (Deser et al., 2105). Despite qualitatively similar temperature responses, the zonal wind responses to quadrupled CO_2 and Antarctic sea-ice loss differ, particularly the eddy-driven jet responses. Quadrupled CO_2 causes a strengthening on the poleward side of the Southern Hemisphere tropospheric westerly jet, in contrast to the weakening seen in response to Antarctic sea-ice loss.

In the stratosphere, quadrupled CO_2 causes cooling year-round in both hemispheres, whereas Antarctic sea-ice loss causes Southern Hemisphere stratospheric cooling, but little change in the Northern Hemisphere stratospheric temperature. Correspondingly, the SPV in each hemisphere is strengthened in response to quadrupled CO_2, but strengthens only in the Southern Hemisphere in response to Antarctic sea-ice loss.

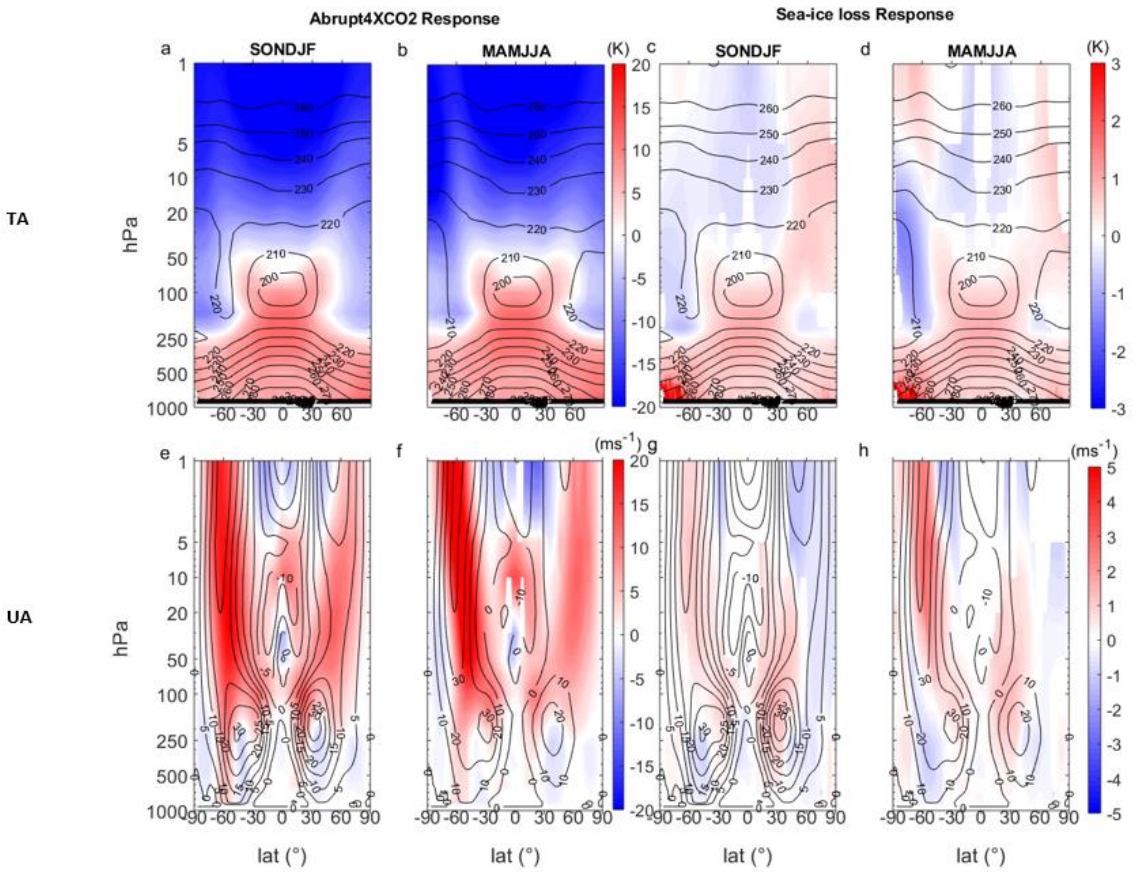

***Figure 5.14**: Zonal-mean air temperature Abrupt4xCO₂ response from PiControl in austral (a) warm season (September-February; SONDJF), (b) cold season (March-August; MAMJJA). (c&d) As (A&b) for the response to Antarctic sea-ice loss. (e-h) As (a-d), but for zonal-mean westerly wind.*

5.3 Discussion

Previous atmosphere-only studies suggest a largely locally-confined impact on the climate, with debated effects on the tropospheric eddy-driven jet and SAM (Bader et al., 2013; England et al., 2018; Kidston et al., 2011; Menéndez et al., 1999; Raphael et al., 2011; Smith et al., 2017). However, the results presented in this chapter, using the HadGEM3-GC3.1 low resolution model, suggest that the impacts of abrupt Antarctic sea-ice loss have global reach and represent a sizeable fraction of the total projected climate change response, inducing a 'mini

global warming' signal, approximately 10-20 % of the magnitude of that in a quadrupled CO_2 scenario.

This chapter broadly supports previous studies regarding the local response to Antarctic sea-ice loss, showing a weakening and small, but significant, shift in the southern westerly jet. Although a significant shift is found, this study only uses one model and previous studies (Ayres & Screen, 2019; Bracegirdle et al., 2018; Holmes et al., 2019) have shown model biases, such as the initial position of the tropospheric eddy-driven jet, may influence the magnitude of the jet shift. Changes to the SAM index, inferred from changes in surface pressure patterns over the Southern Hemisphere, consist mostly of negative anomalies, but are small and vary from month to month. The ASL, however, does show a significant decrease in strength, with pressure anomalies increasing over the Amundsen Sea.

Near-surface warming is greatest over regions of sea-ice loss in the Southern Ocean, but extended over the whole Antarctic continent. Significant Antarctic continental warming is not seen in previous atmosphere-only modelling studies (Ayres & Screen, 2019; England et al., 2018), but is simulated in coupled simulations (England et al., 2020). This result shows that coupling is important for Antarctic continental warming. This may be for similar reasons to those proposed in the Arctic (e.g., Blackport & Kushner, 2017), whereby the coupling allows for the surrounding oceans to warm and then warm anomalies are transported along isentropic surfaces (Laliberté & Kushner, 2013) from the mid-latitude ocean surface to the high-latitude mid-troposphere.

In the regions of warming over the Southern Ocean there is an increase in total precipitation. Vertical patterns of temperature change above the Antarctic region display a general warming throughout the lower troposphere, centred above the Southern Ocean, with a cooling of varying magnitudes in all seasons in the upper troposphere and into the stratosphere. In the upper stratosphere, there is a slight warming over the high latitudes. Associated wind changes exhibit a predominant weakening of the tropospheric eddy-driven jet over the Southern Ocean throughout the troposphere, with an increase at higher altitudes in all months apart from winter. With time, the air temperature displays a steady increasing trend, suggesting a further 'slow' secondary response. This chapter is only the second study to have found clear tropical responses to Antarctic sea-ice loss, the other study being the recent work of (England et al., 2020a) who used a different model, CESM-WACCM.

A notable tropical result is the upper tropospheric warming, a key component of the 'mini global warming' fingerprint, reminiscent of a similar response to Arctic sea-ice loss (Deser et al., 2016, 2015).(The upper tropospheric warming response to abrupt Antarctic sea-ice loss presented here is approximately 10-20 % that in response to quadrupled CO_2. Additionally, in the tropics, the ITCZ and Hadley cell experience a southern shift and weakening, specifically in the Pacific region. The idea that a heat imbalance between hemispheres can shift the ITCZ is not a new one. When forced with interhemispheric heating, GCM studies have found that the Hadley cell, and thus, the ITCZ moves towards the hemisphere with the heating or away from the hemisphere with cooling (e.g., Kay et al., 2016;

Tomas et al., 2016). In contrast, it is found that the corresponding changes to the tropical convergence zone in the ocean of a GCM act to dampen this shift via Ekman advection reducing the need for atmospheric energy transport (Green et al., 2019; Kang et al., 2018). Therefore, the shift in the ITCZ is weakened in coupled models compared to atmospheric only modelling studies. This chapter suggests that Antarctic sea-ice loss, by disproportionately warming the Southern Hemisphere, can induce an ITCZ shift, consistent with England et al., (2020a).

The chapter has also demonstrated that the impacts of Antarctic sea-ice loss can extend into the Northern Hemisphere, as far north as the Arctic. Antarctic sea-ice loss induced surface warming in the Arctic, reaching as high as 3 K, and significant changes to Arctic sea ice, with reductions across the Arctic in the summer and in the Barents-Kara Sea all year round, agreeing with similar results in England et al. (2020b). It is hypothesised that the mechanism for this pole-to-pole connection involves the ocean, as there is an approximate 20-year lag between the initial Antarctic sea-ice loss and the resulting Arctic sea ice response. One possible mechanism is tropical to northern extratropical teleconnections triggered by changes in tropical precipitation (i.e. convection). Antarctic sea-ice loss causes a deepening of the Aleutian Low, observed in the surface pressure response, which may be triggered by a Rossby wave train from the tropical Pacific (e.g. England et al., 2020b; McCrystall et al., 2020; Yuan et al., 2018). Seasonally, the deepening of the Aleutian Low is greatest in boreal winter, when tropical to extratropical teleconnections are known to be most active. The seasonality of this response is also in agreement with England et al. (2020b), however, in order to explore this response further, additional atmosphere-only models, forced with the tropical SST response, would be required.

The results presented in this chapter support the importance of tropical-to-polar (and vice versa) teleconnections (e.g., Ding et al., 2014; Dong et al., 2019; McCrystall et al., 2020) in communicating the effects of sea-ice loss to the rest of the globe. This study also agrees with England et al. (2020a), that the location of the greatest tropical warming in response to Antarctic sea-ice loss is the Central and eastern equatorial Pacific. Whilst the strongest links to the Arctic may originate from warming in the Western Pacific (e.g., Dong et al., 2019), it is noted that there is significant warming in both the eastern and western Pacific in response to Antarctic sea-ice loss (Figure 5.10).

It is acknowledged that all responses away from the Antarctic are minor compared to the effects of general warming from increased greenhouse gasses, and in some regions is small compared to internal variability even though the responses are statistically significant over a 290-year period.

5.4 Summary of Chapter 5

The climate impacts of Antarctic sea-ice loss have not been researched to the same extent as the impacts of Arctic sea-ice loss, with the limited studies of the former relying on atmosphere-only models. This study was one of the first to assess the coupled climate response to Antarctic sea-ice loss. In this chapter, the atmospheric response to Antarctic sea-ice loss was assessed in a fully coupled climate model, HadGEM3-GC3.1, by modifying the sea ice albedo to induce abrupt Antarctic sea-ice loss. These results suggested the atmospheric response

to Antarctic sea-ice loss can be separated into two categories: a ‘fast’ local response and a ‘slow’ global response. The local responses were consistent with previous studies, with local warming, increased precipitation, and a weakening of the tropospheric eddy-driven jet. A key difference with past studies was that ocean coupling allowed the warming signal to spread across the Southern Ocean and onto the Antarctic continent. After around 50 years, tropospheric warming had global reach, including in the tropical upper troposphere, which is thought to be driven primarily through warmer tropical Pacific SSTs and enhanced convection. The response to Antarctic sea-ice loss reached as far as the Arctic, where a warming and decrease in Arctic sea ice, primarily in the Barents-Kara Seas, were simulated.

Chapter 6

Oceanic Response to Abrupt Antarctic Sea-Ice Loss in HadGEM3-GC3.1.

This chapter examines the oceanic response to abrupt Antarctic sea-ice loss using the low resolution HadGEM3-GC3.1 coupled model. Section 6.1 discusses the previous literature on Southern Ocean dynamics, their connections to the global climate, and the oceanic response to Antarctic sea-ice loss. Sections 6.2.1 to 6.2.4 describe the physical oceanographic response to Antarctic sea-ice loss, starting with a full global perspective, and then focusing regionally on the Southern Ocean, the tropical Pacific Ocean, and finally, the Arctic Ocean and AMOC. Section 6.3 discusses these results, with a summary in Section 6.4.

6.1 Introduction

Since accurate satellite records began in 1979, Antarctic SIE has shown a small but significant increasing trend (Parkinson, 2019). However, Antarctic sea-ice extent is predicted to significantly decrease by the end of the century (e.g., Collins et al., 2013; Vaughan, 2013). The relatively limited number of modelling studies assessing the climate impacts of Antarctic sea-ice loss have focussed on the atmosphere (Ayres & Screen, 2019; Bader et al., 2013; England et al., 2018; England et al., 2020a; England et al., 2020b; Kidston et al., 2011; Menéndez et al., 1999; Raphael et al., 2011; Smith et al., 2017), with far less attention on the ocean.

The Southern Ocean plays a key role in the global climate system. The MOC connects the global oceans and is partly driven by vertical transport and water

mass transformation at the southern high latitudes. At the surface, air-sea interaction drives the transport of heat, momentum, freshwater, carbon, tracers, and greenhouse gasses into the depths. These processes are essential for the global energy budget (Trenberth & Fasullo, 2010) and better understanding of them is needed to improve weather and climate models (e.g., Dong et al., 2010; Trenberth & Fasullo, 2010). The consistently strong winds and seasonal sea-ice extent, make the Southern Ocean a central regulator of the global climate (e.g., Frölicher et al., 2015; Rintoul, 2018; Sabine et al., 2004).

Water masses are transformed in the surface mixed layer. Deep waters upwell and are then downwelled to sub-surface layers (Whitworth et al., 1998). This process is particularly important in the Southern Ocean, associated with large amounts of water mass overturning (Ludicone et al., 2008). Within the eddy-driven ACC, in the SAF and PF zones, SAMW and AAIW are formed from the upwelled deep waters as they flow equatorward across the ACC (Sabine et al., 2004). In scenarios of increased greenhouse gas, models predict that the subduction of these water masses will increase as surface waters are warmed and freshened (Downes et al., 2010). The surface mixed layer has a seasonal cycle, with deep destabilisation in winter from changes to air-sea fluxes, Ekman transport and vertical entrainment (e.g., Dong et al., 2007; Ren, et al., 2011; Sallée et al., 2006).

The strength of the tropospheric eddy-driven jet is thought to have minimal impact on the transport and isopycnic tilt of the ACC, due to the balance of changes in eddy-induced and Eulerian mean transports (Böning et al., 2008; Farneti &

Delworth, 2010; Farneti et al., 2010; Hallberg and Gnanadesikan, 2006). In an eddy-permitting coupled simulation, a poleward shift and intensification of the westerly winds, driven by increased sea ice, led to a small increase in the net ACC transport and a slight shift in its position. Enhanced wind stress leads to a stronger northward Ekman transport of colder surface waters, leading to an increase in the winter mixed layer depth. This results in a small increase in the subduction rates of SAMW and AAIW between the SAF and PF (Downes et al., 2010).

Interactions between the ocean and sea ice have been examined in situ, with the use of Argo floats, buoys, and also from satellite data. In situ data is limited, particularly during the winter months, which hampers understanding of air-sea interaction. Sea-ice growth leads to a flux of brine into the ocean, which enhances vertical mixing. As the sea ice melts, freshwater fluxes restratify the water column. These processes create a strong annual cycle of mixed layer depth and density south of the ACC, with summer freshwater input lightening the mixed layer, and winter sea-ice growth causing densification and deepening the mixed layer (Barthélemy et al., 2015; Petty et al., 2014; Ren et al., 2011), and play a crucial role in the transformation of water masses (e.g., Abernathey et al., 2016; Haumann et al., 2016; Pellichero et al., 2017; Swart et al., 2018).

Increased SIE has been found to enhance stratification and reduce entrainment of warm deep waters into the mixed layer. With increased SIE, the seasonal cycle is enhanced, causing greater flux of freshwater from sea-ice loss in the melt season, and increased brine rejection from sea-ice formation in the growth

season (Abernathey et al., 2016; Goosse & Zunz, 2014; Olivier Lecomte et al., 2017). Within the subpolar gyre regions, these seasonal interactions are thought to be even more prominent (Barthélemy et al., 2015; Petty et al., 2014; Ren et al., 2011). This process is again associated with significant water mass transformation, particularly in association with AABW (Whitworth et al., 1998), in addition to the upwelling of deep waters (Rintoul et al., 2001). In both current and paleoclimates, increased sea ice cover has been shown to enhance the volume of AABW formation, accompanied by a stronger poleward export of CDW, in addition to increased brine rejection causing enhanced deep ocean stratification and decreasing vertical mixing (Shin et al., 2003; Stein et al., 2020).

The influence of the Southern Ocean on the AMOC is debated in the literature. The AMOC is primarily driven by the southward transport of NADW and the northward transport of AABW (e.g., Lumpkin & Speer, 2007). Some studies suggest that Southern Ocean surface buoyancy forcing controls the AMOC depth, shallowing the AMOC with an increase in SIE, and greater buoyancy loss causes the contraction of the upper overturning cell, shifting NADW upward. (Ferrari et al., 2014; Jansen & Nadeau, 2016). However, these theories were challenged, where models did not include diabatic processes and diapycnal mixing in the Southern Ocean (Newsom & Thompson, 2018; Sun et al., 2018). Others suggest that the North Atlantic surface forcing or interior diabatic mixing is more dominant, for instance, increased NADW formation from stronger westerly winds, leads to a deepened AMOC depth (e.g., Muglia & Schmittner, 2015; Wolfe & Cessi, 2014). A recent study, suggests that the AMOC depth is more strongly constrained by changes to the surface density, rather than the

buoyancy fluxes, suggesting that the surface density fields in both the North Atlantic and Southern Ocean control the AMOC depth (Sun et al., 2020).

Changes in the Southern Ocean have been found to impact global paleoclimates, most notably through the bipolar seesaw hypothesis (Blunier & Brook, 2001; Broecker, 1998; Marino et al., 2015; Pedro et al., 2018). This hypothesis theorises that the Southern Ocean drives the Northern Hemisphere climate through the NADW circulation and transformation. It is suggested that increased AABW formation caused the little ice age of the 16th-19th century. Proxy records of the last glacial and deglacial periods show that warming in the northern high-latitudes and cooling in the southern high-latitudes coincide with each other, and vice versa (e.g., Blunier & Brook, 2001; Pedro et al., 2011; Blunier et al., 1998). Studies suggest that this phenomenon is driven by deep ocean circulation at the poles (Knutti et al., 2004; Stocker, 1998; Stocker & Johnsen, 2003).

This chapter presents the oceanographic results from the coupled HadGEM3-GC3.1 abrupt Antarctic sea-ice loss experiment described in section 3.2. Recall, this experiment used the HadGEM3-GC3.1 low resolution (n96 ORCA1) global coupled model, with abrupt Antarctic sea-ice loss induced by perturbing the sea ice albedo in the Southern Hemisphere only, and was run for 300 years to quasi-equilibrium. All stated seasons refer to austral seasons, unless otherwise indicated.

6.2 Results

6.2.1 Global Ocean

In the perturbation experiment, SIC is reduced all year round in the Southern Hemisphere (Figure 6.1 a-d), being of greatest magnitude near the ice edge, which migrates with the seasons. In the Arctic, there is a SIC reduction that is focused mostly in the Barents-Kara Sea in boreal winter and spring, but extending across the Arctic Ocean in boreal summer and autumn.

An increase in SST is observed globally in ice-free waters, in all seasons (Figure 6.1 a-d). In the coastal regions of the Southern Ocean, SSTs increase by as much as 4 K in summer, with significant warming extending to the northern regions of the Southern Ocean, up to 40° S. In the tropics and mid-latitudes of both hemispheres, SST increases by approximately 1 K in all ocean basins, with a slightly greater increase in the tropical Pacific than the tropical Atlantic. In the Northern Hemisphere, north of 50° N, there is an increase in SSTs of up to 2 K in the North Atlantic region and Barents-Kara Sea.

A decrease in sea surface salinity in the Arctic Ocean is simulated in all seasons, with the largest decrease of -1.5 ppt in the Beaufort Sea (Figure 6.1 i-l). This salinity decrease is an expected result from sea-ice loss (increased freshwater input and/or reduced brine rejection from ice formation), in addition to the increased precipitation (See Chapter 5). Surface salinity is increased over the Kara and Laptev Seas in the Arctic all year round, and over the Amundsen and Weddell Seas in the Antarctic, predominantly in summer and autumn. These increases in salinity may relate to changes in advection and mixing.

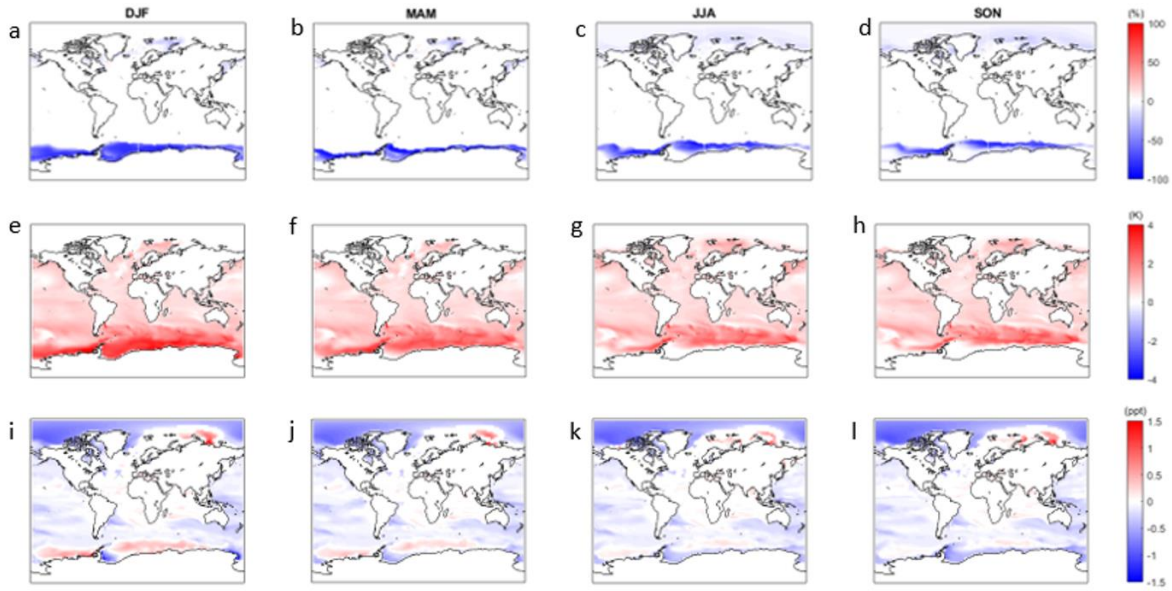

***Figure 6.1**: Sea ice concentration (SIC) response associated with Antarctic sea-ice loss in austral (a) summer (December-February; DJF), (b) autumn (March-May MAM), (c) winter (June-August; JJA) and (d) spring (September-November SON). (e-h) As (a-d) for sea surface temperature (SST). (i-l) As (a-d) for sea surface salinity.*

The zonal-mean temperature response as a function of depth shows warming at all latitudes and depths, suggesting warming of all global water masses (Figure 6.2 a-d). The overall warming pattern is comparable to that seen in the RCP4.5 scenario (Collins et al., 2013), suggesting that sea-ice loss induces a 'mini global warming' signature in the ocean, analogous to that in the atmosphere. Water in the top 1000 m shows the largest increases, with the greatest warming south of 30° S in all basins, followed by north of 60° N, and then hotspots around the equator. Warming is not limited to the mixed layer, highlighting the role of ocean circulation and mixing in the global response to Antarctic sea-ice loss.

In the Southern Ocean, the largest warming at intermediate depths is found in the Atlantic basin (Figure 6.2b). AABW is a crucial water mass for the MOC and its temperature increases by up to 1 K and becomes less dense, potentially reducing downwelling in the region. NADW, another crucial water mass in global circulation, warms by ~0.5 K. Away from the Southern Ocean, Atlantic Intermediate waters warm, but to a lesser magnitude than those at the poles, with the greatest increase at the equator. The equatorial warming at depth may be related to changes in upwelling in the tropical convergence zone, discussed later in this chapter. In the Northern Hemisphere, the greatest warming is in the North Atlantic. The Pacific and Indian Oceans (Figure 6.2 c&d) display similar spatial patterns to the Atlantic Ocean, but with slightly lesser magnitudes, particularly in the Northern Hemisphere where there are geographical constraints.

Changes in zonal-mean salinity have similar patterns in all ocean basins (Figure 6.2 e-h). Salinity decreases by ~ 0.9 ppt in surface and intermediate waters at most latitudes, and increases by ~ 0.2 ppt in the deep-water masses of the Southern Ocean. In the Atlantic (Figure 6.2f), this salinity increase extends northward to intermediate depths in the southern mid-latitudes, reaching the surface in the tropics and into the Northern Hemisphere. Salinity can be controlled by a variety of factors. The simulated increase in precipitation acts to reduce salinity at the surface, and ice melt and reduced ice growth (brine rejection) also contribute to freshening. Salinity increases at depth are more likely due to changes in advection by both the meridional and vertical transports.

A combination of the freshening and warming leads to a reduction in density in surface waters globally, and in deep waters generated near the Antarctic coast

(Figure 6.2 i-l). The increase in the temperature of AABW is partially counteracted by the increase in salinity, but not enough to offset it, so its density is still reduced. Surface waters show a maximum decrease in density of ~ 0.5 kgm^{-3}, with AABW and NADW decreasing by ~ 0.2 kgm^{-3}. Having less dense water at the surface may reduce upwelling, acting as a stable lid in polar regions.

The zonal-mean vertical velocity (Figure 6.3) provides insight into changes in mixing resulting from density and wind driven processes. In all ocean basins, the largest changes are in the polar regions. Throughout the Southern Ocean, downwelling of bottom waters at the very high latitudes off the coastal shelf is reduced (i.e., although patchy, there is generally an upward velocity response in regions of climatological downwelling). Also, upwelling of deep waters in latitudes 60-70 °S is reduced (i.e., generally a downward velocity response in regions of climatological upwelling). At lower latitudes of the Southern Ocean, climatological downwelling is reduced by sea-ice loss. Equatorial upwelling of cold water in the tropics is also weakened. In the Arctic, results are patchy and vary between ocean basins.

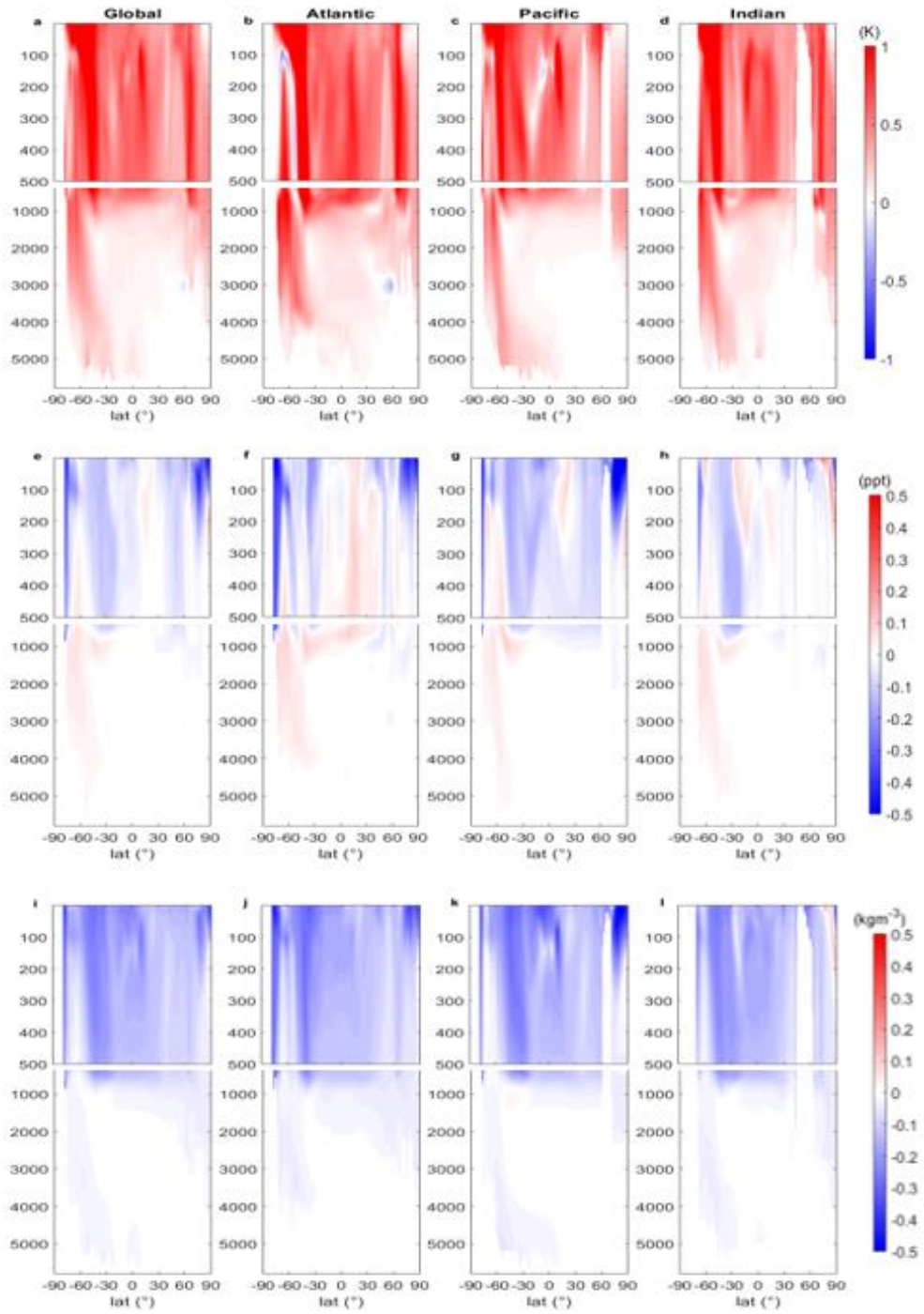

***Figure 6.2**: Zonal-mean potential seawater temperature as a response to Antarctic sea-ice loss, (a) global zonal-mean, (b) Atlantic zonal-mean, (c) Pacific zonal-mean, (d) Indian zonal-mean. Top panel is the top 500m of the ocean, bottom panel is the full ocean depth profile. (e-h) As (a-d) for salinity. (i-l) As (d) for density.*

The zonal-mean zonal velocity (Figure 6.4) in the Southern Ocean is dominated by the ACC and the Antarctic coastal current, both driven by the wind. The ACC shows a mixed result in the upper ocean, with strengthening on the southern flank, and a decrease on the northern flank. With depth, a clearer decrease in velocity is seen throughout the ACC. In the lower latitudes of South Pacific, there is an increase in zonal velocity in the surface and intermediate waters. The differences between basins are likely due to the ACC being located at different latitudes in each basin. In the tropics, there is a reduction in the equatorial currents most prominent in the Pacific and Indian oceans.

Changes in the zonal-mean meridional transport are small in comparison to the zonal transport response (Figure 6.5). Northward transport is increased at the surface in southern high-latitude regions of the Atlantic and Pacific basins, but decreased in the Indian basin. The response directly within the ACC (~ 60° S - 40° S), shows a decrease in northward transport in the Atlantic and Pacific basins. With depth, the northward velocity of AABW is decreased at all latitudes. The surface water of the tropics shows a reduced south velocity in the Southern Hemisphere, and reduced northward velocity in the Northern Hemisphere. This is likely related to the reduced equatorial upwelling (Figure 6.3 & 6.4 e-h), representing a weakened overturning of the tropical convergence cell. Southward transport of NADW is slightly reduced.

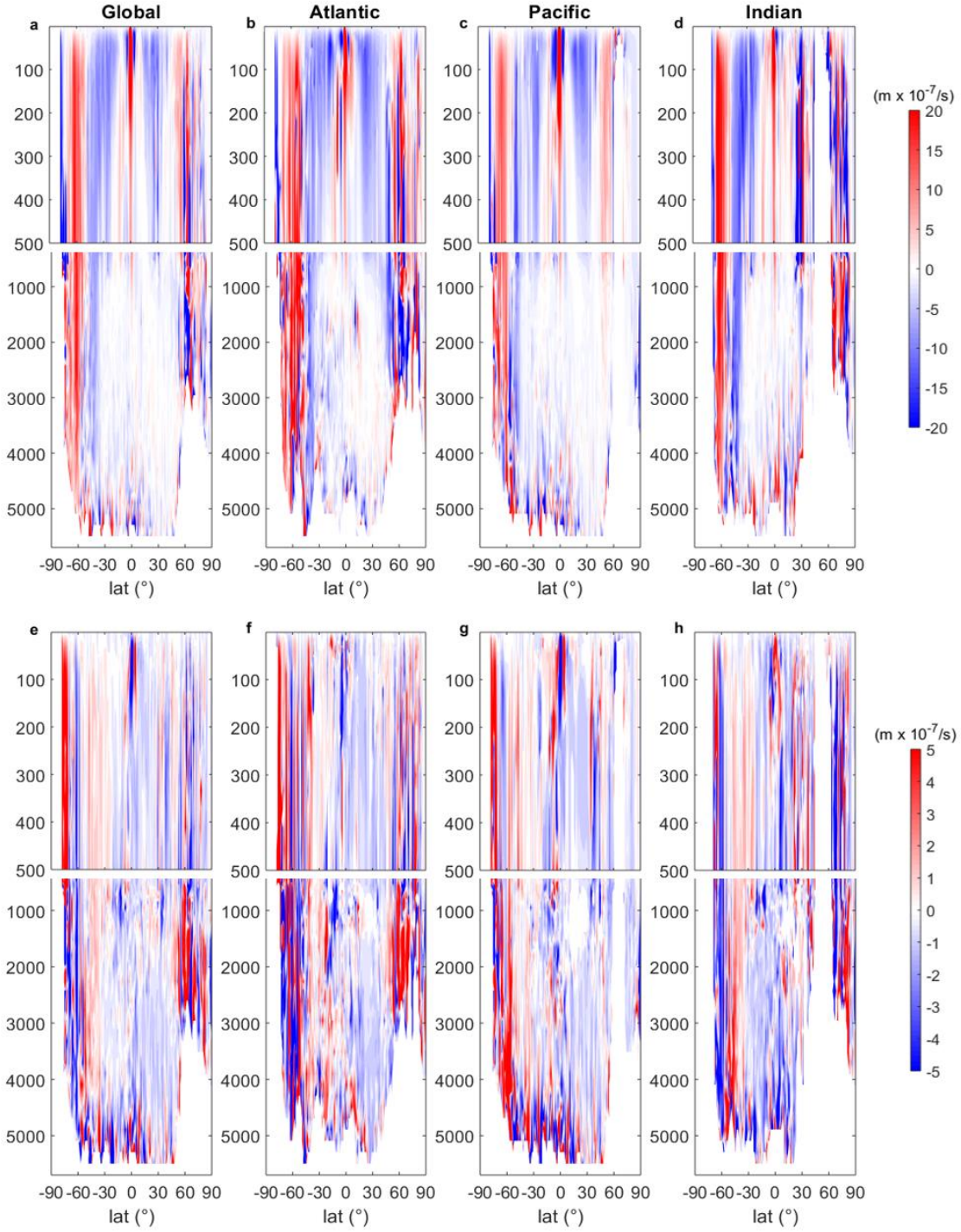

***Figure 6.3**: Zonal-mean vertical velocity PiControl, (a) global zonal-mean, (b) Atlantic zonal-mean, (c) Pacific zonal-mean, (d) Indian zonal-mean. Top panel is the top 500m of the ocean, bottom panel is the full ocean depth profile. (e-h) As (a-d) for zonal-mean vertical velocity as a response to Antarctic sea-ice loss.*

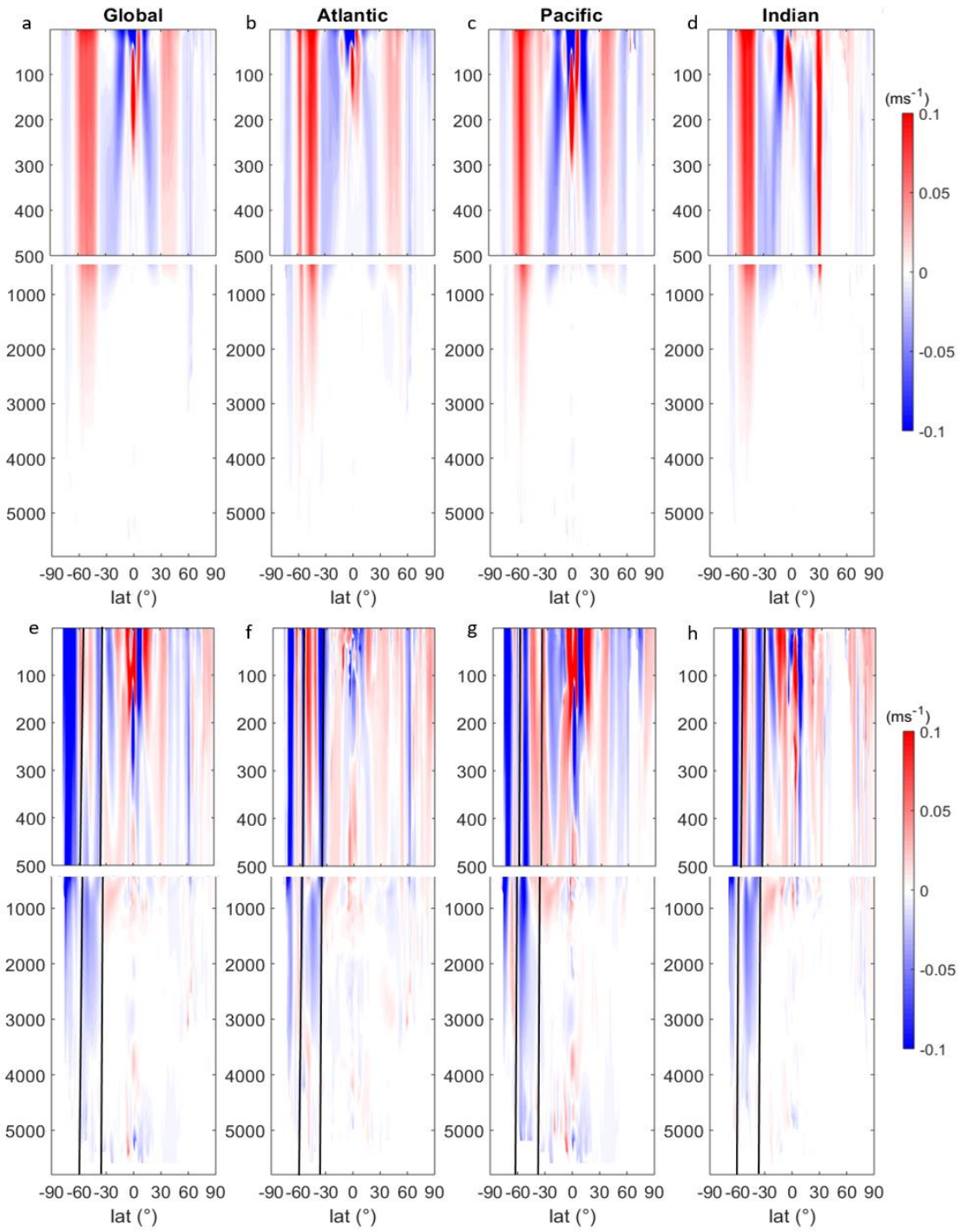

***Figure 6.4**: Zonal-mean zonal velocity PiControl, (a) global zonal-mean, (b) Atlantic zonal-mean, (c) Pacific zonal-mean, (d) Indian zonal-mean. Top panel is the top 500m of the ocean, bottom panel is the full ocean depth profile. (e-h) As (a-d) for zonal-mean zonal velocity as a response to Antarctic sea-ice loss. The Antarctic circumpolar current (ACC) is marked as between the two vertical black lines.*

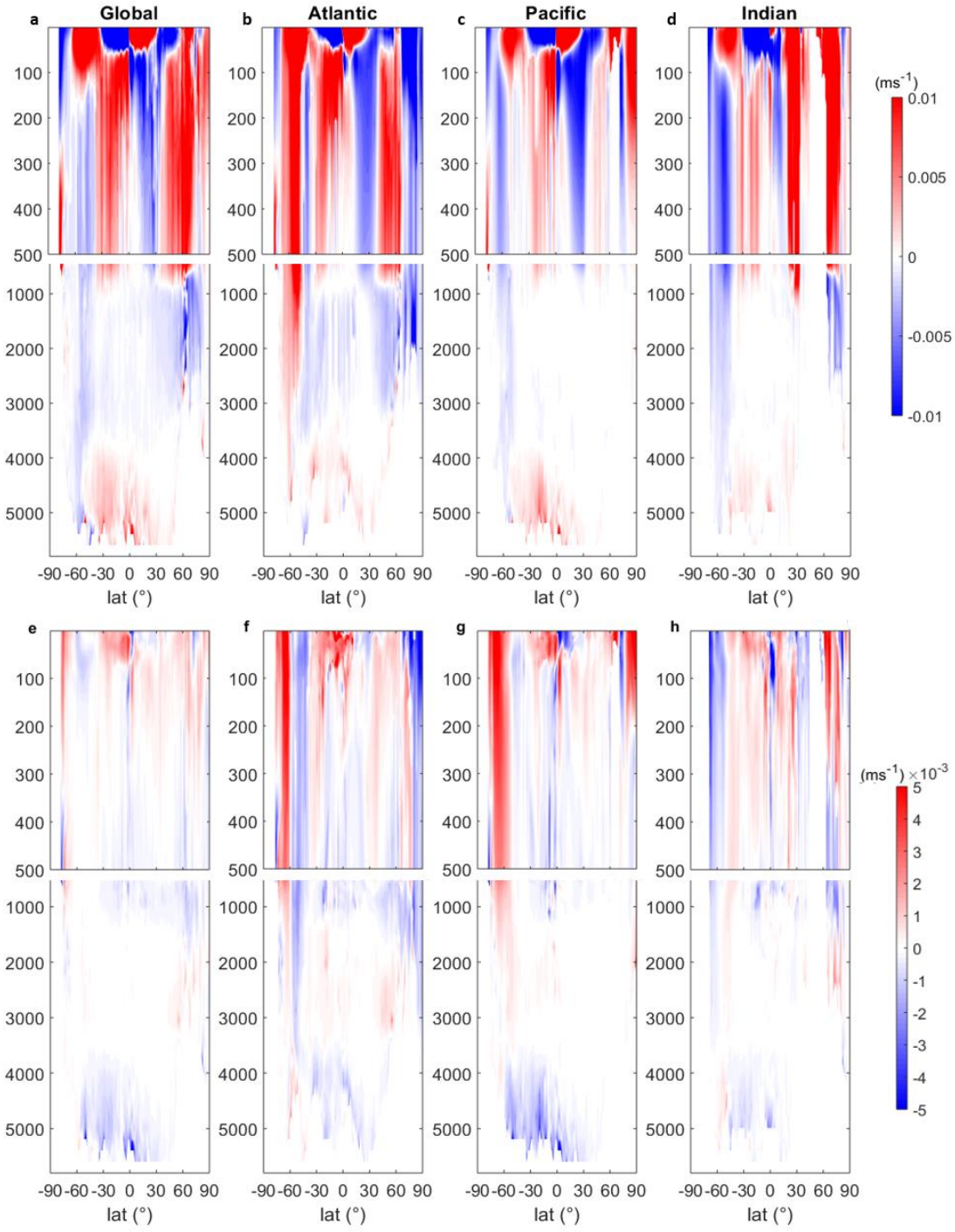

***Figure 6.5**: Zonal-mean meridional velocity PiControl, (a) global zonal-mean, (b) Atlantic zonal-mean, (c) Pacific zonal-mean, (d) Indian zonal-mean. Top panel is the top 500m of the ocean, bottom panel is the full ocean depth profile. (e-h) As (a-d) for zonal-mean meridional velocity as a response to Antarctic sea-ice loss.*

6.2.2 The Southern Ocean

Changes in the ACC transport were assessed by integrating the zonal velocities through Drake Passage (Figure 6.6). A notable decrease in the ACC transport of 25-30 Sv is simulated, with little seasonal variation (Figure 6.6a). This is a reduction of 18 % compared to the mean ACC transport in the control run. The time evolution of the annual-mean ACC volume transport (Figure 6.6b) exhibits a decrease in volume transport gradually from the beginning of the simulation to seventy years in, and thereafter, the ACC transport fluctuates around a lower mean, not recovering back to its original state. The decreased ACC transport appears to partially be in response to the weakened overlying zonal wind stress (Figure 6.6 c-f). Zonal wind stress is broadly reduced along the path of the ACC in all seasons except summer. The wind stress reductions are circumpolar in winter, and in the Pacific and Indian sectors in spring and autumn. Zonal wind stress is increased over the region of sea-ice loss, most strongly in winter and spring, due to the increased exposure of open water.

Whilst the depth integrated ACC transport through Drake Passage decreases, there is both spatial and vertical variability in the zonal velocity response to sea-ice loss. In the top 500 m, there are filaments of increased and decreased zonal flow within the latitudes of the ACC (Figure 6.7 a, d). At 500-2000 m depth, a clearer pattern of decreased zonal velocity emerges over the latitudes of the ACC (Figure 6.7 b, e). A greater depth, below 2000 m, the zonal velocity is broadly decreased, but with lesser magnitude than at intermediate depths. However, the mean ACC transport at depth is also weaker (Figure 6.7f).

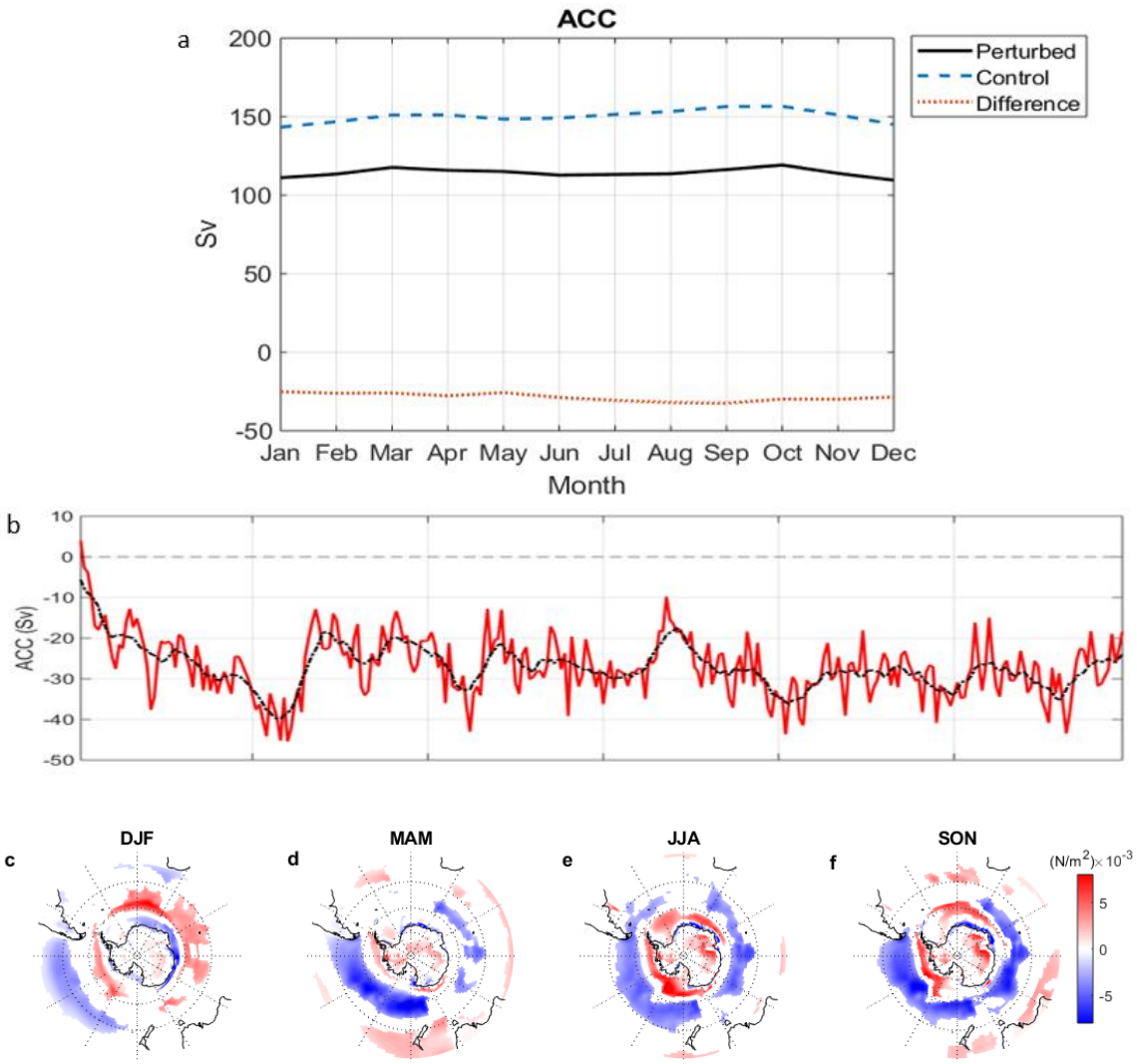

***Figure 6.6**: (a) Monthly change in Antarctic Circumpolar Current (ACC) transport (Sv) at Drake Passage control in blue dashed, experiment in black solid and the difference in red dotted lines. (b) Annual average ACC transport (Sv) at Drake Passage difference between perturbed and PiControl data with ten year running mean (black dashed line). (c-f) The zonal wind stress response to Antarctic sea-ice loss in austral (a) summer (December-February; DJF), (b) autumn (March-May MAM), (c) winter (June-August; JJA) and (d) spring (September-November SON).*

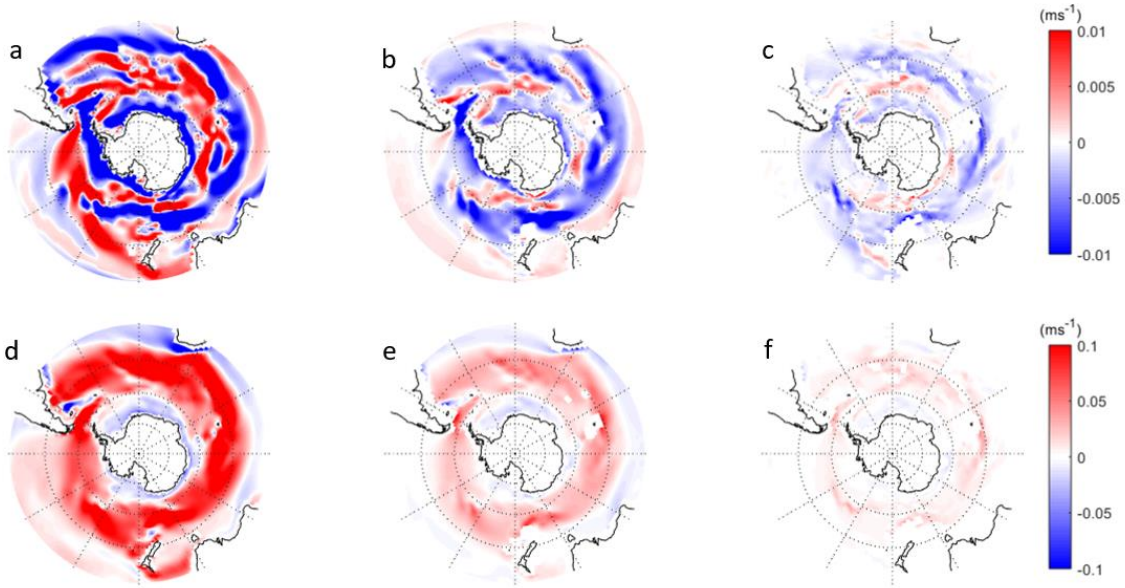

***Figure 6.7**: Zonal-mean zonal velocity as a response to Antarctic sea-ice loss, (a) averaged between 0-500 m, (b) averaged between 500-2000 m, (c) averaged between 2000-4000 m. (d-f) As (a-c) for the PiControl mean fields.*

Vertical temperature and salinity profiles at 50° S, 60° S and 70° S can be used to assess the seasonal changes to the water column and in characteristic water masses. Temperature and salinity profiles show how the density of the water changes as a function of potential temperature and salinity. Usually read from left to right, if density increases with depth the water column is considered stable, which restricts vertical mixing. Conversely, decreasing density with depth implies an unstable water column, conducive to vertical mixing. Key water masses can be recognised on a T-S diagram by their specific tracer properties. So long as a water parcel is away from the surface and in the absence of mixing, potential temperature and salinity is conserved. Water masses can be identified by the turning points (bends) in the profile. Typically, the bend point identifies the core of the water mass and the lines between the bend points represent mixing

between adjacent water masses. Due to the non-linear relationship between temperature and density, temperature change is the dominant driver of density change in warmer waters (visually, this appears in the T-S plot as more tilted isopycnals), whereas salinity change is the dominant driver of density change in colder waters (seen as more vertically aligned isopycnals).

At 50° S, the entire water column warms in response to sea-ice loss, in all seasons, with the biggest increase of 1.5 °C at the surface, above the seasonal thermocline (Figure 6.8 a-d). Salinity is reduced in the surface and intermediate waters, again in all seasons. Sea-ice loss results in less dense surface waters in all seasons (warmer and fresher; recall that at this latitude, temperature change dominates over salinity change in the density response), meaning a more stable water column and increased stratification in the upper ocean. Although a year-round increase in both temperature and salinity is found in the Deep Waters and AABW, the density of these waters remains largely the same, and hence the structure of the water column at these depths is unchanged. Therefore, at 50° S the greatest changes to density occur toward the top of the water column.

At 60° S in summer and autumn (Figure 6.8 e&f), the seasonal thermocline displays a reduction in density from a decrease in salinity. The density gradient between the surface and the seasonal thermocline is increased due to a 2 °C warming at the surface. As at 50 °S, the greatest changes to the density occur in the upper parts of the water column. Deep Waters warm, but there is relatively little change in salinity, meaning that density remains unchanged. Recall that at this latitude, density is more strongly driven by salinity than temperature (steeper isopycnals). The density of AABW also remains unchanged. In winter and spring,

there is no longer a seasonal thermocline (Figure 6.8 g&h). In these seasons, surface waters are cooler and fresher than waters below, leading to a different profile in the upper layers compared to summer and autumn (Figure 6.8 g&h). In response to sea-ice loss temperature is increased in the upper layers, making the water column more stratified, with a reduced density gradient between water masses. In spring, surface warming and freshening due to sea-ice loss is sufficient to cause the development of a small thermocline that is not present in the control experiment.

The vertical water column structure at 70° S (Figure 6.8 i-l) is largely consistent with that just described at 60° S, with cold surface waters overlying less cold waters at depth. In summer and autumn, surface waters above the seasonal thermocline are warmed and freshened by sea-ice loss, leading to a weakened density gradient in the upper layers, as also seen at 60° S. Below the seasonal thermocline in summer and autumn, and throughout the water column in winter and spring, water masses remain approximately the same density, despite warming (i.e., the profiles are shifted along isopycnals). Recall that at this latitude, density is controlled by salinity more than temperature (i.e., the isopycnals are nearly vertical). In spring, a shallow seasonal thermocline is established in response to sea-ice loss, like that also seen at 60° S, suggesting an earlier seasonal formation of the thermocline.

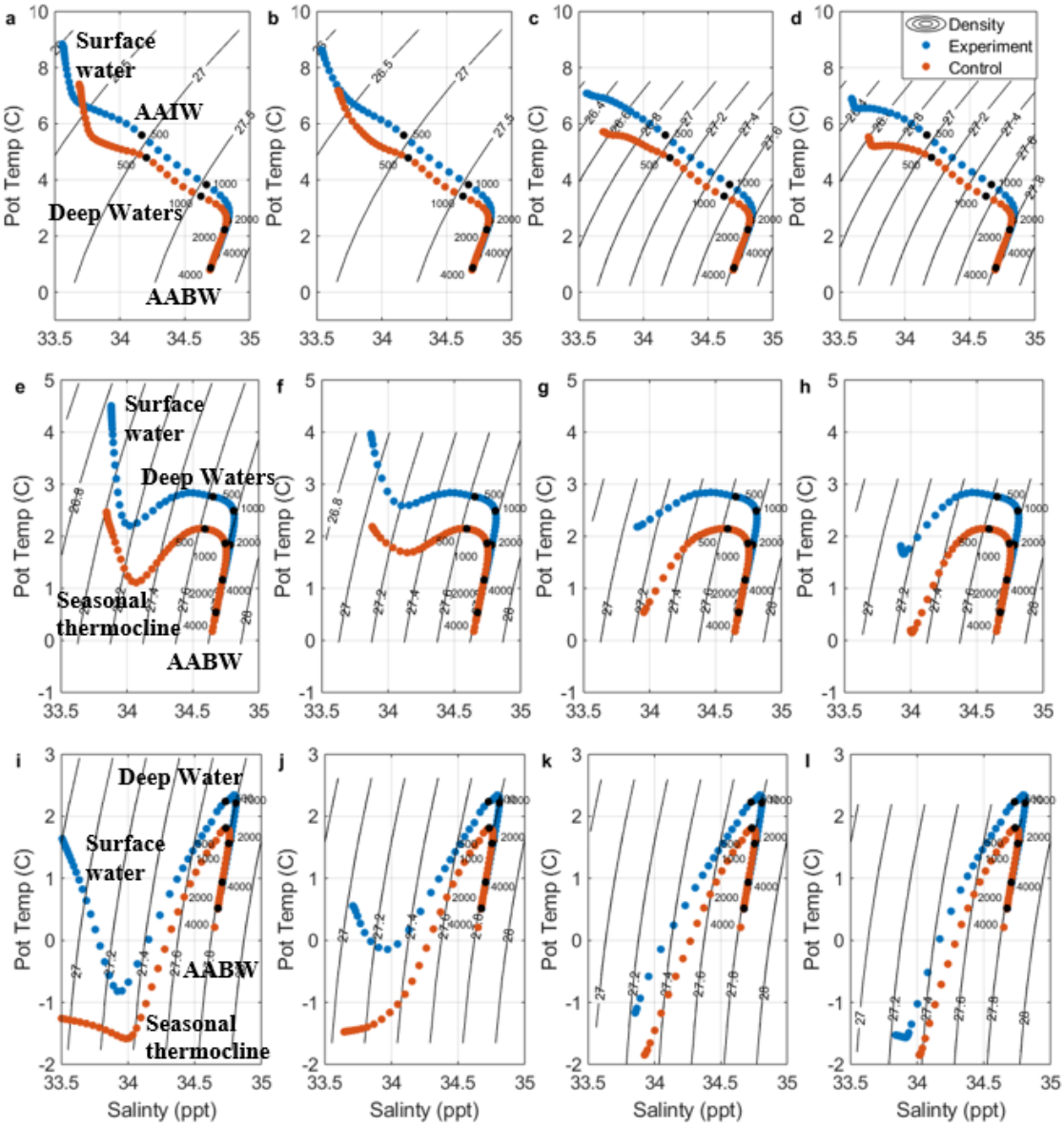

Figure 6.8: *Temperature and salinity profiles at latitude bands of the Southern Ocean. The perturbed result (blue dots) and the PIControl result (red dots) are compared to assess the differences in density of the water column (Contours). Water increases with depth and densitiy from left to right across the figure. This can be used to assess the changes to the regional water masses (lables). 50° S (a) summer (December-February; DJF), (b) autumn (March-May MAM), (c) winter (June-August; JJA) and (d) spring (September-November SON). (e-h) As (a-d) for 60° S. (i-l) As (a-d) for 70° S.*

Southern Ocean fronts can be inferred from local absolute maxima in the meridional SST or sea surface height (SSH) gradients across a somewhat arbitrary threshold, chosen to match the number of fronts within the Southern Ocean. Altering this value has no effect on the overall conclusions, and is here used as a guideline for frontal position (Graham et al., 2012; Sokolov & Rintoul, 2007). Here, fronts are identified as local maxima along the Greenwich Meridian (0° E). Using the SSH values, this places the fronts as follows: the Southern Boundary Front at ~57° S, the SACCF at ~54° S, the APF at ~50° S, the SAF at ~47° S and the STF at ~36° S (Figure 6.9).

Figure 6.9 suggests that frontal positions are relatively unchanged by sea-ice loss, defining the fronts based on either the SST gradient (Figure 6.9a) or SSH gradient (Figure 6.9b), albeit the STF shows a small southward shift. This suggests the ACC frontal positions are primarily determined by bathymetry, consistent with past work (e.g., Graham et al., 2012).

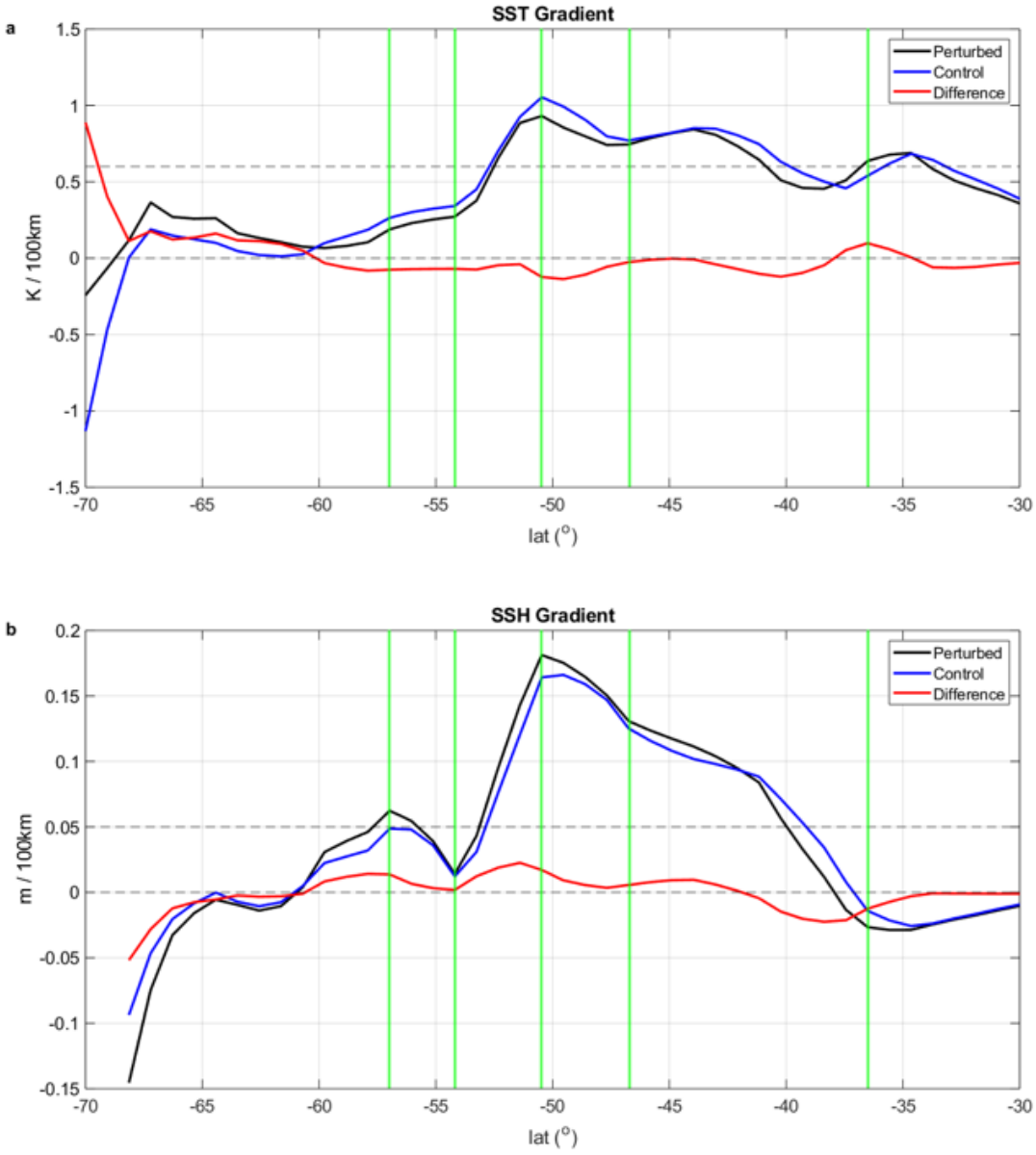

***Figure 6.9**: Sea surface temperature (SST) gradient transcet along the Greenwhich Meridian (0° E) throughout the Southern Ocean (70° S to 30° S). The perturbed rewsponse to sea-ice loss in (black line), the PiControl (blue line), and the difference (red line) for comparrison. The threshold is inidicated by the grey dashed line, fronts are included for reference, identified as the local absolute maxima along the meridional SSH transect (green lines) (a). (b) As (a) for the sea surface height (SSH) graditent.*

6.2.3 The Tropics

The previous chapter revealed changes to the ITCZ, specifically a southward shift towards the equator, hypothesised to be induced by the interhemispheric heating difference (Figure 5.7). Figure 6.10 shows the oceanic tropical convergence cell, which is weakened in response to sea-ice loss. This is likely driven by the weakening of the equatorial easterly trade winds (i.e., westerly wind anomaly) and is qualitatively comparable to a similar response seen in scenarios of increased greenhouse gases (Figure 6.10a).

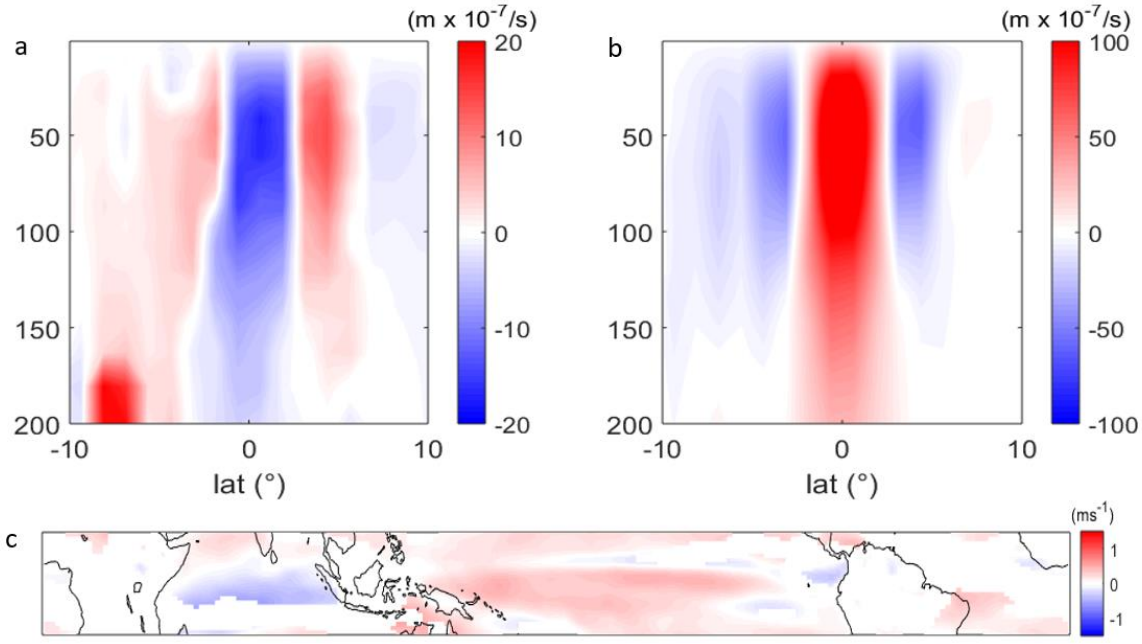

Figure 6.10*: Zonal-mean tropical Pacific surface upwelling as a response to Antarctic sea-ice loss, in the top 100 m. (b) As (a) but for the PiControl as a direct comparison. (c) Zonal wind at 850 hPa as a response of Antarctic sea-ice loss, over the tropics.*

At the tropics, the water column is warmer than at higher latitudes (Figure 6.11 a-d) and thus, changes in temperature are more important than changes in salinity for determining the density response (note the near-horizontal isopycnals). Temperature and salinity profiles at the equator show minimal differences in salinity or temperature in response to sea-ice loss, with little seasonality. In all seasons, the maximum response in the water column is at the surface, where there is warming of ~1 K and a slight freshening of 0.1 ppt. At depth, there is a small decrease in salinity and warming of intermediate waters, but minimal change in Deep Waters. Overall, the profiles show a slight decrease in density in response to sea-ice loss from intermediate levels to the surface.

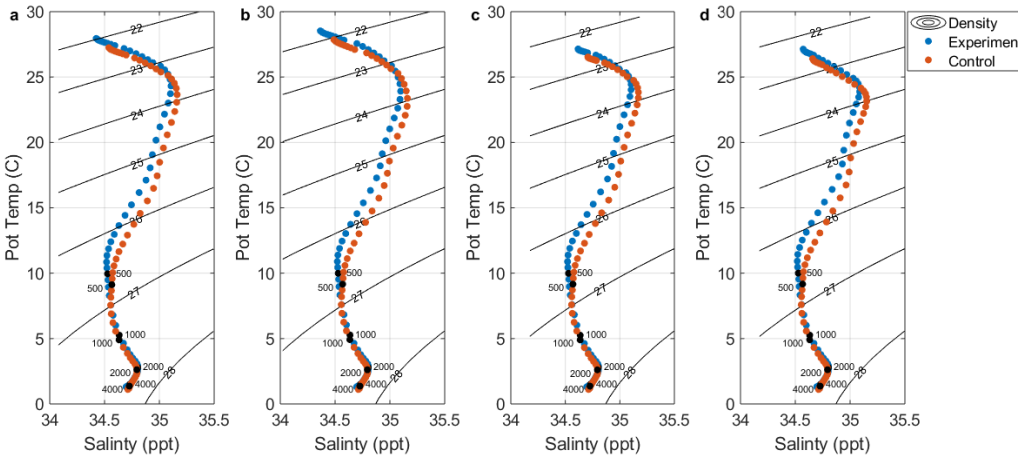

Figure 6.11*: Temperature and salinity profiles of the Equator. The perturbed result (blue dots) and the PiControl result (red dots) are compared to assess the differences in desnisty of the water collumn (contours). (a) (December-February; DJF), (b) (March-May MAM), (c) (June-August; JJA) and (d) (September-November SON).6.2.4 The Arctic and the AMOC*

Temperature and salinity profiles in the Arctic at 85° N (Figure 6.12 a-d) reveal that sea-ice loss induces warming of 0.5 °C in the surface and intermediate waters. At greater depth, the response is completely dominated by changes in

salinity (i.e., the curves are shifted horizontally), specifically freshening, likely in response to induced Arctic sea-ice loss. In the Arctic Ocean, density changes are very strongly determined by salinity changes (i.e., near-vertical isopycnals) and hence, salinity determines stratification. The vertical density structure of the water column is largely unchanged, but density is reduced at depth, which increases the stability of the water column and reduces vertical mixing.

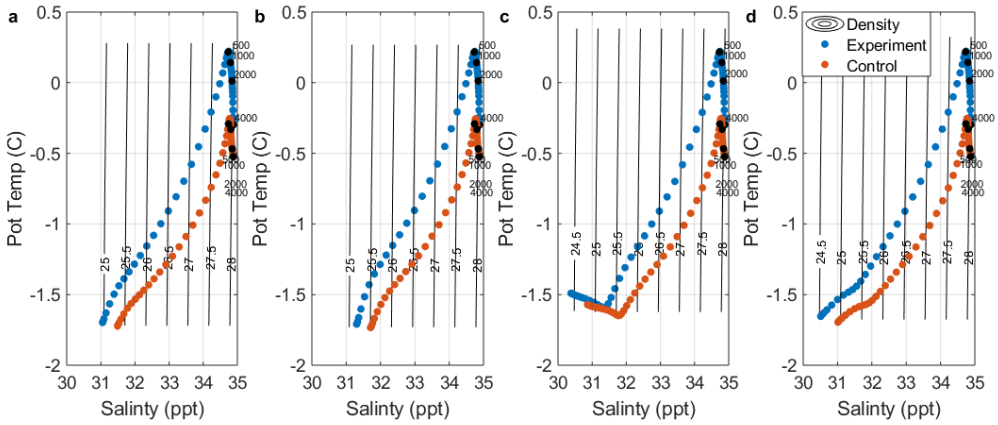

***Figure 6.12**: T-S profiles at 85° N of the Arctic Ocean. The perturbed result (blue dots) and the PIControl result (red dots) are compared to assess the differences in desnisty of the water collumn (contours). Boreal (a) winter (December-February; DJF), (b) spring (March-May MAM), (c) summer (June-August; JJA) and (d) autumn (September-November SON).*

The AMOC is commonly defined as the maximum meridional streamfunction with depth at 26.5° N in the Atlantic. Figure 6.13 shows no difference in the AMOC strength between the control and perturbed simulations, although density change between the perturbed and control is reduced at depth.

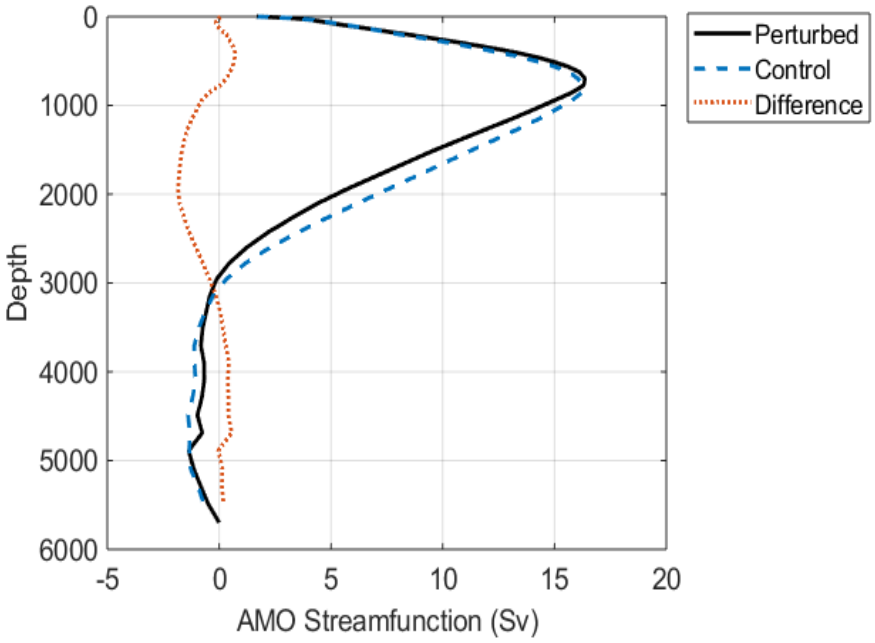

***Figure 6.13**: Annual average change in North Atlantic Meridional Streamfunction transport (Sv) at 26.5° N, control in blue dashed, experiment in black solid and the difference in red dotted lines.*

6.3 Discussion

The literature directly assessing the impacts of Antarctic sea-ice loss on the ocean circulation is limited. However, it is understood that changes in seasonal salinity fluxes affect water mass overturning and, the transformation of key water masses (e.g., Abernathey et al., 2016; Haumann et al., 2016; Pellichero et al., 2017; Swart et al., 2018). The results presented within this chapter evaluate the impacts of Antarctic sea-ice loss on the ocean circulation, using the low resolution HadGEM3-GC3.1 coupled climate model. These include changes to density, stratification, and mixing, in the Southern Ocean, a reduction in the ACC transport at mid-depths, a weakening of the tropical convergence cell, and freshening of the Arctic Ocean due to Arctic sea-ice loss.

One of the most novel results of this study is the weakened ACC transport in response to Antarctic sea-ice loss. Drake Passage transport is reduced by ~20% in the perturbed simulation in comparison to the control. Weakened ACC transport is consistent with reduced surface wind stress, due to the weakening of the tropospheric eddy-driven jet (refer to Chapter 5). The reverse - a small increase in ACC transport in response to increased sea ice and a strengthened westerly jet - was found by Downes et al. (2011). However, the effect of changes in westerly jet strength on the ACC is debated (e.g., Böning et al., 2008; Farneti & Delworth, 2010; Farneti et al., 2010; Hallberg and Gnanadesikan, 2006). A possible limitation of the low resolution HadGEM3 model is that it does not explicitly resolve mesoscale eddies. It is plausible that a different ACC response to sea-ice loss would have been obtained if the model were eddy resolving (e.g., Munday et al., 2013) although it is unclear from the literature on what that difference may be.

The reduction in wind speed may also be responsible for a reduction in the transformation of water masses in the region. The results presented in this chapter suggest a weakening of vertical velocities, stabilisation of upper levels, and reduced northern Ekman transport within the ACC; all in response to sea-ice loss. Decreased northward Ekman transport of cold water would be expected to contribute to the simulated near-surface warming at the latitudes of the ACC. These changes are consistent in character, but of opposite sign, to those reported by Downes et al. (2010), a study that used an eddy-permitting model, in response to increased sea ice and a strengthened westerly jet. Downes et al. (2010) found

an increase in northward Ekman transport of cold water, leading to an increase in the subduction rates of SAMW and AAIW.

Another oceanic response likely caused by the wind stress changes is that of the weakened tropical convergence cell. The equatorial upwelling and downwelling on either side of the equator is reduced, in addition to the associated surface meridional transport, in response to sea-ice loss induced weakening of the equatorial trade winds. It is possible that the tropical response of the atmosphere may be mediated by this reduction in vertical transport within the tropical convergence cell (England et al., 2020a), as reduced upwelling of the cold waters from depth will amplify warming in the upper levels.

The zonally averaged temperature response with depth is comparable to a ‘mini global warming’ response (Collins et al., 2013). The warming response is spread across all global ocean basins, and is greatest in the surface and intermediate waters, but also impacts the deep ocean, particularly within AABW formation regions. The global response in salinity is also alike that in response to increased greenhouse gases, with a general freshening of surface and intermediate waters, but varying in magnitude and spatial detail between ocean basins.

The overall response in density is a decrease in surface and intermediate waters, driven by warming and freshening, and a relatively smaller decrease at depth, where warming and increased salinity have compensating effects on density. Water mass transformation appears to be affected by sea-ice loss, with a

reduction in downwelling AABW, and upwelling of Deep Waters. The transformation of CDW occurs throughout the mixed layer of the ACC. Interestingly, there is an increase in salinity below 200m in the region of AABW, which is likely a response to changes in advection. The overall effect of the density changes is to stabilise and increase stratification of the upper water column, which might be expected to impact the MOC, via reduced entrainment and less mixing.

However, there is minimal change in the AMOC in response to Antarctic sea-ice loss, perhaps because the density changes are minimal in deep and bottom water masses in both hemispheres. The influence of Southern Ocean buoyancy forcing and density on the AMOC is debated in the literature (e.g., Ferrari et al., 2014; Jansen & Nadeau, 2016; Newsom & Thompson, 2018; Sun et al., 2018, 2020). Generally, the AMOC depth would be expected to deepen with Antarctic sea-ice loss, based on studies that state the opposite effect for sea-ice growth (e.g., Ferrari et al., 2014; Jansen & Nadeau, 2016), due to the increased surface buoyancy and reduced density of the Southern Ocean.

6.4 Summary

The ocean response to projected Antarctic sea-ice loss has been relatively unstudied, in comparison the response to Arctic sea-ice loss. In this chapter, the oceanographic response to Antarctic sea-ice loss was assessed in a fully coupled climate model, HadGEM3-GC3.1, by modifying the sea-ice albedo to induce abrupt Antarctic sea-ice loss. These results suggested a ~20% reduction in ACC transport, likely driven by a reduction in zonal wind stress. Temperature, salinity

and density changes were found throughout the global oceans, much alike those projected for scenarios of increased greenhouse gases, but with lesser magnitude. Strong warming and freshening of surface waters at the poles, led to more stratified and stable water columns, most strongly in the Southern Ocean but also in the Arctic Ocean. Despite these changes, the response of the AMOC was minimal. Away from the polar regions, another notable response to Antarctic sea-ice loss was a weakening of the tropical convergence cell.

Chapter 7

Role of Ocean Coupling in the Atmospheric Response to Abrupt Antarctic Sea-Ice Loss

This chapter examines the atmospheric response to abrupt Antarctic sea-ice loss in the absence of ocean coupling, using an atmospheric-only model prescribed with sea ice conditions from the coupled model experiments in previous chapters. It then compares the results from the atmosphere-only and coupled versions of the model to assess the role of ocean coupling in the atmospheric response to abrupt Antarctic sea-ice loss. Section 7.1 discusses the previous literature on atmospheric responses to Antarctic and Arctic sea-ice loss, and in particular, the potential importance of atmosphere-ocean coupling. Sections 7.2.1 to 7.2.3 present the sea ice forcing, the spatial pattern of the atmospheric response to Antarctic sea-ice loss, and the zonal-mean and tropospheric eddy-driven jet responses; in all cases comparing the atmosphere-only and coupled simulations. Section 7.3 discusses these results, with a brief summary in Section 7.4.

7.1 Introduction

The atmospheric response to changes in Antarctic sea ice has been minimally assessed in the literature, and principally focuses on the response of the Southern Hemisphere extratropical circulation (e.g., Ayres & Screen, 2019; Bader et al., 2013; England et al., 2018; Kidston et al., 2011; Menéndez et al., 1999; Raphael et al., 2011; Smith et al., 2017). This is partially due to the primary use of atmosphere-only model configurations, that may not capture the further-afield

responses to sea-ice loss, as seen in coupled models (e.g., England et al., 2020a; 2020b).

Atmosphere-only modelling studies, prescribed with projected Antarctic sea-ice loss, have found contrasting results on the impact on the location of the mid-latitude tropospheric eddy-driven jet, but generally agree that there is a reduction in its strength (Bader et al., 2013; England et al., 2018; Kidston et al., 2011; Menéndez et al., 1999). For example, Bader et al. (2013) found that in austral winter there was a clear equatorward shift in the jet, agreeing with Menéndez et al. (1999). However, Kidston et al. (2011) found no significant jet shift. Bracegirdle et al. (2018) found when comparing CMIP5 models, that the initial position of the jet mediated the subsequent jet shift in response to increased greenhouse gases. Atmosphere-only modelling studies have demonstrated that the response to Antarctic sea-ice loss may be more vertically confined, of smaller amplitude, and less seasonally variable than the relatively well-studied response to Arctic sea-ice loss (England et al., 2018). Model studies forced by observed sea ice trends and observational studies, suggest that increased sea ice may drive a poleward shift in the tropospheric eddy-driven jet and a positive SAM anomaly in winter months (Raphael et al., 2011; Smith et al., 2017). Raphael et al. (2011) suggests that there may be an atmospheric circulation response to sea ice trends in the summer months also.

The important role of ocean coupling in the atmospheric response to Arctic sea-ice loss has been established (Deser et al., 2016; Smith et al., 2017; Tomas et al., 2016), but much less is known about the importance of ocean-atmosphere

coupling for the response to Antarctic sea-ice loss (England et al., 2020a; 2020b). Atmosphere-only models depict fairly locally-confined changes in response to Arctic sea-ice loss, as far south as the mid-latitudes, whereas coupled models suggest more widespread effects, reaching the tropics and even into the Southern Hemisphere (e.g., Blackport & Kushner, 2016; Deser et al., 2016; Deser et al., 2015; Oudar et al., 2017). For example, Deser et al. (2015) found that the response to Arctic sea-ice loss was limited to north of 30° N when an atmosphere-only model was used, but with ocean-atmosphere coupling, the responses were seen over the whole globe. Remote responses included tropical upper-tropospheric warming, an enhanced global hydrological cycle, and an equatorward shift of the ITCZ (Deser et al., 2016, 2015). In the northern hemisphere extratropics, ocean coupling enhanced the magnitude of the response to Arctic sea-ice loss by up to 50%, but did not appreciably change its overall spatial pattern (Deser et al., 2016). The character of the global response appears to depend on the type of ocean model used, whether a slab ocean or full ocean model. For example, the response was largely symmetric about the equator with a full ocean model, whereas the response was antisymmetric with a slab ocean model, (Tomas et al., 2016). More recently, Chemke et al., (2019) found that the Hadley Cell demonstrates negligible response in the absence of coupling. Thermodynamic coupling to a slab ocean model resulted in a weakening and expansion of the Hadley Cell in response to Arctic sea-ice loss, whereas coupling to a dynamical full-depth ocean model led to narrowing of the Hadley Cell in response to Arctic sea-ice loss.

Only two studies, using the same set of model experiments, have assessed the coupled response to Antarctic sea-ice loss (England et al., 2020a; 2020b). In

these coupled simulations, responses included tropical warming, which induced atmospheric teleconnections to the Arctic, where there was warming of up to 1°C. Therefore with ocean coupling, prescribed Antarctic sea-ice loss caused Arctic sea-ice loss (England et al., 2020b).

This chapter presents results from the HadGEM3-A atmosphere-only model simulation. Recall, this experiment used the low resolution (N96) HadGEM3-GA7.1 atmospheric-only model, forced with Antarctic sea ice conditions from the coupled model simulations. The atmosphere-only model was run with 200 ensemble members, in order to obtain robust results. All stated seasons refer to the austral seasons, unless otherwise specified.

7.2. Results

7.2.1 Sea ice

Antarctic SIC is reduced all year round (Figure 7.1 a-d) with the greatest reductions near the ice edge. The net heat flux response (Figure 7.1 e-h) shows its greatest increase (ocean-to-atmosphere) in the regions and seasons of largest sea-ice loss. Reductions in the net heat flux are seen northward of the sea ice edge in the Southern Ocean, reflecting anomalous heat input due to atmospheric warming.

SIA loss in square kilometres (Figure 7.1c) is largest in early summer, leading to near-complete loss of ice at a time of year when the effect of the albedo change is largest; and is smallest in late summer, when there is little ice to begin with. In

the winter, sea-ice loss is ~7x10^6 km^2, which is a 40 % reduction sea ice. Compared to the simulated sea-ice loss in the coupled model, from which the specified sea ice boundary conditions were derived, there are small differences, primarily in summer and early autumn, arising from a technical problem explained fully in Chapter 3.

The total turbulent heat flux to the atmosphere peaks in winter (July) at 550 TW and is smallest in summer (December) at 50 TW (Figure 7.1d). This annual cycle reflects both the magnitude of sea-ice loss in each month and the magnitude of the air-sea temperature difference. The heat flux response in the coupled model is near equivalent to the atmospheric-only model, with the atmosphere-only response being slightly greater at its annual maximum, and peaking a month earlier (in July, rather than August). However, these subtle differences between the coupled and atmosphere-only model are modest compared to the magnitude of the heat flux response to sea-ice loss.

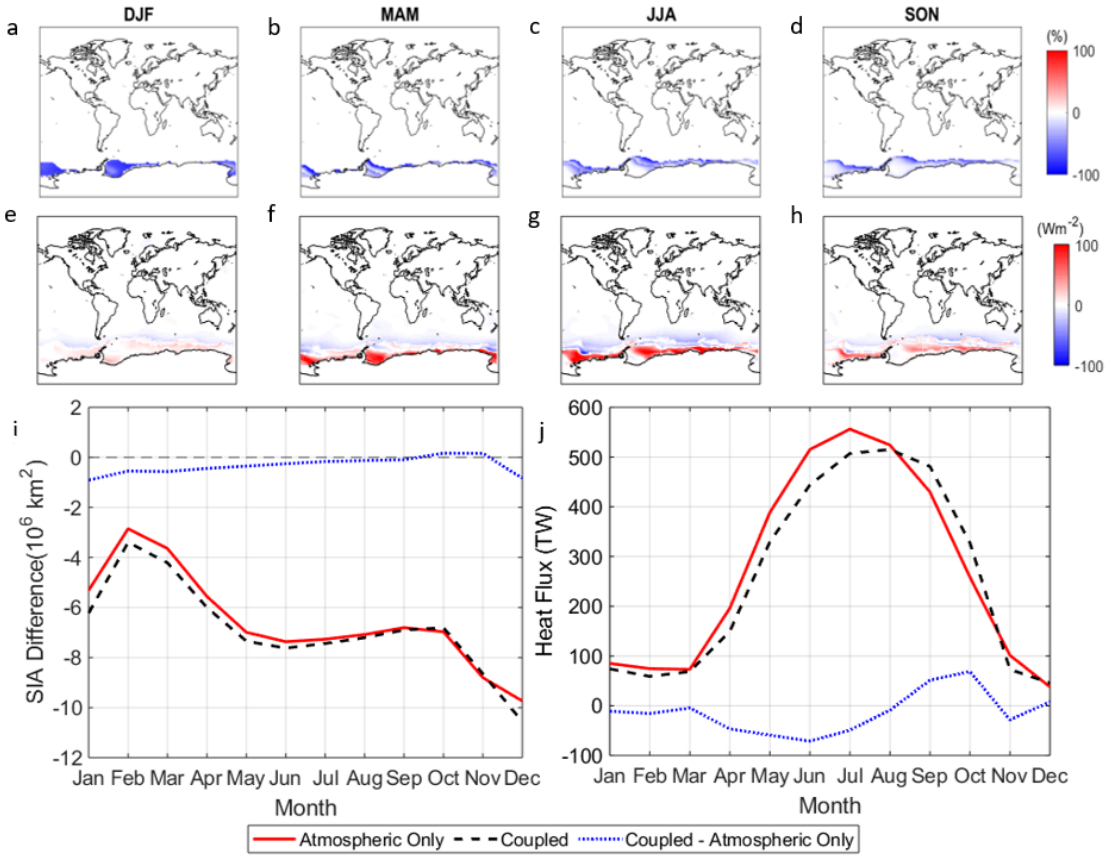

Figure 7.1: *Sea ice concentration (SIC) response to Antarctic sea-ice loss in austral (a) summer (December-February; DJF), (b) autumn (March-May MAM), (c) winter (June-August; JJA) and (d) spring (September-November SON). (e-h) as (a-d) for surface turbulent heat flux response. The heat flux is defined as positive in the upward direction. (i) Total sea ice area (SIA) response to Antarctic sea-ice loss as a function of calendar month, with the solid red line showing the Southern Hemisphere ice response in the atmospheric-only simulation, the dashed black line showing the ice response in the coupled simulation, and the blue dotted line showing the difference between the coupled and the atmospheric-only sea ice. (j) As (i) for the surface turbulent heat flux response, calculated as the area-weighted surface turbulent (sensible plus latent) heat flux response, summed over grid points where the sea ice concentration differs between the control and the Antarctic sea-ice loss states.*

7.2.2 Spatial pattern of atmospheric response

The near-surface air temperature response extends over the regions of sea-ice loss, the Southern Ocean, and the coastal regions of the Antarctic continent (Figure 7.2 a-d). There is a clear seasonal cycle, with the largest warming in autumn and winter, reaching as high as 10 K. Over the Antarctic continent, coastal regions warm by up to 2 K in the autumn and winter, but this warming does not extend to the high-altitude plateau in any season.

The mean sea level pressure (MSLP) response (Figure 7.2 e-h) to Antarctic sea-ice loss shows a decrease in pressure of up to 300 Pa over the Southern Ocean and Antarctic continent in all seasons apart from autumn, when there is a slight increase at the highest latitudes and in the ASL region. Few regions beyond the Southern Ocean show a significant MSLP response, with perhaps the exception of summer, when there are patchy MSLP increases over mid-latitudes.

The zonal wind response at 500 hPa (U500) (Figure 7.2 i-l) displays a decrease of up to 1 ms^{-1} close to the continent in all seasons, and a decrease in the latitudes of the westerly eddy-driven jet of up to 3 ms^{-1}, significant in only autumn and winter. On the northern flank of the jet, there is a slight increase in westerly velocity, but this is not statistically significant at all longitudes or in all seasons. Farther north, there are again only small, patchy regions of significant change.

Precipitation (Figure 7.2 m-p) significantly increases over areas of Antarctic sea-ice loss, most strongly in autumn and winter. However, there is no significant

response over the continent. Over the lower latitude Southern Ocean there is a small, but significant, precipitation decrease.

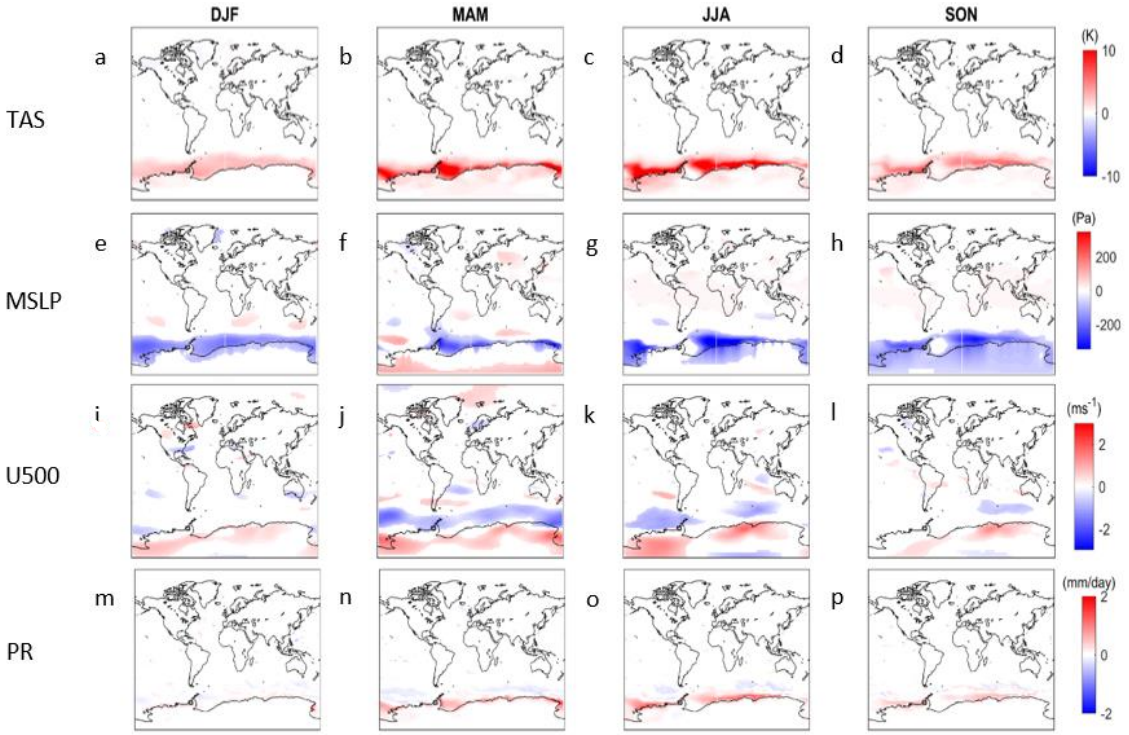

***Figure 7.2**: Surface air temperature (TAS) response to Antarctic sea-ice loss in austral (a) summer (December-February; DJF), (b) autumn (March-May MAM), (c) winter (June-August; JJA) and (d) spring (September-November SON). (e-h) As (a-d), for mean sea level pressure (MSLP). (i-l) As (a-d), for 500 hPa westerly wind (U500). (m-p) As (a-d) but for total precipitation (PR).*

A comparison of the cold season (March – August; Figure 7.3 a-c) and warm season (September – February; Figure 7.4 a-c) near-surface air temperature responses in the atmosphere-only and coupled configurations (Figure 7.3 a-c) shows similarities over the Southern Ocean and regions of sea-ice loss, but clear differences elsewhere. The coupled model response is ~2 K warmer than the maximum increase in the atmospheric-only response. In the differences between

coupled and atmosphere-only versions (Figure 7.3c), there is a ring around the sea ice edge where there is no difference between the two responses. This likely occurs where sea-ice loss does not match in the coupled and atmosphere-only models, due to values below 0.3 being set to 0 in the latter (see chapter 3 for details). Over the continent, the warming response in the atmosphere-only model does not reach the high-altitude plateau, unlike in the coupled model. It is suspected that mid-latitude ocean warming, simulated in the coupled model but not in the atmosphere-only model, is needed to drive the continental warming signal, through advection of temperature anomalies along isentropic surfaces, from the lower troposphere in mid-latitudes to the mid-troposphere at high latitudes. Away from the continent, the warming response in the atmosphere-only model is confined to south of 50° S, whereas the warming in the coupled model extends toward to the tropics (and beyond; see Chapter 5).

The cold season mean sea level pressure (MSLP) responses in the coupled and atmosphere-only models are of opposite sign in many regions. The coupled model response shows a MSLP increase over the continent whereas the atmosphere-only model shows a decrease, although not significant at highest latitudes. The ASL does not change strength significantly in the atmosphere-only version but weakens in response to sea-ice loss in the coupled model. Similarities between the coupled and atmosphere-only model responses include a decrease in the Atlantic sector of the Southern Ocean and Weddell Sea, albeit with the decrease being of greater magnitude in the atmosphere-only model. Overall, the coupled model response bears closer resemblance to the negative SAM phase than the atmosphere-only model response (Figure 7.3f). The MSLP response

differences, between coupled and atmosphere-only configuration, are similar in the warm season (Figure 7.4 d-f) to those in the cold season.

The cold season 500 hPa zonal wind (U500) responses (Figure 7.3 g-i) show similarities in their spatial patterns between the coupled and atmosphere-only versions. Both display an increase in zonal wind over the Antarctic and a weakening of the tropospheric eddy-driven jet. The main difference between the two cases is the magnitude of this weakening, being more than twice as large in the coupled experiment compared to the atmosphere-only experiment. The weakening is also more latitudinally confined in the atmosphere-only model response, with a slight but significant increase on the equatorward flank of the jet that is absent in the coupled counterpart. The jet response difference is more pronounced in the warm season (Figure 7.4 g-i), when the coupled model depicts a strong decrease in westerly wind in the latitudes of the tropospheric eddy-driven jet, whereas the atmosphere-only version depicts minimal change. Thus, the weakened westerly response is seen year-round in the coupled model, but only during the cold season in the atmosphere-only model.

The precipitation responses are similar between the cold (Figure 7.3 j-l) and warm seasons (Figure 7.4 j-l). In both the coupled and atmosphere-only models, the overall responses are an increase in precipitation over the regions of sea-ice loss. In the coupled model, the wetting signal is seen over much of the Southern Ocean, whereas it is locally confined to the high latitudes in the atmosphere-only model. In fact, over the Indian Ocean sector of the Southern Ocean, precipitation decreases in the atmosphere-only case. This greater spatial extent of the wetting

signal in the coupled model, compared to that in the atmosphere-only model, is likely due to the more widespread warming (Figure 7.3 a-c) in the coupled model, which is expected to increase moisture availability.

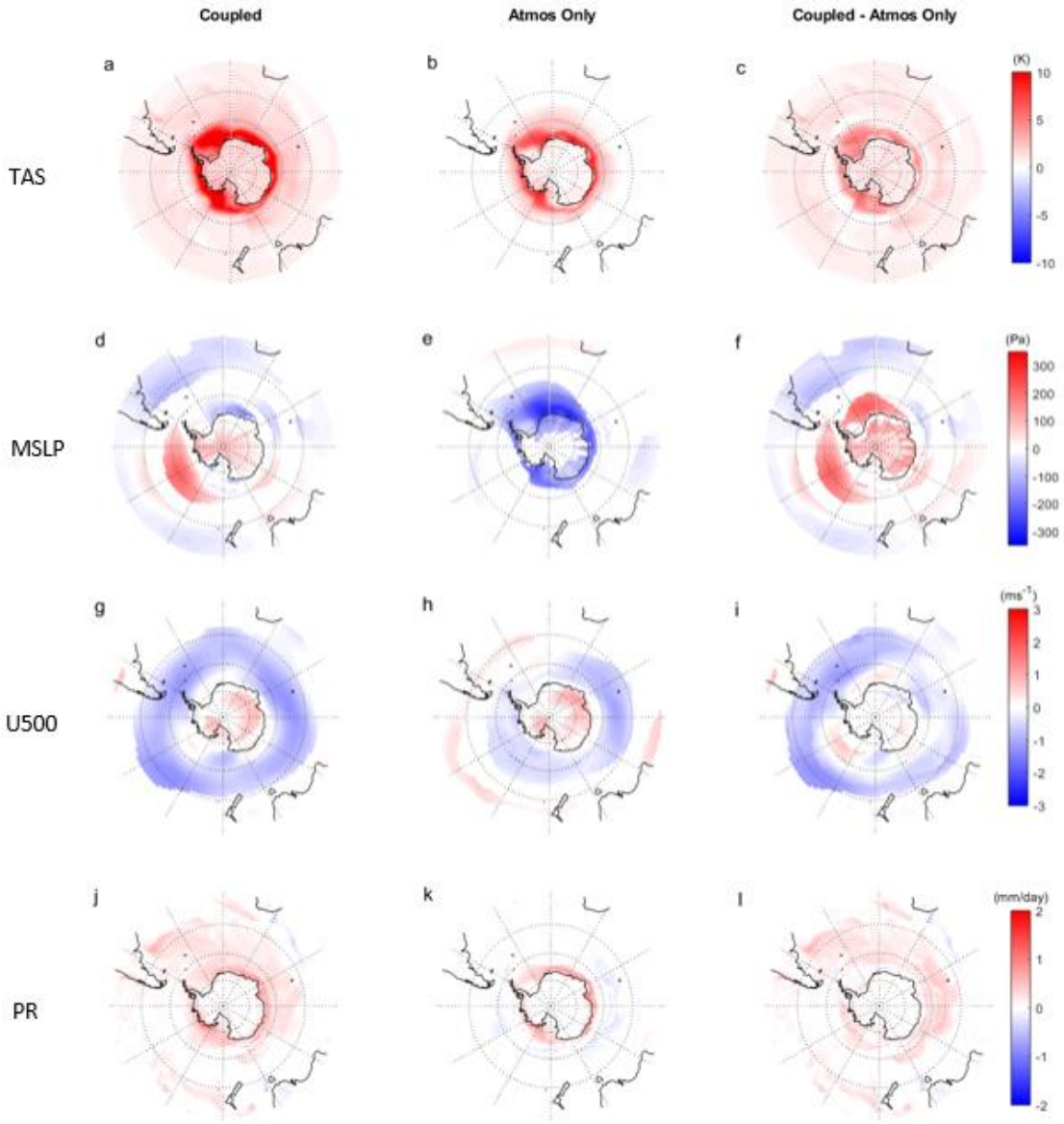

***Figure 7.3**: Surface air temperature (TAS) (a) coupled model response to Antarctic sea-ice loss in austral cold season (March-August; MAMJJA), (b as (a) for atmospheric-only response, (c) for the difference between the coupled and atmospheric-only response. (d-f) As (a-c), for mean sea level pressure (MSLP). (g-h) As (a-c), for 500 hPa westerly wind (U500). (j-l) As (a-c) for total precipitation (PR).*

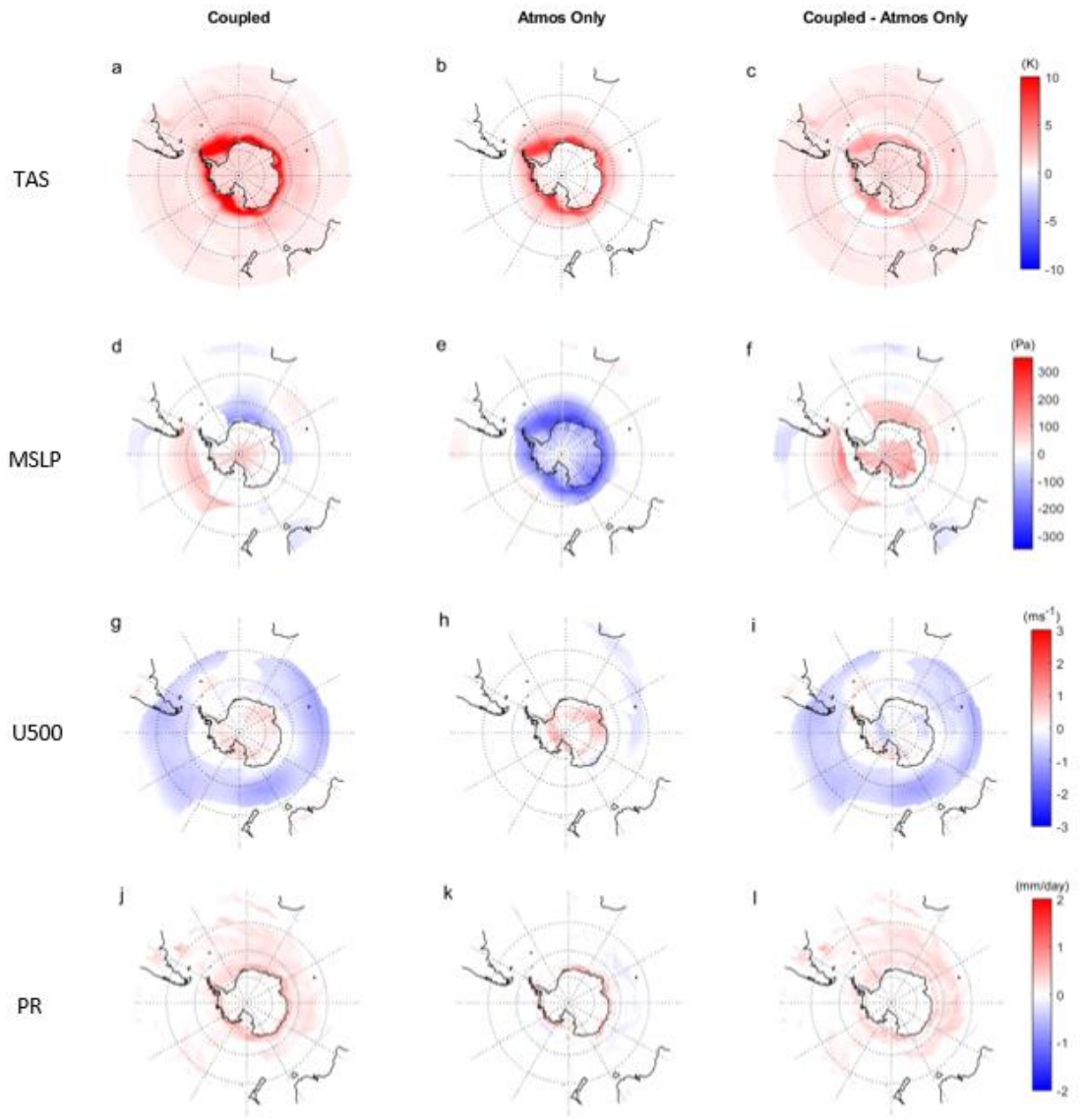

***Figure 7.4**: Surface air temperature (TAS) (a) coupled model response to Antarctic sea-ice loss in austral warm season (September - February; SONDJF), (b) as (a) for atmospheric-only response, (c) for the difference between the coupled and atmospheric-only response. (d-f) As (a-c), for mean sea level pressure (MSLP). (g-h) As (a-c), for 500 hPa westerly wind (U500). (j-l) As (a-c) for total precipitation (PR).*

7.2.3 Vertical structure of atmospheric response

In the absence of ocean coupling the zonal-mean temperature response to Antarctic sea-ice loss (Figure 7.5 a-d) displays lower tropospheric warming (up to 500 hPa) over Antarctica and the Southern Ocean, of greatest magnitude in autumn and winter. In the Antarctic upper troposphere and stratosphere, the temperature responses vary with season: warming in autumn and winter and cooling in spring and summer. The temperature response is weak over low latitudes and in the Northern Hemisphere apart from boreal winter, where there is notable stratospheric cooling over the Arctic.

The zonal-mean zonal wind response (Figure 7.5 e-h) also has marked seasonality. In autumn and winter, there is a decrease in the speed of the mid-latitude eddy-driven jet throughout the troposphere, with an increase on the equatorward flank in autumn. In spring and summer, the zonal wind changes are weak in the vicinity of the jet, but large increases are simulated over the Antarctic into the stratosphere. Related to the stratospheric cooling over the Arctic in boreal winter, there is a strengthening of the northern stratospheric polar vortex.

Comparing the coupled and atmosphere-only models, the zonal-mean temperature responses to Antarctic sea-ice loss in the cold season (March – August) (Figure 7.6 a-c) are similar in terms of sign and spatial pattern over the high-latitude Southern Hemisphere, but very different elsewhere. Although both model versions depict tropospheric warming over the Antarctic and Southern Ocean, this warming is of greater magnitude and extends to higher altitudes in the coupled model. Warming reaches the tropopause over the Antarctic (250

hPa) in the coupled model, whereas it is confined to below 500 hPa in the atmosphere-only model. The upper tropospheric and lower stratospheric cooling is also of greater magnitude in the coupled model. Away from Antarctica, there is a clear global tropospheric warming signature in the coupled model, which is not present in the atmospheric-only model. The tropical upper tropospheric warming and Arctic lower tropospheric warming seen in the coupled model response are absent from the atmosphere-only model response. The differences in responses in the warm season (September - February) (Figure 7.7 a-c) are comparable to those just described for the cold season.

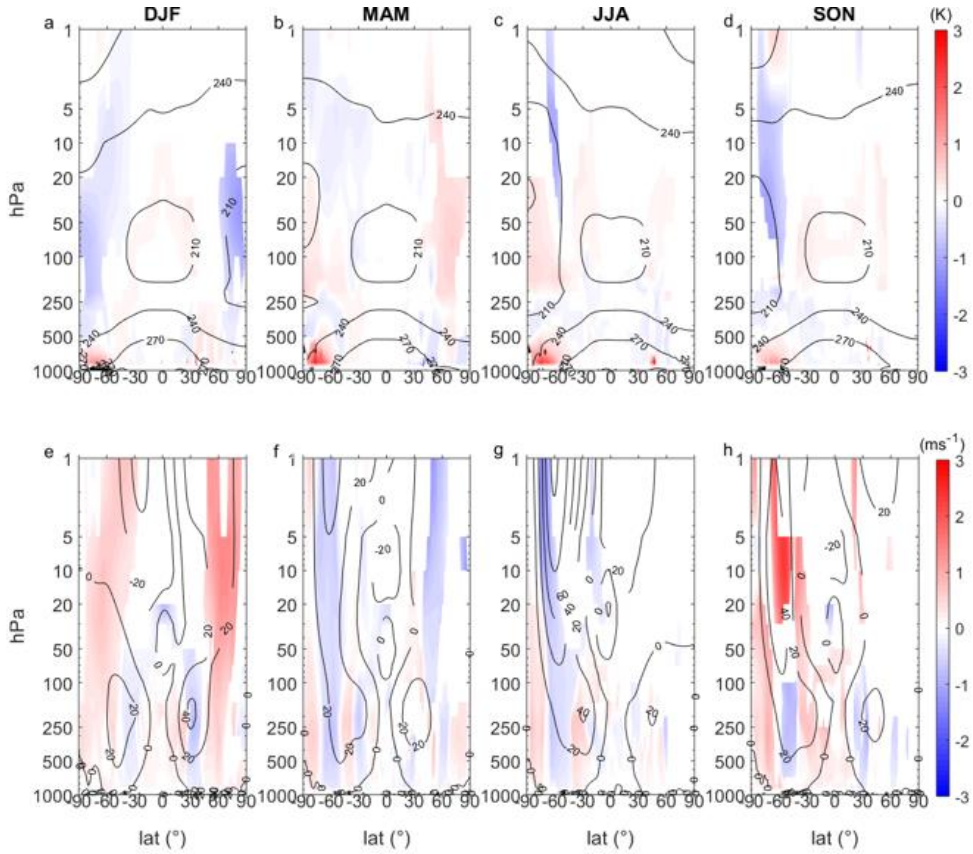

***Figure 7.5**: Zonal-mean air temperature response to Antarctic sea-ice loss in austral (a) summer (December-February; DJF), (b) autumn (March-May MAM), (c) winter (June-August; JJA) and (d) spring (September-November SON). (e-h) As (a-d), for zonal-mean westerly wind.*

The main differences between the zonal-mean zonal wind responses in the coupled and uncoupled models are in the vicinity of the subtropical jets, in both the cold (Figure 7.6 d-f) and warm (Figure 7.7 d-f) seasons. In the coupled model, the westerly winds increase in the tropical upper troposphere, in both hemispheres, related to the upper tropospheric tropical warming. These features are absent in the atmosphere-only configuration. The coupled model depicts larger reductions in the tropospheric westerly winds over southern mid-latitudes, compared to the uncoupled version, especially in the warm season. The southern polar vortex strengthens in the cold season in the coupled model but not in the uncoupled model.

The Southern Hemisphere mid-latitude tropospheric eddy-driven jet latitude (Figure 7.8a) shifts equatorwards in months from March to August, with a maximum of 0.95° in August, in the atmosphere-only model. This shift is broadly comparable to response in the coupled model. The largest difference between the coupled and uncoupled versions is found in September, when the jet shifts equatorwards in the coupled model, but poleward in the uncoupled model. The jet weakens in the atmosphere-only model throughout the entire year, apart from late spring and early summer (Figure 7.8b), with a maximum weakening in September of -0.3 ms^{-1}. Although a robust feature across the two model versions, the jet weakening is of notably greater magnitude in the coupled model than the atmosphere-only model. Ocean coupling appears to be more important for the jet strength response than the jet latitude response to Antarctic sea-ice loss. These differences in the jet response, between coupled and uncoupled versions, occur despite similar mean states of the two model versions (Figure 7.8 c&d),

suggesting ocean-atmosphere coupling rather than state dependencies is the main cause of cause the jet response differences.

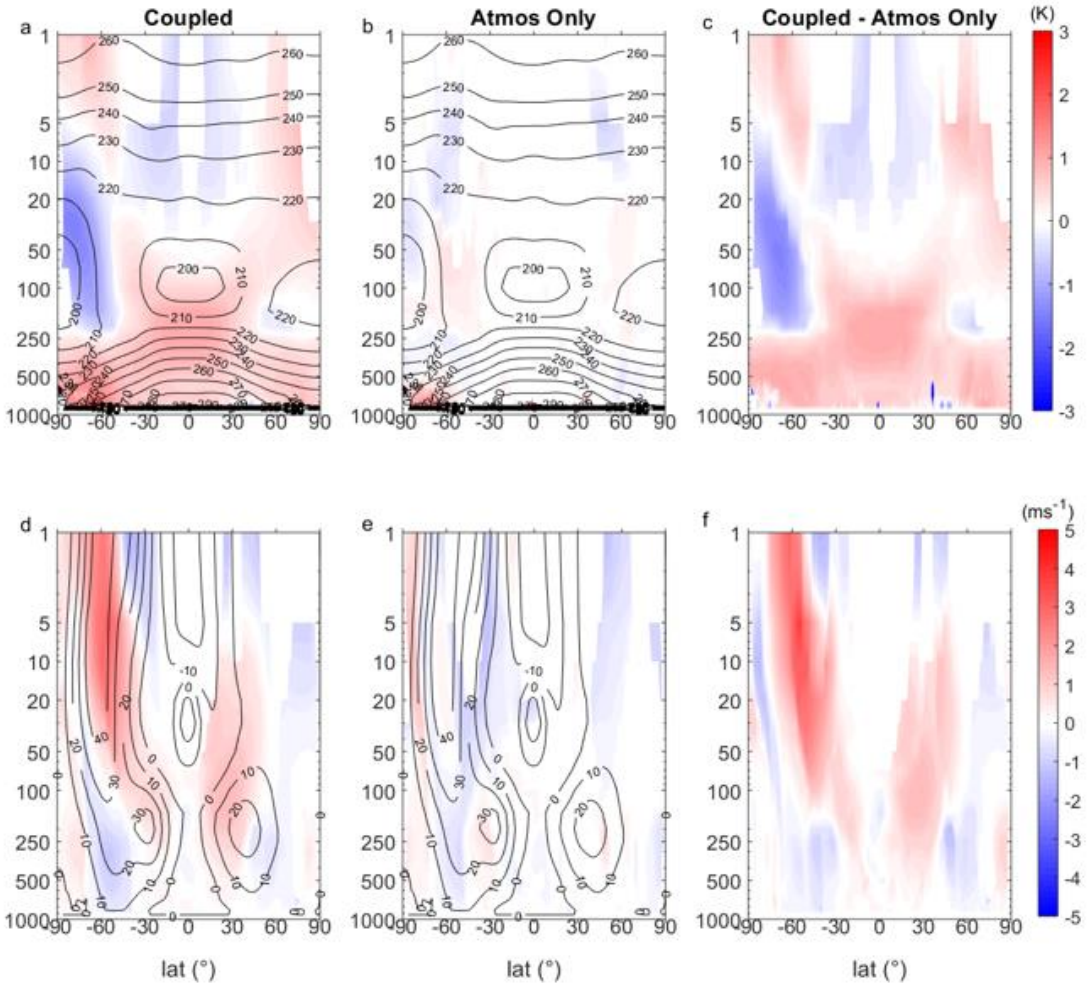

***Figure 7.6**: Zonal-mean air temperature (a) coupled model response to Antarctic sea-ice loss in austral cold season (March-August; MAMJJA). (b) As (a) for atmospheric-only response, (c) for the difference between the coupled and atmospheric-only response. (d-f) As (a-c) for zonal-mean westerly wind.*

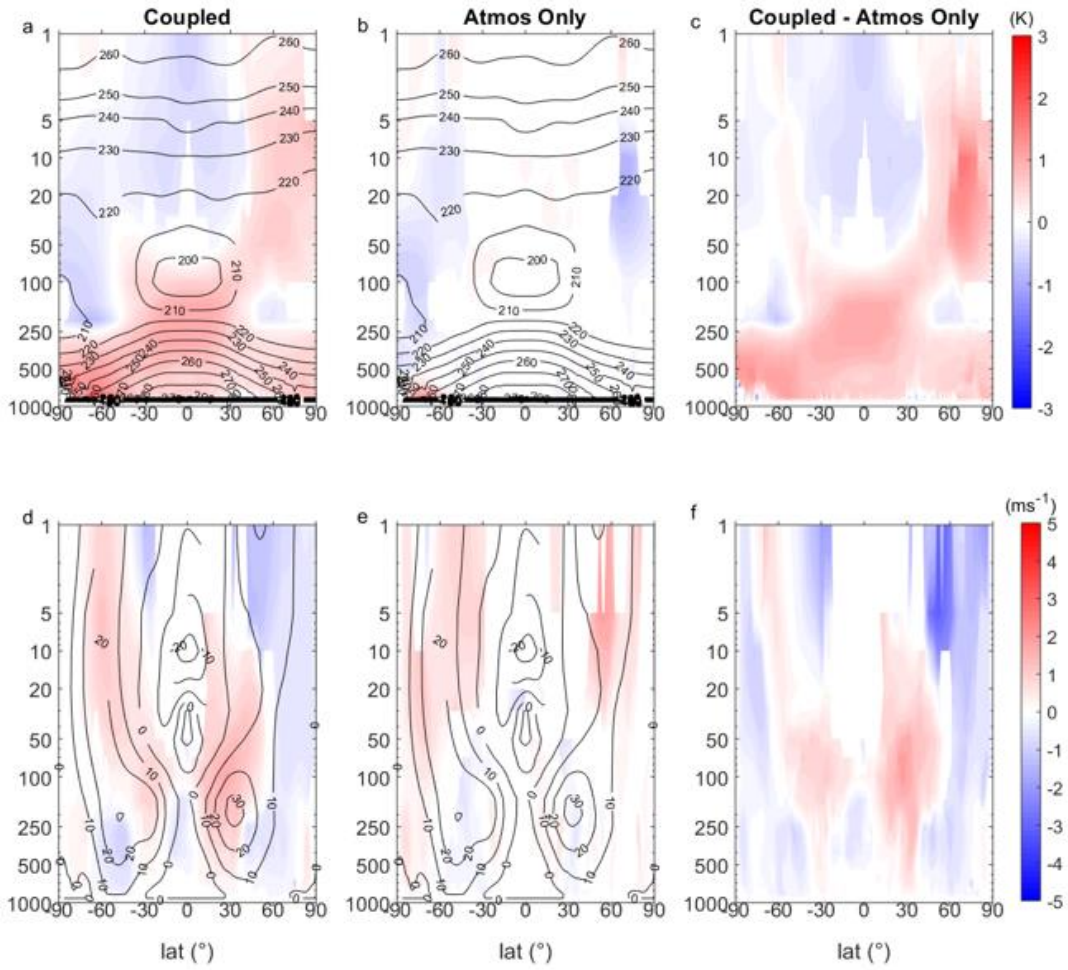

***Figure 7.7**: Zonal-mean air temperature (a) coupled model response to Antarctic sea-ice loss in austral warm season (September - February; SONDJF). (b) As (a) for atmospheric-only response, (c) for the difference between the coupled and atmospheric-only response. (d-f) As (a-c) for zonal-mean westerly wind.*

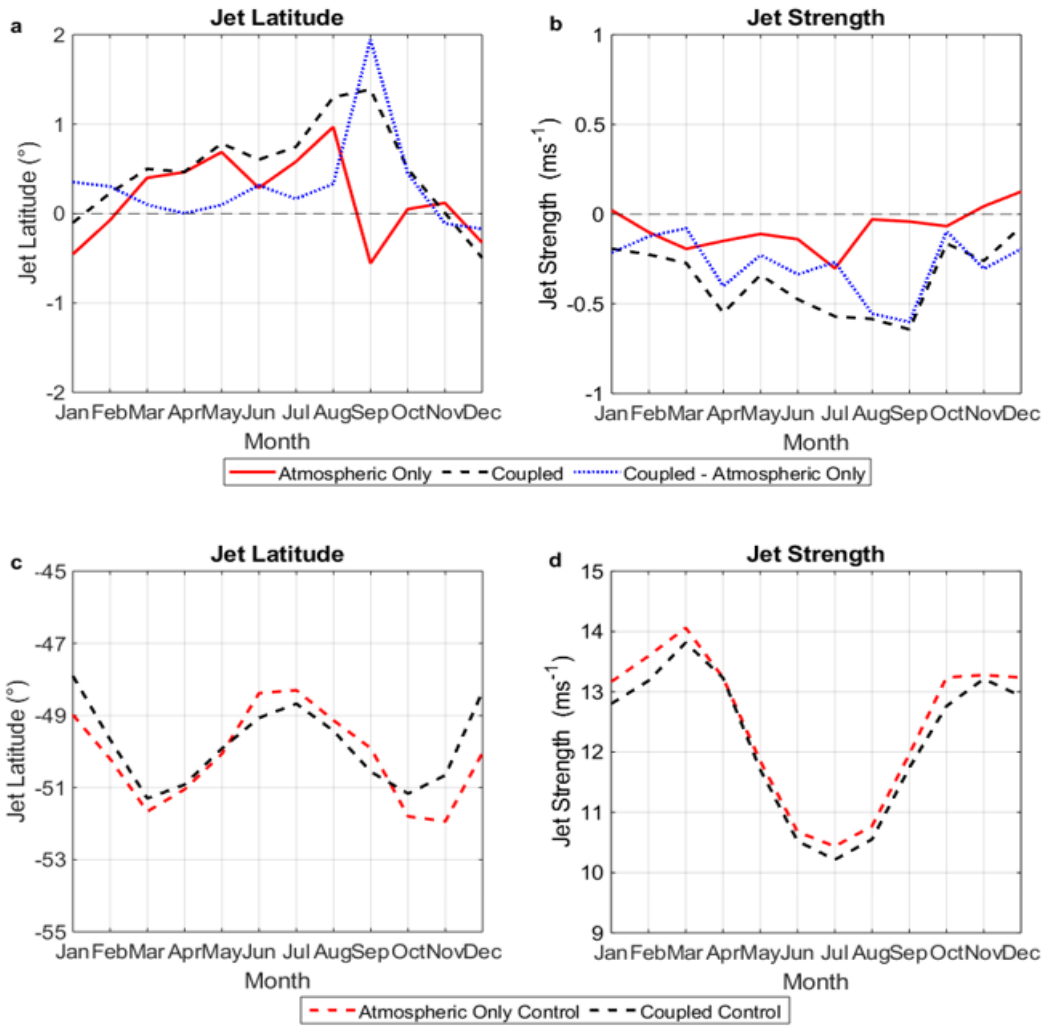

***Figure 7.8**: The Southern Hemispheric tropospheric jet latitude response to Antarctic sea-ice loss with the solid red line showing the jet response in the atmospheric-only simulation, the dashed black line showing the jet response in the coupled simulation, and the blue dotted line showing the difference between the coupled and the atmospheric-only response. (b) As (a), for jet strength. (c&d) As (a&b) for the controls of the atmospheric only (red) and coupled model (black).*

7.3. Discussion

This chapter provided a direct comparison between the coupled and atmosphere-only model responses to Antarctic sea-ice loss. The results presented highlight key differences between the atmosphere-only and coupled model experiments, which suggest an important role for ocean coupling. The atmosphere-only model response to Antarctic sea-ice loss shows a localised warming response, greatest in autumn and winter, which does not reach the high-altitude Antarctic plateau or extend to lower latitudes. In comparison, warming in the coupled model reached the continental interior, suggesting ocean-atmosphere interaction is critical to the Antarctic warming response, consistent with England et al. (2020a; 2020b). As discussed in Chapter 2, this may be due to the coupled model allowing for the mid-latitude oceans to warm. Warm anomalies are then advected along isentropic surfaces from the mid-latitude ocean surface to the high-latitude mid-troposphere (Laliberté & Kushner, 2013). Precipitation increased over the southern high latitudes in both model configurations, but with greater magnitude and spatial extent in the coupled model, consistent with the larger and more widespread warming response.

The local warming and wetting responses were approximately twice as large in the coupled model as the uncoupled model. This is comparable to Deser et al., 2016, which reported that ocean coupling amplified the warming response to Arctic sea-ice loss by approximately 50 %. The coupled model displays a clear “mini-global warming” signature, with warming maxima in the high-latitude lower troposphere and tropical upper-troposphere. However, this global response is absent in the atmosphere-only model, which supports the interpretation in Chapter 2 that ocean coupling is important in communicating Antarctic changes

to the rest of the globe. This result is consistent with England et al. (2020a; 2020b), whom also demonstrated the important role of ocean coupling in creating a “mini-global warming” response from Antarctic sea-ice loss, but in a different climate model. This result also echoes numerous studies on the response to Arctic sea-ice loss (e.g Blackport & Kushner, 2016; Deser et al., 2016; Deser et al., 2015; Oudar et al., 2017), wherein the response in atmospheric-only models was locally confined in comparison to the global response in coupled models.

The sea level pressure response in the atmosphere-only model was dominated by pressure reductions over the regions of sea-ice loss, which can be understood as a direct thermal “heat low” response. In contrast, the sea level response in the coupled model is more complex. Reduced pressure is still seen over many regions of sea-ice loss, but additionally, there is a pressure reduction in the ASL region, not seen in the atmosphere-only model. The coupled model greatly resembles a negative SAM phase in all seasons, whereas the atmospheric only model does not.

The zonal wind response in the vicinity of the mid-latitude jet is similar in coupled and uncoupled models, but the coupled response is of greater magnitude. The zonal wind response in the atmosphere-only model is, again, latitudinally confined compared to the coupled model. In the coupled model, there is an increase in tropical upper-tropospheric westerly winds in both hemispheres, not present in the atmospheric-only response.

Focussing on the mid-latitude tropospheric eddy-driven jet, there is a significant shift equatorward, most prominent in autumn and winter, in both the coupled and atmospheric-only responses. Jet strength is weakened during most months of the year, but with lesser magnitude in the atmosphere-only model compared to the coupled model. This result agrees with previous literature on the reduction of jet strength, but the result of a significant equatorward shift is still debated (Ayres & Screen, 2019; Bader et al., 2013; Bracegirdle et al., 2018; England et al., 2018; Kidston et al., 2011; Menéndez et al., 1999; Raphael et al., 2011; Smith et al., 2017). The atmosphere-only and coupled models show greater consistency in the jet latitude response than the jet strength response. Jet strength is highly dependent on the meridional temperature gradient (and baroclinity), which is decreased more in the coupled model than in the atmosphere-only model. By contrast, the jet shift seems less dependent on the magnitude of high-latitude warming, in agreement with Bracegirdle et al., (2018). Previous studies have found the response in jet latitude to be dependent on the initial position of the jet (Bracegirdle et al., 2018). Although the initial jet latitude is closely comparable in coupled and uncoupled control runs, it is possible that even these seemingly small differences influence the resultant response to sea-ice loss.

7.4. Summary

The chapter has assessed the response to Antarctic sea-ice loss in an atmosphere-only model and conducted a direct comparison to response in the coupled model discussed in Chapter 5. The atmosphere-only model yielded a response that was lesser in magnitude, locally confined and seasonally dependent compared to the coupled model response. More specifically, the surface temperature response in the atmosphere-only model was largely confined to the regions of sea-ice and the adjacent coastal regions of the Antarctic continent, and did not reach the high-altitude Antarctic plateau. The response in the coupled model, however, was global in reach. The response in the tropospheric jet latitude was closely comparable in the coupled and atmosphere-only models, but the response in jet strength was stronger in the coupled model, likely related to the greater weakening of the meridional temperature gradient. Whilst atmosphere-only models have advantages, for example, they are cheaper and faster to run, coupled models are needed in order to evaluate the full magnitude and global scale of response to Antarctic sea-ice loss.

Chapter 8

Conclusions

8.1 Key Findings

This thesis has provided the first comprehensive examination of the climate response to Antarctic sea-ice loss, isolating the atmospheric and oceanic responses, and their coupled interactions. Three distinct modelling approaches were used. First, the CMIP5 multi-model ensemble was used to infer the atmospheric response to Antarctic sea-ice loss at quadrupled CO_2. Due to limitations of the indirect method, focus was on sea-ice induced changes to the extratropical Southern Hemisphere atmosphere. Second, a novel coupled modelling framework was used to isolate the full global response, in both the atmosphere and ocean, to abrupt sea-ice loss in HadGEM3. Third, a large ensemble of atmosphere-only model experiments was conducted, mimicking the sea ice conditions in the coupled experiment, to provide the first clear determination of the role of ocean coupling in the climate response to Antarctic sea-ice loss.

Robust results across all models and experimental approaches included tropospheric warming (Figure 5.5 & 5.8), of greatest magnitude in austral autumn and winter, over the regions of sea-ice loss and nearby Southern Ocean, but not extending to the Antarctic interior (Figure 4.2 & 7.3). Associated with warming, a robust increase in precipitation was also found (Figure 5.5 & 7.3). These local responses are much alike those found in the high-latitude Northern Hemisphere in response to Arctic sea-ice loss (e.g. Deser et al., 2010; England et al., 2018; Screen & Simmonds, 2010; Screen et al., 2013).

A weakening and slight equatorward shift of the Southern Hemisphere tropospheric eddy-driven jet, leading to a more negative SAM index, was also common across all models and experiments (Figures 4.9, 5.5 & 7.3). The weakened jet is likely a consequence of the weakened near-surface meridional temperature gradient, being of greatest magnitude in autumn and winter when the high-latitude warming is also most pronounced (Figure 5.5). The jet weakening in response to Antarctic sea-ice loss acts to slightly offset the strengthening of the jet in response to increased CO_2 (Figure 4.9 & 5.13).

The weakening of the jet in response to Antarctic sea-ice loss is in broad agreement with past work (Bader et al., 2013; England et al., 2018; Kidston et al., 2011; Menéndez et al., 1999; Raphael et al., 2011; Smith et al., 2017) and again, is analogous to the robust weakening of the Northern Hemisphere eddy-driven jet in response to Arctic sea-ice loss (e.g., Blackport & Kushner, 2016; Deser et al., 2015; Kim et al., 2014; Peings & Magnusdottir, 2014; Screen & Simmonds, 2013; Screen et al., 2013). Despite the jet response being qualitatively similar to past studies using atmosphere-only models, it is notable that the jet response was larger and found year-round (rather than just in the colder months) in the coupled model (Figure 7.5 & 7.6), due to the greater weakening of the meridional temperature gradient. Thus, past studies may have underestimated the jet response to Antarctic sea-ice loss.

Although the aforementioned atmospheric responses were independent of ocean coupling, at least qualitatively, other atmospheric responses were found only in

the coupled model experiment. In addition to the 'fast' and largely local responses seen across all experiments, the coupled model experiments revealed 'slow' and global responses. Ocean coupling allowed the warming response to spread globally, including into the Antarctic interior (Figure 5.5). Warming did not reach the high-altitude Antarctic continent plateau in neither the CMIP5 analysis nor the atmosphere-only experiments (Figure 4.2 & 7.3), due to the lack of warming in the mid-latitude oceans. After a period of around 50 years after abrupt sea-ice loss, lower tropospheric warming was global in reach and upper tropospheric warming was simulated in the tropics, thought to be primarily driven through warmer tropical SSTs and enhanced convection (Figure 5.10).

The spatial pattern of sea-ice induced warming at (quasi-)equilibrium is reminiscent of that in response to increased CO_2, but with lesser magnitude (Figure 5.13 & 5.14). This pattern is also alike that seen in response to Arctic sea-ice loss in coupled models (Deser et al., 2015; 2016; Smith et al., 2017; Tomas et al., 2016; 2016b; Blackport & Kushner, 2016; Oudar et al., 2017; Sun et al., 2020), which Deser et al. (2015) referred to as a 'mini global warming' response. This thesis has shown that the concept of a 'mini global warming' is also applicable to the response to Antarctic sea-ice loss (Figure 5.14), as simulated by HadGEM3, and further supported by recent work with the CESM-WACCM model (England et al. 2020a; 2020b).

Another distinct aspect of the response to Antarctic sea-ice loss, seen in HadGEM3 but not in the atmosphere-only model experiments, is warming in the Arctic, and associated Arctic sea-ice loss (Figures 5.2, 5.3 & 5.4). Again, this

response in HadGEM3 is confirmed by the CESM-WACCM experiments in England et al. (2020b).

The results presented in this thesis highlight that ocean coupling is important to capture the full magnitude, and global scale of the atmospheric response to Antarctic sea-ice loss. Atmosphere-only models still have their place as tool to assess and understand the local and shorter-term impacts of Antarctic sea-ice loss. They are cheaper and faster to run, making larger ensembles or a greater diversity of experiments possible. Large ensembles, to better separate the forced response from internal variability (Mori et al., 2014; Screen et al., 2014), may be more advantageous than ocean coupling for some applications. However, coupled models are evidently needed to accurately quantify the extratropical Southern Hemisphere climate response to Antarctic sea-ice loss, and are essential to capture the responses in the tropics and Northern Hemisphere.

This thesis has also provided the first detailed examination of the oceanic response to Antarctic sea-ice loss, using a coupled model framework. A novel result is the simulated ~20 % reduction in ACC transport, likely in response to reduced surface wind stress from a weakened tropospheric eddy-driven jet (Figure 6.6). Whether or not surface wind stresses changes would be expected to influence ACC transport is debated in the literature (Böning et al., 2008; Farneti & Delworth, 2010; Farneti et al., 2010; Hallberg and Gnanadesikan, 2006). However, at least in the low resolution HadGEM3 model, ACC transport was significantly reduced in response to Antarctic sea-ice loss.

Surface waters became warmer, more stable, and more stratified in the Southern Ocean in response to Antarctic sea-ice loss (Figure 6.8). Similar changes were simulated in the Arctic Ocean, but with lesser magnitude (Figure 6.12). Globally, the pattern of warming and salinity change with latitude and depth was alike that in response to increased CO_2, but lesser in magnitude (Figure 6.2). Thus, it is also appropriate to think of the oceanic response to Antarctic sea-ice loss as a 'mini global warming' response. Despite this, there were no notable change to the AMOC (Figure 6.13).

To summarise the overall response to Antarctic sea-ice loss, the key climatic processes are as follows. Antarctic sea-ice loss causes an initial heat flux from ocean to atmosphere, triggering a localised tropospheric warming. This warming creates a surface pressure change, namely in the spatial pattern of a negative SAM index. The equator-to-pole temperature gradient is reduced, and thus, the tropospheric eddy driven jet is weakened. Surface atmospheric warming conveys with it an increase in Southern Ocean SSTs, which through atmospheric and wind driven circulation, warms the Antarctic continent and plateau, and, over several decades, spreads northward towards the equator. A weakening of the easterly equatorial winds leads to a reduction in equatorial upwelling in the upper ocean tropical convergence cell, causing reduced upwelling of cold water from below, and enhancing the surface warming. From the tropical Pacific, a Rossby wave causes a strengthening of the Aleutian Low in the North Pacific, contributing to Arctic warming, in addition to triggering Northern Hemisphere sea-ice loss.

The ocean response is just as global in reach. Initially, there is an overall warming of the surface mixed layer in the Southern Ocean, due to the reduced albedo and exposure to short wave radiation. With the reduction of sea ice comes an overall reduction of brine rejection, which in turn reduces salinity, alongside the increased precipitation. However, surface salinity is also increased in the melt season, due to the reduction of saltwater flux in the formation season. The combined effect of these changes leads to a decrease in surface density, which stabilises and shallows the surface layer, in addition to reducing vertical mixing. The temperature gradient across the ACC is reduced, and alongside the reduction of wind stress at the atmospheric boundary layer, ACC transport is reduced by approximately 20 %. The reduction in the wind stress also reduces the Ekman driven northward transport of cold water, increasing surface transport of warm water into the Southern Ocean.

8.2 Future work and possible extensions

This thesis demonstrated a clear response to Antarctic sea-ice loss across varying methodologies, however, these methods had limitations. The multimodel response to sea-ice loss, indirectly inferred from CMIP5 models, relied on imperfect scaling approaches. As a result, the SST scaling used meant that any tropical response to sea-ice loss would be missed by this method. The coupled model used in Chapter 5 and 6 was the low resolution HadGEM3 GC3.1 model. The benefits of using the low resolution version of the model out-wayed the potential problems, for example, the low resolution model has been shown to perform better in many aspects of the climate, including the ACC (See Chapter 3.2 for more details). However, the high resolution version of the model explicitly resolves mesoscale eddy interactions. This experiment used a melt pond albedo

scheme, whereby the model gave a different seasonal cycle to projections, however, maintained better water and energy conversation than other methods (Sun et al., 2020). The final method, used in Chapter 7, utilised the atmosphere-only version of the coupled model used in Chapter 5 and Chapter 6. When applying the sea ice conditions to the model, an issue arose whereby all sea ice concentrations less than 30% were set to zero (Figure 3.10). Although unfixable within the scope of this work, this limitation made little difference to the overall results (Figure 7.1). A second issue, where sea ice thickness was unable to be prescribed in the atmosphere only version of the model, made the sea ice thickness unalike in the coupled and atmosphere-only versions (Figure 3.11). However, due to the short seasonal cycle of Antarctic sea ice, sea ice thickness is thought to have less of an impact than it would have in the Arctic. Possible extensions that address these issues are discussed below.

One caveat of this thesis is it's heavy reliance on a single model, namely HadGEM3. Although key results are substantiated by CMIP5 multi-model analysis, and by England et al. (2020a; 2020b) using CESM-WACCM - the only other coupled model study of the response to Antarctic sea-ice loss - it remains possible that aspects of the response may be model dependent. Indeed, a number of studies have highlighted aspects of the atmospheric response vary between models (Ayres & Screen, 2019; Bracegirdle et al., 2018; Holmes et al., 2019). Given the importance of ocean coupling in the global response to Antarctic sea-ice loss, demonstrated in this thesis, sea ice perturbation experiments with greater diversity of coupled models is encouraged.

This thesis assessed the effect of Antarctic sea-ice loss on the ocean, using a low-resolution version of HadGEM3, for practical reasons (i.e. speed and computing cost), and also because the high-resolution version performs poorly in the Southern Ocean (Menary et al., 2018) - in many regards, worse than the low-resolution version. The relatively low-resolution ocean in HadGEM3 is a potential source of model error in the response to sea-ice loss, however. For example, past work has suggested that mesoscale eddies may be important for ACC transport response to changed wind stress (e.g., Downes et al., 2011; Munday et al., 2013). A valuable extension to the work presented in this thesis would be to perform analogous simulations with a high resolution, eddy-resolving model; ideally one that performs well in the Southern Ocean. It would be especially interesting to see if the reduction in ACC transport, in response to sea-ice loss, is also simulated at higher resolution.

The thesis has focussed on the equilibrium response to sea-ice loss. However, Chapter 5 suggested different timescales to responses, with ‘fast’ responses governed by atmospheric processes and ‘slow’ responses that rely on oceanic adjustments. Future work could examine the transient response in closer detail, perhaps by conducting multiple ensemble members for the first 50-100 years after abrupt sea-ice loss. This would allow clearer separation of the forced response from internal variability, and of the time evolution of the forced response.

The novel method developed here to induce sea-ice loss within the coupled climate system, by altering the melt pond scheme, could be applied to examine

the global response to Arctic sea-ice loss, which would complement work using alternative methods of perturbing sea ice (e.g., Blackport & Kushner, 2016; Deser et al., 2015; Oudar et al., 2017; Sun et al., 2018; Sun et al., 2020). Lastly, a logical and worthwhile extension to the CMIP5 analysis, would be to replicate it with the newer (and potentially, improved) CMIP6 models, to assess whether the conclusions are robust in another large multi-model ensemble.

Bibliography

Abernathey, R. P., Cerovecki, I., Holland, P. R., Newsom, E., Mazloff, M., & Talley, L. D. (2016). Water-mass transformation by sea ice in the upper branch of the Southern Ocean overturning. Nature Geoscience, 9(8), 596–601. https://doi.org/10.1038/ngeo2749

Alexander Haumann, F., Gruber, N., Münnich, M., Frenger, I., & Kern, S. (2016). Sea-ice transport driving Southern Ocean salinity and its recent trends. Nature, 537(7618), 89–92. https://doi.org/10.1038/nature19101

Armour, K. C., Marshall, J., Scott, J. R., Donohoe, A., & Newsom, E. R. (2016). Southern Ocean warming delayed by circumpolar upwelling and equatorward transport. Nature Geoscience, 9(7), 549–554. https://doi.org/10.1038/ngeo2731

Ayres, H. C., & Screen, J. A. (2019). Multimodel Analysis of the Atmospheric Response to Antarctic Sea Ice Loss at Quadrupled CO 2. Geophysical Research Letters, 46(16), 9861–9869. https://doi.org/10.1029/2019GL083653

Bader, J., Flügge, M., Kvamstø, N. G., Mesquita, M. D. S., & Voigt, A. (2013). Atmospheric winter response to a projected future Antarctic sea-ice reduction: A dynamical analysis. Climate Dynamics, 40(11–12), 2707–2718. https://doi.org/10.1007/s00382-012-1507-9

Bandoro, J., Solomon, S., Donohoe, A., Thompson, D. W. J., & Santer, B. D. (2014). Influences of the antarctic ozone hole on southern hemispheric summer climate change. Journal of Climate, 27(16), 6245–6264. https://doi.org/10.1175/JCLI-D-13-00698.1

Barthélemy, A., Fichefet, T., Goosse, H., & Madec, G. (2015). Modeling the interplay between sea ice formation and the oceanic mixed layer: Limitations of simple

brine rejection parameterizations. Ocean Modelling, 86, 141–152. https://doi.org/10.1016/j.ocemod.2014.12.009

Belkin, I. M., & Gordon, A. L. (1996). Southern Ocean fronts from the Greenwich meridian to Tasmania. Journal of Geophysical Research C: Oceans, 101(C2), 3675–3696. https://doi.org/10.1029/95JC02750

Bintanja, R., Van Oldenborgh, G. J., Drijfhout, S. S., Wouters, B., & Katsman, C. A. (2013). Important role for ocean warming and increased ice-shelf melt in Antarctic sea-ice expansion. Nature Geoscience, 6(5), 376–379. https://doi.org/10.1038/ngeo1767

Bitz, C. M., & Polvani, L. M. (2012). Antarctic climate response to stratospheric ozone depletion in a fine resolution ocean climate model. Geophysical Research Letters, 39(20), 1–5. https://doi.org/10.1029/2012GL053393

Blackport, R., & Kushner, P. J. (2016). The transient and equilibrium climate response to rapid summertime sea ice loss in CCSM4. Journal of Climate, 29(2), 401–417. https://doi.org/10.1175/JCLI-D-15-0284.1

Blackport, R., & Kushner, P. J. (2017). Isolating the atmospheric circulation response to arctic sea ice loss in the coupled climate system. Journal of Climate, 30(6), 2163–2185. https://doi.org/10.1175/JCLI-D-16-0257.1

Blackport, R., Screen, J. A., & Sciences, P. (2020). Insignificant effect of Arctic amplification on the amplitude of mid- latitude atmospheric waves. 1–10.

Blunier, T., & Brook, E. J. (2001). Timing of millennial-scale climate change in Antarctica and Greenland during the last glacial period. Science, 291(5501), 109–112. https://doi.org/10.1126/science.291.5501.109

Bodas-Salcedo, A., Williams, K. D., Ringer, M. A., Beau, I., Cole, J. N. S., Dufresne, J. L., … Yokohata, T. (2014). Origins of the solar radiation biases over the Southern Ocean in CFMIP2 models. Journal of Climate, 27(1), 41–56. https://doi.org/10.1175/JCLI-D-13-00169.1

Böning, C. W., Dispert, A., Visbeck, M., Rintoul, S. R., & Schwarzkopf, F. U. (2008). The response of the antarctic circumpolar current to recent climate change. Nature Geoscience, 1(12), 864–869. https://doi.org/10.1038/ngeo362

Bracegirdle, T. J., Hyder, P., & Holmes, C. R. (2018). CMIP5 diversity in Southern Westerly jet projections related to historical sea ice area: Strong link to strengthening and weak link to shift. Journal of Climate, 31(1), 195–211. https://doi.org/10.1175/JCLI-D-17-0320.1

Bracegirdle, T. J., Shuckburgh, E., Sallee, J. B., Wang, Z., Meijers, A. J. S., Bruneau, N., … Wilcox, L. J. (2013). Assessment of surface winds over the Atlantic, Indian, and Pacific Ocean sectors of the southern ocean in cmip5 models: Historical bias, forcing response, and state dependence. Journal of Geophysical Research Atmospheres, 118(2), 547–562. https://doi.org/10.1002/jgrd.50153

Briegleb, B. P., & Light, B. (2007). A Delta-Eddington Multiple Scattering Parameterization for Solar Radiation in the Sea Ice Component of the Community Climate System Model. (February), 100 pp.

Broecker, W. S. (1998). Paleocean circulation during the last deglaciation: A bipolar seesaw? Paleoceanography, 13(2), 119–121. https://doi.org/10.1029/97PA03707

Bromwich, D. H., Nicolas, J. P., Monaghan, A. J., Lazzara, M. A., Keller, L. M., Weidner, G. A., & Wilson, A. B. (2013). Central West Antarctica among the

most rapidly warming regions on Earth. Nature Geoscience, 6(2), 139–145. https://doi.org/10.1038/ngeo1671

Bryan, F. O., Hecht, M. W., & Smith, R. D. (2007). Resolution convergence and sensitivity studies with North Atlantic circulation models. Part I: The western boundary current system. Ocean Modelling, 16(3–4), 141–159. https://doi.org/10.1016/j.ocemod.2006.08.005

Ceppi, P., Zappa, G., Shepherd, T. G., & Gregory, J. M. (2017). Fast and slow components of the extratropical atmospheric circulation response to CO 2 forcing. Journal of Climate, 31(3), 1091–1105. https://doi.org/10.1175/JCLI-D-17-0323.1

Chambers, S. D., Preunkert, S., Weller, R., Hong, S. B., Humphries, R. S., Tositti, L., … Dommergue, A. (2018). Characterizing atmospheric transport pathways to Antarctica and the remote southern ocean using radon-222. Frontiers in Earth Science, 6(November), 1–28. https://doi.org/10.3389/feart.2018.00190

Chapman, C., Lea, M., Meyer, A., Sallée, J.-B., & Hindell, M. (2020). Defining Southern Ocean fronts and their influence on biological and physical processes in a changing climate. Nature Climate Change. https://doi.org/10.1038/s41558-020-0705-4

Chapman, C., & Sallée, J. B. (2017). Isopycnal mixing suppression by the Antarctic Circumpolar Current and the Southern Ocean meridional overturning circulation. Journal of Physical Oceanography, 47(8), 2023–2045. https://doi.org/10.1175/JPO-D-16-0263.1

Chemke, R., & Polvani, L. M. (2020). Using multiple large ensembles to elucidate the discrepancy between the 1979-2019 modelled and observed Antarctic sea-ice trends. Geophysical Research Letters. https://doi.org/10.1029/2020GL088339

Chemke, R., Polvani, L. M., & Deser, C. (2019). The Effect of Arctic Sea Ice Loss on the Hadley Circulation. Geophysical Research Letters. https://doi.org/10.1029/2018GL081110

Chidichimo, M. P., Donohue, K. A., Watts, D. R., & Tracey, K. L. (2014). Baroclinic transport time series of the Antarctic Circumpolar Current measured in Drake Passage. Journal of Physical Oceanography, 44(7), 1829–1853. https://doi.org/10.1175/JPO-D-13-071.1

Clem, K. R., Renwick, J. A., McGregor, J., & Fogt, R. L. (2016). The relative influence of ENSO and SAM on Antarctic Peninsula climate. Journal of Geophysical Research, 121(16), 9324–9341. https://doi.org/10.1002/2016JD025305

Coggins, J. H. J., & McDonald, A. J. (2015). The influence of the Amundsen Sea Low on the winds in the Ross Sea and surroundings: Insights from a synoptic climatology. Journal of Geophysical Research, 120(6), 2167–2189. https://doi.org/10.1002/2014JD022830

Comiso, J. C., Parkinson, C. L., Markus, T., Cavalieri, D. J. and Gersten. R., (2020). “Current State of Sea Ice Cover”. Available: https://earth.gsfc.nasa.gov/cryo/data/current-state-sea-ice-cover. Last accessed November 2020.

Cohen, J., Screen, J. A., Furtado, J. C., Barlow, M., Whittleston, D., Coumou, D., … Jones, J. (2014). Recent Arctic amplification and extreme mid-latitude weather. Nature Geoscience, 7(9), 627–637. https://doi.org/10.1038/ngeo2234

Collins, M., Knutti, R., Arblaster, J., Dufresne, J.-L., Fichefet, T., Friedlingstein, P., … Wehner, M. (2013). Long-term Climate Change: Projections, Commitments and Irreversibility. Climate Change 2013: The Physical Science Basis. Contribution of Working Group I to the Fifth Assessment Report of the Intergovernmental Panel on Climate Change, 1029–1136. https://doi.org/10.1017/CBO9781107415324.024

de Boyer Montégut, C., Madec, G., Fischer, A. S., Lazar, A., & Iudicone, D. (2004). Mixed layer depth over the global ocean: An examination of profile data and a profile-based climatology. Journal of Geophysical Research C: Oceans, 109(12), 1–20. https://doi.org/10.1029/2004JC002378

Deser, C., Sun, L., Tomas, R. A., & Screen, J. (2016). Does ocean coupling matter for the northern extratropical response to projected Arctic sea ice loss? Geophysical Research Letters, 43(5), 2149–2157. https://doi.org/10.1002/2016GL067792

Deser, C., Tomas, R. A., & Sun, L. (2015). The role of ocean-atmosphere coupling in the zonal-mean atmospheric response to Arctic sea ice loss. Journal of Climate, 28(6), 2168–2186. https://doi.org/10.1175/JCLI-D-14-00325.1

Deser, C., Tomas, R., Alexander, M., & Lawrence, D. (2010). The seasonal atmospheric response to projected Arctic sea ice loss in the late twenty-first century. Journal of Climate, 23(2), 333–351. https://doi.org/10.1175/2009JCLI3053.1

Ding, Q., Steig, E. J., Battisti, D. S., & Küttel, M. (2011). Winter warming in West Antarctica caused by central tropical Pacific warming. Nature Geoscience, 4(6), 398–403. https://doi.org/10.1038/ngeo1129

Ding, Q., Wallace, J. M., Battisti, D. S., Steig, E. J., Gallant, A. J. E., Kim, H. J., & Geng, L. (2014). Tropical forcing of the recent rapid Arctic warming in northeastern Canada and Greenland. Nature, 509(7499), 209–212. https://doi.org/10.1038/nature13260

Doddridge, E. W., & Marshall, J. (2017). Modulation of the Seasonal Cycle of Antarctic Sea Ice Extent Related to the Southern Annular Mode. Geophysical Research Letters, 44(19), 9761–9768. https://doi.org/10.1002/2017GL074319

Dong, S., Gille, S. T., & Sprintall, J. (2007). An assessment of the Southern Ocean mixed layer heat budget. Journal of Climate, 20(17), 4425–4442. https://doi.org/10.1175/JCLI4259.1

Dong, S., Gille, S. T., Sprintall, J., & Fetzer, E. J. (2010). Assessing the potential of the Atmospheric Infrared Sounder (AIRS) surface temperature and specific humidity in turbulent heat flux estimates in the southern Ocean. Journal of Geophysical Research: Oceans, 115(5), 1–16. https://doi.org/10.1029/2009JC005542

Dong, Y., Proistosescu, C., Armour, K. C., & Battisti, D. S. (2019). Attributing Historical and Future Evolution of Radiative Feedbacks to Regional Warming Patterns using a Green's Function Approach: The preeminence of the Western Pacific. Journal of Climate, 32(17), 5471–5491. https://doi.org/10.1175/JCLI-D-18-0843.1

Donohue, K. A., Tracey, K. L., Watts, D. R., Chidichimo, M. P., & Chereskin, T. K. (2016). Mean Antarctic Circumpolar Current transport measured in Drake Passage. Geophysical Research Letters, 43, 1–8. https://doi.org/10.1002/2016GL070319

Downes, S. M., Budnick, A. S., Sarmiento, J. L., & Farneti, R. (2011). Impacts of wind stress on the Antarctic Circumpolar Current fronts and associated subduction. Geophysical Research Letters, 38(11), 3–8. https://doi.org/10.1029/2011GL047668

Downes, Stephanie M., Bindoff, N. L., & Rintoul, S. R. (2010). Changes in the subduction of Southern Ocean water masses at the end of the twenty-first century in eight IPCC models. Journal of Climate, 23(24), 6526–6541. https://doi.org/10.1175/2010JCLI3620.1

Downes, Stephanie M., & Hogg, A. M. C. C. (2013). Southern Ocean Circulation and Eddy Compensation in CMIP5 Models. Journal of Climate, 26(18), 7198–7220. https://doi.org/10.1175/JCLI-D-12-00504.1

Emery, W. J. (1977). Antarctic Polar Frontal Zone from Australia to the Drake Passage. Journal of Physical Oceanography, 7(6), 811–822. https://doi.org/10.1175/1520-0485(1977)007<0811:APFZFA>2.0.CO;2

England, M., Polvani, L., & Sun, L. (2018). Contrasting the Antarctic and Arctic atmospheric responses to projected sea ice loss in the late twenty-first century. Journal of Climate, 31(16), 6353–6370. https://doi.org/10.1175/JCLI-D-17-0666.1

England, M. R., Polvani, L. M., & Sun, L. (2020). Robust Arctic warming caused by projected Antarctic sea ice loss. Environmental Research Letters, in press, 0–31. https://doi.org/10.1088/1748-9326/abaada

England, M. R., Polvani, L. M., Sun, L., & Deser, C. (2020). Tropical climate responses to projected Arctic and Antarctic sea-ice loss. Nature Geoscience, 13(4), 275–281. https://doi.org/10.1038/s41561-020-0546-9

Eyring, V., Bony, S., Meehl, G. A., Senior, C. A., Stevens, B., Stouffer, R. J., & Taylor, K. E. (2016). Overview of the Coupled Model Intercomparison Project Phase 6 (CMIP6) experimental design and organization. Geoscientific Model Development, 9(5), 1937–1958. https://doi.org/10.5194/gmd-9-1937-2016

Fan, T., Deser, C., & Schneider, D. (2014). Recent sea ice trend in the context of Southern Ocean surface climate variations since 1950. Geophysical Research Letters, 41, 2419–2426. https://doi.org/10.1002/2014GL059239.Received

Farneti, R., & Delworth, T. L. (2010). The Role of Mesoscale Eddies in the Remote Oceanic Response to Altered Southern Hemisphere Winds. Journal of Physical Oceanography, 40(1999), 2348–2354. https://doi.org/10.1175/2010JPO4480.1

Farneti, R., Delworth, T. L., Rosati, A. J., Griffies, S. M., & Zeng, F. (2010). The role of mesoscale eddies in the rectification of the Southern ocean response to climate change. Journal of Physical Oceanography, 40(7), 1539–1557. https://doi.org/10.1175/2010JPO4353.1

Ferrari, R., Jansen, M. F., Adkins, J. F., Burke, A., Stewart, A. L., & Thompson, A. F. (2014). Antarctic sea ice control on ocean circulation in present and glacial climates. Proceedings of the National Academy of Sciences of the United States of America, 111(24), 8753–8758. https://doi.org/10.1073/pnas.1323922111

Ferreira, D., Marshall, J., Bitz, C. M., Solomon, S., & Plumb, A. (2015). Antarctic ocean and sea ice response to ozone depletion: A two-time-scale problem. Journal of Climate, 28(3), 1206–1226. https://doi.org/10.1175/JCLI-D-14-00313.1

Ferry, A. J., Prvan, T., Jersky, B., Crosta, X., & Armand, L. K. (2015). Statistical modeling of Southern Ocean marine diatom proxy and winter sea ice data:

Model comparison and developments. Progress in Oceanography, 131, 100–112. https://doi.org/10.1016/j.pocean.2014.12.001

Fetterer, F., K. Knowles, W. N. Meier, M. Savoie, and A. K. Windnagel, (2017). “(updated daily): Sea ice Index, Version 3. Regional Daily Data. National Snow and Ice Data Center”. Last accessed August 2019, https://doi.org/10.7265/N5K072F8.

Flocco, D., Feltham, D. L., & Turner, A. K. (2010). Incorporation of a physically based melt pond scheme into the sea ice component of a climate model. Journal of Geophysical Research: Oceans, 115(8), 1–14. https://doi.org/10.1029/2009JC005568

Flocco, D., Schroeder, D., Feltham, D. L., & Hunke, E. C. (2012). Impact of melt ponds on Arctic sea ice simulations from 1990 to 2007. Journal of Geophysical Research: Oceans, 117(9), 1–17. https://doi.org/10.1029/2012JC008195

Fogt, R. L., & Bromwich, D. H. (2006). Decadal variability of the ENSO teleconnection to the high-latitude south pacific governed by coupling with the Southern Annular mode. Journal of Climate, 19(6), 979–997. https://doi.org/10.1175/JCLI3671.1

Fogt, R. L., Bromwich, D. H., & Hines, K. M. (2011). Understanding the SAM influence on the South Pacific ENSO teleconnection. Climate Dynamics, 36(7), 1555–1576. https://doi.org/10.1007/s00382-010-0905-0

Frölicher, T. L., Sarmiento, J. L., Paynter, D. J., Dunne, J. P., Krasting, J. P., & Winton, M. (2015). Dominance of the Southern Ocean in anthropogenic carbon and heat uptake in CMIP5 models. Journal of Climate, 28(2), 862–886. https://doi.org/10.1175/JCLI-D-14-00117.1

Gagné, M.-È., Gillett, N. P., Fyfe, J. C., Gagne, M.-E., Gillett, N. P., & Fyfe, J. C. (2015). Observed and simulated changes in Antarctic sea ice extent over the past 50 years. Geophysical Research Letters, 42(1), 90–95. https://doi.org/10.1002/2014GL062231

Gent, P. R. (2016). Effects of Southern Hemisphere Wind Changes on the Meridional Overturning Circulation in Ocean Models. Annual Review of Marine Science, 8(August), 79–94. https://doi.org/10.1146/annurev-marine-122414-033929

Gersonde, R., Crosta, X., Abelmann, A., & Armand, L. (2005). Sea-surface temperature and sea ice distribution of the Southern Ocean at the EPILOG Last Glacial Maximum - A circum-Antarctic view based on siliceous microfossil records. Quaternary Science Reviews, 24(7-9 SPEC. ISS.), 869–896. https://doi.org/10.1016/j.quascirev.2004.07.015

Gille, S. T. (2014). Meridional displacement of the Antarctic Circumpolar Current. Philosophical Transactions of the Royal Society A: Mathematical, Physical and Engineering Sciences, 372(2019). https://doi.org/10.1098/rsta.2013.0273

Gillett, N. P., & Thompson, D. W. J. (2003). Simulation of recent Southern Hemisphere climate change. Science, 302(5643), 273–275. https://doi.org/10.1126/science.1087440

Gnanadesikan, A., & Hallberg, R. W. (2000). On the relationship of the circumpolar current to Southern Hemisphere winds in coarse-resolution ocean models. Journal of Physical Oceanography, 30(8), 2013–2034. https://doi.org/10.1175/1520-0485(2000)030<2013:OTROTC>2.0.CO;2

Gong, D., & Wang, S. (1999). Definition of Antarctic oscillation index. Geophysical Research Letters, 26(4), 459–462. https://doi.org/10.1029/1999GL900003

Goosse, H., & Zunz, V. (2014). Decadal trends in the Antarctic sea ice extent ultimately controlled by ice-ocean feedback. Cryosphere, 8(2), 453–470. https://doi.org/10.5194/tc-8-453-2014

Graham, R. M., De Boer, A. M., Heywood, K. J., Chapman, M. R., & Stevens, D. P. (2012). Southern Ocean fronts: Controlled by wind or topography? Journal of Geophysical Research: Oceans, 117(8), 1–14. https://doi.org/10.1029/2012JC007887

Green, B., Marshall, J., & Campin, J. M. (2019). The 'sticky' ITCZ: ocean-moderated ITCZ shifts. Climate Dynamics, 53(1–2), 1–19. https://doi.org/10.1007/s00382-019-04623-5

Gupta, A. Sen, & England, M. H. (2006). Coupled ocean-atmosphere-ice response to variations in the southern annular mode. Journal of Climate, 19(18), 4457–4486. https://doi.org/10.1175/JCLI3843.1

Hall, A., & Visbeck, M. (2002). Synchronous variability in the Southern Hemisphere atmosphere, sea ice, and ocean resulting from the annular mode. Journal of Climate, 15(21), 3043–3057. https://doi.org/10.1175/1520-0442(2002)015<3043:SVITSH>2.0.CO;2

Hallberg, R., Gnanadesikan, A.. (2006). The Role of Eddies in Determining the Structure and Response of the Wind-Driven Southern Hemisphere Overturning: Results from the Modeling Eddies in the Southern Ocean (MESO) Project. Journal of Physical Oceanography, 36, 2232–2252.

Hassler, B., Bodeker, G. E., Solomon, S., & Young, P. J. (2011). Changes in the polar vortex: Effects on Antarctic total ozone observations at various stations.

Geophysical Research Letters, 38(1), 1–5. https://doi.org/10.1029/2010GL045542

Hermanson, L., Ren, H. L., Vellinga, M., Dunstone, N. D., Hyder, P., Ineson, S., … Williams, K. D. (2018). Different types of drifts in two seasonal forecast systems and their dependence on ENSO. Climate Dynamics, 51(4), 1411–1426. https://doi.org/10.1007/s00382-017-3962-9

Heuzé, C., Ridley, J. K., Calvert, D., Stevens, D. P., & Heywood, K. J. (2015). Increasing vertical mixing to reduce Southern Ocean deep convection in NEMO3.4. Geoscientific Model Development, 8(10), 3119–3130. https://doi.org/10.5194/gmd-8-3119-2015

Hobbs, W. R., Massom, R., Stammerjohn, S., Reid, P., Williams, G., & Meier, W. (2016). A review of recent changes in Southern Ocean sea ice, their drivers and forcings. Global and Planetary Change, 143(August), 228–250. https://doi.org/10.1016/j.gloplacha.2016.06.008

Holland, M. M., Landrum, L., Kostov, Y., & Marshall, J. (2017). Sensitivity of Antarctic sea ice to the Southern Annular Mode in coupled climate models. Climate Dynamics, 49(5–6), 1813–1831. https://doi.org/10.1007/s00382-016-3424-9

Holland, P. R. (2014). The seasonality of Antarctic sea ice trends. Geophysical Research Letters, 41(12), 4230–4237. https://doi.org/10.1002/2014GL060172

Holmes, C. R., Holland, P. R., & Bracegirdle, T. J. (2019). Compensating biases and a noteworthy success in the CMIP5 representation of Antarctic sea ice processes. Geophysical Research Letters, 2018GL081796. https://doi.org/10.1029/2018GL081796

Hosking, J. S., Orr, A., Marshall, G. J., Turner, J., & Phillips, T. (2013). The influence of the amundsen-bellingshausen seas low on the climate of West Antarctica and its representation in coupled climate model simulations. Journal of Climate, 26(17), 6633–6648. https://doi.org/10.1175/JCLI-D-12-00813.1

Hosking, S & National Center for Atmospheric Research Staff (Eds). (2020). "The Climate Data Guide: Amundsen Sea Low indices". Available: https://climatedataguide.ucar.edu/climate-data/amundsen-sea-low-indices. Last accessed September 2020.

Houseago-Stokes, R. E., & McGregor, G. R. (2000). Spatial and temporal patterns linking southern low and high latitudes during south Pacific warm and cold events. International Journal of Climatology, 20(7), 793–801. https://doi.org/10.1002/1097-0088(20000615)20:7<793::AID-JOC502>3.0.CO;2-9

Hunke, E. C., Lipscomb, W. H., Turner, A. K., Jeffery, N., and Elliott, S.: CICE: the Los Alamos Sea ice Model Documentation and Software User's Manual Version 5.1, LA-CC-06-012, Los Alamos National Laboratory, Los Alamos, NM, 2015.

Hyder, P., Edwards, J. M., Allan, R. P., Hewitt, H. T., Bracegirdle, T. J., Gregory, J. M., … Belcher, S. E. (2018). Critical Southern Ocean climate model biases traced to atmospheric model cloud errors. Nature Communications, 9(1). https://doi.org/10.1038/s41467-018-05634-2

Iudicone, D., Mades, G., Blanke, B., & Speich, S. (2008). The role of Southern Ocean surface forcings and mixing in the global conveyor. Journal of Physical Oceanography, 38(7), 1377–1400. https://doi.org/10.1175/2008JPO3519.1

Jacobs, S. S. (2004). Bottom water production and its links with the thermohaline circulation. Antarctic Science, 16(4), 427–437. https://doi.org/10.1017/S095410200400224X

Jansen, M. F., & Nadeau, L. P. (2016). The effect of Southern Ocean surface buoyancy loss on the deep-ocean circulation and stratification. Journal of Physical Oceanography, 46(11), 3455–3470. https://doi.org/10.1175/JPO-D-16-0084.1

Jin, D., & Kirtman, B. P. (2009). Why the Southern Hemisphere ENSO responses lead ENSO. Journal of Geophysical Research Atmospheres, 114(23), 1–15. https://doi.org/10.1029/2009JD012657

Jones, J. M., Gille, S. T., Goosse, H., Abram, N. J., Canziani, P. O., Charman, D. J., … Vance, T. R. (2016). Assessing recent trends in high-latitude Southern Hemisphere surface climate. Nature Climate Change, 6(10), 917–926. https://doi.org/10.1038/nclimate3103

Kang, S. M., Shin, Y., & Xie, S. P. (2018). Extratropical forcing and tropical rainfall distribution: energetics framework and ocean Ekman advection. Npj Climate and Atmospheric Science, 1(1), 1–10. https://doi.org/10.1038/s41612-017-0004-6

Karoly, D. J. (1989). Southern Hemisphere Circulation Features Associated with El Niño-Southern Oscillation Events. Journal of Climate, 2(11), 1239–1252. https://doi.org/10.1175/1520-0442(1989)002<1239:SHCFAW>2.0.CO;2

Kay, J. E., Deser, C., Phillips, A., Mai, A., Hannay, C., Strand, G., … Vertenstein, M. (2015). The community earth system model (CESM) large ensemble project : A community resource for studying climate change in the presence of internal

climate variability. Bulletin of the American Meteorological Society, 96(8), 1333–1349. https://doi.org/10.1175/BAMS-D-13-00255.1

Kay, J. E., Wall, C., Yettella, V., Medeiros, B., Hannay, C., Caldwell, P., & Bitz, C. (2016). No access global climate impacts of fixing the Southern Ocean shortwave radiation bias in the Community Earth System Model (CESM). Journal of Climate, 29(12), 4617–4636. https://doi.org/10.1175/JCLI-D-15-0358.1

Kidston, J., & Gerber, E. P. (2010). Intermodel variability of the poleward shift of the austral jet stream in the CMIP3 integrations linked to biases in 20th century climatology. Geophysical Research Letters, 37(9), 1–5. https://doi.org/10.1029/2010GL042873

Kidston, J., Taschetto, A. S., Thompson, D. W. J., & England, M. H. (2011). The influence of Southern Hemisphere sea-ice extent on the latitude of the mid-latitude jet stream. Geophysical Research Letters, 38(15), 1–5. https://doi.org/10.1029/2011GL048056

Kidston, J., Scaife, A. A., Hardiman, S. C., Mitchell, D. M., Butchart, N., Baldwin, M. P., & Gray, L. J. (2015). Stratospheric influence on tropospheric jet streams, storm tracks and surface weather. Nature Geoscience, 8(6), 433–440. https://doi.org/10.1038/NGEO2424

Kim, B. M., Son, S. W., Min, S. K., Jeong, J. H., Kim, S. J., Zhang, X., … Yoon, J. H. (2014). Weakening of the stratospheric polar vortex by Arctic sea-ice loss. Nature Communications, 5, 1–8. https://doi.org/10.1038/ncomms5646

Klekociuk, A., Wienecke, B., (2017). Australia State of the Environment 2016: Antarctic Environment, Independent Report to the Australian Government Minister for the

Environment and Energy. Australian Government Department of the Environment and Energy, Canberra. https://doi.org/10.4226/94/58b65b2b307c0.

Knutti, R., Flückiger, J., Stocker, T. F., & Timmermann, A. (2004). Strong hemispheric coupling of glacial climate through freshwater discharge and ocean circulation. Nature, 430(7002), 851–856. https://doi.org/10.1038/nature02786

Kohyama, T., & Hartmann, D. L. (2016). Antarctic sea ice response to weather and climate modes of variability. Journal of Climate, 29(2), 721–741. https://doi.org/10.1175/JCLI-D-15-0301.1

Kostov, Y., Marshall, J., Hausmann, U., Armour, K. C., Ferreira, D., & Holland, M. M. (2017). Fast and slow responses of Southern Ocean sea surface temperature to SAM in coupled climate models. Climate Dynamics, 48(5–6), 1595–1609. https://doi.org/10.1007/s00382-016-3162-z

Kuhlbrodt, T., Jones, C. G., Sellar, A., Storkey, D., Blockley, E., Stringer, M., … Walton, J. (2018). The Low-Resolution Version of HadGEM3 GC3.1: Development and Evaluation for Global Climate. Journal of Advances in Modeling Earth Systems, 10(11), 2865–2888. https://doi.org/10.1029/2018MS001370

Kurtz, N. T., & Markus, T. (2012). Satellite observations of Antarctic sea ice thickness and volume. Journal of Geophysical Research: Oceans, 117(8), 1–9. https://doi.org/10.1029/2012JC008141

Kwok, R., & Comiso, J. C. (2002). Spatial patterns of variability in Antarctic surface temperature: Connections to the Southern Hemisphere Annular Mode and the

Southern Oscillation. Geophysical Research Letters, 29(14), 2–5. https://doi.org/10.1029/2002GL015415

Labe, Z., Peings, Y., & Magnusdottir, G. (2019). The Effect of QBO Phase on the Atmospheric Response to Projected Arctic Sea Ice Loss in Early Winter. Geophysical Research Letters, 46(13), 7663–7671. https://doi.org/10.1029/2019GL083095

Laliberté, F., & Kushner, P. J. (2013). Isentropic constraints by midlatitude surface warming on the Arctic midtroposphere. Geophysical Research Letters, 40(3), 606–611. https://doi.org/10.1029/2012GL054306

Landrum, L., Holland, M., Raphael, M., & Polvani, L. (2017). Stratospheric ozone depletion: an unlikely driver of the regional trends in Antarctic sea ice in austral fall in the late 20 th Century. Geophysical Research Letters. https://doi.org/10.1002/2017GL075618

Lecomte, O., Goosse, H., Fichefet, T., Holland, P. R., Uotila, P., Zunz, V., & Kimura, N. (2016). Impact of surface wind biases on the Antarctic sea ice concentration budget in climate models. Ocean Modelling, 105, 60–70. https://doi.org/10.1016/j.ocemod.2016.08.001

Lecomte, O., Goosse, H., Fichefet, T., De Lavergne, C., Barthélemy, A., & Zunz, V. (2017). Vertical ocean heat redistribution sustaining sea-ice concentration trends in the Ross Sea. Nature Communications, 8(1), 258. https://doi.org/10.1038/s41467-017-00347-4

Lefebvre, W., Goosse, H., Timmermann, R., & Fichefet, T. (2004). Influence of the Southern Annular Mode on the sea ice - Ocean system. Journal of Geophysical Research C: Oceans, 109(9), 1–12. https://doi.org/10.1029/2004JC002403

Li, L., McClean, J. L., Miller, A. J., Eisenman, I., Hendershott, M. C., & Papadopoulos, C. A. (2014). Processes driving sea ice variability in the Bering Sea in an eddying ocean/sea ice model: Mean seasonal cycle. Ocean Modelling, 84, 51–66. https://doi.org/10.1016/j.ocemod.2014.09.006

Liu, J., & Curry, J. A. (2010). Accelerated warming of the Southern Ocean and its impacts on the hydrological cycle and sea ice. Proceedings of the National Academy of Sciences of the United States of America, 107(34), 14987–14992. https://doi.org/10.1073/pnas.1003336107

Ludescher, J., Yuan, N., & Bunde, A. (2018). Detecting the statistical significance of the trends in the Antarctic sea ice extent: an indication for a turning point. Climate Dynamics, 53(1), 237–244. https://doi.org/10.1007/s00382-018-4579-3

Lumpkin, R., & Speer, K. (2007). Global ocean meridional overturning. Journal of Physical Oceanography, 37(10), 2550–2562. https://doi.org/10.1175/JPO3130.1

Maksym, T., Stammerjohn, S., Ackley, S., & Massom, R. (2012). “Antarctic Sea ice: A Polar Opposite?”, Oceanography, 25(3), 140-151. Accessed November 2020, from http://www.jstor.org/stable/24861407

Marino, G., Rohling, E. J., Rodríguez-Sanz, L., Grant, K. M., Heslop, D., Roberts, A. P., … Yu, J. (2015). Bipolar seesaw control on last interglacial sea level. Nature, 522(7555), 197–201. https://doi.org/10.1038/nature14499

Marshall, G. J. (2003). Trends in the Southern Annular Mode from observations and reanalyses. Journal of Climate, 16(24), 4134–4143. https://doi.org/10.1175/1520-0442(2003)016<4134:TITSAM>2.0.CO;2

Marshall, J., Armour, K. C., Scott, J. R., Kostov, Y., Hausmann, U., Ferreira, D., … Bitz, C. M. (2014). The ocean’s role in polar climate change: asymmetric Arctic

and Antarctic responses to greenhouse gas and ozone forcing. Philosophical Transactions. Series A, Mathematical, Physical, and Engineering Sciences, 372(2019), 20130040. https://doi.org/10.1098/rsta.2013.0040

Marshall, Gareth & National Center for Atmospheric Research Staff (Eds). (2018). "The Climate Data Guide: Marshall Southern Annular Mode (SAM) Index (Station-based)." Available: https://climatedataguide.ucar.edu/climate-data/marshall-southern-annular-mode-sam-index-station-based. Last Accessed September 2020.

Martinson, D. G. (1990). Evolution of the southern ocean winter mixed layer and sea ice: Open ocean deepwater formation and ventilation. Journal of Geophysical Research, 95(C7), 11641. https://doi.org/10.1029/jc095ic07p11641

Mayewski, P. A., Meredith, M. P., Summerhayes, C. P., Turner, J., Worby, A., Barrett, P. J., … Van Ommen, T. (2009). State of the antarctic and southern ocean climate system. Reviews of Geophysics, 47(1), 1–38. https://doi.org/10.1029/2007RG000231

McCabe, M. V., Stansby, P. K., & Apsley, D. D. (2013). Random wave runup and overtopping a steep sea wall: Shallow-water and Boussinesq modelling with generalised breaking and wall impact algorithms validated against laboratory and field measurements. Coastal Engineering, 74, 33–49. https://doi.org/10.1016/j.coastaleng.2012.11.010

McCrystall, M. R., Hosking, J. S., White, I. P., & Maycock, A. C. (2020). The Impact of Changes in Tropical Sea Surface Temperatures over 1979–2012 on Northern Hemisphere High-Latitude Climate. Journal of Climate, 33(12), 5103–5121. https://doi.org/10.1175/jcli-d-19-0456.1

Meehl, G. A., Arblaster, J. M., Chung, C. T. Y., Holland, M. M., DuVivier, A., Thompson, L., … Bitz, C. M. (2019). Sustained ocean changes contributed to sudden Antarctic sea ice retreat in late 2016. Nature Communications, 10(1), 14. https://doi.org/10.1038/s41467-018-07865-9

Menary, M. B., Kuhlbrodt, T., Ridley, J., Andrews, M. B., Dimdore-Miles, O. B., Deshayes, J., … Xavier, P. (2018). Preindustrial Control Simulations With HadGEM3-GC3.1 for CMIP6. Journal of Advances in Modeling Earth Systems, 10(12), 3049–3075. https://doi.org/10.1029/2018MS001495

Menéndez, C. G., Serafini, V., & Le Treut, H. (1999). The effect of sea-ice on the transient atmospheric eddies of the Southern Hemisphere. Climate Dynamics, 15(9), 659–671. https://doi.org/10.1007/s003820050308

Meredith, M., M. Sommerkorn, S. Cassotta, C. Derksen, A. Ekaykin, A. Hollowed, G. Kofinas, A. Mackintosh, J. Melbourne-Thomas, M.M.C. Muelbert, G. Ottersen, H. Pritchard, and E.A.G. Schuur, 2019: (2019). Polar Regions. In: IPCC Special Report on the Ocean and Cryosphere in a Changing Climate. IPCC, 3(SUPPL.), S129–S131. https://doi.org/10.1016/S1366-7017(01)00066-6

Meredith, M. P., & Hogg, A. M. (2006). Circumpolar response of Southern Ocean eddy activity to a change in the Southern Annular Mode. Geophysical Research Letters, 33(16), 2–5. https://doi.org/10.1029/2006GL026499

Mo, K. C., & Higgins, R. W. (1998). The Pacific-South American modes and tropical convection during the Southern Hemisphere winter. Monthly Weather Review, 126(6), 1581–1596 .https://doi.org/10.1175/1520-0493(1998)1262.0.CO;2

Mori, M., Watanabe, M., Shiogama, H., Inoue, J., & Kimoto, M. (2014). Robust Arctic sea-ice influence on the frequent Eurasian cold winters in past decades. Nature Geoscience, 7(12), 869–873. https://doi.org/10.1038/ngeo2277

Morrison, A. K., & Hogg, A. M. C. (2013). On the relationship between southern ocean overturning and ACC transport. Journal of Physical Oceanography, 43(1), 140–148. https://doi.org/10.1175/JPO-D-12-057.1

Muglia, J., & Schmittner, A. (2015). Glacial Atlantic overturning increased by wind stress in climate models. Geophysical Research Letters, 42(22), 9862–9869. https://doi.org/10.1002/2015GL064583

Munday, D. R., Johnson, H. L., & Marshall, D. P. (2013). Eddy saturation of equilibrated circumpolar currents. Journal of Physical Oceanography, 43(3), 507–532. https://doi.org/10.1175/JPO-D-12-095.1

Nakamura, T., Yamazaki, K., Iwamoto, K., Honda, M., Miyoshi, Y., Ogawa, Y., … Ukita, J. (2016). The stratospheric pathway for Arctic impacts on midlatitude climate. Geophysical Research Letters, 43(7), 3494–3501. https://doi.org/10.1002/2016GL068330

Newsom, E. R., & Thompson, A. F. (2018). Reassessing the Role of the Indo-Pacific in the Ocean's Global Overturning Circulation. Geophysical Research Letters, 45(22), 12,422-12,431. https://doi.org/10.1029/2018GL080350

Nicholls, K. W., Boehme, L., Biuw, M., & Fedak, M. A. (2008). Wintertime ocean conditions over the southern Weddell Sea continental shelf, Antarctica. Geophysical Research Letters, 35(21), 1–5. https://doi.org/10.1029/2008GL035742

Nicolas, J. P., & Bromwich, D. H. (2014). New reconstruction of antarctic near-surface temperatures: Multidecadal trends and reliability of global reanalyses. Journal of Climate, 27(21), 8070–8093. https://doi.org/10.1175/JCLI-D-13-00733.1

NOAA. (2020). “Multivariate ENSO Index Version 2 (MEI.v2)”. Available: https://psl.noaa.gov/enso/mei/. Last accessed September 2020.

Ohshima, K. I., Fukamachi, Y., Williams, G. D., Nihashi, S., Roquet, F., Kitade, Y., … Wakatsuchi, M. (2013). Antarctic Bottom Water production by intense sea-ice formation in the Cape Darnley polynya. Nature Geoscience, 6(3), 235–240. https://doi.org/10.1038/ngeo1738

Orsi, A. H., Whitworth, T., & Nowlin, W. D. (1995). On the meridional extent and fronts of the Antarctic Circumpolar Current. Deep-Sea Research Part I, 42(5), 641–673. https://doi.org/10.1016/0967-0637(95)00021-W

Orsi, A. H., & Wiederwohl, C. L. (2009). A recount of Ross Sea waters. Deep-Sea Research Part II: Topical Studies in Oceanography, 56(13–14), 778–795. https://doi.org/10.1016/j.dsr2.2008.10.033

Oudar, T., Sanchez-Gomez, E., Chauvin, F., Cattiaux, J., Terray, L., & Cassou, C. (2017). Respective roles of direct GHG radiative forcing and induced Arctic sea ice loss on the Northern Hemisphere atmospheric circulation. Climate Dynamics, 0(0), 1–21. https://doi.org/10.1007/s00382-017-3541-0

Panassa, E., Völker, C., Wolf-Gladrow, D., & Hauck, J. (2018). Drivers of Interannual Variability of Summer Mixed Layer Depth in the Southern Ocean Between 2002 and 2011. Journal of Geophysical Research: Oceans, 123(8), 5077–5090. https://doi.org/10.1029/2018JC013901

Parkinson, C. L., & Cavalieri, D. J. (2012). Antarctic sea ice variability and trends, 1979-2010. Cryosphere, 6(4), 871–880. https://doi.org/10.5194/tc-6-871-2012

Parkinson, C L. (2019). A 40-y record reveals gradual Antarctic sea ice increases followed by decreases at rates far exceeding the rates seen in the Arctic. Proceedings of the National Academy of Sciences, 201906556. https://doi.org/10.1073/pnas.1906556116

Patara, L., & Böning, C. W. (2014). Abyssal ocean warming around Antarctica strengthens the Atlantic overturning circulation. Geophysical Research Letters, 41(11), 3972–3978. https://doi.org/10.1002/2014GL059923

Pauling, A. G., Bitz, C. M., Smith, I. J., & Langhorne, P. J. (2016). The response of the Southern Ocean and Antarctic sea ice to freshwater from ice shelves in an earth system model. Journal of Climate, 29(5), 1655–1672. https://doi.org/10.1175/JCLI-D-15-0501.1

Pedro, J. B., Van Ommen, T. D., Rasmussen, S. O., Morgan, V. I., Chappellaz, J., Moy, A. D., … Delmotte, M. (2011). The last deglaciation: Timing the bipolar seesaw. Climate of the Past, 7(2), 671–683. https://doi.org/10.5194/cp-7-671-2011

Pedro, Joel B., Jochum, M., Buizert, C., He, F., Barker, S., & Rasmussen, S. O. (2018). Beyond the bipolar seesaw: Toward a process understanding of interhemispheric coupling. Quaternary Science Reviews, 192, 27–46. https://doi.org/10.1016/j.quascirev.2018.05.005

Peings, Y., & Magnusdottir, G. (2014). Response of the wintertime northern hemisphere atmospheric circulation to current and projected arctic sea ice

decline: A numerical study with CAM5. Journal of Climate, 27(1), 244–264. https://doi.org/10.1175/JCLI-D-13-00272.1

Pellichero, V., Sallée, J.-B., Schmidtko, S., Roquet, F., & Charrassin, J.-B. (2017). The ocean mixed layer under Southern Ocean sea-ice: Seasonal cycle and forcing. Journal of Geophysical Research: Oceans, 122(2), 1608–1633. https://doi.org/10.1002/2016JC011970

Petty, A. A., Holland, P. R., & Feltham, D. L. (2014). Sea ice and the ocean mixed layer over the Antarctic shelf seas. Cryosphere, 8(2), 761–783. https://doi.org/10.5194/tc-8-761-2014

Physics, E., Bern, C.-, Clausen, H. B., Hammer, C. U., Johnsen, S. J., & Blunier, T., Chappellaz, J., Schander, J., et al. (1998). Asynchrony of Antarctic and Greenland climate change during the last glacial period. Nature, 394, 739–743.

Pollard, R. T., Lucas, M. I., & Read, J. F. (2002). Physicalcontrol on biogeochemical zonation in the southern ocean. Deep-Sea Research II, 49(2002), 3289–3305. Retrieved from http://www.sciencedirect.com/science/article/pii/S096706450200084X

Polvani, L. M., & Smith, K. L. (2013). Can natural variability explain observed Antarctic sea ice trends? New modeling evidence from CMIP5. Geophysical Research Letters, 40(12), 3195–3199. https://doi.org/10.1002/grl.50578

Polvani, L. M., Waugh, D. W., Correa, G. J. P., & Son, S. W. (2011). Stratospheric ozone depletion: The main driver of twentieth-century atmospheric circulation changes in the Southern Hemisphere. Journal of Climate, 24(3), 795–812. https://doi.org/10.1175/2010JCLI3772.1

Purich, A., Cai, W., England, M. H., & Cowan, T. (2016). Evidence for link between modelled trends in Antarctic sea ice and underestimated westerly wind changes. Nature Communications, 7(May 2015), 10409. https://doi.org/10.1038/ncomms10409

Purkey, S. G., & Johnson, G. C. (2012). Global contraction of Antarctic Bottom Water between the 1980s and 2000s. Journal of Climate, 25(17), 5830–5844. https://doi.org/10.1175/JCLI-D-11-00612.1

Purkey, S. G., & Johnson, G. C. (2013). Antarctic bottom water warming and freshening: Contributions to sea level rise, ocean freshwater budgets, and global heat gain. Journal of Climate, 26(16), 6105–6122. https://doi.org/10.1175/JCLI-D-12-00834.1

Rae, J. G. L., Hewitt, H. T., Keen, A. B., Ridley, J. K., West, A. E., Harris, C. M., … Walters, D. N. (2015). Development of the Global Sea Ice 6.0 CICE configuration for the Met Office Global Coupled model. Geoscientific Model Development, 8(7), 2221–2230. https://doi.org/10.5194/gmd-8-2221-2015

Rafferty, A. R., Johnstone, C. P., Garner, J. A., & Reina, R. D. (2017). A 20-year investigation of declining leatherback hatching success: Implications of climate variation. Royal Society Open Science, 4(10). https://doi.org/10.1098/rsos.170196

Randel, W. J., Shine, K. P., Austin, J., Barnett, J., Claud, C., Gillett, N. P., … Yoden, S. (2009). An update of observed stratospheric temperature trends. Journal of Geophysical Research Atmospheres, 114(2). https://doi.org/10.1029/2008JD010421

Raphael, M. N., Hobbs, W., & Wainer, I. (2011). The effect of Antarctic sea ice on the Southern Hemisphere atmosphere during the southern summer. Climate Dynamics, 36(7), 1403–1417. https://doi.org/10.1007/s00382-010-0892-1

Ren, L., Speer, K., & Chassignet, E. P. (2011). The mixed layer salinity budget and sea ice in the Southern Ocean. Journal of Geophysical Research: Oceans, 116(8), 1–17. https://doi.org/10.1029/2010JC006634

Ridley, J. K., Blockley, E. W., Keen, A. B., Rae, J. G. L., West, A. E., & Schroeder, D. (2018). The sea ice model component of HadGEM3-GC3.1. Geoscientific Model Development, 11(2), 713–723. https://doi.org/10.5194/gmd-11-713-2018

Rintoul, S., Hughes, C., & Olbers, D. (2001). The Antarctic Circumpolar Current System. In Ocean Circulation and Climate. https://doi.org/10.1002/ajp.20122

Rintoul, S. R. (2018). The global influence of localized dynamics in the Southern Ocean. Nature, 558(7709), 209–218. https://doi.org/10.1038/s41586-018-0182-3

Roach, L. A., Dean, S. M., & Renwick, J. A. (2018). Consistent biases in Antarctic sea ice concentration simulated by climate models. Cryosphere, 12(1), 365–383. https://doi.org/10.5194/tc-12-365-2018

Rosenblum, E., & Eisenman, I. (2017). Sea ice trends in climate models only accurate in runs with biased global warming. Journal of Climate, 30(16), 6265–6278. https://doi.org/10.1175/JCLI-D-16-0455.1

Sabine, C. L., Feely, R. A., Gruber, N., Key, R. M., Lee, K., Bullister, J. L., … Rios, A. F. (2004). The oceanic sink for anthropogenic CO2. Science, 305(5682), 367–371. https://doi.org/10.1126/science.1097403

Sallée, J. B., Shuckburgh, E., Bruneau, N., Meijers, A. J. S., Bracegirdle, T. J., & Wang, Z. (2013). Assessment of Southern Ocean mixed-layer depths in CMIP5 models: Historical bias and forcing response. Journal of Geophysical Research: Oceans, 118(4), 1845–1862. https://doi.org/10.1002/jgrc.20157

Sallée, J. B., Shuckburgh, E., Bruneau, N., Meijers, A. J. S. S., Bracegirdle, T. J., Wang, Z., & Roy, T. (2013). Assessment of Southern Ocean water mass circulation and characteristics in CMIP5 models: Historical bias and forcing response. Journal of Geophysical Research: Oceans, 118(4), 1830–1844. https://doi.org/10.1002/jgrc.20135

Sallée, Jean Baptiste, Wienders, N., Speer, K., & Morrow, R. (2006). Formation of subantarctic mode water in the southeastern Indian Ocean. Ocean Dynamics, 56(5–6), 525–542. https://doi.org/10.1007/s10236-005-0054-x

Schlosser, E., Haumann, F. A., & Raphael, M. N. (2017). Atmospheric influences on the anomalous 2016 Antarctic sea ice decay. The Cryosphere Discussions, 13(3), 1–31. https://doi.org/10.5194/tc-2017-192

Schneider, D. P., & Deser, C. (2018). Tropically driven and externally forced patterns of Antarctic sea ice change: reconciling observed and modeled trends. Climate Dynamics, 50(11–12), 4599–4618. https://doi.org/10.1007/s00382-017-3893-5

Schneider, D. P., & Reusch, D. B. (2016). Antarctic and Southern Ocean surface temperatures in CMIP5 models in the context of the surface energy budget. Journal of Climate, 29(5), 1689–1716. https://doi.org/10.1175/JCLI-D-15-0429.1

Schneider, D. P., & Steig, E. J. (2008). Ice cores record significant 1940s Antarctic warmth related to tropical climate variability. Proceedings of the National

Academy of Sciences of the United States of America, 105(34), 12154–12158. https://doi.org/10.1073/pnas.0803627105

Schroeter, S., Hobbs, W., & Bindoff, N. L. (2017). Interactions between Antarctic sea ice and large-scale atmospheric modes in CMIP5 models. The Cryosphere, 11(2), 789–803. https://doi.org/10.5194/tc-11-789-2017

Scott, F., & Feltham, D. L. (2010). A model of the three-dimensional evolution of Arctic melt ponds on first-year and multiyear sea ice. Journal of Geophysical Research: Oceans, 115(12), 1–37. https://doi.org/10.1029/2010JC006156

Screen, J. A., Bracegirdle, T. J., & Simmonds, I. (2018). Polar Climate Change as Manifest in Atmospheric Circulation. Current Climate Change Reports, 4(4), 383–395. https://doi.org/10.1007/s40641-018-0111-4

Screen, J. A., Gillet, N. P., Stevens, D. P., Marshall, G. J., & Roscoe, H. K. (2009). The role of eddies in the Southern Ocean temperature response to the southern annular mode. Journal of Climate, 22(3), 806–818. https://doi.org/10.1175/2008JCLI2416.1

Screen, J A, Blackport, R., & Screen, J. (2019). How Robust is the Atmospheric Response to Projected Arctic Sea-Ice Loss Across Climate Models? (2018), 1–10. https://doi.org/10.1029/2019GL084936

Screen, James A., Deser, C., Simmonds, I., & Tomas, R. (2014). Atmospheric impacts of Arctic sea-ice loss, 1979-2009: Separating forced change from atmospheric internal variability. Climate Dynamics, 43(1–2), 333–344. https://doi.org/10.1007/s00382-013-1830-9

Screen, James A., Deser, C., Smith, D. M., Zhang, X., Blackport, R., Kushner, P. J., … Sun, L. (2018). Consistency and discrepancy in the atmospheric response to

Arctic sea-ice loss across climate models. Nature Geoscience, 11(3), 155–163. https://doi.org/10.1038/s41561-018-0059-y

Screen, James A., & Simmonds, I. (2010). Increasing fall-winter energy loss from the Arctic Ocean and its role in Arctic temperature amplification. Geophysical Research Letters, 37(16), 1–5. https://doi.org/10.1029/2010GL044136

Screen, James A., & Simmonds, I. (2013). Exploring links between Arctic amplification and mid-latitude weather. Geophysical Research Letters, 40(5), 959–964. https://doi.org/10.1002/grl.50174

Screen, James A., Simmonds, I., Deser, C., & Tomas, R. (2013). The atmospheric response to three decades of observed arctic sea ice loss. Journal of Climate, 26(4), 1230–1248. https://doi.org/10.1175/JCLI-D-12-00063.1

Shen, X., Wang, L., & Osprey, S. (2020). Tropospheric Forcing of the 2019 Antarctic Sudden Stratospheric Warming. Geophysical Research Letters, 47(20), 1–8. https://doi.org/10.1029/2020GL089343

Shi, J. R., Xie, S. P., & Talley, L. D. (2018). Evolving relative importance of the Southern Ocean and North Atlantic in anthropogenic ocean heat uptake. Journal of Climate, 31(18), 7459–7479. https://doi.org/10.1175/JCLI-D-18-0170.1

Shin, S. I., Liu, Z., Otto-Bliesner, B. L., Kutzbach, J. E., & Vavrus, S. J. (2003). Southern Ocean sea-ice control of the glacial North Atlantic thermohaline circulation. Geophysical Research Letters, 30(2), 68–71. https://doi.org/10.1029/2002GL015513

Sigmond, M., & Fyfe, J. C. (2010). Has the ozone hole contributed to increased Antarctic sea ice extent? Geophysical Research Letters, 37(18), 2–6. https://doi.org/10.1029/2010GL044301

Simmonds, I., & Jacka, T. H. (1995). Relationships between the Interannual Variability of Antarctic Sea Ice and the Southern Oscillation. Journal of Climate, 8(3), 637–647. https://doi.org/10.1175/1520-0442(1995)008<0637:RBTIVO>2.0.CO;2

Simpkins, G. R., Ciasto, L. M., & England, M. H. (2013). Observed variations in multidecadal Antarctic sea ice trends during 1979-2012. Geophysical Research Letters, 40(14), 3643–3648. https://doi.org/10.1002/grl.50715

Simpkins, G. R., Ciasto, L. M., Thompson, D. W. J. J., & England, M. H. (2012). Seasonal relationships between large-scale climate variability and antarctic sea ice concentration. Journal of Climate, 25(16), 5451–5469. https://doi.org/10.1175/JCLI-D-11-00367.1

Simpkins, G. R., McGregor, S., Taschetto, A. S., Ciasto, L. M., & England, M. H. (2014). Tropical connections to climatic change in the extratropical Southern Hemisphere: The role of atlantic SST trends. Journal of Climate, 27(13), 4923–4936. https://doi.org/10.1175/JCLI-D-13-00615.1

Smith, D. M., Dunstone, N. J., Scaife, A. A., Fiedler, E. K., Copsey, D., & Hardiman, S. C. (2017). Atmospheric response to Arctic and Antarctic sea ice: The importance of ocean-atmosphere coupling and the background state. Journal of Climate, 30(12), 4547–4565. https://doi.org/10.1175/JCLI-D-16-0564.1

Smith, D. M., Screen, J. A., Deser, C., Cohen, J., Fyfe, J. C., García-Serrano, J., … Zhang, X. (2018). The Polar Amplification Model Intercomparison Project (PAMIP) contribution to CMIP6: investigating the causes and consequences of

polar amplification. Geoscientific Model Development Discussions, 1–42. https://doi.org/10.5194/gmd-2018-82

Sokolov, S., & Rintoul, S. R. (2002). Structure of Southern Ocean fronts at 140°E. Journal of Marine Systems, 37(1–3), 151–184. https://doi.org/10.1016/S0924-7963(02)00200-2

Sokolov, S., & Rintoul, S. R. (2007). Multiple jets of the antarctic circumpolar current South of Australia. Journal of Physical Oceanography, 37(5), 1394–1412. https://doi.org/10.1175/JPO3111.1

Sokolov, S., & Rintoul, S. R. (2009). Circumpolar structure and distribution of the antarctic circumpolar current fronts: 1. Mean98 circumpolar paths. Journal of Geophysical Research: Oceans, 114(11), 1–19. https://doi.org/10.1029/2008JC005108

Solomon, S., Ivy, D. J., Kinnison, D., Mills, M. J., Neely III, R. R., & Schmidt, A. (2016). Antarctic ozone layer. Science, 353(6296), 269–274.

Speer, K., Rintoul, S. R., & Sloyan, B. (2000). The diabatic Deacon cell. Journal of Physical Oceanography, 30(12), 3212–3222. https://doi.org/10.1175/1520-0485(2000)030<3212:TDDC>2.0.CO;2

Stammerjohn, S. E., Martinson, D. G., Smith, R. C., & Iannuzzi, R. A. (2008). Sea ice in the western Antarctic Peninsula region: Spatio-temporal variability from ecological and climate change perspectives. Deep-Sea Research Part II: Topical Studies in Oceanography, 55(18–19), 2041–2058. https://doi.org/10.1016/j.dsr2.2008.04.026

Stein, K., Timmermann, A., Kwon, E. Y., & Friedrich, T. (2020). Timing and magnitude of southern ocean sea ice/carbon cycle feedbacks. Proceedings of the National

Academy of Sciences of the United States of America, 117(9), 4498–4504. https://doi.org/10.1073/pnas.1908670117

Stocker, T. F. (1998, October 2). The seesaw effect. Science, Vol. 282, pp. 61–62. https://doi.org/10.1126/science.282.5386.61

Stocker, T. F., & Johnsen, S. J. (2003). A minimum thermodynamic model for the bipolar seesaw. Paleoceanography, 18(4), 1–9. https://doi.org/10.1029/2003PA000920

Stocker, T. F., Qin, D., Plattner, G. K., Tignor, M., Allen, S. K., Boschung, J., … Midgley, P. M. (2013). Climate change 2013: the physical science basis. Intergovernmental panel on climate change, working group I contribution to the IPCC fifth assessment report (AR5). New York, (October 2015). https://doi.org/10.1017/cbo9781107415324

Storkey, D., Blaker, A. T., Mathiot, P., Megann, A., Aksenov, Y., Blockley, E. W., … Sinha, B. (2018). UK Global Ocean GO6 and GO7: A traceable hierarchy of model resolutions. Geoscientific Model Development, 11(8), 3187–3213. https://doi.org/10.5194/gmd-11-3187-2018

Student (1908) The probable error of a mean. Biometrika 6:1–25

Stuecker, M. F., Bitz, C. M., & Armour, K. C. (2017). Conditions leading to the unprecedented low Antarctic sea ice extent during the 2016 austral spring season. Geophysical Research Letters, 1–12. https://doi.org/10.1002/2017GL074691

Stuut, J. B. W., Crosta, X., van der Borg, K., & Schneider, R. (2004). Relationship between Antarctic sea ice and southwest African climate during the late Quaternary. Geology, 32(10), 909–912. https://doi.org/10.1130/G20709.1

Sun, L., Alexander, M., & Deser, C. (2018). Evolution of the global coupled climate response to Arctic sea ice loss during 1990-2090 and its contribution to climate change. Journal of Climate, 31(19), 7823–7843. https://doi.org/10.1175/JCLI-D-18-0134.1

Sun, L., Deser, C., Tomas, R., & Alexander, M. (2020). Global coupled climate response to polar sea ice loss: Evaluating the effectiveness of different ice-constraining approaches. Geophysical Research Letters, 1–9. https://doi.org/10.1029/2019gl085788

Sun, S., Eisenman, I., & Stewart, A. L. (2018). Does Southern Ocean Surface Forcing Shape the Global Ocean Overturning Circulation? Geophysical Research Letters, 45(5), 2413–2423. https://doi.org/10.1002/2017GL076437

Sun, S., Eisenman, I., Zanna, L., & Stewart, A. L. (2020). Surface constraints on the depth of the Atlantic meridional overturning circulation: Southern Ocean versus North Atlantic. Journal of Climate, 33(8), 3125–3149. https://doi.org/10.1175/JCLI-D-19-0546.1

Swart, N. C., & Fyfe, J. C. (2013). The influence of recent Antarctic ice sheet retreat on simulated sea ice area trends. Geophysical Research Letters, 40(16), 4328–4332. https://doi.org/10.1002/grl.50820

Swart, N. C., Fyfe, J. C., Gillett, N., & Marshall, G. J. (2015). Comparing trends in the southern annular mode and surface westerly jet. Journal of Climate, 28(22), 8840–8859. https://doi.org/10.1175/JCLI-D-15-0334.1

Swart, Neil C., Gille, S. T., Fyfe, J. C., & Gillett, N. P. (2018). Recent Southern Ocean warming and freshening driven by greenhouse gas emissions and ozone

depletion. Nature Geoscience, 11(11), 836–841. https://doi.org/10.1038/s41561-018-0226-1

Thompson, D. W. J., Baldwin, M. P., & Solomon, S. (2005). Stratosphere–Troposphere Coupling in the Southern Hemisphere. Journal of the Atmospheric Sciences, 62(3), 708–715. https://doi.org/10.1175/jas-3321.1

Thompson, D. W. J., & Solomon, S. (2002). Interpretation of recent Southern Hemisphere climate change. Science, 296(5569), 895–899. https://doi.org/10.1126/science.1069270

Thompson, D. W. J., Solomon, S., Kushner, P. J., England, M. H., Grise, K. M., & Karoly, D. J. (2011). Signatures of the Antarctic ozone hole in Southern Hemisphere surface climate change. Nature Geoscience, 4(11), 741–749. https://doi.org/10.1038/ngeo1296

Thompson, D. W. J., & Wallace, J. M. (2000). Annular modes in the extratropical circulation. Part II: Trends. Journal of Climate, 13(5), 1018–1036. https://doi.org/10.1175/1520-0442(2000)013<1018:AMITEC>2.0.CO;2

Tomas, R. A., Deser, C., & Sun, L. (2016). The role of ocean heat transport in the global climate response to projected arctic sea ice loss. Journal of Climate, 29(19), 6841–6859. https://doi.org/10.1175/JCLI-D-15-0651.1

Trenberth, K. E., & Fasullo, J. T. (2010). Simulation of present-day and twenty-first-century energy budgets of the southern oceans. Journal of Climate, 23(2), 440–454. https://doi.org/10.1175/2009JCLI3152.1

Turner, J. (2004). The El Niño-Southern Oscillation and Antarctica. International Journal of Climatology, 24(1), 1–31. https://doi.org/10.1002/joc.965

Turner, J., Bracegirdle, T. J., Phillips, T., Marshall, G. J., & Scott Hosking, J. (2013). An initial assessment of antarctic sea ice extent in the CMIP5 models. Journal of Climate, 26(5), 1473–1484. https://doi.org/10.1175/JCLI-D-12-00068.1

Turner, J., Comiso, J. C., Marshall, G. J., Lachlan-Cope, T. A., Bracegirdle, T., Maksym, T., … Orr, A. (2009). Non-annular atmospheric circulation change induced by stratospheric ozone depletion and its role in the recent increase of Antarctic sea ice extent. Geophysical Research Letters, 36(8), 1–5. https://doi.org/10.1029/2009GL037524

Turner, J., Guarino, M. V., Arnatt, J., Jena, B., Marshall, G. J., Phillips, T., … Cavanagh, R. (2020). Recent Decrease of Summer Sea Ice in the Weddell Sea, Antarctica. Geophysical Research Letters, 47(11). https://doi.org/10.1029/2020GL087127

Turner, J., Hosking, J. S., Bracegirdle, T. J., Marshall, G. J., & Phillips, T. (2015). Recent changes in Antarctic Sea Ice. Philosophical Transactions of the Royal Society A: Mathematical, Physical and Engineering Sciences, 373(2045), 20140163. https://doi.org/10.1098/rsta.2014.0163

Turner, J., Hosking, J. S., Bracegirdle, T. J., Phillips, T., & Marshall, G. J. (2017). Variability and trends in the Southern Hemisphere high latitude, quasi-stationary planetary waves. International Journal of Climatology, 37(5), 2325–2336. https://doi.org/10.1002/joc.4848

Turner, J., Lu, H., White, I., King, J. C., Phillips, T., Hosking, J. S., … Deb, P. (2016). Absence of 21st century warming on Antarctic Peninsula consistent with natural variability. Nature. https://doi.org/10.1038/nature18645

Turner, J., Phillips, T., Hosking, J. S., Marshall, G. J., & Orr, A. (2013). The amundsen sea low. International Journal of Climatology, 33(7), 1818–1829. https://doi.org/10.1002/joc.3558

Turner, J., Phillips, T., Marshall, G. J., Hosking, J. S., Pope, J. O., Bracegirdle, T. J., & Deb, P. (2017). Unprecedented springtime retreat of Antarctic sea ice in 2016. Geophysical Research Letters, 44(13), 6868–6875. https://doi.org/10.1002/2017GL073656

Turner, J., Scott Hosking, J., Marshall, G. J., Phillips, T., & Bracegirdle, T. J. (2016). Antarctic sea ice increase consistent with intrinsic variability of the Amundsen sea low. Climate Dynamics, 46(7–8), 2391–2402. https://doi.org/10.1007/s00382-015-2708-9

Valcke, S.: OASIS3 User Guide (prism_2-5), PRISM Support Initiative No. 3, 68 pp., CERFACS, Toulouse, France, 2006.

Vaughan, D.G., J.C. Comiso, I. Allison, J. Carrasco, G. Kaser, R. Kwok, P. Mote, T. Murray, F. Paul, J. Ren, E. Rignot, O. Solomina, K. S. and T. Z. (2013). Observations: Cryosphere. In Intergovernmental Panel on Climate Change (Ed.), Climate Change 2013: The Physical Sci- ence Basis. Contribution of Working Group I to the Fifth Assessment Report of the Intergovernmental Panel on Climate Change (Vol. 9781107057, pp. 317–382). https://doi.org/10.1017/CBO9781107415324.012

Vavrus, S. J. (2018). The Influence of Arctic Amplification on Mid-latitude Weather and Climate. Current Climate Change Reports, 4(3), 238–249. https://doi.org/10.1007/s40641-018-0105-2

Walters, D., Baran, A. J., Boutle, I., Brooks, M., Earnshaw, P., Edwards, J., … Zerroukat, M. (2017). The Met Office Unified Model Global Atmosphere 7.0/7.1 and JULES Global Land 7.0 configurations. Geoscientific Model Development, 12(5), 1909–1963. https://doi.org/10.5194/gmd-12-1909-2019

Wang, G., Hendon, H. H., Arblaster, J. M., Lim, E.-P., Abhik, S., & van Rensch, P. (2019). Compounding tropical and stratospheric forcing of the record low Antarctic sea-ice in 2016. Nature Communications, 10(1), 13. https://doi.org/10.1038/s41467-018-07689-7

Wang, X., & Wu, Z. (2020). Variability in Polar Sea Ice (1989-2018). IEEE Geoscience and Remote Sensing Letters, 1–5. https://doi.org/10.1109/lgrs.2020.3004257

Waugh, D. W., & Randel, W. J. (1999). Climatology of Arctic and Antarctic Polar Vortices Using Elliptical Diagnostics. Journal of the Atmospheric Sciences, 56(11), 1594–1613. https://doi.org/10.1175/1520-0469(1999)056<1594:COAAAP>2.0.CO;2

Williams, K. D., Copsey, D., Blockley, E. W., Bodas-Salcedo, A., Calvert, D., Comer, R., … Xavier, P. K. (2017). The Met Office Global Coupled Model 3.0 and 3.1 (GC3.0 and GC3.1) Configurations. Journal of Advances in Modeling Earth Systems, 10(2), 357–380. https://doi.org/10.1002/2017MS001115

Whitworth T., III, Orsi, A.H., Kim, S.-J., and Nowlin, W.D. Jr., 1998. Water masses and mixing near the Antarctic Slope Front. In Jacobs, S.S., and Weiss, R.F. (eds.), Ocean, Ice and Atmosphere: Interactions at the Antarctic Continental Margin. Washington, DC: American Geophysical Union, Antarctic Research Series, No. 75, pp. 1–27.

Wolfe, C. L., & Cessi, P. (2014). Salt feedback in the adiabatic overturning circulation. Journal of Physical Oceanography, 44(4), 1175–1194. https://doi.org/10.1175/JPO-D-13-0154.1

Worby, A. P., Geiger, C. A., Paget, M. J., Van Woert, M. L., Ackley, S. F., & DeLiberty, T. L. (2008). Thickness distribution of Antarctic sea ice. Journal of Geophysical Research: Oceans, 113(5), 1–14. https://doi.org/10.1029/2007JC004254

Yu, J. Y., Lu, M. M., & Kim, S. T. (2012). A change in the relationship between tropical central Pacific SST variability and the extratropical atmosphere around 1990. Environmental Research Letters, 7(3). https://doi.org/10.1088/1748-9326/7/3/034025

Yu, Lejiang, Zhong, S., & Sun, B. (2020). The Climatology and Trend of Surface Wind Speed over Antarctica and the Southern Ocean and the Implication to Wind Energy Application. Atmosphere, 11(1), 108. https://doi.org/10.3390/atmos11010108

Yu, Lisan, & Weller, R. A. (2007). Objectively analyzed air-sea heat fluxes for the global ice- free oceans (1981-2005). Bulletin of the American Meteorological Society, 88(4), 527–539. https://doi.org/10.1175/BAMS-88-4-527

Yuan, X. (2004). ENSO-related impacts on Antarctic sea ice: A synthesis of phenomenon and mechanisms. Antarctic Science, 16(4), 415–425. https://doi.org/10.1017/S0954102004002238

Yuan, X., Kaplan, M. R., & Cane, M. A. (2018). The interconnected global climate system-a review of tropical-polar teleconnections. Journal of Climate, 31(15), 5765–5792. https://doi.org/10.1175/JCLI-D-16-0637.1

Yuan, X., & Li, C. (2008). Climate modes in southern high latitudes and their impacts on Antarctic sea ice. Journal of Geophysical Research: Oceans, 113(6), 1–13. https://doi.org/10.1029/2006JC004067

Zappa, G., Pithan, F., & Shepherd, T. G. (2018). Multimodel Evidence for an Atmospheric Circulation Response to Arctic Sea Ice Loss in the CMIP5 Future Projections. Geophysical Research Letters, 45(2), 1011–1019. https://doi.org/10.1002/2017GL076096

Zhang, J. (2007). Increasing antarctic sea ice under warming atmospheric and oceanic conditions. Journal of Climate, 20(11), 2515–2529. https://doi.org/10.1175/JCLI4136.1

Zhang, P., Wu, Y., Simpson, I. R., Smith, K. L., Zhang, X., De, B., & Callaghan, P. (2018). A stratospheric pathway linking a colder Siberia to Barents-Kara Sea sea ice loss. Science Advances, 4(7), 1–9. https://doi.org/10.1126/sciadv.aat6025

Zhang, T., Hoell, A., Perlwitz, J., Eischeid, J., Murray, D., Hoerling, M., & Hamill, T. M. (2019). Towards Probabilistic Multivariate ENSO Monitoring. Geophysical Research Letters, 46(17–18), 10532–10540. https://doi.org/10.1029/2019GL083946

Zunz, V., Goosse, H., & Massonnet, F. (2013). How does internal variability influence the ability of CMIP5 models to reproduce the recent trend in Southern Ocean sea ice extent? Cryosphere, 7(2), 451–468. https://doi.org/10.5194/tc-7-451-2013

Data Sources

CMIP data were obtained from the British Atmospheric Data Centre. I acknowledge the World Climate Research Programme Working Group on Coupled Modelling, which is responsible for CMIP, and the modeling groups, for producing the simulations and making available their output.